Advancing Cancer Therapy Predictions with Patient-Derived Organoid Models of Metastatic Breast Cancer

Dissertation

der Mathematisch-Naturwissenschaftlichen Fakultät

der Eberhard Karls Universität Tübingen

zur Erlangung des Grades eines

Doktors der Naturwissenschaften

(Dr. rer. nat.)

vorgelegt von

Cansu Ebru Önder

aus Stuttgart

Tübingen

2024

Gedruckt mit Genehmigung der Mathematisch-Naturwissenschaftlichen Fakultät der Eberhard Karls Universität Tübingen.

Tag der mündlichen Qualifikation:	25.11.2024
Dekan:	Prof. Dr. Thilo Stehle
1. Berichterstatter:	Prof. Dr. Robert Feil
2. Berichterstatter:	Jun. Prof. Dr. Martin Weiss

Acknowledgements

I would first like to voice my profound gratitude to Dr. André Koch for giving me the opportunity to do my PhD at the Institute for women's health and his guidance. His expertise has been invaluable in determining the direction of this thesis. It was truly a great honor to be a member of AG Koch.

Also, I would like to convey many thanks to Prof. Dr. Robert Feil and Prof. Dr. Martin Weiss, who were exceptionally kind and willing to review my thesis. Their constructive feedback has enhanced the content of this work.

Special thanks go to Ingrid Teufel and Anjali Singh, who shared their great knowledge, taught me various techniques, and supported me tirelessly. I will be forever grateful for their exceptional guidance and friendship.

My heartfelt thanks to all the colleagues of AG Koch for the admirable working environment and enjoyable conversations. I highly appreciate Teresa Ziegler for her consistent support and companionship. I extend my appreciation to further participants of this study: Franziska Leibfarth, Stella Asmanidou, Jasmin Müller, Henrike Held, and Alica Fehrenbach. Their contributions have added value to the research that shaped this thesis.

Many thanks also go to my friends Demet Tanriverdi, Susanne Klute, Shakira Wafa, Betül Findik, Carolina Schröder, Barbara Volz, Yacine Maringer, Sinja Kieninger, Johanna Geiger and Nicole Vogt for always standing by my side. Their encouragement has provided me with much-needed resilience.

Finally, I must express my deepest appreciation to my parents Filay and Öner, my brother Baris, and my partner Moustafa for their extraordinary support during my studies. Their unconditional love and understanding have been my driving force throughout my academic journey.

This thesis would not have been possible without the support of all those mentioned above. Thank you.

Contents

I. List of figures

Supplementary figures

II. List of tables

III. List of abbreviations

% ..... percent
× g ..... relative centrifugal force (RCF)
× ..... fold; times
°C ..... degree(s) Celsius
µg ..... microgram(s)
µL ..... microliter(s)
µm ..... micrometer(s)
µM ..... micromolar(s)
2D 2-dimensional
3D 3-dimensional
4-1BB (alias CD137) ..... cluster of differentiation 137
A ..... adenine
AdCAR ..... Adapter CAR
AdCARs ..... Adapter CAR-T cells
ADP ..... adenosine diphosphate
AdvDMEM ..... Advanced DMEM/F-12
AKT (1/2/3) ..... RAC-alpha/beta/gamma serine/threonine-protein kinase
AKT1 ..... gene encoding RAC-alpha serine/threonine-protein kinase
AM(s) ..... Adapter molecule(s)
Arg ..... arginine
ATCC ..... American Type Culture Collection
ATP ..... adenosine triphosphate
BC ..... breast cancer
BCM ..... breast cancer medium
BF ..... brightfield
BME ..... basement membrane extract
bp ..... basepairs
BRAF ..... v-Raf murine sarcoma viral oncogene homolog B1
BRCA1/2 ..... breast cancer type 1/2 susceptibility protein
BRCA1/2 ..... tumor suppressor gene encoding BRCA1/2
BSA ..... Albumin fraction V from bovine serum
C ..... cytosine
CAR(s) ..... chimeric antigen receptor(s)
CD276 ..... cluster of differentiation 276
CD28 ..... cluster of differentiation 28
CD3ζ ..... cluster of differentiation 3 zeta

CD4 ..... cluster of differentiation 4
CD8 ..... cluster of differentiation 8
CDH1 ..... cadherin-1 or epithelial cadherin
CDH1 ..... gene encoding CDH1
CDK4/6 ..... cyclin-dependent kinase 4/6
CO_2 ..... carbon dioxide
conc. ..... concentration
DCIS ..... ductal carcinoma in situ
DMEM ..... Dulbecco's Modified Eagle's Medium
DMSO ..... dimethyl sulfoxide
DNA ..... deoxyribonucleic acid
dNTP(s) ..... deoxynucleosidtriphophate(s)
DPBS ..... Dulbecco's phosphate-buffered saline
E ..... glutamic acid
E:T ..... effector:target ratio
EDTA ..... ethylenediaminetetraacetic acid
EGF ..... epidermal growth factor
EGFR ..... epidermal growth factor receptor
EpCAM ..... epithelial cell adhesion molecule
ERK1/2 ..... extracellular-signal regulated kinases 1/2
ERα ..... estrogen receptor alpha
FACS ..... fluorescence activated cell sorting
FBS ..... fetal bovine serum
FC ..... flow cytometry
FFPE ..... formalin-fixed paraffin-embedded tissue
FGF ..... fibroblast growth factor
FL ..... fluorescence
g ..... gram(s)
G ..... guanine
GATA3 ..... GATA binding protein 3 (transcription factor)
GATA3 ..... gene encoding GATA3
GFP ..... green fluorescent protein
Glu ..... glutamic acid
h ..... hour(s)
H ..... histidine
H&E ..... hematoxylin and eosin stain
HER2 ..... human epidermal growth factor receptor 2

HER4 ..... human epidermal growth factor receptor 4
HF ..... high-fidelity
His ..... histidine
HRP ..... horseradish peroxidase
HSA ..... human serum albumin
IC50 ..... half maximal inhibitory concentration
IDC ..... invasive ductal carcinoma
IHC ..... immunohistochemistry
IL ..... interleukin
IL-2Rβ ..... interleukin-2 receptor subunit beta
ILC ..... invasive lobular carcinoma
K ..... lysine
$KHCO_3$ ..... potassium bicarbonate
Ki67 ..... marker of proliferation protein
L ..... liter(s)
LCIS ..... lobular carcinoma in situ
LLE ..... linker-label-epitope
Lys ..... lysine
M ..... molar(s)
MA ..... malignant ascites
mAbs ..... monoclonal antibodies
MAPK ..... mitogen-activated protein kinase
MBC-PDO(s) ..... metastatic breast cancer patient-derived organoid line(s)
MEK ..... mitogen-activated protein kinase kinase
min ..... minute(s)
mL ..... milliliter(s)
mm ..... millimeter(s)
MOI ..... multiplicity of infection
MPE ..... malignant pleural effusion
mTORC1 ..... mammalian target of rapamycin complex 1
n ..... number(s)
Na_2EDTA ..... ethylenediaminetetraacetic acid disodium salt dihydrate
ng ..... nanogram(s)
NH_4Cl ..... ammonium chloride
NIC ..... nicotinamide
nm ..... nanometer(s)
nM ..... nanomolar(s)

NST ..... no special type
OX-40 (alias CD134) ..... cluster of differentiation 134
P ..... passage(s)
p ..... phospho(rylated)
p ..... significance value
p53 ..... tumor protein P53
PARP ..... Poly (ADP-ribose) polymerase
PCR ..... polymerase chain reaction
PDX ..... patient-derived xenografts
PE ..... pleural effusion
Pen/Strep ..... penicillin-streptomycin
pH ..... potential of hydrogen
PI3K ..... phosphoinositide 3-kinase, alias phosphatidylinositol-4,5-biphosphate 3-kinase
PIK3CA ..... gene encoding PIK3CA
PIK3CA ..... phosphatidylinositol-4,5-biphosphate 3-kinase, catalytic subunit alpha
PR ..... progesterone receptor
PTEN ..... phosphatase and tensin analog
PTEN ..... tumor suppressor gene encoding PTEN
R ..... arginine
R1/2/3 ..... replicate 1/2/3
RBC ..... red blood cell
RNA ..... ribonucleic acid
ROR1 ..... receptor tyrosine kinase-like orphan receptor 1
rpm ..... rounds per minute
RPMI ..... Roswell Park Memorial Institute (medium)
RT ..... room temperature
RTK(s) ..... receptor tyrosine kinase(s)
SD ..... standard deviation
Ser ..... serine
STAT3 ..... signal transducer and activator of transcription 3
T ..... thymine
TAA(s) ..... tumor-associated antigen(s)
TAE ..... Tris-acetate-EDTA
Thr ..... threonine
TNBC ..... triple-negative breast cancer
TP53 ..... tumor suppressor gene encoding p53
Tris ..... tris(hydroxymethyl)aminomethan

TROP2 ..... tumor-associated calcium signal transducer 2
Tyr ..... tyrosine
UKT ..... Uniklinikum Tübingen
V ..... Volt
w/o ..... without
WT ..... wild type
X ..... amino acid

IV. Zusammenfassung

Brustkrebs wurde bereits in verschiedenen Modellen und Zelltypen untersucht. Von Patienten stammende metastasierte Brustkrebs-Organoide müssen jedoch näher erforscht werden. So wurde in dieser Arbeit die Auswirkung von therapeutischen Wirkstoffen auf Brustkrebs-Zelllinien und von Patienten stammende metastasierte Organoide untersucht, um eine zuverlässige Anwendung für *in vitro* Wirkstoff-Screenings zu kreieren. Im ersten Teil dieser Studie wurden verschiedene Konzentrationen von zahlreichen Wirkstoffen auf 2-dimensionale Brustkrebszelllinien getestet, um Medikamenten-Wirkungskurven zu generieren und sensitive Linien zu identifizieren. Die meisten Studien zu Brustkrebs involvieren typischerweise Brustkrebszelllinien und Primärtumorgewebe für die Herstellung von Organoid-Modellen. Deshalb wurde im zweiten Teil dieser Studie metastasierter Brustkrebs adressiert. Da metastasierter Brustkrebs eine schlechte Prognose hat, besteht ein Bedarf an zuverlässiger Präzisionsonkologie sowie Modelle, welche die heterogene Natur des Brustkrebses repräsentieren. Ein häufiges Symptom von metastasiertem Brustkrebs schließt unter anderem die Akkumulation von Flüssigkeit und metastasierten Zellen im Peritoneum, bezeichnet als maligner Aszites (MA), oder in der Pleurahöhle, sogenannter maligner Pleuraerguss (MPE), ein. In dieser Arbeit wurden metastasierte Tumorzellen, welche von MA- und MPE-Proben von fortgeschrittenen Brustkrebspatienten stammen, als Organoide kultiviert. Etablierte Organoid-Kulturen wurden als metastasierte Brustkrebs-Patienten-abgeleiteter Organoide (in Englisch: metastatic BC patient-derived organoids; abgekürzt: MBC-PDO) bezeichnet. Die Eigenschaften von MBC-PDO-Linien wurden mittels Immunhistochemie und Mutationsanalysen von Hotspot-Regionen identifiziert. MBC-PDO-Linien konnten im Vergleich zu ihren originalen Proben ihre Expressionsmuster und Hotspot-Mutationen präservieren, was sie zu einem angemessenen *in vitro* Modell für metastasierten Brustkrebs macht. Anschließend wurden MBC-PDO-Linien mit zahlreichen Inhibitoren und chemotherapeutischen Wirkstoffen behandelt, um eine zuverlässige Anwendung für Wirkstoff-Screenings von metastasierten Brustkrebszellen zu implementieren. Diese 3-dimensionalen Wirkstoff-Assays demonstrierten, dass die Medikamentenwirkungen nicht immer mit den Expressionsmustern und Hotspot-Mutationen übereinstimmt. Diese Diskrepanz hebt die Wichtigkeit der Kombination von Immunhistochemie und Mutationsanalysen von MBC-PDO-Linien mit *in vitro* Wirkstoff-Assays hervor. Unsere MBC-PDO-Linien rekapitulieren die Eigenschaften der originalen Proben, welche von MA und MPE stammen, und dienen als wertvolle Modelle, die in einem präklinischen Rahmen genutzt werden können, um Therapieentscheidungen zu erleichtern. Beispielsweise wurden hämatologische bösartige Erkrankungen erfolgreich mit chimärischen-antigenspezifischen-Rezeptor-T-Zellen (CAR-T-Zellen) behandelt. Die Wirksamkeit von CAR-T-Zellen bei der Bekämpfung von soliden Tumoren wie Brustkrebs muss jedoch noch verbessert werden. Zu guter Letzt wurde das

Potential von MBC-PDO-Linien hinsichtlich der Nutzung in Adapter CAR-(AdCAR) T-Zell-vermittelten Zytotoxizität-Assays erforscht. MBC-PDO-Linien wurden transduziert, um Luciferase und GFP zu exprimieren. Tumor-assoziierte Antigene der MBC-PDO-Linien wurden mittels Flow Cytometry charakterisiert. Ein Assay für die Behandlung von metastasierten Brustkrebszellen mit AdCAR-T-Zellen wurde implementiert, um die Wirkungen personalisiert zu bewerten. MBC-PDO-Linien wurden als eine Screening-Plattform verwendet, um die AdCAR-T-Zell-basierte Präzisionsimmuntherapie für flexibles Abzielen auf tumorassoziierte Antigene zu evaluieren. Abhängig von ihrer Antigenexpression wurden MBC-PDO-Linien mit AdCAR-T-Zellen und biotinylierten monoklonalen Antikörpern gegen CD276, HER2, EGFR, TROP2, and EpCAM behandelt. Flow-Cytometry-Daten und Ko-Kultur-Assays zeigten, dass die Zytolyse mittels AdCAR-T-Zellen mit der Antigenexpression der MBC-PDO-Linien korrelierte. Diese Erkenntnisse deuten drauf hin, dass MBC-PDO-Linien als ein zuverlässiges Modell für die Erforschung der Wirksamkeit von AdCAR-T-Zellen auf metastasierten Brustkrebs dienen können. Zusammengefasst: MBC-PDO-Linien haben das Potential, als ein Instrument zur Untersuchung von metastasiertem Brustkrebs zu dienen, um dazu beizutragen, das Überleben der Patienten zu verlängern und ihre Lebensqualität zu steigern.

V. Abstract

Breast cancer (BC) has been studied in various models and cell types, yet patient-derived metastatic BC organoids remain to be further explored. Here, the impact of therapeutic compounds on BC cell lines and patient-derived metastatic organoids was investigated, to create a reliable application for *in vitro* drug screenings. In the first part of this study, different concentrations of various drugs were tested on two-dimensional BC cell lines to generate drug-response curves and identify sensitive lines. Most studies on BC typically involve BC cell lines and primary tumor tissue for creating organoid models. Therefore, metastatic BC was addressed in the second part of this study. As metastasized BC has a poor outcome, there is a requirement for dependable precision oncology and models representing the heterogeneous nature of BC. A frequent symptom of metastasized BC includes the accumulation of fluid and metastatic cells in the peritoneum called malignant ascites (MA) or in the pleural cavity referred to as malignant pleural effusion (MPE). In this thesis, metastatic tumor cells derived from MA or MPE from advanced BC patients were cultured applying organoid technology. The resulting organoid cultures were referred to as metastatic BC patient-derived organoids (MBC-PDO). The characteristics of MBC-PDO lines were identified by applying immunohistochemistry and mutation analysis of hotspot regions. MBC-PDO lines could preserve their expression patterns and hotspot mutations when compared to their original metastatic counterpart and are therefore a suitable *in vitro* model for metastasized BC. Subsequently, MBC-PDO lines were treated with various inhibitors and chemotherapy drugs to implement a reliable application for drug screenings of metastasized BC cells. These three-dimensional drug assays demonstrated that drug responses are not always in accord with expression patterns and hotspot mutations. This discrepancy highlights the importance of combining immunohistochemistry stainings and mutational analysis of MBC-PDO lines with *in vitro* drug assays. Our MBC-PDO lines recapitulate the characteristics of their original sample derived from MA and MPE and serve as a valuable model that can be used in a preclinical setting for guiding therapy decisions. For instance, hematologic malignancies have been shown to be effectively treated with chimeric antigen receptor (CAR) T cell therapy. Yet, CAR-T efficacy in battling solid tumors, like BC, still needs improvement. Lastly, the capability of utilizing MBC-PDO lines for Adapter CAR (AdCAR) T cell-mediated cytotoxicity assays was therefore investigated. MBC-PDO lines were transduced to express luciferase and GFP. Tumor-associated antigens of MBC-PDO lines were characterized by flow cytometry. An assay for the treatment of metastasized BC cells with AdCAR-T cells was implemented to assess responses in a personalized manner. MBC-PDO lines were used as a screening platform to evaluate AdCAR-T cell-based precision immunotherapy for flexible targeting of tumor-associated antigens. Based on their antigen expression, MBC-PDO lines were targeted with AdCAR-T cells and biotinylated monoclonal antibodies against CD276, HER2, EGFR, TROP2, and

EpCAM. Flow cytometry data and co-culture assays demonstrated that cytolysis by AdCAR-T cells correlated with the antigen expression of MBC-PDO lines. The results suggest that MBC-PDO lines can serve as a reliable model for assessing the efficacy of AdCAR-T on metastatic BC. Overall, MBC-PDOs have the potential to serve as a tool to study metastasized BC and help prolong patients' survival time and improve their quality of life.

1 Introduction

Some of the following contents have been previously published (see chapter 8 and 9).

Onder, C.E., T.J. Ziegler, R. Becker, S.Y. Brucker, A.D. Hartkopf, T. Engler, and A. Koch, Advancing Cancer Therapy Predictions with Patient-Derived Organoid Models of Metastatic Breast Cancer. Cancers (Basel), 2023. 15(14).

Onder, C.E., M. Moustafa-Oglou, S.M. Schroder, A.D. Hartkopf, A. Koch, and C.M. Seitz, Precision Immunotherapy Utilizing Adapter CAR-T Cells (AdCAR-T) in Metastatic Breast Cancer Leads to Target Specific Lysis. Cancers (Basel), 2023. 16(1).

1.1 Breast cancer

Representing 11.7% of all cancer cases in 2020, breast cancer (BC) ranks as the most frequent type of cancer and is one of the leading causes of cancer-associated deaths among women globally [1]. Its frequency is based, among other things, on age, genetic predisposition, and geographic location [2]. According to American Cancer Society, BC accounts for about 30% of all new female cancers and one in eight women in the United States develops BC [3]. BC incidences are increased in developed countries due to advanced detection techniques and a higher prevalence of known risk factors associated with the disease. Risk factors include early onset of menstruation, nulliparity, low parity, late age at birth, and late menopause [4]. These factors are linked to the hormonal (mainly estrogen) milieu to which breasts are exposed from menarche until menopause [4, 5]. In contrast, women in developing countries tend to have more and earlier age of pregnancies, which contributes to lower BC incidences. In addition to that, longer period of breastfeeding reduces the risk of BC, as shown by recent studies [5, 6]. Even though the incidence of BC is lower in developing countries, the mortality is higher [7]. Approximately 1% of BC occur in men [8].

BC is a heterogeneous disease, with different types based on various factors, such as the cells involved and the expression of specific receptors (**Figure 1**) [9]. Each BC type has distinct biological features, clinical behavior and treatment approaches [9]. Most commonly, breast tumors commence in the epithelial cells of the ducts, that carry milk to the nipple, or the lobules, that produce milk [10]. Preinvasive cancer refers to ductal and lobular carcinoma in situ (DCIS and LCIS). Invasive cancer describes lobular, ductal or any form of BC that has invaded the surrounding tissue [9, 10]. The commonest BC type is invasive BC of no special type (NST), so called invasive ductal carcinoma (IDC), which makes up about 50-80% of all BC, followed by the special type invasive lobular carcinoma (ILC), accounting for approx. 25% of invasive BC [9, 11]. Subtypes of BC are defined by the status of estrogen receptor α (ERα),

progesterone receptor (PR), and human epidermal growth factor receptor 2 (HER2) [9]. The expression status of these receptors guides the therapy proposal and estimates the prognosis of BC patients [12-14]. “Hormone receptor-positive” breast tumors express ER and/or PR, while tumors that lack expression of ER, PR, or HER2 are considered “triple-negative” BC (TNBC) [10].

Just like in any other type of cancer, there are genetic mutations that commonly occur in BC. While somatic mutations are acquired during a lifetime and can only be found in tumor cells, germline mutations are inherited and are present in every cell of the human’s body [10, 15]. Also, germline mutations are more important for the prognosis of an individual’s genetic risk [15].

Most well-known genes linked to hereditary BC are *BRCA1* and *BRCA2* coding for “breast cancer type 1/2 susceptibility protein”. Mutations in these genes can increase the risk of developing BC [15]. *TP53* and *PTEN* are tumor suppressor genes encoding p53 and phosphatase and tensin homolog (PTEN), respectively; mutations in these genes are also associated with elevated risk of BC [16-18]. Mutations in the *CDH1* gene (encoding cadherin-1 alias epithelial cadherin) can promote the development of lobular BC [19]. GATA binding protein 3 (GATA3) is a transcription factor expressed in various tissues including the mammary gland, and genetic mutations in *GATA3* are associated with luminal BC [20].

Of note, tumorigenesis in BC cells can be driven by the phosphoinositide 3-kinase (PI3K) and the mitogen-activated protein kinase (MAPK) signaling pathway [21]. Sometimes, a mutation of genes encoding key proteins involved in these pathways can be responsible for the activation of these pathways. For instance, mutations in *PIK3CA* (encoding PI3K, catalytic subunit alpha) and *AKT1* genes (encoding RAC-alpha serine/threonine-protein kinase, which acts downstream of PI3K) can result in abnormal protein production and have been linked to the proliferation and survival of cancer cells, as well as enhanced risk of BC [22, 23]. The proto-oncogene *PIK3CA* is one of the most frequently mutated genes in BC [24]. Hotspot mutations in *PIK3CA* often occur in exon 9 (E543 and E545) and exon 20 (H1047) [22, 24, 25]. These hotspot mutations are associated with a hyperactivation of the PI3K-AKT pathway, which promotes cell growth and proliferation [22]. The hotspot mutation in *AKT1* (E17) is linked to a constant activation of the AKT protein, that potentially drives the uncontrolled cell growth and survival of tumor cells [26].

The identification of both somatic and germline mutations in BC influences diagnosis, prognosis, and therapy proposal. For example, mutations in *PIK3CA* or *AKT1* could be more susceptible to treatments targeting the PI3K-AKT pathway [27]. Depending on its specific characteristics and the patient, BC can be treated with a combination of therapies. Treatment options for BC include surgery, radiation, and systemic therapy. The latter approach includes

endocrine therapy for hormone receptor-positive (luminal) BC, targeted therapy for HER2-positive BC, chemotherapy especially for (basal) TNBC, poly adenosine diphosphate (ADP) ribose polymerase (PARP) inhibitors, such as Olaparib, for BC patients with *BRCA* mutations, and immunotherapy [28].

Surgery is performed to eliminate cancerous tissue from the primary tumor site. The range of surgery can vary from a lumpectomy (removal of tumor tissue) to a mastectomy (removal of the breast) and additional removal of adjacent lymph nodes [28]. Post-surgery (adjuvant) radiation therapy utilizes high-energy rays to damage tumor cells and stop their growth [10, 28]. Endocrine therapy, also known as hormone therapy, can be applied before (neoadjuvant) and after (adjuvant) surgery to hormone receptor-positive BC and consists of drugs that reduce hormone production or inhibit their effects [10, 28]. Targeted therapy involves drugs that specifically inhibit proteins that are crucial for the growth of tumor cells [10, 28]. For instance, HER2-positive BC can be treated with inhibitors or antibodies (in combination with chemotherapy) that specifically target HER2. Furthermore, BC can be treated with immunotherapy which involves drugs that help the immune system attack cancer cells [10, 28]. Depending on several factors, BC can also be treated with chemotherapy. Adjuvant chemotherapy can be applied to try to eliminate tumor cells that might have been left behind or spread. Hence, adjuvant chemotherapy can decrease the risk of BC relapse. Neoadjuvant chemotherapy can be useful to shrink the tumor mass before surgery so that lumpectomy instead of a mastectomy might be performed. [10, 28]. Finally, patients with advanced or metastatic BC can receive palliative care, which focuses on managing pain and side effects, and improving the quality of life.

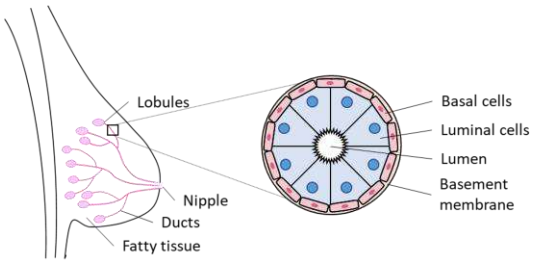

Histological subtype	Ductal	Lobular
Preinvasive	Ductal carcinoma in situ (DCIS)	Lobular carcinoma in situ (LCIS)
Invasive	Invasive ductal carconima (IDC)	Invasive lobular carcinoma (ILC)

Cancer cell phenotype	Luminal	Basoluminal		Basal
Molecular subtype	Luminal A	Luminal B	HER2+	Triple negative
Receptor status	ER+/PR+		HER2+	
Prognosis	Good			Poor
Medical therapy	Endocrine therapy	Targeted therapy	Chemotherapy	

Figure 1: BC subtypes.*(A) Scheme of a breast with lobules and ducts, which are the origin of BCs. Ducts consist of luminal and basal cells. (B) Histological subtypes of BC. (C) Molecular subtype, receptor*

status, prognosis, and therapy options of BC. The figure was created using Microsoft® PowerPoint® and is a modified version of a previously published figure [29].

1.2 Malignant pleural effusion and malignant ascites

Early BC, which describes cancer restricted to the breast or having only spread to the axillary lymph nodes, is potentially curable [10]. Nonetheless, during the progression of cancer, invasive tumor cells can spread through the bloodstream and the lymphatic system to various organs and locations where they form metastasis [30, 31].

Although BC is often detected in early stages, many patients with BC experience a relapse even up to approximately 30 years after primary diagnosis [32]. In some cases, dormant metastatic cells may persist in the patients for years after the surgical removal of the primary BC, and can start proliferating even decades after the primary BC treatment [33]. Primary BC is well studied and has favorable outcome. In contrast, metastatic BC is not curable with today's therapeutic options. However, metastatic BC can be treated by prolonging survival and managing symptoms [10]. Metastatic BC is frequently hindered by heterogeneity, which describes the presence of diverse traits within the tumor cells and is a common cause behind therapy failures [34]. Furthermore, metastatic BC has a poor outcome due to persistent and treatment-resistant tumor cells and their impact on vital organs [34].

Metastatic biopsies are very rare, because of hindered accessibility to the metastatic source and associated risk considerations. Therefore, therapy recommendation generally depends on the characteristics of primary tumors. Yet, primary tumors do not necessarily recapitulate the properties of metastatic lesions, which may exhibit discordance in markers such as receptor expression [35]. Additionally, there can be differences in mutational signatures and increase of tumor mutational burden in metastatic BC [36]. Hence, therapy that is based on the characteristics of the primary tumor alone can lead to a poorer prognosis [37-39].

Sometimes, advanced BC can lead to ascites and pleural effusion, which define the abnormal accumulation of fluid in the peritoneal cavity (the space between the abdominal organs and the wall) and pleural cavity (the space between the lung and the chest wall), respectively (**Figure 2**) [40, 41]. Malignant ascites (MA) is a condition in which the accumulation of fluid in the peritoneal cavity is caused by the spread of cancer cells to the peritoneum [40]. This accumulation of fluid can cause swelling and pain resulting in a reduced quality of life. Malignant pleural effusion (MPE) describes the buildup of fluid and presence of malignant cells in the pleural cavity. MPE is caused by tumor cells that metastasized to the pleura, which can lead to chest pain, reduced lung function and difficulty breathing [41]. Both MA and MPE are

a frequent issue for patients with advanced cancer and are an indication of metastatic disease [40, 41]. BC is a common driver of MA and MPE with 3% of BC patients developing MA and 7% developing MPE [42, 43]. Patients with MA or MPE endure a poor quality of life defined by chest and abdominal pain and trouble breathing [43, 44].

The diagnosis of MA and MPE has an influence on tumor stage and prognosis. The median survival rate of cancer patients with MA and MPE is relatively low and reaches from 5 to 13 months [43, 45, 46]. To relieve the pressure and pain for the patients, the fluid of MA and MPE can be removed through a simple puncture. Consequently, obtained MA and MPE, containing metastatic tumor cells, offer opportunities for metastatic biopsies. Moreover, they present a potential source for the characterization of metastatic BC [47, 48]. MA and MPE can be further used as a source for the creation of *in vitro* models to improve therapy outcomes. The treatment of MA and MPE is focused on managing symptoms and improving quality of life. Apart from drainage, treatment options can include targeted therapy, immunotherapy, and chemotherapy depending on the attributes of BC [49-51].

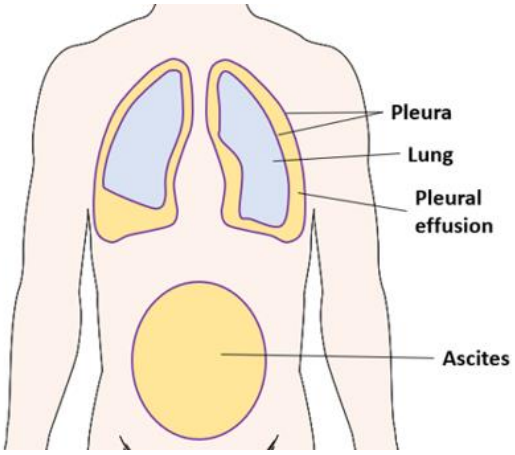

Figure 2: MA and MPE. *Accumulation of fluid in the peritoneal (ascites) and pleural (pleural effusion) cavity. In the presence of malignant cells, both accumulations are referred to as malignant ascites (MA) and malignant pleural effusion (MPE). The figure was created using Microsoft® PowerPoint®.*

1.3 Two-dimensional (2D) BC cell lines

In the nineteen-seventies, the first BC cell lines, including the MDA-series and MCF-7, were established amongst others from pleural effusions derived from metastatic BC patients [52, 53]. Two-dimensional (2D) BC cell lines are established cell lines that grow on a flat surface, such as a petri dish or culture flask, and are widely used in research as they are easy to use and reproducible [54]. Some of the benefits of 2D BC cell lines are their use in basic cancer

research, drug development, drug screening, identification of biomarkers, studying genetic and molecular mechanisms, and even cancer immunology.

In BC, biomarkers can function as important indicators for cancer prognosis and therapy effectiveness. The discovery of biomarkers in 2D BC cell lines can pave the way to the development of targeted or precision therapies [55, 56]. Moreover, 2D BC cell lines can serve as a crucial tool to study the genetic and molecular alterations that take place in BC [57]. Hence, a deeper knowledge on the genetic drivers of BC can be gained, which can also lead to the progress of precision medicine [10].

In terms of drug development, BC cell lines can be fundamental in the first stages of drug discovery, as they can be utilized to investigate the effects of potential drug candidates [58]. Since they can be cultured in multi-well plates, BC cell lines are applicable to high-throughput screening methods [59]. Consequently, many compounds or conditions can be investigated, and outperforming drug candidates can be detected and used for subsequent testing in preclinical and clinical studies. Regarding cancer immunology, BC cell lines permit the investigation of how the immune system interacts with tumor cells [59]. Hence, for the treatment of specific BC types, these approaches are important for the development of immunotherapies.

MCF-7 is one of the most popular BC cell lines and is derived from a pleural effusion from a metastasized BC patient [53]. MCF-7 cells are ERα-positive, which makes them valuable for studying hormonal studies and therapies [60, 61]. The HER2-positive cell line SKBR3 is a useful model to study HER2-targeted therapies [62, 63]. The TNBC cell line MDA-MB-231 is frequently used to investigate the biology of TNBC and its responsiveness to certain drugs, especially chemotherapy [64].

Although 2D BC cell lines are convenient to use in the mentioned approaches and offer various benefits, they also have their restrictions [65]. That is, BC cell lines do not reflect the complex pathophysiology and the multi-faceted tumor microenvironment of living organisms [58]. Therefore, results from 2D cell lines need to be validated not only in three-dimensional (3D) models, but also in *in vivo* models and clinical studies.

1.4 Three-dimensional (3D) BC organoids

Metastasized BC is known for its poor outcome. Therefore, the demand for personalized oncology and the importance of models reflecting the features of BC is high. Cell lines are widely utilized in BC research, yet they only represent a miniscule subset of the BC diversity and are not capable of covering the heterogeneity of BC nor can they predict the specific drug responses for patients [66]. Patient-derived xenograft (PDX) models are commonly used in

translational research and make up a fundamental part of drug development and response studies. They play a great role in mimicking the complex environment and interactions within the body. Despite their importance, high costs and low efficiency demonstrate a hindrance in the utilization of PDX [66].

As 3D structures cultured in an extracellular matrix, patient-derived organoids serve as a relatively modern alternative to 2D cell lines and PDX models (**Figure 3**). Organoids can self-organize and mimic specific tissues of the human body [67]. Due to their multiple benefits, organoids of various sources have already been used in numerous methods. Organoids can be generated from pluripotent and adult stem cells, as well as tissue- and organ-derived cells [68]. While stem cells can differentiate into any cell type of the body and can be guided to form specific organoids, organ-specific progenitor and organ-derived cells are more limited to forming specific cell types within that tissue or organ. Importantly, the success of culturing organoids depends not only on the primary cells but also on the culture conditions [68].

Examples of methods organoids are used in include disease modeling, drug development, precision medicine, biomarker discovery, and even regenerative medicine [69]. Organoids can be cultivated to resemble various diseases including cancer and provide a platform for the study of molecular mechanisms and responses to specific treatments [69]. Also, the safety and efficacy of drug candidates can be screened in a high-throughput manner, which leads to the reduction of dependance on animal models [70]. Patient-derived organoids can aid clinicians predict individual therapy responses, which marks a milestone in precision medicine [69]. This approach may pave the way to optimize treatments to the needs of individual patients. Furthermore, patient-derived organoids may help identify new biomarkers associated with different diseases and drug responses [70]. New biomarkers can lead to optimized disease diagnosis and therapy proposals.

BC organoids have shown to be an invaluable 3D model for research, since they accurately capture the characteristics of their respective origin and are utilized for long-term culturing [71]. BC organoids are obtained by culturing patient-derived BC cells in an extracellular matrix which allows them to self-organize in a way that resembles BC. Patient-specific models can reflect the characteristics of a patient's particular BC and therefore they offer a valuable tool for testing personalized therapy strategies [67, 71, 72]. Consequently, BC organoids have been used in drug screenings to assess the effectiveness of certain treatments [71, 72]. Such methods allow researchers to determine which therapies are most effective for the individual's BC, potentially leading to more personalized treatments. Furthermore, BC organoids can be applied to test new therapies that have not been screened in clinical trials [73]. Consequently, BC organoids can be applied in screenings of drug candidates to discover outstanding drugs for further research [74]. BC organoids can further be utilized in the identification of new biomarkers that

correlate with specific BC subtypes or drug responses. Accordingly, these biomarkers can become important for diagnosis and predicting outcomes [75]. Hence, organoids can serve as inexpensive and valuable *in vitro* models for individualized oncology and high-throughput drug assays [71, 76].

Still, there is a remaining shortage of models portraying the most lethal breast cancers: drug-resistant, metastatic tumors. An extended collection of advanced BC models to propagate these tumors is required to get a better understanding of sensitivity and resistance to therapeutic approaches across BC subtypes.

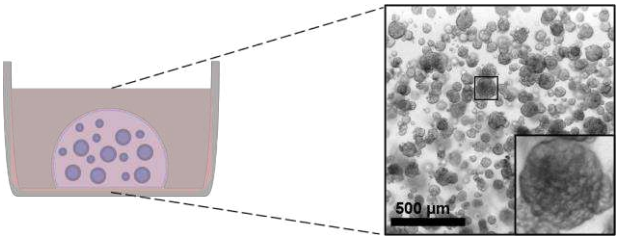

Figure 3: BC organoids. *Patient-derived BC organoids cultured in an extracellular matrix and organoid medium can mimic BC tissue and serve as a model for fundamental and advanced BC studies. Here, an example of an organoid model derived from a BC patient and grown in a 3D manner is shown. The figure was created using Microsoft® PowerPoint®.*

1.5 Drug screening and clinical application

An important step in drug discovery and development is *in vitro* drug screening. Potential drug candidates can be identified, and their effectiveness can be tested in a preclinical setting [73]. *In vitro* drug assays are often conducted in cell lines, primary cells or tissues that represent a specific disease or an organ, before continuing with time-consuming and costly *in vivo* studies [67]. Cultured cells are exposed to varying concentrations of a drug to assess its influence on cell proliferation, viability, and function, which are all important to set the optimal dosages for patients [77, 78]. Additionally, *in vitro* drug response assays can help uncover the molecular mechanism of action of compounds, including receptor binding and activation or inhibition of signaling pathways [78, 79]. Gained information contributes to drug design and the revelation of off-target effects [80, 81]. *In vitro* assays have also the potential to reduce animal testing. They serve as an ethical, low-priced, and time-efficient alternative to animal models. Upcoming therapies for BC aim for personalized treatment based on tumor characteristics [76].

As mentioned above, treatment options for BC consist of surgery, radiation, and systemic therapy [28]. Systemic therapy proposal for BC patients depends on the tumor characteristics. For instance, hormone-receptor-positive (ERα+/PR+; luminal) BC can be treated with endocrine therapy, HER2-positive BC is usually treated with targeted therapy, and

chemotherapy is especially applied in (basal) TNBC. Furthermore, BC patients with *BRCA1/2* mutations are often treated with PARP inhibitors [28].

As stated previously, tumorigenesis in BC cells can be steered by both the PI3K-AKT and the MAPK signaling pathway [21]. HER2 belongs to the ERBB family of receptor tyrosine kinases (RTKs) and acts upstream of the PI3K-AKT and MAPK signaling pathways, both resulting in cell survival and proliferation [82]. Overexpression of HER2 has been detected in several cancers, including BC [83]. Afatinib, Neratinib, Lapatinib, and Tucatinib are inhibitors that target HER2 (**Figure 4**) [84]. Importantly, Afatinib and Neratinib also target human epidermal growth factor receptor 4 (HER4) and epidermal growth factor receptor (EGFR), while Lapatinib targets EGFR but not HER4 [84]. Of these four inhibitors, Afatinib is the only drug not used for clinical BC treatments [84].

Activation of the PI3K-AKT pathway can sometimes be traced back to mutations of *PIK3CA* and *AKT1*, which can lead to abnormal protein production and increased risk of BC [22]. PI3K inhibitors Alpelisib and Pictilisib as well as AKT inhibitors Ipatasertib and Capivasertib, and mammalian target of rapamycin complex 1 (mTORC1) inhibitor Everolimus can be useful in cancer cells that are driven by the PI3K-AKT pathway [85]. Further downstream, Abemaciclib and Palbociclib target cyclin-dependent kinases (CDK) 4 and 6, which promote cell cycle progression [86]. Both drugs arrest the cell cycle in cancer cells and have been approved for the treatment of hormone-receptor positive and HER2-negative BC [86]. Tamoxifen and Fulvestrant are both drugs that target the ER and are therefore used in hormone-receptor positive BC [87]. Olaparib is a PARP inhibitor, commonly used in BC patients with *BRCA1/2* mutations [88]. Gemcitabine and Paclitaxel are both chemotherapy drugs used in BC treatment [89]. While Gemcitabine interferes with the DNA synthesis of cancer cells which leads to their death, Paclitaxel disrupts the disassembly of microtubule and inhibits cell division [90, 91]. Lastly, Selumetinib and Trametinib are mitogen-activated protein kinase kinase (MEK) inhibitors commonly used in neurofibroma, melanoma and lung cancer [92]. Yet, they are also being studied for their potential in other types of cancer including BC [93, 94].

Adjuvant systemic treatment in BC patients is applied to inhibit the spread of metastatic cells. The requirement of finding the optimal treatment plan for metastasized BC is tremendously high. Hence, the subsequent necessity would be the implementation of *in vitro* assays in clinical therapy. Yet, therapy proposals still depend on clinical studies only, and do not take into account interpatient heterogeneity in drug sensitivity. Here, I show a drug screening method that is reliable and helps determine the best drug treatment in an individualized manner.

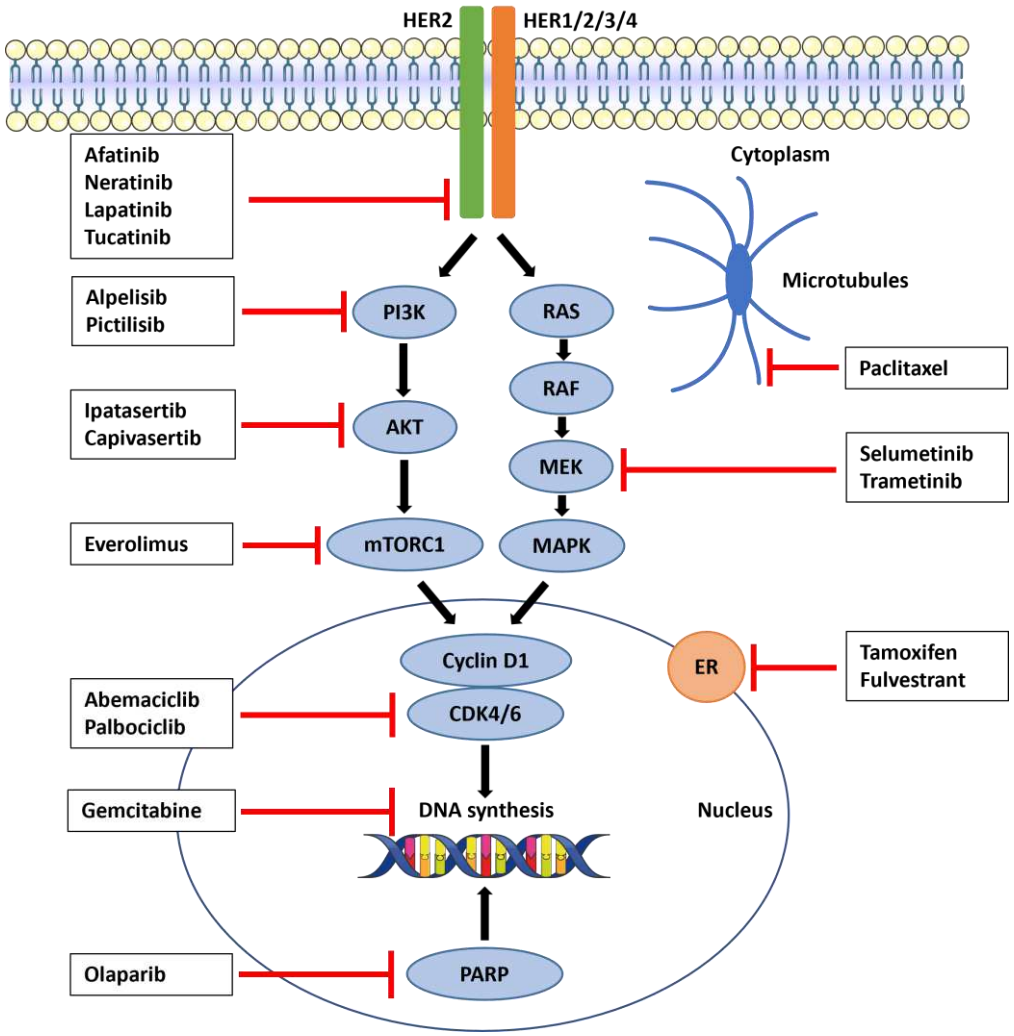

Figure 4: Signaling pathways and drug targets. *Overview of drugs used in the assays and their targets. HER2 receptor is targeted intracellularly by inhibitors Afatinib, Lapatinib, Neratinib, and Tucatinib. Alpelisib and Pictilisib inhibit PI3K, whereas Ipatasertib and Capivasertib target AKT. Everolimus targets mTORC1, while Abemaciclib and Palbociclib aim for CDK4/6 in the nucleus. BC patients with a BRCA1/2 mutation/deletion are usually treated with Olaparib, which inhibits PARP. Gemcitabine enters the cell through nucleoside transporters and is phosphorylated into Gemcitabine triphosphate, which in turn is incorporated into the DNA and results in the termination of DNA synthesis. Like Gemcitabine, Paclitaxel is a chemotherapeutical drug which stabilizes β-tubulin and leads to the blockage of depolymerization. This interrupts the mitotic spindle assembly, chromosome segregation, and mitosis. Selumetinib and Trametinib are MEK inhibitors, while Tamoxifen and Fulvestrant target the hormone receptor ERα. The figure was created using Microsoft® PowerPoint®.*

1.6 CAR-T cell therapy

Despite advances in BC treatment, BC remains the most frequent type of cancer among women [1]. Immunotherapy, which is a branch of targeted therapy, has shown promising results and mild safety concerns [95]. Genetically modified T cell therapies, that incorporate a chimeric antigen receptor (CAR) produced successful and long-lasting clinical responses in patients with hematologic malignancies [96]. CAR-T cell therapy offers new potential in the treatment of different types of cancer and involves using a patient's own T cells (autologous) for targeting cancer [97]. Isolated T cells are genetically engineered to express CARs on the T cell surface [98]. Once CAR-T cells are infused back into the patient's blood stream, these CARs recognize and bind a specific antigen on the surface of cancer cells. Consequently, the CAR-T cells become activated and release cytokines and cytotoxic compounds that result in the killing of cancer cells [97, 99].

Allogeneic CAR-T cells have made great progress in recent years, including the engineering of different generations of CAR-T cells [100]. CAR-T cell generations differ in the composition of the intracellular co-stimulatory domains. The first generation contained a CD3ζ signaling domain, which activated T cells upon binding to the target antigen [101]. Since the initial generation had a short T cell survival and low activation, the second and third generations of were introduced, to overcome these limitations. They incorporated at least one additional co-stimulatory molecule, such as cluster of differentiation 28 (CD28), 4-1BB (alias CD137), and OX-40 (alias CD134) [101, 102]. These molecules conferred greater potency, persistence, activation of CAR-T cells and lead to their enhanced proliferation and cytokine secretion, upon antigen binding [102]. Cancer cells which down-regulate the targeted antigen are not recognized by the CAR-T cells and can lead to tumor relapse. This may happen especially in heterogenic solid cancer lesions [103]. Hence, the fourth generation of CAR-T cells focuses on modulating the tumor microenvironment by the secretion of cytokines such as interleukin (IL)-12 into the targeted tissue [103]. Treatments of the fourth generation can lead to therapeutic concentrations in the targeted area while reducing systemic toxicity (on-target off-tumor activation of CAR-T cells) [103]. Quite recently, the fifth generation of CAR-T cells has been engineered, that carries a fragment of the IL-2 receptor β-chain (IL-2Rβ) and a STAT3-binding tyrosine-X-X-glutamine motif. These molecules prevented the terminal differentiation of CAR-T cells, promoting their persistence and antitumor cytotoxic effects [104].

The progress of CAR-T cell generations brings us closer to advanced immunotherapeutic approaches for cancer treatment. Nevertheless, all five generations face the same challenges in their potential to deliver adjustable cytotoxicity and flexibility against heterogeneous tumors. These limitations may lead to uncontrollable CAR-T cell proliferation and exhaustion, cytotoxic

on-target off-tumor effects, and lack of activation towards antigen-negative tumor cells [105-107].

One approach to achieve control over CAR-T function is to separate target antigen recognition from the activation of CAR-T cells by including adapter molecules (AMs) and Adapter CAR-T cells (AdCARs), as previously described by Seitz et al. [108]. AdCARs are redirected to target antigens via biotin-labeled AMs, as they combine the components of both an antigen binding and a CAR-T cell binding moiety (**Figure 5A and B**). Hence, clinically approved therapeutical antibodies can be conjugated and reshaped into AMs, which not only allows flexible redirection of AdCAR against a multiplicity of tumor-associated antigens (TAAs), but also introduces a controllable on/off-switch [108]. In recent studies, Seitz et al. and Atar et al. presented the efficiency of the AdCAR technology *in vitro* and *in vivo* by aiming at tumors with a TAAs across different cancer types [108-110]. This approach enables the universal targeting of numerous cancer types, allows adjustable modulation of AdCAR function, and addresses antigen-loss-caused immune evasion.

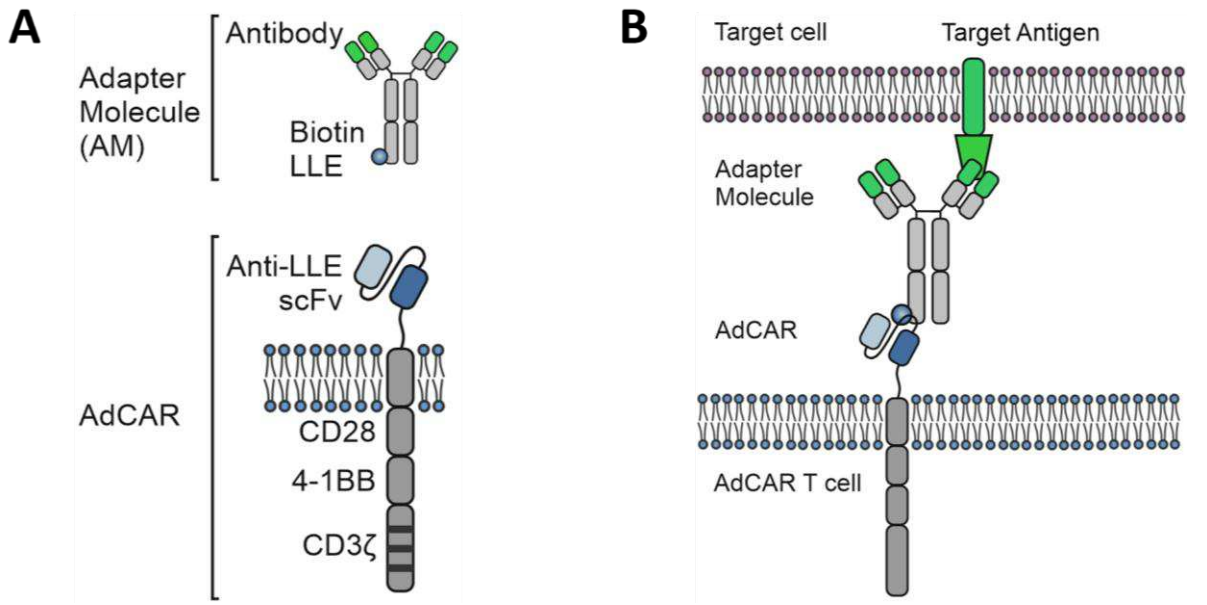

Figure 5: Adapter molecule (AM) and Adapter CAR-T cell (AdCAR). (A) *Schematic illustration of an AM and an AdCAR. The AM is a biotin-labeled antibody with a linker-label-epitope (LLE). The AdCAR consists of costimulatory molecules (e.g., CD28, 4-1BB, CD3ζ), and an anti-LLE single chain variable domain (scFv).* ***(B)*** *AdCARs are directed against the target antigen via LLE-conjugated biotinylated AMs. The figure was created using Microsoft® PowerPoint®. This figure has been previously published (9.2).*

1.7 Aim of this thesis

BC has been investigated in various models and cell types, but patient-derived metastatic BC organoids remain to be further investigated. The aim of this project was to study the impact of therapeutic compounds on BC cell lines and patient-derived metastatic organoids, to create a reliable application for drug screenings.

In the first part of the thesis, I tested varying concentrations of specific drugs, some of which are applied in clinical BC therapy, on BC cell lines to produce drug-response curves and identify sensitive cell lines.

Studies with BC organoids typically use primary tumor tissue for creating patient-derived models [71, 111, 112]. Therefore, in the second part of this study, I established organoid lines from patients with metastatic BC (metastatic breast cancer patient-derived organoids, MBC-PDO) derived from MA and MPE and cultivated them for *in vitro* experiments. To characterize the original tissue and corresponding organoid lines, paraffin-embedded samples were immunohistochemically stained, and hotspot mutation analysis of extracted DNA was performed. The goal was to use these MBC-PDOs to create a reliable application for drug screenings. 3D drug-response assays were carried out to determine the sensitivity MBC-PDOs towards inhibitors and chemotherapeutic drugs in an individualized manner.

While hematologic malignancies have been shown to be successfully treated with CAR-T cell therapy, CAR-T efficiency in battling solid tumors, such as BC, requires improvement. Lastly, the potential of utilizing MBC-PDOs for AdCAR-T cell-mediated cytotoxicity assays was therefore tested. MBC-PDOs were transduced to stably express luciferase and GFP and characterized by flow cytometry (FC). Subsequently, AdCAR-T cells in combination with adapter molecules were applied to MBC-PDOs according to their surface markers. The aim was to use MBC-PDOs as a screening platform, that can be assessed to evaluate AdCAR-T cell-based precision immunotherapy for flexible targeting of tumor-associated antigens.

All in all, once established, MBC-PDOs could serve as a tool to study the most lethal BCs and consequently help prolong patients' survival time and improve their quality of life.

2 Material and methods

Some of the following contents have been previously published (see chapter 8 and 9).

2.1 Material

2.1.1 Patient cohort

All pleural effusion (PE) and ascites samples were obtained from advanced BC patients treated at the Department of Women's Health in Tübingen after informed written consent. The study was approved by the Ethics Committee of the Eberhard Karl University of Tübingen (Ethical approval 150/2018BO2 and 288/2022BO2) and is compliant with all relevant ethical regulations regarding research involving human participants. MPEs and MAs were collected during drainage of the patients in sterile containers. For this study, MPE or MA from six patients with metastatic BC was collected. For full patient characteristics see **Table 23**.

2.1.2 Cell lines and virus

Table 1: Cell lines used for in vitro experiments and virus used for T cell transduction.

Cell line	Details	Company
L-WRN	CRL-3276; inserts: Wnt, R-spondin, Noggin	American Type Culture Collection (ATCC) (Manassas, VA, USA)
MCF-7	BC cell line (ER+/PR-/HER2-) Mutation in *PIK3CA*	American Type Culture Collection (ATCC) (Manassas, VA, USA)
SKBR3	BC cell line (ER-/PR-/HER2+) Mutation in *TP53*	American Type Culture Collection (ATCC) (Manassas, VA, USA)
MDA-MB-453	BC cell line (ER-/PR-/HER2+) Mutation in *PIK3CA* and *PTEN*	American Type Culture Collection (ATCC) (Manassas, VA, USA)
MDA-MB-468	BC cell line (ER-/PR-/HER2-) Mutation in *TP53* and *PTEN*	American Type Culture Collection (ATCC) (Manassas, VA, USA)
T47D	BC cell line (ER+/PR+/HER2-) Mutation in *TP53* and *PIK3CA*	American Type Culture Collection (ATCC) (Manassas, VA, USA)
HCC1500	BC cell line (ER+/PR+/HER2-) Mutation in *TP53* and *PIK3CA*	American Type Culture Collection (ATCC) (Manassas, VA, USA)
MDA-MB-231	BC cell line (ER-/PR-/HER2-) Mutation in *TP53* and *BRAF*	American Type Culture Collection (ATCC) (Manassas, VA, USA)

HEY	Ovarian cancer cell line Mutation in *BRAF* and *KRAS*	American Type Culture Collection (ATCC) (Manassas, VA, USA)
Lenti-X™ 293T cells	Human embryonic kidney cell line	Clontech, TaKaRa Bio Company (San Jose, California, USA) (632180)
AdCAR lentivirus	AdCAR (LLE-CAR) lentivirus	Miltenyi Biotec B.V. & Co. KG (Bergisch Gladbach, Germany)

2.1.3 Plasmids

Table 2: Plasmids used for AdCAR-T methods (generation of lentiviral vector and viral transduction of MBC-PDOs and MCF-7).

Plasmid	Details	Company	Catalog number
Packaging plasmid	Lentiviral packaging plasmid	Addgene Europe (Teddington, UK)	12259
VSV-G envelope plasmid	VSV-G envelope expressing plasmid	Addgene Europe (Teddington, UK)	631276
Lentiviral vector plasmid	Contains luciferase and GFP	Irmela Jeremias, Helmholtz Center Munich, Germany	12260

2.1.4 Cell culture media

Table 3: Commercial cell culture media.

Medium	Company	Catalog number
Advanced DMEM/F-12 (AdvDMEM)	Thermo Fisher Scientific (Waltham, MA, USA)	12634-028
Dulbecco's Modified Eagle Medium (DMEM)	Thermo Fisher Scientific (Waltham, MA, USA)	41965-039
Recovery™ Cell Culture Freezing Medium	Thermo Fisher Scientific (Waltham, MA, USA)	12648-010
Roswell Park Memorial Institute (RPMI) medium	Thermo Fisher Scientific (Waltham, MA, USA)	31870
TexMACS™ Medium	Miltenyi Biotec B.V. & Co. KG (Bergisch Gladbach, Germany)	130-097-196

Table 4: Content of cell culture media.

Medium	Content
Conditioning-DMEM	500 mL AdvDMEM+++, 10% FBS
DMEM	500 mL DMEM, 1% Pen/Strep
DMEM-FBS	500 mL DMEM, 10% FBS, 1% Pen/Strep
DMEM-selection	500 mL DMEM, 10% FBS, 500 µg/mL Geneticin, 500 µg/mL Hygromycin B
AdvDMEM +++	500 mL AdvDMEM, 1% Pen/Strep, 1x GlutaMAX™-I, 10 mM HEPES

Table 5: Content of homemade BC medium (BCM) for organoid culturing. *Composition was previously published [71, 111].*

Reagent	Concentration
AdvDMEM +++	Up to desired volume
Neuregulin 1	5 nM
FGF-7	5 ng/mL
FGF-10	20 ng/mL
EGF	5 ng/mL
A83-01	500 nM
SB202190	500 nM
Y-27632	5 µM
B-27™ Supplement	1x
Nicotinamide (NIC)	5 mM
N-Acetylcysteine (NAC)	1.25 mM
Primocin	50 µg/mL
L-WRN conditioned medium	50%

2.1.5 Buffers

Table 6: Commercial buffers

Buffer	Company	Catalog number
Dulbecco's Phosphate Buffered Saline (DPBS)	Pan Biotech GmbH (Aidenbach, Germany)	P04-36500
Rotiphorese 50x TAE (1x with dH_2O)	Carl Roth GmbH & Co. Kg (Karlsruhe, Germany)	CL86.1
CliniMACS® PBS/EDTA Buffer	Miltenyi Biotec B.V. & Co. KG (Bergisch Gladbach, Germany)	700-25

Table 7: Content of homemade buffers and solutions.

Buffer/Solution	Content
Citrate buffer, 0.05% Tween, pH 6	10 mM Tri-sodium citrate dihydrate, 0.05% Tween® 20 in H_2O
Crystal Violet	0.1% Crystal Violet, 5% Methanol, 15% dH_2O in DPBS
DPBS/ Y-27632	5 µM Y-27632 in DPBS
Red blood cell (RBC) lysis buffer 1x, sterile filtered	155 mM NH_4Cl, 10 mM $KHCO_3$, 100 µM Na_2EDTA in H_2O, pH 7.4
Tris/EDTA Buffer, 0.05% Tween, pH 9	10 mM Trizma® base, 100 nM Na_2EDTA, 0.05% Tween® 20 in dH_2O

2.1.6 Chemicals and reagents

Table 8: Chemicals and reagents used in the experiments.

Chemical/reagent	Company	Catalog number
A83-01	Tocris Bioscience (Bristol, UK)	2939
Acetic acid	Merck KGaA (Darmstadt, Germany)	1.00063
AdCAR detection reagent	Miltenyi Biotec B.V. & Co. KG (Bergisch Gladbach, Germany)	-
Agarose, SeaKem® LE Agarose	Lonza (Basel, Switzerland)	50004
Albumin fraction V from bovine serum (BSA)	Sigma-Aldrich (St. Louis, MO, USA)	1.12018.0100
Ammonium chloride (NH_4Cl)	Sigma-Aldrich (St. Louis, MO, USA)	9718
B-27™ Supplement (50x)	Thermo Fisher Scientific (Waltham, MA, USA)	17504-44
CellTiter-Glo® 3D Cell Viability Assay	Promega (Madison, WI, USA)	G9682
Crystal Violet	Merck KGaA (Darmstadt, Germany)	42555
Cultrex Reduced Growth Factor Basement Membrane Extract, Type 2, Select (BME)	Bio-techne, R&D Systems (Minneapolis, MN, USA)	3533-005-02
Cytoseal™ XYL	Thermo Fisher Scientific (Waltham, MA, USA)	8312-4
Descosept Sensitive, 1L	Dr. Schumacher (Malsfeld, Germany)	00-323DS-010
Dimethyl sulfoxide (DMSO)	PanReac Applichem (Darmstadt, Germany)	A3672
Dispase	Sigma-Aldrich (St. Louis, MO, USA)	D4693
D-Luciferin	Sigma-Aldrich (St. Louis, MO, USA)	L9504
dNTP Mix (10 mM) (deoxynucleosidtriphosphate)	Bioline, Meridian Bioscience® (London, Great Britain)	BIO-39044
Epidermal growth factor (EGF)	Peprotech (Cranbury, NJ, USA)	AF-100-15
Eosin	Merck KGaA (Darmstadt, Germany)	1.15935.0100
Ethanol 99% (denatured)	SAV Liquid Production	ETO 5000-99-1
Ethylenediaminetetraacetic acid disodium salt dihydrate (Na_2EDTA)	Sigma-Aldrich (St. Louis, MO, USA)	E5134

EZ-Link™ NHS-LC-LC-Biotin	Thermo Fisher Scientific (Waltham, MA, USA)	21343
Fetal Bovine Serum (FBS)	Thermo Fisher Scientific (Waltham, MA, USA)	10270-106
Fibroblast growth factor 10 (FGF-10)	Peprotech (Cranbury, NJ, USA)	100-26
Fibroblast growth factor 7 (FGF-7)	Peprotech (Cranbury, NJ, USA)	100-19
Ficoll (Biocoll®)	BIO&SELL GmbH (Nürnberg, Germany)	L 6115
Formaldehyde solution (37%)	Merck KGaA (Darmstadt, Germany)	1.04003.1000
GelPilot® DNA Loading Dye, 5x	QIAGEN GmbH (Hilden, Germany)	239901
GelRed Nucleic Acid Gel Stain	VWR International (Radnor, PA, USA)	U1003
Gene Ruler 100 bp (DNA ladder)	Thermo Fisher Scientific (Waltham, MA, USA)	SM0243
Geneticin (G418-BC)	Biochrom GmbH	A2912
GlutaMAX™-I (100x)	Thermo Fisher Scientific (Waltham, MA, USA)	35050-038
HEPES buffer solution (1M)	Thermo Fisher Scientific (Waltham, MA, USA)	15630-056
Histogel™ (Epredia™ HG-4000-012)	Thermo Fisher Scientific (Waltham, MA, USA)	12006679
Human serum albumin (HSA)	CSL Behring GmbH (Marburg, Germany)	4356500002
Hygromycin B	Thermo Fisher Scientific (Waltham, MA, USA)	10687-010
Interleukin 7 (IL-7, human)	Miltenyi Biotec B.V. & Co. KG (Bergisch Gladbach, Germany)	130-095-367
Interleukin 15 (IL-15, human)	Miltenyi Biotec B.V. & Co. KG (Bergisch Gladbach, Germany)	130-093-955
Lenti-X Concentrator	TaKaRa Bio Company (San Jose, California, USA)	631231
Lipofectamine 3000	Thermo Fisher Scientific (Waltham, MA, USA)	L3000001
Mayer's hemalum solution	Sigma-Aldrich (St. Louis, MO, USA)	1.09249
Methanol	Honeywell (Charlotte, NC, USA)	32213
Microbeads, anti-CD4	Miltenyi Biotec B.V. & Co. KG (Bergisch Gladbach, Germany)	130-045-101
Microbeads, anti-CD8	Miltenyi Biotec B.V. & Co. KG (Bergisch Gladbach, Germany)	130-045-201
N-Acetyl-L-Cysteine (NAC)	Sigma-Aldrich (St. Louis, MO, USA)	A9165-5G
Neuregulin-1	Peprotech (Cranbury, NJ, USA)	100-03
Nicotinamide (NIC)	Sigma-Aldrich (St. Louis, MO, USA)	NO636
Paraplast Plus	McCormick Scientific (Berkeley, MO, USA)	39502004
Penicillin-Streptomycin (Pen/Strep)	Thermo Fisher Scientific (Waltham, MA, USA)	15140-122
Phusion® High-Fidelity DNA Polymerase	New England BioLabs Inc. (Ipswich, MA, USA)	M0530L
Potassium bicarbonate ($KHCO_3$)	Sigma-Aldrich (St. Louis, MO, USA)	P9144
Primocin	InvivoGen (San Diego, CA, USA)	Ant-pm-1
SB202190	Sigma-Aldrich (St. Louis, MO, USA)	S7067
Sephadex G25 column	Cytiva Europe GmbH (Freiburg, Germany)	17085101
TransAct™	Miltenyi Biotec B.V. & Co. KG (Bergisch Gladbach, Germany)	130-128-758

Tri-sodium citrate dihydrate	Carl Roth GmbH & Co. Kg (Karlsruhe, Germany)	3580.3
Trizma® base	Sigma-Aldrich (St. Louis, MO, USA)	T1503-1KG
Trypan blue solution	Sigma-Aldrich (St. Louis, MO, USA)	T8154
TrypLE™ Express Enzyme (1X)	Thermo Fisher Scientific (Waltham, MA, USA)	12604013
Trypsin-EDTA 0.05% (1x), phenol red	Thermo Fisher Scientific (Waltham, MA, USA)	25300-054
Tween® 20	Carl Roth Gmbh & Co. Kg (Karlsruhe, Germany)	P1379-250 ML
Water, nuclease-free	Merck KGaA (Darmstadt, Germany)	95284
Xylol	VWR® (Darmstadt, Germany)	28975.325
Y-27632	Hölzel Diagnostika Handels GmbH (Köln, Germany)	TMO-T1725-50 mg
Zytomed antibody diluent	Zytomed Systems GmbH (Berlin, Germany)	ZUC025-100

2.1.7 Drugs

Table 9: Inhibitors, drugs and antibodies used for drug assays. *Inhibitors and drugs were dissolved in DMSO, antibodies Pertuzumab and Trastuzumab were delivered already dissolved in water.*

Inhibitor/Drug	Company	Catalog number
Abemaciclib	Hycultec (Beutelsbach, Germany)	HY-16297A
Afatinib	Hycultec (Beutelsbach, Germany)	HY-10261
Alpelisib	Hycultec (Beutelsbach, Germany)	HY-15244
Capivasertib	Selleckchem (Houston, TX, USA)	S8019
Everolimus	Selleckchem (Houston, TX, USA)	S1120
Fulvestrant	Hycultec (Beutelsbach, Germany)	HY-13636
Gemcitabine	Selleckchem (Houston, TX, USA)	S1714
Ipatasertib	Hycultec (Beutelsbach, Germany)	HY-15186
Lapatinib	Hycultec (Beutelsbach, Germany)	HY-50898
Neratinib	Hycultec (Beutelsbach, Germany)	HY-32721
Olaparib	Hycultec (Beutelsbach, Germany)	HY-10162
Paclitaxel	Sigma-Aldrich (St. Louis, MO, USA)	T7191
Palbociclib	Hycultec (Beutelsbach, Germany)	HY-59767
Pertuzumab	Perjeta (UKT pharmacy, Tübingen, Germany)	-
Pictilisib	Selleckchem (Houston, TX, USA)	S1065
Selumetinib	Hycultec (Beutelsbach, Germany)	HY-50706
Tamoxifen	Hycultec (Beutelsbach, Germany)	HY-13757A
Tariquidar	Selleckchem (Houston, TX, USA)	S8028
Trametinib	Hycultec (Beutelsbach, Germany)	HY-10999
Trastuzumab	Kanjinti (UKT pharmacy, Tübingen, Germany)	-
Tucatinib	Hycultec (Beutelsbach, Germany)	HY-16069

2.1.8 Antibodies

Table 10: Antibodies used for immunohistochemistry (IHC).

Antibody	Dilution	Species	Target	Company	Catalog number
Anti-TROP2 antibody (162-56.2)	1:100	Mouse	TROP2	Abcam (Cambridge, United Kingdom)	AB79976
c-erbB-2 Oncoprotein	1:500	Rabbit	HER2	Agilent Technologies (Santa Clara, CA, USA)	A048529-2
E-cadherin (CDH1) (clone NCH-38)	1:50	Mouse	CDH1	Agilent Technologies (Santa Clara, CA, USA)	M3612
Epithelial Antigen - EPCAM (clone Ber-EP4)	1:50	Mouse	EpCAM	Agilent Technologies (Santa Clara, CA, USA)	M0804
ER alpha (F-10)	1:50	Mouse	ER	Santa Cruz Biotechnology (Dallas, TX, USA)	SC-8002
GATA-3 (HG3-31)	1:200	Mouse	GATA3	Santa Cruz Biotechnology (Dallas, TX, USA)	SC-268
Ki67-antibody	1:500	Rabbit	Ki67	Abcam (Cambridge, United Kingdom)	AB16667
p53 Protein (DO-7) - Unconjugated	1:50	Mouse	p53	Agilent Technologies (Santa Clara, CA, USA)	M700129-2
Phospho-Akt (Ser473) (D9E) XP® (p-AKT)	1:200	Rabbit	p-AKT	Cell Signaling Technology (Danvers, MA, USA)	4060S
Phospho-p44/42 MAPK (Erk1/2) (Thr202/Tyr204) (D13.14.4E) XP® (p-ERK 1/2)	1:500	Rabbit	p-ERK 1/2	Cell Signaling Technology (Danvers, MA, USA)	4370S
Progesterone Receptor (Concentrate) Clone PgR 636	1:50	Mouse	PR	Agilent Technologies (Santa Clara, CA, USA)	M356929-2

Table 11: Antibodies used for FC and AdCAR-T assays.

Antibody	Dilution	Species	Target	Company	Catalog number
Biotin Antibody, REAfinity™ (REA746)	1:50	Human	Biotin	Miltenyi Biotec B.V. & Co. KG (Bergisch Gladbach, Germany)	130-111-069
CD276 Antibody, Anti-human, Biotin, REAfinity™ (REA1094)	1:50	Human	CD276	Miltenyi Biotec B.V. & Co. KG (Bergisch Gladbach, Germany)	130-118-579

Cetuximab (Erbitux®), Biotin conjugated	1:50	Human	EGFR	Merck KGaA (Darmstadt, Germany)	G0157D
EpCAM (CD326) antibody, anti-human, Biotin, REAfinity™, (REA764) Biotin conjugate)	1:50	Human	EpCAM	Miltenyi Biotec B.V. & Co. KG (Bergisch Gladbach, Germany)	130-111-114
ROR1 antibody, anti-human, Biotin, REAfinity™, (REA1051)	1:50	Human	ROR1	Miltenyi Biotec B.V. & Co. KG (Bergisch Gladbach, Germany)	130-118-018
Trastuzumab (Kanjinti®), Biotin conjugated	1:50	Human	HER2	Amgen GmbH (Rotkreuz, Switzerland); UKT pharmacy (Tübingen, Germany)	1144554A
TROP2 antibody, anti-human, Biotin, REAfinity™, (REA916)	1:50	Human	TROP2	Miltenyi Biotec B.V. & Co. KG (Bergisch Gladbach, Germany)	130-115-096

2.1.9 Primers

Table 12: Primers used in the polymerase chain reactions (PCRs). *All primers were purchased from Sigma-Aldrich. *Reverse primer for PIK3CA E542 and E545 mutation was designed based on a previous publication, to eliminate the amplification of a pseudogene [113].*

Primer	Sequence (5' → 3')	Purpose
Forward primer for *PIK3CA* mutation (exon 9 covering E542 and E545)	AATCTGGTCTTGTTGTTGGCT	PCR
Reverse primer for *PIK3CA* mutation * (exon 9 covering E542 and E545)	CCATTTTAGCACTTACCTGTGAC	PCR
Sequencing primer for *PIK3CA* mutation (exon 9 covering E542 and E545)	ATCATCTGTGAATCCAGAGGGGA	Sequencing
Forward primer for *PIK3CA* mutation (exon 20 covering H1047)	TGGTAAGAGAAGTGAGAGAGGA	PCR
Reverse primer for *PIK3CA* mutation (exon 20 covering H1047)	CAGCCTTTGTTGTGTCCACATT	PCR
Sequencing primer for *PIK3CA* mutation (exon 20 covering H1047)	CGACAGCATGCCAATCTCTTC	Sequencing
Forward primer for *AKT* mutation (exon 1 covering E17)	CTGGTTGATTGGGGAATGCT	PCR
Reverse primer for *AKT* mutation (exon 1 covering E17)	AAATCTGAATCCCGAGAGGC	PCR
Sequencing primer for *AKT* mutation (exon 1 covering E17)	TCGCTGGCCCTAAGAAACAG	Sequencing
Forward primer for *ESR1* mutation (exon 8 covering Y537 and D538)	GGGCAGCACAAAAATCAGTGT	PCR

Reverse primer for *ESR1* mutation (exon 8 covering Y537 and D538)	AAGTGGTGCATGATGAGGGT	PCR
Sequencing primer for *ESR1* mutation (exon 8 covering Y537 and D538)	GCCATGAGTTCCAGATTAGGG	Sequencing

2.1.10 Kits

Table 13: Kits used in the experiments.

Kit	Company	Catalog number	Purpose
DAB Substrate Kit	Zytomed Systems GmbH (Berlin, Germany)	DAB057	IHC staining
PCR detection Kit	abm (Richmond, BC, Canada)	G238	Mycoplasma check
QIAquick PCR Purification Kit (250)	QIAGEN GmbH (Germany)	28106	Mutation analysis
Quick-DNA/RNA Miniprep	Zymo Research Europe GmbH (Freiburg, Germany)	D7001	Mutation analysis
ZytoChem Plus HRP Polymer Kit	Zytomed Systems GmbH (Berlin, Germany)	POLHRP-100	IHC-staining

2.1.11 Devices

Table 14: Instruments and devices used in the experiments.

Device	Company	Catalog number
BD FACSCanto II	BD Biosciences (Heidelberg, Germany)	338962
Cell Counter, Bio-Rad TC20™ Automated	Bio-Rad Laboratories, Inc. (Hercules, CA, USA)	508BR10204
Cell Counting Slides for TC20™ Cell Counter, Dual Chamber	Bio-Rad Laboratories, Inc. (Hercules, CA, USA)	145-0011
Cell culture hood	Heraeus, Kendro (Hanau, Germany)	51016687
Cell strainer, Easystrainer 100 µm	Greiner Bio-One GmbH (Frickenhausen, Germany)	542000
Cell strainer, Easystrainer 40 µm	Greiner Bio-One GmbH (Frickenhausen, Germany)	542040
Cell strainer, Easystrainer small 20 µm	Greiner Bio-One GmbH (Frickenhausen, Germany)	542120
Cell strainer, PluriStrainer® 300 µm	PluriSelect Life Science (Leipzig, Germany)	43-50300-03
Cell-culture dish, CELLSTAR®, 100 mm	Greiner Bio-One GmbH (Frickenhausen, Germany)	664160
Cell-culture flask, T175	Greiner Bio-One GmbH (Frickenhausen, Germany)	660175

Cell-culture flask, T25	Greiner Bio-One GmbH (Frickenhausen, Germany)	690160
Cell-culture flask, T75	Greiner Bio-One GmbH (Frickenhausen, Germany)	658175
Cell-culture plate, 24-well	Corning Incorporated (Glendale, AZ, USA)	CLS3524
Cell-culture plate, 48-well	Corning Incorporated (Glendale, AZ, USA)	CLS3548
Cell-culture plate, 96-well	Falcon™, Thermo Fisher Scientific (Waltham, MA, USA)	353072
Cell-culture white plate, 96-well	Thermo Fisher Scientific (Waltham, MA, USA)	136102
Centrifuge, Heraeus Biofuge Pico	Heraeus (Hanau, Germany)	75003235
Centrifuge, Heraeus Multifuge 3SR	Heraeus (Hanau, Germany)	75004371
Centrifuge, Mini	Labnet (Iselin, NJ, USA)	C-1200
CoolCell LX, BioCision	Brooks Life Sciences GmbH (Griesheim, Germany)	BCS-405PK
Cryogenic storage vials	Greiner Bio-One GmbH (Frickenhausen, Germany)	3002998
Cuvette/reagent reservoir, 50 mL	Corning® Costar® (Glendale, AZ, USA)	CSL4870
Deep-well plate	Thermo Fisher Scientific (Waltham, MA, USA)	260251
DNA electrophoresis system (model B2, 0-150 V, 0-100 mA)	Owl Separation System, Inc. (Portsmouth, NH, USA)	128448
Electronic pipette Picus, 50-1000 µL	Sartorius (Goettingen, Germany)	735081
EVOS M7000 Imager	Thermo Fisher Scientific (Waltham, MA, USA)	AMF7000
FACS tubes	Greiner Holding (Kremsmünster, Austria)	352008
Filter, Minisart® Syringe 0,45 µm	Sartorius AG (Göttingen, Germany)	17598-K
SuperFrost® Plus microscope slides	R. Langenbrinck GmbH (Emmendingen, Germany)	03-0060
iBright™ CL1000 Instrument	Thermo Fisher Scientific (Waltham, MA, USA)	A32747
Incubator for cell culture	Binder (Tuttlingen, Germany)	9040-0012
Micropipettes	Eppendorf (Hamburg, Germany); Gilson Inc. (Middleton, WI, USA)	-
Microscope cover glasses	Paul Marienfeld GmbH & Co.KG (Lauda-Königshofen, Germany)	0102242
Microtome (Type HM 355S)	Microm GmbH (Walldorf, Germany)	90545C
Microwave	Robert Bosch GmbH (Gerlingen, Germany)	FFL023MW0
Multichannel pipette, 1200 µL	Eppendorf (Hamburg, Germany)	3125 000.214
Multichannel pipette, 300 µL	Eppendorf (Hamburg, Germany)	3125 000.052

PCR reaction tubes	Sarstedt AG & Co. KG (Nümbrecht, Germany)	72.737.002
Pasteur Capillary Pipettes, 230 mm	Wilhelm Ulbrich™ (Bamberg, Germany)	10230
Pipette tips, 10 µL	Biozym Scientific GmbH (Hessisch Oldendorf, Germany)	720011
Pipette tips, 1000 µL	Sarstedt AG & Co. KG (Nümbrecht, Germany)	70.3050
Pipette tips, 1000 µL, filtered	TipOne® STARLAB GmbH (Hamburg, Germany)	S1126-7810-C
Pipette tips, 200 µL	Sarstedt AG & Co. KG (Nümbrecht, Germany)	70.3030
Pipette, 10 mL, graduated 1/10 mL, sterile	Greiner Bio-One GmbH (Frickenhausen, Germany)	607160
Pipette, 25 mL, graduated 2/10 mL, sterile	Greiner Bio-One GmbH (Frickenhausen, Germany)	760160
Pipette, 5 mL, graduated 1/10 mL, sterile	Greiner Bio-One GmbH (Frickenhausen, Germany)	606160
Power supply Consort (300 V, 1000 mA)	Consort bvba (Turnhout, Belgium)	E831
Reaction tubes, 0.5 mL	Eppendorf (Hamburg, Germany)	0030121.023
Reaction tubes, 1.5 mL	Greiner Bio-One GmbH (Frickenhausen, Germany)	G.616201
Reaction tubes, 2.0 mL	Greiner Bio-One GmbH (Frickenhausen, Germany)	G.623201
Scanner, Perfection V800 Photo	Epson (Meerbusch, Germany)	B11B223401
ScanScope®	Leica biosystems (Wetzlar, Gemany)	Model: CS
Shaker, Titramax 1000, 150-1350 rpm	Heidolph Instruments GmbH & Co. KG (Schwabach, Germany)	544-12200-00-3
Stericup Quick Release-GP Sterile Vacuum Filtration System (0.22 µm)	Merck-Millipore (Burlington, MA, USA)	S2GPU05RE
Syringe, Original Perfusor, 50 mL	B. Braun Group (Melsungen, Germany)	8728844F-06
T100™ Thermal Cycler	Bio-Rad Laboratories, Inc. (Hercules, CA, USA)	621BR57740
Thermomixer Comfort	Eppendorf (Hamburg, Germany)	5355 06849
Tube, 15 mL	Greiner Bio-One GmbH (Frickenhausen, Germany)	188271-N
Tube, 50 mL	Greiner Bio-One GmbH (Frickenhausen, Germany)	227261
Vacuum aspirator	Thomas (Memmingen, Germany)	3120005
Varioskan LUX	Thermo Fisher Scientific (Waltham, MA, USA)	VLBL0TD2
Vortex	IKA®-Werke GmbH & CO. KG (Staufen, Germany)	Model: MS2
Water bath	GFL Gesellschaft für Labortechnik (Burgwedel, Deutschland)	Model: 1013

2.1.12 Softwares

Table 15: Softwares used for this thesis.

Software	Provider
Adobe Photoshop	Adobe (Dublin, Republic of Ireland)
Aperio ImageScope	Leica Biosystems (Wetzlar, Gemany)
Benchling	Benchling.com (San Francisco, CA, USA)
EndNote™ X9	Clarivate™ Analytics, EndNote™
GraphPad Prism	GraphPad Software Inc. (San Diego, CA, USA)
ImageJ 1.8.0_172	National Institutes of Health (Bethesda, MD, USA)
Invitrogen™ EVOS™ M7000 Imaging System	Thermo Fisher Scientific (Waltham, MA, USA)
Microsoft Office 365 (Excel, PowerPoint, Word)	Microsoft Corporation (Redmond, WA, USA)
SnapGene Viewer 6.0.2	GSL Biotech LLC (Chicago, IL, USA)

2.2 Cell culture methods

2.2.1 Culturing 2D cell lines

Cell lines (**Table 1**; all except CAR-T cells) were cultured in DMEM with 10% FBS (DMEM-FBS) and incubated at 37 °C and 5% CO_2. Confluent cells were passaged by washing the cells with DPBS and treating them with Trypsin-EDTA (0.05%) for 5-7 min at 37 °C. Detached cells were resuspended in DMEM-FBS to inactivate Trypsin. Cells were then used for further culturing, cryopreservation (2.2.7), and/or 2D drug assays (2.2.9).

2.2.2 Processing of pleural and ascites

MPE and MA samples were obtained from BC patients treated at the Department of Women's Health in Tübingen. Samples were centrifuged at 500 × g for 10 minutes (min) (Kendro, Multifuge 3S-R) to separate cells from fluid (**Figure 6**). Cell pellets were pooled and when necessary, red blood cells were lysed with 10 mL of RBC lysis buffer on ice for 5-10 min. Cells were diluted in DPBS and centrifuged at 500 × g for 10 min. The final cell pellet was resuspended in AdvDMEM+++. When necessary, the cell suspension was subjected to 40 µm and 100 µm cell stainers, to obtain various fractions. Thus, small cells (below 40 µm) including blood cells and fibroblasts could be eliminated. Cells on the strainers were recovered by washing the strainers with DMEM and transferring the suspension into 15 mL tubes. Fractions were pelleted and used for cryopreservation (2.2.7), culturing organoids (2.2.3), FFPE embedding (2.3.1) and for snap-freezing (2.2.6).

2.2.3 Organoid culture setup

For organoid culture setup, the desired amount of cell suspension, e.g., from fraction 40-100 µm, was mixed with Basement Membrane Extract (Type 2; BME) at a ratio of 30% cell suspension to 70% BME. Twenty µL droplets (domes) were plated out on 48-well plates and placed upside-down in an incubator (37 °C, 5% CO_2) to solidify for 30 min. BC culture medium (BCM; **Table 5**) was added to each well and renewed every 3-4 days. Empty wells received PBS to increase humidity and reduce BCM evaporation. Cells were incubated at 37 °C and 5% CO_2, and pictures were taken regularly with an EVOS M7000 microscope.

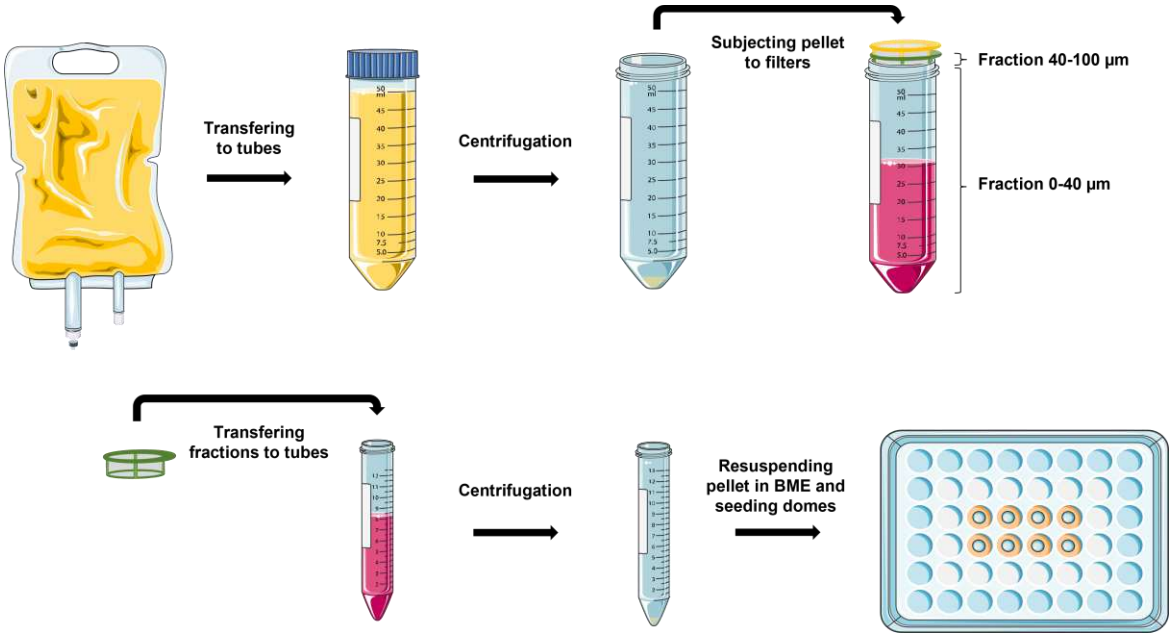

Figure 6: Processing of MA and MPE samples and organoid setup. *Samples were collected in sterile containers and transferred to tubes. Pelleted cells were subjected to strainers and desired fractions were seeded in BME droplets and cultured in BCM. The figure was created using Microsoft® PowerPoint®.*

2.2.4 Preparation of conditioned L-WRN medium

L-WRN cells (Inserts: Wnt, R-spondin, Noggin) were thawed and cultured in DMEM-FBS (without Pen/Strep) at 37 °C and 5% CO_2 for one day. The medium was exchanged with DMEM-selection (**Table 4**) in which the cells were cultured until confluency. L-WRN cells were passaged using 0.05% Trypsin-EDTA and expanded in several flasks under DMEM-FBS (without Pen/Strep), until they became overconfluent. Cells were washed and cultured in conditioning-DMEM (**Table 4**). After 24 hours (h), conditioned medium was recovered and new conditioning-DMEM was added. The recovered medium was centrifuged at 3000 × g for 5 min and the supernatant was stored at -80 °C. Every 24 h, recovering and replenishing was repeated for 12 days in total. Collected conditioned L-WRN medium was filtered through a 0.22 µm “Stericup Quick Release-GP Sterile Vacuum Filtration System” and stored in aliquots at -80 °C.

2.2.5 Passaging of organoid cultures

MBC-PDOs were passaged every 7 to 21 days, depending on organoid size and density. Organoids were recovered from the wells by resuspending the BME-droplets in ice-cold DPBS/Y-27632. The organoid suspension was centrifuged at 500 × g for 10 min and the supernatant was carefully removed. The BME-organoid pellet was enzymatically dispersed

with 1 mL of 1x TrypLE Express Enzyme at 37 °C in a water bath for 5 min. The suspension was then centrifuged at 500 × g for 10 min, and the supernatant was removed. For further culture, the desired amount of cell pellet was resuspended in AdvDMEM+++ and mixed with BME at a ratio of 30% cell suspension to 70% BME and cultured as described in 2.2.3.

2.2.6 Snap-Freeze

At least 100.000 cells in a 1.5 mL reaction tube were centrifuged for 1 min and the supernatant was removed. The vial was then snap-frozen in liquid nitrogen and stored at -80 °C until deoxyribonucleic acid (DNA) and ribonucleic acid (RNA) extraction.

2.2.7 Cryopreservation

For cryopreservation of 2D and 3D cultures, cell pellets were resuspended in Recovery™ Cell Culture Freezing Medium (Gibco) and transferred to cryovials. Cells were then slowly cooled down in CoolCell™ LX Freezing Containers (Merck) at -80 °C for at least 4 h. Frozen cryovials were transferred to liquid nitrogen tanks for long-term storage.

2.2.8 Thawing cells

10 mL DMEM-FCS (for 2D cells) or AdvDMEM+++ (for 3D cells) were prewarmed in a 15 mL tube in the 37 °C water bath. Cryovials were thawed in the water bath for 1-2 min and the cell suspensions were transferred to the prewarmed media. Cells were centrifuged at 500 × g for 10 min and used for downstream methods.

2.2.9 2D drug screening

Relative cell viability of BC cell lines in 2D were determined using Crystal Violet staining and CellTiter-Glo®. BC cell lines (**Table 1**) were trypsinized as described in 2.2.1 and resuspended in DMEM-FBS in a 50 mL tube. Cells were diluted 1:1 with Trypan Blue and counted using the Bio-Rad TC20™ Cell Counter with the according Cell Counting Slides according to manufacturer's protocol. The required cell number was resuspended in DMEM-FBS in a fresh 50 mL tube and 100 µL/well were seeded in 96-well plates using an electronic pipette. Cell number per well depended on doubling time of each cell line (**Table 16**). Technical triplicates were done for each drug – one replicate in clear plates for Crystal Violet staining and 2 replicates in white plates for CellTiter Glo® assay. Wells in the outer margin were filled with 200 µL of DPBS to increase humidity and reduce medium loss. Plates were incubated at 37 °C and 5% CO_2 overnight, until the cells attached to the bottom. The following day, drug dilution

series were prepared in triplicates in DMEM-FCS in 2-fold concentrations. The medium of 100 µL/well was not removed and 100 µL/well of the 2-fold concentrated drugs were added to the wells to reach the desired final 1-fold concentration. Drug assays were stopped once the untreated control wells of the clear plates were confluent, which took 6-7 days.

For Crystal Violet staining, all steps were performed at room temperature (RT). The content of clear plates was shaken off and 50 µL/well of 100% methanol were added using a multi-channel pipette, to fix the cells for 10 min. Afterwards, the content was shaken off, again and the plates were dried for a few minutes. 50 µL/well of 0,1% Crystal Violet were added, and the plates incubated covered in foil at RT for 3 hours. Finally, the staining was carefully removed, and plates were washed in dH_2O. Dried plates were scanned and cell intensity per well was analyzed using the "ColonyArea" plugin on ImageJ according to instructor's protocol [114].

For CellTiter-Glo Assay, the CellTiter-Glo® 3D Cell Viability Assay reagent (Promega) was used to quantify adenosine triphosphate (ATP) as a luminescent readout. First, the reagent, AdvDMEM+++ and all plates were equilibrated to RT. Second, lights were switched off and the reagent was mixed 1:1 with the same volume of AdvDMEM+++. Next, the content of the wells was shaken off and 50 µL of the reagent mixture was added to all wells using a multichannel pipette. Then, plates were covered with aluminum foil and incubated on the plate shaker for 2 min (900 rpm). After an additional 10 min-incubation, luminescence values were read by Varioskan LUX. Results of Crystal Violet stainings, as well as luminescence values were normalized to lowest drug concentration (100% cell viability).

Table 16: BC cell lines used for 2D drug assays. *BC cell lines were used in different amounts per well in 96-well-plates.*

Cell line	MCF-7	SKBR3	MDA-MB-453	MDA-MB-468	T47D	HCC1500	MDA-MB-231
Cells/well	3,000	4,000	6,000	4,000	6,000	8,000	4,000

2.2.10 3D drug screening

CellTiter-Glo® 3D Cell Viability Assay reagent was used to determine the relative cell viability of organoids. For the heat map assays, specific concentrations of drugs (**Table 9**) were applied. For the dose-dependent assays, dilution series of selected drugs were prepared in BCM using multichannel pipettes and deep-well plates. BC cell line MCF-7 (and ovarian cancer cell line HEY for the Olaparib assay) serving as control was passaged according to 2.2.1 and suspensions were stored at 4 °C until cell counting and seeding. MBC-PDOs were passaged as follows: Two BME droplets containing organoids were resuspended in 500 µL of TryplE and

incubated at 37 °C for 10 min. Afterwards, suspensions were thoroughly pipetted up and down to disrupt organoids into single cells. Cells were shortly spun down (National Labnet Co, Mini centrifuge C-1200) and the supernatant was removed entirely. Cell pellets of cell lines and MBC-PDOs were resuspended in 110 µL of AdvDMEM+++ and counted as described in the previous section (2.2.9).

To seed 1,000 cells/well, the required cell number of each line was resuspended in BME in a ratio of 30% cell suspension and 70% BME. Three µL of this suspension, containing 1000 cells, were seeded in each well of white flat-bottom 96-well plates. Plates were turned upside down and incubated at 37 °C, 5% CO_2 for 30 min. Finally, drug dilutions in BCM were added to the wells using a multichannel pipette. Margin wells were filled with DPBS.

After four days of treatment, relative cell viability was determined using CellTiter-Glo® 3D Cell Viability Assay reagent. First, the reagent, AdvDMEM+++ and all plates were equilibrated to RT. The reagent was mixed 1:1 with the same volume of AdvDMEM+++. The content of the wells was removed and 100 µL of the reagent mixture was added to all wells using a multichannel pipette. Then, plates were covered with aluminum foil and incubated on an orbital plate shaker for 15 min (900 rpm). After a 10 min resting phase, luminescence values were read using a Varioskan LUX. Assays were performed in technical triplicates. Untreated wells and 0.1% DMSO served as controls. For the heat map assay, results were normalized to viability in 0.1% DMSO, and for the drug response curves, results were normalized to the lowest drug concentration (set as 100% cell viability).

2.2.11 Isolation and transduction of T cells

Peripheral blood samples were obtained from healthy donors at the University of Children's Hospital Tübingen, and peripheral blood mononuclear cells (PBMCs) were isolated *via* Ficoll centrifugation. T cells were isolated with anti-CD4 and anti-CD8 microbeads before they were activated with TransAct™ and cultured in TexMACS™ media supplemented with 10 ng/mL IL-7 and 5 ng/mL IL-15. After 36 h, activated T cells were transduced with AdCAR (LLE-CAR) lentivirus at a multiplicity of infection (MOI) of 3. Transduced T cells were monitored for lactate and maintained at 0.5-2 × 10^6 cells/mL in IL-7/IL-15-supplemented TexMACS™ media. On day 7, CAR transduction efficiency was determined by FC using AdCAR detection reagent.

2.2.12 Freezing and thawing of AdCAR-T cells

Cultured cells were pelleted at 350 × g for 5 min and resuspended in human serum albumin (HSA) containing 10% DMSO at a cell concentration of 1-10 × 10^7 cells/mL. 1mL aliquots were frozen overnight at -80 °C and transferred to liquid nitrogen storage. To thaw cells, frozen

aliquots were quickly thawed in a 37 °C water bath, diluted in pre-warmed TexMACS™ medium without interleukins or antibiotics and spun at 350 × g for 5 min. Subsequently, T cells were resuspended in TexMACS™ medium without any supplementation in a concentration of 4 × 10^6 cells/mL and incubated for 4 h. Finally, IL-7/IL-15-supplemented TexMACS™ media was added to achieve a cell density of 1 x 10^6 cells/mL.

2.2.13 Adapter molecule conjugation

Adapter conjugation of HER2-antibody (Trastuzumab, Kanjinti®) and epidermal growth factor receptor (EGFR)-antibody (Cetuximab, Erbitux®) with biotin was carried out at 30 °C for 1 h in DPBS buffer using 5-fold molar excess of EZ-Link™ NHS-LC-LC-Biotin. Subsequently, separation of the antibody/label mix was performed on a Sephadex G25 column. Protein containing fractions were collected, measured by absorption at 280 nm and pooled. Successful conjugation was confirmed via FC on cell lines expressing the target.

2.2.14 Generation of lentiviral vector

Lentivirus carrying luciferase and GFP was produced as previously described [108]. Following lipofection with Lipofectamine 3000 of Lenti-X™ 293T cells with second-generation packaging plasmid, VSV-G envelope plasmid and transfer plasmid, lentivirus containing supernatants were concentrated and cryopreserved at -80 °C.

2.2.15 Viral transduction of MCF-7 and MBC-PDO lines

Transfer plasmids, that are based on a third-generation lentiviral vector plasmid and contain luciferase and GFP were provided by Irmela Jeremias, Helmholtz Center Munich, Germany. Lentiviral particles were generated as described above.

MCF-7 cells were seeded in a 24-well-plate to achieve 60% confluency the following day. MBC-PDO lines #03, #04, #06, and #07 were treated with TrypLE, pelleted, resuspended in AdvDMEM+++ and counted. MCF-7 cells and all MBC-PDO lines were transduced with the lentivirus at a MOI of 3. Transduction was performed in a 24-well-plate via spinoculation (600 × g, 90 min, 37 °C) in a total volume of 300 µL per line. 6 h later, 500 µL of RPMI medium were added to MCF-7, while MBC-PDO lines were recovered from the wells, pelleted, and seeded in BME droplets. MCF-7 and the MBC-PDO lines were cultured to be expanded. Subsequent transgene expression was confirmed by FC using the co-expressed GFP. Expanded cells were pelleted and filtered with a 40 µm cell strainer. The filtered fraction of 0-40 µm was sorted and enriched by bulk fluorescence activated cell sorting (FACS) at the sorting facility at UKT. The brightest GFP-signaling cells were selected for further culturing and expansion.

2.2.16 Flow cytometry (FC)

FC analysis was performed by staining 0.2 × 10^6 cells in FACS tubes. The biotinylated antibodies targeting cluster of differentiation 276 (CD276), receptor tyrosine kinase-like orphan receptor 1 (ROR1), tumor-associated calcium signal transducer 2 (TROP2), epithelial cell adhesion molecule (EpCAM), human epidermal growth factor receptor 2 (HER2) and epidermal growth factor receptor (EGFR) (**Table 11**) were used to determine antigen expression. CliniMACS® buffer containing antibodies at an equimolar concentration of 20 µg/mL was added to each sample. The cells were furthermore stained with anti-biotin and analyzed via BD FACSCanto II.

2.2.17 3D luciferase-based cytotoxicity assay

For the treatment of MBC-PDOs and MCF-7 with AdCAR-T cells, organoids were cultured 7 to 21 days. On the day before treatment, MBC-PDOs were retrieved from the BME droplets by incubating the droplets in 1 mg/mL dispase at 37 °C for 20 minutes. Tubes and pipette tips were coated with 1% BSA. The resulting droplet suspensions were diluted in 1% BSA and centrifuged at 250 × g for 10 min. The supernatant was discarded, and organoid pellets were resuspended in the required amount of Assay Medium (BCM without Nicotinamide and Y-27632). Per well, 125 µL of organoid suspensions were seeded in clear and white 96-well-plates coated with 40 µL BME-advDMEM (in a ratio of 50% BME and 50% AdvDMEM+++).

AdCAR-T cells were thawed the day before treatment and pelleted (10 min, 350 × g). Cells were cultured in TexMACS™ medium lacking cytokines and including 10% FBS at 37 °C for 4 h. Cells were then diluted to a concentration of 1 × 10^6 cells/mL with TexMACS™ supplemented with IL-7 (10 ng/mL), IL-15 (5 ng/mL), penicillin (100 units/mL)/ streptomycin (100 µg/mL) and cultured at 37 °C until the following day.

On the day of treatment, MBC-PDO cells were counted by the addition of TrypLE to one well per line. Organoids dispersed into single cells at 37 °C for 10 min and were subsequently pelleted and resuspended in 100 µL of AdvDMEM+++. MBC-PDO and AdCAR-T cells were counted using the Bio-Rad TC20™ Automated Cell Counter according to manufacturer's protocol.

Of note, in CAR-T related assays, CAR-T cells are referred to as effector cells and cancer cells are referred to as target cells. Assays are carried out in various effector:target (E:T) ratios. Diluted in Assay Medium, 25 µL of AdCAR-T cells (various E:T ratios), 25 µL of biotinylated antibodies (80 ng/mL) and 25 µL D-Luciferin (2 ng/µL) were added to the wells, reaching a total volume of 200 µL. Wells of clear plates received Assay Medium instead of D-Luciferin; also, control wells received Assay Medium as a replacement for AdCAR-T cells and/or

biotinylated antibodies. Readouts were conducted after 24 h, 48 h and 72 h by measuring the luminescence (white plates) with a Varioskan LUX and capturing brightfield (BF) and fluorescence (FL) images (clear plates) of MCF-7 organoids and MBC-PDOs. Assays were performed in multiple replicates, and results were normalized to untreated controls.

2.3 Immunohistochemistry

2.3.1 Fixation and FFPE-embedding of tissue and organoids

For the fixation of tissue and primary cells from MPE and MA, samples were fixed in 5-10 mL of 4% formaldehyde. The following day, the 4% formaldehyde was renewed. The next day, formaldehyde was replaced with 5-10 mL of 70% ethanol. Samples were always stored at 4 °C until they were embedded.

For the fixation of organoids, wells were washed with DPBS. 250 µL of 1 mg/mL dispase were added per well and BME domes were lightly scraped with the pipette tip. The plate was incubated at 37 °C for 15-20 min. The BME-dispase mixture was then resuspended with 1% BSA (in DPBS) and transferred to a 15 mL tube coated with 2 mL of 1% BSA. For subsequent steps, tubes and pipette tips were coated with 1% BSA. The suspension was centrifuged at 250 × g for 10 min (Kendro, Multifuge 3S-R) and the supernatant was removed. The organoid pellet was resuspended with 3.7% formaldehyde and the suspension was carefully transferred into a 1.5 mL tube. Organoids were incubated in formaldehyde for 30 min at RT before they were centrifuged at 250 × g for 3 min (National Labnet Co, Mini centrifuge C-1200) and washed with DPBS. Ethanol was added stepwise to fixed organoids, until a final concentration of 70% was reached. Samples were stored at 4 °C until they were embedded in paraffin.

For embedding organoids in paraffin to generate formalin-fixed paraffin-embedded (FFPE) samples, the ethanol supernatant of fixed samples was removed. With a 1% BSA-coated tip, 80 µL of prewarmed histogel (65 °C) were added to cells and organoids in the tube, which was incubated thermocycler at 65 °C for 30 seconds. A 100 µL pipette tip was cut and placed on parafilm to be used as a mold in which the tube content was transferred to. The resulting samples were stored at -20 °C until the histogel was solidified. The histogel cylinder was put into a plastic cassette and dehydrated at RT as shown in **Table 17**. Prewarmed paraffin (65 °C) was added to another mold in which the histogel cylinder containing the sample was placed into and stored at -20 °C for 15 min. FFPE blocks were stored at RT until 2.5 µm sections were cut with a microtome and stored at 4 °C.

Table 17: Solution and incubation time of fixed samples for FFPE embedding.

Solution	Incubation time
70% ethanol	1 h
70% ethanol	1 h
96% ethanol	1 h
96% ethanol	1 h
100% ethanol	1 h
100% ethanol	16 h
100% xylol	1 h
100% xylol	1 h

2.3.2 H&E staining

To stain FFPE sections with hemalum/hematoxylin and eosin (H&E), 2.5 µm thick sections were cut with a microtome before they were shortly fixed in 100% ethanol and washed with water. Afterwards, samples were stained according to **Table 18**. Mayer's hemalum was a ready-to-use solution, while eosin was dissolved in water (1% eosin Y-solution in approx. 200 mL of dH_2O with 3 drops of acetic acid). Finally, samples were mounted with Cytoseal™ XYL.

Table 18: H&E staining protocol.

Solution	Incubation time
Mayer's hemalum solution	1 min
Warm tap water	30-60 sec
Eosin solution	5 sec
Tap water	3 sec
70% ethanol	3 sec
96% ethanol	3 sec
100% ethanol	3 sec
100% ethanol	3 sec
100% ethanol	30 sec
100% xylol	5 sec
100% xylol	Wash until grease is gone

2.3.3 Immunohistochemistry (IHC) staining

FFPE sections (2.5 µm) were deparaffinized according to **Table 19**. For antigen retrieval, the slides were put either in Citrate buffer or Tris/EDTA buffer (**Table 7**) for 10 min at 90-94 °C, using a microwave. After the buffer cooled down to RT, the slides were placed into dH_2O. For IHC staining, the ZytoChem HRP-Kit and DAB Kit were used according to manufacturer's protocol. Primary antibodies were diluted with Zytomed antibody diluent as listed in **Table 10**.

The counterstain was done by dipping the slides into 1:10 diluted Mayer's hemalum for 10 sec and subsequently into dH_2O. Finally, the slides were dehydrated as listed in **Table 20** and fixed with Cytoseal™ XYL and a coverslip. Slides were captured with ScanScope or EVOS M7000 microscope and images were processed with Aperio ImageScope, Image J and Photoshop.

Table 19: Deparaffinization of FFPE sections.

Solution	Incubation time
100% xylol	10 min
100% xylol	10 min
100% xylol	10 min
100% ethanol	3 min
100% ethanol	3 min
96% ethanol	3 min
96% ethanol	3 min
75% ethanol	3 min
75% ethanol	5 min
dH_2O	5 min

Table 20: Dehydration of slides after IHC staining.

Solution	Incubation time
70% ethanol	10 seconds
70% ethanol	1 min
96% ethanol	10 seconds
96% ethanol	1 min
100% ethanol	10 seconds
100% ethanol	1 min
100% xylol	10 seconds
100% xylol	1 min

2.4 Mutation Analysis

2.4.1 DNA and RNA extraction

Snap-frozen cells (2.2.6) were used for DNA and RNA extraction. Nucleic acids were extracted using the Quick-DNA/RNA miniprep kit (Zymo Research) according to manufacturer's protocol. DNA and RNA concentration was determined using a Varioskan LUX.

2.4.2 Polymerase chain reaction

Six different hotspot regions were investigated for mutation analysis. Primers were designed using NCBI and Benchling (**Table 12**). The reverse primer for *PIK3CA* E542 and E545 mutation

was designed based on a previous publication, to eliminate the amplification of a pseudogene [113]. Polymerase chain reaction (PCR) was performed by preparing 20 µL reactions with 1x Phusion HF buffer, 200 µM dNTPs, 0.5 µM of forward and reverse primer (**Table 12**), 40 ng of template DNA, 0.4 units Phusion DNA polymerase and nuclease-free water up to 20 µL. PCR tubes were placed in the thermocycler and PCR was run with parameters listed in **Table 21**.

PCR products were analyzed via Agarose-gel electrophoresis. 1% agarose-gel in 1x Tris-acetate-EDTA (TAE) buffer was prepared by boiling the suspension in the microwave. Gel red was added for a final concentration of 0.01% before the gel was poured into the tray. The gel solidified at RT for 30 min and was put in a chamber filled with 1x TAE buffer. 2 µL of PCR product mixed with 1 µL of loading dye were loaded in each well of the gel. 2 µL of DNA ladder were loaded in one well per gel. Agarose-gel electrophoresis was run at 90 V for 60-80 min. Finally, the gel was captured with iBright (Thermo Fisher). PCR products were purified using the QIAquick PCR Purification Kit according to manufacturer's instructions.

Table 21: Thermocycler parameters for the amplification of hotspot regions.

	Step	Temperature	Time
	Initial Denaturation	98 °C	60 sec
34 cycles	Denaturation	98 °C	10 sec
	Annealing	62 °C	30 sec
	Elongation	72 °C	60 sec
	Final elongation	72 °C	10 min
	Hold	4 °C	Infinity

2.4.3 Sequencing

For Sanger sequencing by Eurofins Genomics Germany GmbH, 10 µL containing 2.5 ng/µL of the purified PCR product and 2.5 µM of the according sequencing primer (**Table 12**) were prepared. Results were analyzed and aligned using Benchling and SnapGene Viewer.

3 Results

3.1 Dose-dependent drug response of BC cell lines in 2D

2D BC cell lines are established cell lines derived from, amongst others, pleural effusions of metastatic BC patients [52, 53]. They are widely used in research due to their multiple benefits. These include the convenient and reproducible application of BC cell lines in basic research, drug screenings, biomarker identification and even cancer immunology. Cultured in multi-well-plates, BC cell lines can be used in high-throughput drug screening methods [59]. This way multiple compounds or conditions can be analyzed, and promising drug candidates can be identified and tested in preclinical and clinical studies.

As stated previously, the characteristics of BC influence prognosis and therapy proposals. The approach of systemic therapy involves endocrine therapy for hormone receptor-positive BC, targeted therapy for HER2-positive BC, and chemotherapy especially for TNBC [28]. Since MCF-7, T47D and HCC1500 are ERα-positive, they are often used in hormonal studies [60, 61, 115]. SKBR3 and MDA-MB-453, on the other hand, are HER2-positive and are a commonly used model to study HER2-targeted therapies [62, 63, 116]. The TNBC cell lines MDA-MB-468 and MDA-MB-231 are frequently used to investigate the biology of TNBC and its responsiveness to certain drugs, especially chemotherapy [64, 117].

Not only the receptor status determines therapy proposal for BC, but also specific genetic mutations. For instance, *PIK3CA* mutated BC cells could be more sensitive towards treatments targeting the PI3K pathway [27]. Genes that are frequently mutated in BC include *TP53*, *PIK3CA, AKT1*, and *PTEN*. Mutations in tumor suppressor genes *TP53* and *PTEN* are associated with a higher risk of BC, and have been detected in various BC cell lines (**Table 22**) [16-18]. As mentioned before, tumorigenesis in BC cells can be promoted by PI3K-AKT and the MAPK signaling pathway [21]. Mutations of genes encoding key proteins of these pathways can cause pathway activation. The proto-oncogene *PIK3CA* is one of the most mutated genes in BC [24]. *PIK3CA* mutations can lead to abnormal protein production and to proliferation of cancer cells [22]. The BC cell lines MCF-7, MDA-MB-453, and T47D carry a *PIK3CA* mutation (**Table 22**). Mutations of the proto-oncogene *BRAF*, which encodes BRAF (v-Raf murine sarcoma viral oncogene homolog B1), could result in the activation of the MAPK signaling pathway, and serve as a biomarker in TNBC [118]. MDA-MB-231, for one, is a TNBC cell line and carries such a mutation (**Table 22**).

Table 22: Receptor status and mutations of BC cell lines used in 2D drug response assays. *Receptor statuses were retrieved from American Type Culture Collection [119] and from a previous publication [120]. Mutations were retrieved from several sources [121-123]*

BC cell line	Receptor status			Mutation			
	ERα	PR	HER2	*BRAF*	*PIK3CA*	*PTEN*	*TP53*
MCF-7	+	-	-		+		
SKBR3	-	-	+				+
MDA-MB-453	-	-	+		+	+	
MDA-MB-468	-	-	-			+	+
T47D	+	+	-		+		+
HCC1500	+	+	-				
MDA-MB-231	-	-	-	+			+

To assess the sensitivity of various BC cell lines towards specific drugs (**Figure 7**), dose-dependent drug assays were carried out as described in 2.2.9. BC cell lines (**Table 1**) with different receptor status and mutations (**Table 22**) were used to determine sensitive and non-sensitive lines. Relative cell viability of BC cell lines was determined using Crystal Violet staining (1 technical replicate per drug) and CellTiter-Glo® (2 technical replicates per drug). During cell death, adherent cells detach from the plates. This effect can be quantified for drug treatment of cells with methods such as Crystal Violet staining. While Crystal Violet staining dyes DNA and proteins and was applied to determine the intensity of cells still attached to the wells, the CellTiter-Glo® 3D Cell Viability Assay reagent was used to quantify ATP as a luminescent readout of viable cells (**Figure 8**). In both methods, results were normalized to the lowest drug concentration (100% cell viability).

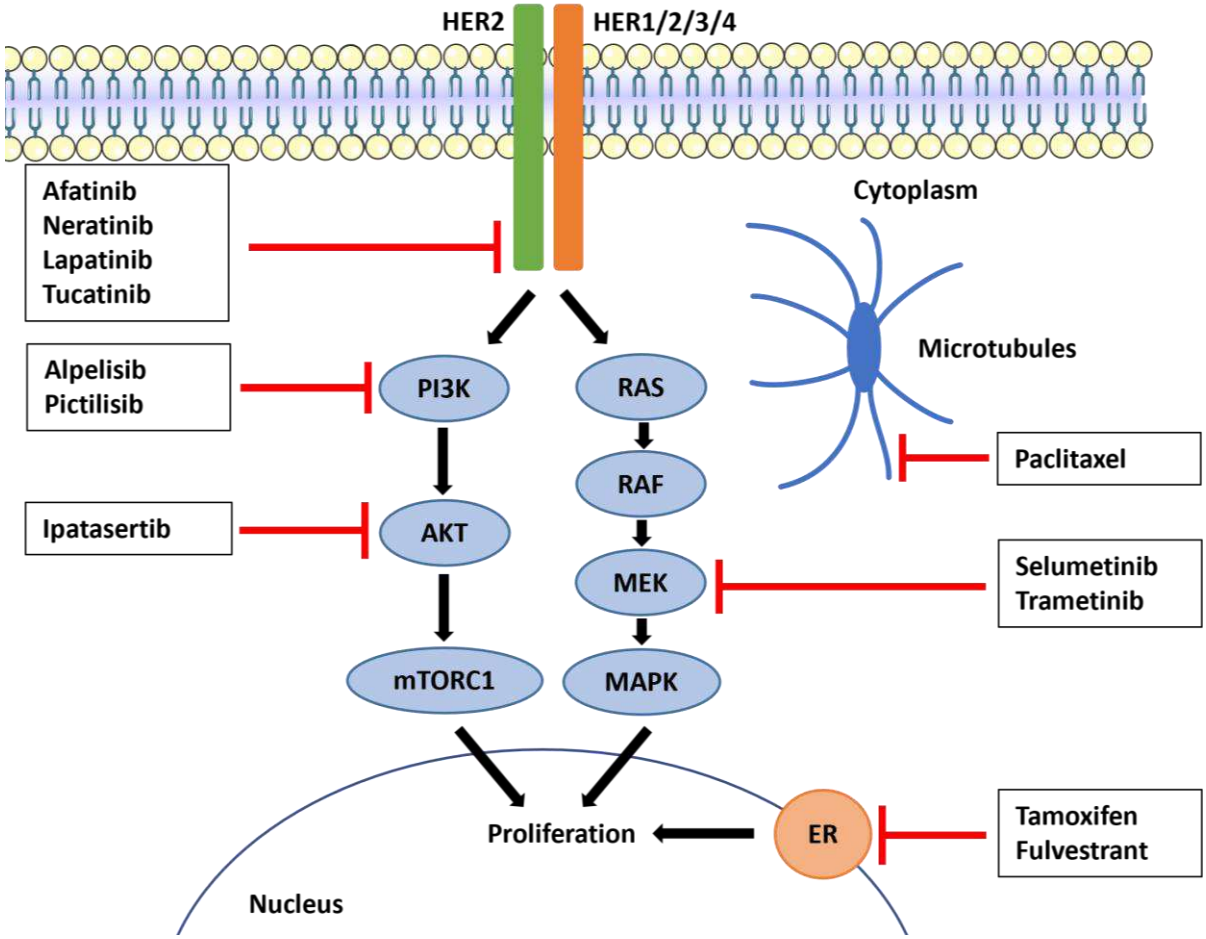

Figure 7: Drug targets of 2D drug assays. *Afatinib, Neratinib, Lapatinib, and Tucatinib target the HER2 receptor intracellularly. Alpelisib and Pictilisib aim for PI3K, while Ipatasertib targets AKT. Selumetinib and Trametinib inhibit MEK, whereas Tamoxifen and Fulvestrant aim for ER. Paclitaxel binds and stabilizes β-tubulin, which results in the blockage of depolymerization. The figure was created using Microsoft® PowerPoint®.*

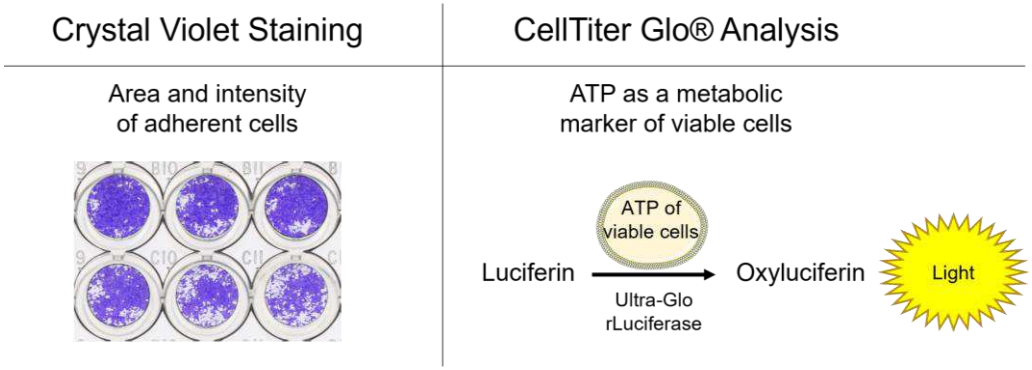

Figure 8: Crystal Violet staining versus CellTiter Glo®. *Crystal Violet staining was applied to determine the area and intensity of cells still attached to the wells, while the CellTiter-Glo® 3D Cell Viability Assay reagent (Promega) was used to quantify ATP of viable cells as a luminescent readout. The figure was created using Microsoft® PowerPoint®.*

Figure 9 demonstrates an example of a Crystal Violet staining and two CellTiter Glo® assays of BC cell lines treated with a serial dilution of MEK inhibitor Selumetinib for 6 days. The Crystal Violet intensity in the control wells (0 µM Selumetinib) and the lowest concentration (0.031 µM Selumetinib) were comparable for all cell lines, as the cell confluency reached almost 100% in both conditions. Same observations were made in the luminescence based CellTiter Glo® assays (not shown here). With increasing drug concentrations, cell proliferation was gradually more inhibited, and the area and intensity of attached cells decreased for each BC cell line. Importantly, inhibition of cell proliferation correlated with drug sensitivity. Hence, the lower the drug concentration was at which the proliferation of BC cell lines was decreased, the more sensitive the BC cell line was towards Selumetinib. As the intensity of Crystal Violet staining indicated cell viability, values were plotted in a graph and compared with the CellTiter Glo® Assay (**Figure 9**). As expected, both approaches produced almost identical cell viability curves. Hence, the values of each BC line were put together and plotted as mean values of triplicates (n=3, error bars shown in the last graph).

The “half maximal inhibitory concentration” (IC50) value defines the concentration of a compound at which 50% cell viability is measured. Thus, low IC50 values indicate sensitive cells lines. In this example, BC cell line MDA-MB-231 showed the lowest IC50 concentration of 1.570 µM, whereas all the other cell lines did not react as sensitively. Since MDA-MB-231 carries a *BRAF* mutation, it is expected to have an activated MAPK signaling pathway. Hence, Selumetinib targeting MEK as a key protein of this pathway led to downregulation of cell survival and proliferation of MDA-MB-231. MDA-MB-453 and MDA-MB-468 reached IC50 values of 9.286 µM and 8.694 µM, respectively, while MCF-7, SKBR3, T47D, and HCC1500 showed relative cell viability of above 50% even at high Selumetinib concentrations.

To further investigate if Crystal Violet staining and CellTiter Glo® Assay generated comparable response curves for other drug applications, both methods were applied for each drug of **Figure 7**. As both methods produced highly comparable response curves, technical triplicates were unified in one response curve plot per drug for which the error bars were removed for better visibility (**Figure 10**, **Figure 11**, **Figure 12**). The same plots were illustrated with error bars in **Supplementary Figure 1**, **Supplementary Figure 2**, and **Supplementary Figure 3**. Furthermore, IC50 values of each component and BC cell line were presented in a heat map (**Figure 13**).

Like Selumetinib, HER2 inhibitors Afatinib, Neratinib, Lapatinib, and Tucatinib were applied as dilution series on BC cell lines (**Figure 10**). In all four treatments, SKBR3 cells reacted most sensitively with low IC50 values (**Figure 13**), followed by MDA-MB-453, as both lines are HER2-positive. In terms of Afatinib and Neratinib treatment, MDA-MB-468 also responded sensitively, since both drugs not only target HER2, but also HER4 and EGFR. Lapatinib inhibits

HER2 and EGFR, resulting in some sensitivity of MDA-MB-468. These results indicate that MDA-MB-468 likely expresses and depends on EGFR, and that inhibitors such as Afatinib, that have multiple molecular targets, can be beneficial for treating BC cells regardless of their HER2 status.

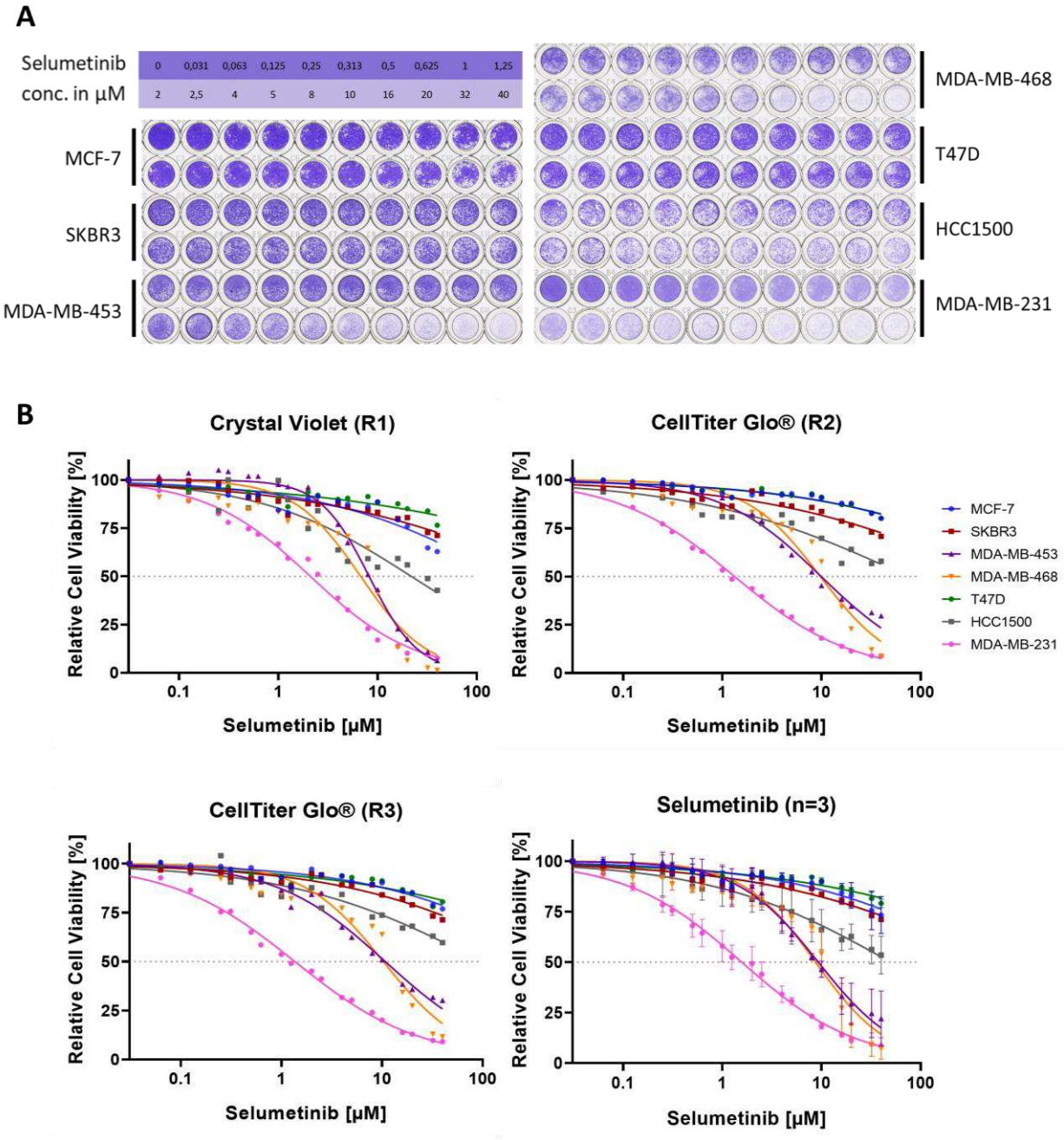

Figure 9: Example of a Crystal Violet staining and CellTiter Glo® assay. (A) *2D cell lines were treated with dilution series of Selumetinib and visualized in Crystal Violet stainings.* ***(B)*** *Drug-response curves of BC cell lines treated with Selumetinib are shown. For each drug, one replicate (R1) was done in clear plates and stained with Crystal Violet, and two replicates (R2 and R3) were carried out in white plates and cell viability was assessed with CellTiter Glo® 3D. Error bars representing standard deviation (SD) of three independent experiments (n=3) were visualized in the last graph.*

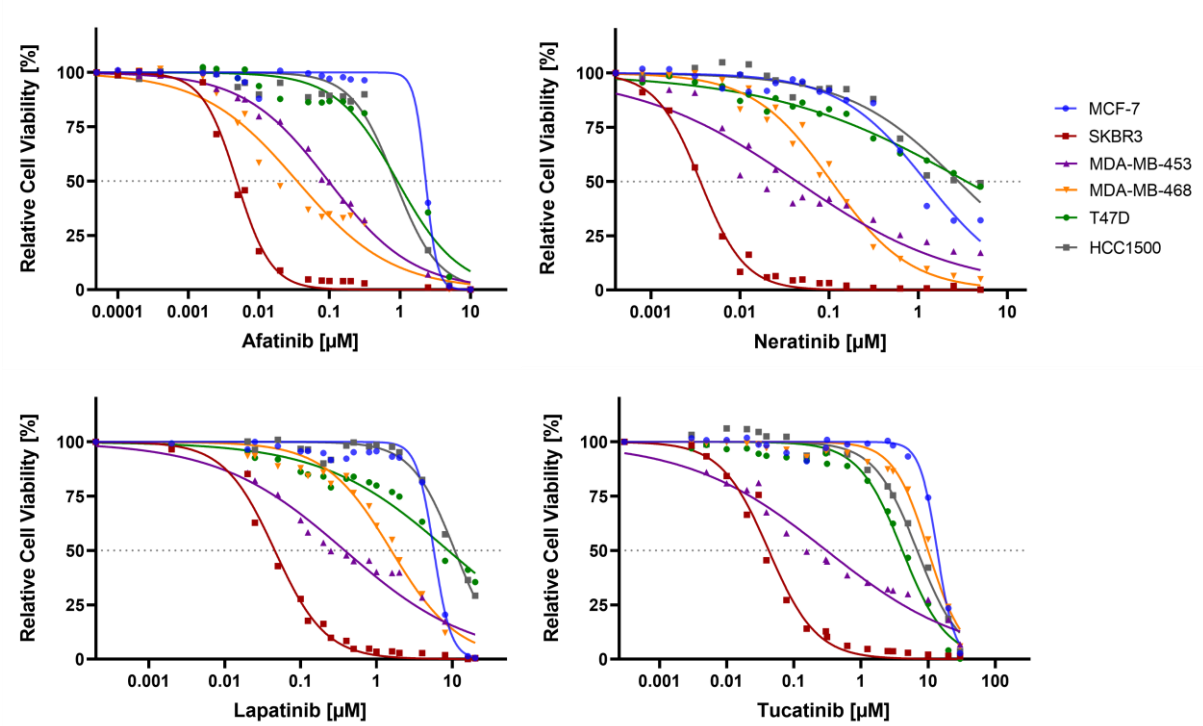

Figure 10: 2D drug response curves of HER2 inhibitors Afatinib Neratinib, Lapatinib, and Tucatinib. *2D BC cell lines were treated with dilution series of HER2 inhibitors. For each drug, one replicate was done in clear plates and stained with Crystal Violet, and two replicates were carried out in white plates and cell viability was assessed with CellTiter Glo® 3D. Error bars representing SD of three independent experiments were removed for better presentation.*

Alpelisib and Pictilisib are inhibitors that target PI3K. Ipatasertib acts downstream by targeting AKT. As shown in **Table 22**, MCF-7, MDA-MB-453, and T47D carry a mutation in *PIK3CA*, which can lead to a hyperactivation of the PI3K-AKT pathway and result in a sensitivity of BC cells towards these drugs. **Figure 11** demonstrates the drug response curves of BC cell lines treated with Alpelisib, Pictilisib, and Ipatasertib. In all three treatments, MCF-7 responded most sensitively, with IC50 values of 0.130 µM, 0.057 µM, and 0.191 µM, respectively (**Figure 13**). The BC cell lines MDA-MB-468 and MDA-MB-231 responded the least sensitively, indicating that they do not depend on PI3K or AKT activation for cell survival and proliferation. The treatment with Paclitaxel, which is a chemotherapy medication, resulted in BC cell lines responding similarly to each other.

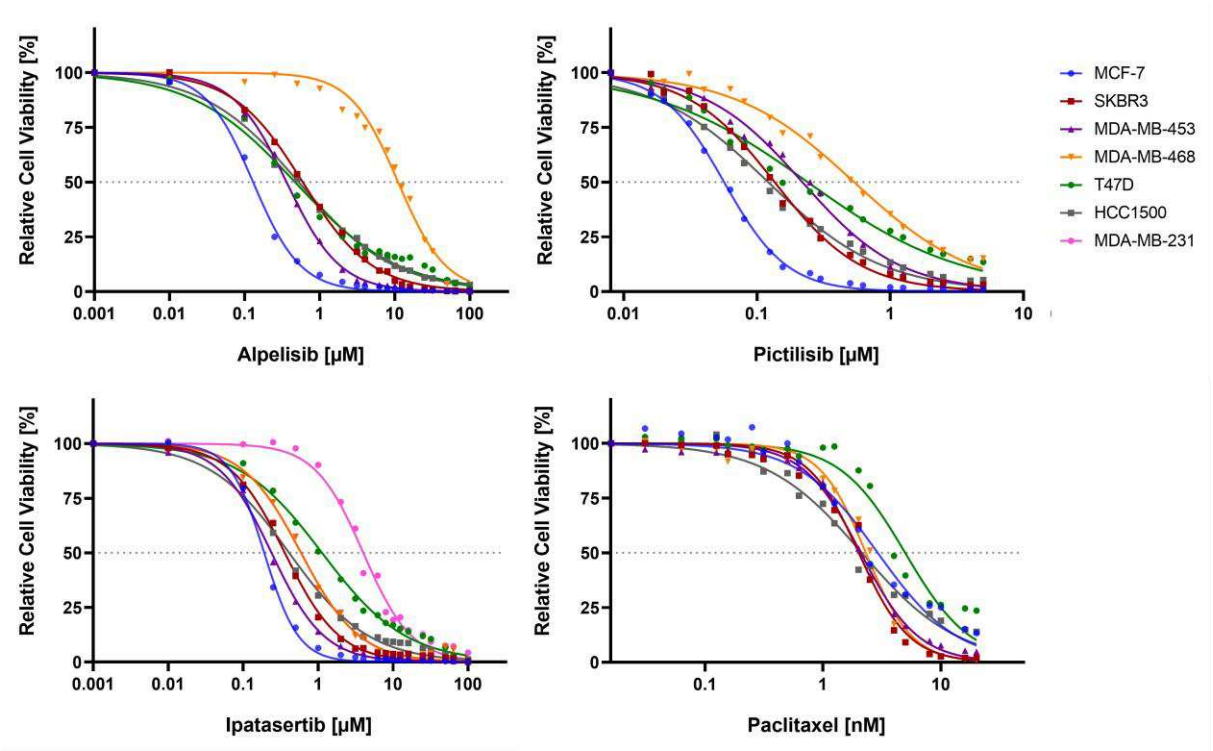

Figure 11: 2D drug response curves of PI3K inhibitors Alpelisib and Pictilisib, as well as AKT inhibitor Ipatasertib and chemotherapeutic drug Paclitaxel. *2D BC cell lines were treated with dilution series of drugs. For each drug, one replicate was done in clear plates and stained with Crystal Violet, and two replicates were carried out in white plates and cell viability was assessed with CellTiter Glo® 3D. Error bars representing SD of three independent experiments were removed for better presentation.*

Figure 12 presents the response curves of BC cell lines treated with the MEK inhibitors Selumetinib and Trametinib. Although MEK inhibitors are not typically used in BC treatment, they could offer a strategy to target BC cells that have an oncogenic activation of the MAPK signaling pathway. As previously mentioned, MDA-MB-231 is known to carry a *BRAF* mutation leading to the activation of the MAPK signaling pathway. Hence, Selumetinib and Trametinib targeting MEK resulted in low relative cell viability of MDA-MB-231 with IC50 values of 1.570 µM and 5.466 nM, respectively. Surprisingly, MDA-MB-453 and MDA-MB-468 also responded towards the MEK inhibitors with some sensitivity, indicating that their cell proliferation depended on active MEK to some extent.

The endocrine therapy drugs Tamoxifen and Fulvestrant, which target ERα, reduced the cell viability of all three ERα-positive BC cell lines MCF-7, T47D, and HCC1500, while the ERα-negative lines were relatively resistant towards both drugs (**Figure 12**). Regarding Fulvestrant treatment, the IC50 values (**Figure 13**) do not capture the full picture, as T47D and HCC1500 did not reach 50% cell viability. Yet, the drug response curves of **Figure 12** demonstrate that

there is a reduction of cell viability of ERα-positive BC cell lines as compared to the ERα-negative lines.

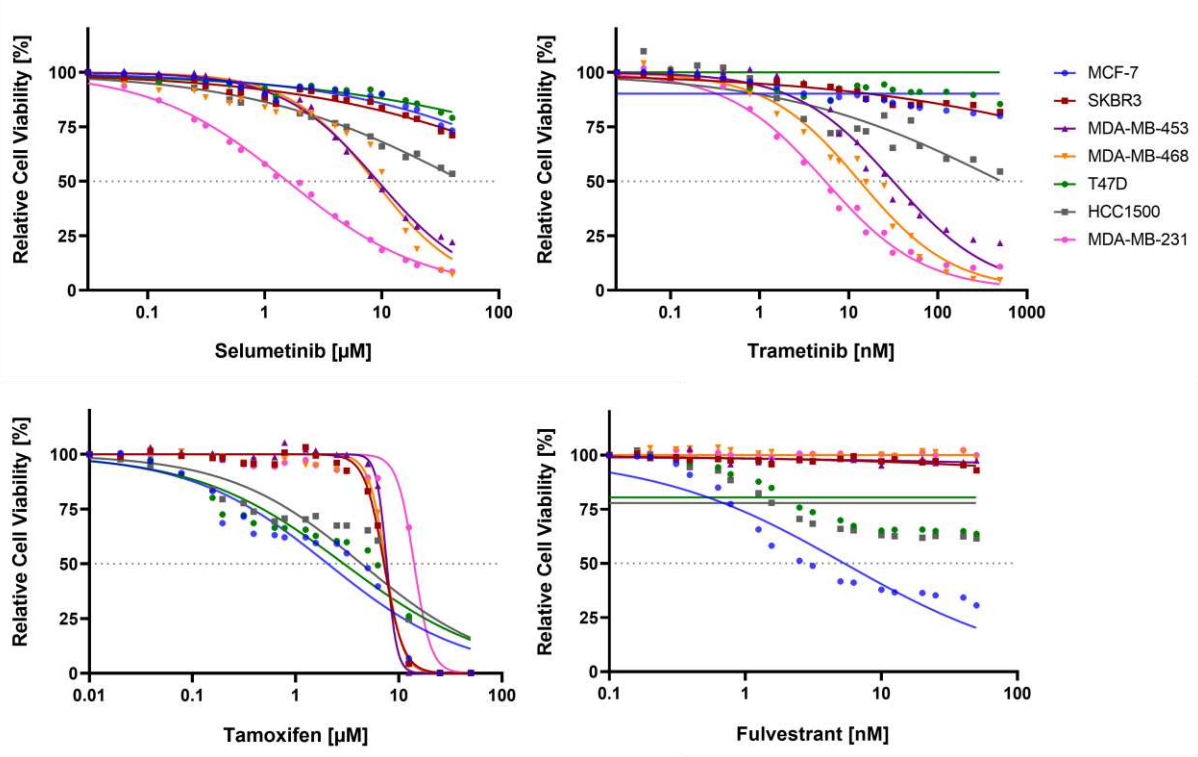

Figure 12: 2D drug response curves of MEK inhibitors Selumetinib and Trametinib, as well as ERα inhibitors Tamoxifen and Fulvestrant. *2D BC cell lines were treated with dilution series of HER2 inhibitors. For each drug, one replicate was done in clear plates and stained with Crystal Violet, and two replicates were carried out in white plates and cell viability was assessed with CellTiter Glo® 3D. Error bars representing SD of three independent experiments were removed for better presentation.*

	MCF-7	SKBR3	MDA-MB-453	MDA-MB-468	T47D	HCC1500	MDA-MB-231
Afatinib [µM]	2.317	0.005	0.097	0.035	0.919	0.849	Not tested
Neratinib [µM]	1.232	0.004	0.044	0.106	3.491	2.837	Not tested
Lapatinib [µM]	5.693	0.046	0.381	1.566	8.811	10.760	Not tested
Tucatinib [µM]	13.650	0.042	0.307	9.997	4.140	6.877	Not tested
Alpelisib [µM]	0.130	0.594	0.362	11.080	0.470	0.525	Not tested
Pictilisib [µM]	0.057	0.136	0.219	0.536	0.240	0.121	Not tested
Ipatasertib [µM]	0.191	0.359	0.239	0.591	1.127	0.411	4.004
Paclitaxel [nM]	2.912	2.010	2.088	2.307	4.971	2.134	Not tested
Selumetinib [µM]	Not reached	Not reached	9.286	8.694	Not reached	Not reached	1.570
Trametinib [nM]	Not reached	Not reached	31.590	13.330	Not reached	Not reached	5.466
Tamoxifen [µM]	2.046	7.175	7.632	7.448	2.928	4.344	14.060
Fulvestrant [nM]	5.333	Not reached	Not reached	Not reached	Not reached	Not reached	Not reached

Resistant
Sensitive

Figure 13: Heat map of IC50 values from 2D drug screenings. *Values were determined by Graphpad Prism. Red fields indicate sensitive response, while blue fields present less-responding lines.*

In conclusion, 2D BC cell lines offer a great platform for testing various drugs and produce drug-response curves. Yet, they also have their limits, as they do not capture the complex heterogeneity of BC tumors. Therefore, these results need to be validated in more complex models, such as 3D organoids.

3.2 Establishment, characterization, and drug screening of MBC-PDOs

Some of the following contents and data have been previously published (see chapter 8 and 9.1). Published figures and tables are labeled accordingly.

Onder, C.E., T.J. Ziegler, R. Becker, S.Y. Brucker, A.D. Hartkopf, T. Engler, and A. Koch, Advancing Cancer Therapy Predictions with Patient-Derived Organoid Models of Metastatic Breast Cancer. Cancers (Basel), 2023. 15(14).

3.2.1 Establishing a biobank of MBC-PDOs from MPE and MA

The aim was to generate suitable 3D models that represent metastasized BC. For this approach, MPE and MA samples were obtained from patients with metastasized BC, who were treated in the women's clinic at the hospital of the University of Tübingen (**Table 23**).

Table 23: List of BC patient data from whom the MBC-PDO lines were established. *All patients were female aged between 52 and 79. Abbreviations: ILC (invasive lobular carcinoma), NST (no special type). This table has been previously published (9.1).*

MBC-PDO	#02	#03	#04	#05	#06	#07
Primary tumor	ILC (1993)	NST (2008)	NST (2009)	ILC (2013)	NST (2019)	NST (2019)
Therapy of primary tumor	No adjuvant drug therapy	Trastuzumab; Aromasin; Carboplatin; Taxol; Avastin (until 2019)	FEC + Docetaxel; Tamoxifen (until 2013)	Not known	Epirubicin/Cyclophosphamide (aborted)	Doxorubicin
Metastasis	Uterus and peritoneal metastasis (2010)	Hepatic and pleural metastasis (2019)	Lymph nodes (2017) Hepatic metastasis (2021)	Peritoneal metastasis (2021) Osseus, ovarian and hepatic metastasis (2021)	Hepatic and osseus metastasis (2020) Pulmonary and medullary metastasis (2021)	Cutaneous, lymphogenic and osseus metastasis (2020-2021)
Therapy of Metastasis	Letrozole; Carboplatin + Taxol; Letrozole (until 2019)	Avastin	Ribociclib + Letrozole; Palbociclib + Letrozole	See "follow-up therapy"	Letrozole + Goserelin + Abemaciclib	Paclitaxel; Eribulin; Abemaciclib + Letrozole
Therapy prior to drainage	Palbociclib + Anastrozole (2019)	Avastin; Nab-Paclitaxel; Eribulin (2020)	Abemaciclib + Fulvestrant (2020-2021)	See "follow-up therapy"	Paclitaxel (2021)	Capecitabin (2021)
Drainage	Ascites (2020)	Pleura (2021)	Pleura (2021)	Ascites (2021)	Pleura (2021)	Pleura (2021)
Follow-up therapy	None, patient deceased	Palbociclib + Letrozole; Vinorelbine + Trastuzumab + Pertuzumab	Everolimus + Aromasin; Doxorubicin	Nab-Paclitaxel + Trastuzumab + Pertuzumab; Fulvestrant + Trastuzumab + Pertuzumab; Abemaciclib + Trastuzumab + Fulvestrant	None, patient deceased	Carboplatin + Olaparib; Olaparib
Additional information	-	Hepatic and pleural metastasis (2019): NST infiltration, *PIK3CA* H1047R mutation	-	Mamma Biopsy (2021): *PIK3CA* E545K mutation	-	NST (2019): *BRCA1/2* deletion, *AKT1* E17K mutation

Primary cells were microscopically analyzed to detect different cell types and to select the appropriate cell strainer sizes. Samples were processed as described in 2.2.2 and **Figure 6**. Isolated metastatic BC cells were seeded in BME droplets and cultured as MBC-PDOs in BCM (**Table 5**). **Figure 14A** presents MBC-PDO #07 as an example of an established organoid line, which has been cultured for at least 10 passages. Importantly, the morphology of the organoids, which had a rough structure, was maintained even in high passage (P) numbers. Multiple organoid lines with various morphologies were established successfully (**Figure 14B**). Morphologies included grape-like structures, dense and massive organoids, as well as organoids with smooth or rough surfaces. In the next step, the suitability of MBC-PDOs as a model for BC was analyzed.

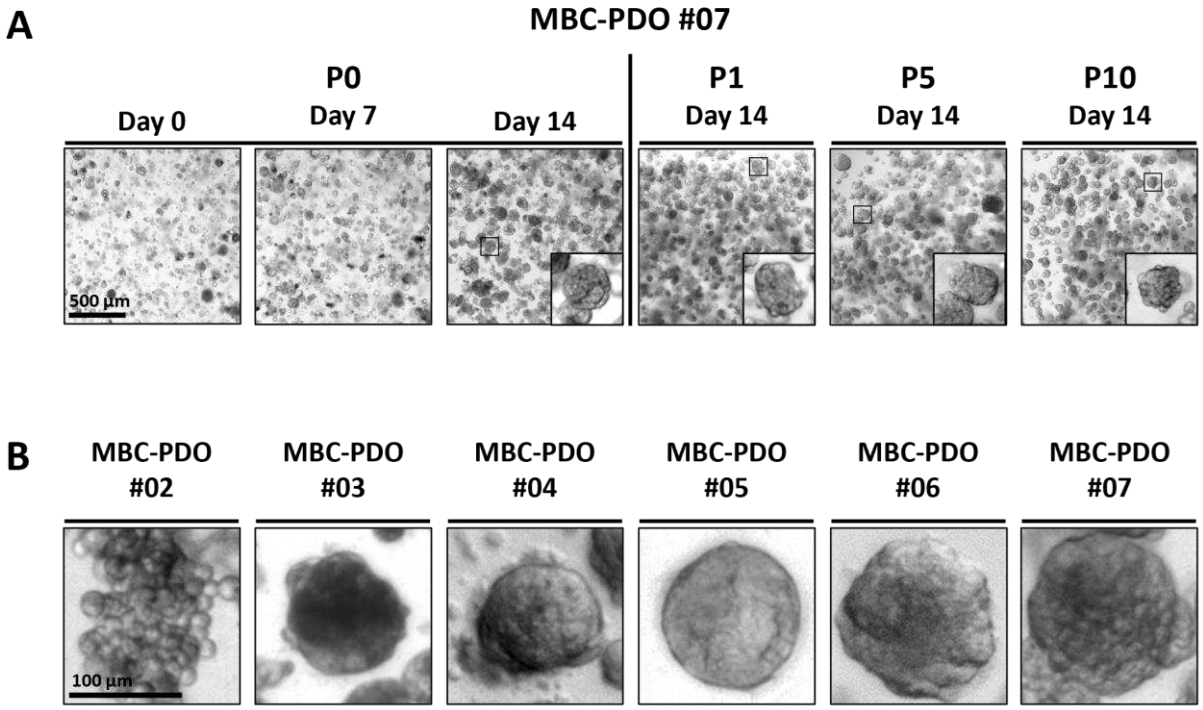

Figure 14: Establishment of a biobank of BC organoids derived from MPE and MA. (A) *Brightfield (BF) images of MBC-PDO #07 in P0, P1, P5, and P10. Throughout the culturing period, the morphology (rough surface) was preserved. Scale bar: 500 µm.* ***(B)*** *BF images of MBC-PDO lines displaying different morphologies. MBC-PDO #02 (first image) has a grape-like phenotype and presents an ILC sample. MBC-PDO lines #03-#07 illustrate NST samples with dense, smooth, and rough phenotypes. Scale bar: 100 µm. This figure has been previously published (9.1).*

3.2.2 Immunohistochemical characterization of MBC-PDOs

The type of therapy patients receive depends on the receptor status of the BC, which is also an indicator for the prognosis. While hormone receptor (ERα and PR)-positive BC can be treated with endocrine therapy, TNBC is associated with a poorer prognosis since it lacks

hormone receptors and has restricted therapy options. HER2-positive tumors, on the other hand, can be targeted with inhibitors and antibodies.

Based on histological characteristics and receptor status, BC is classified into specific subtypes. Here, the suitability of organoid lines as a model for metastasized BC were studied. This included the investigation of preservation of histological characteristics through H&E and IHC staining of pleural samples and the corresponding organoid lines. The patient of MBC-PDO #03 was diagnosed with primary NST in 2008 and developed MPE and liver metastasis over a decade later. Hence, the expression patterns and phenotype of the liver metastasis, MPE, and the corresponding organoids of MBC-PDO #03 were compared. Organoid samples were taken at P3 for paraffin embedding (2.3.1) and H&E/IHC staining (2.3.2; 2.3.3), to validate the expression patterns (**Figure 15**). According to the H&E staining, the histology of liver metastasis, pleural cells, and organoids is comparable. The IHC staining of nuclear hormone receptors ERα and PR revealed positive signals in all three samples, while membranous HER2 expression was observed in some of the cells. According to pathology, HER2 expression had an IHC score of 2+ (out of 3+), which was represented in the organoids. All in all, MBC-PDO #03 organoids preserved the expression patterns of the pleural cells and even carried the same receptor status as the corresponding liver metastasis.

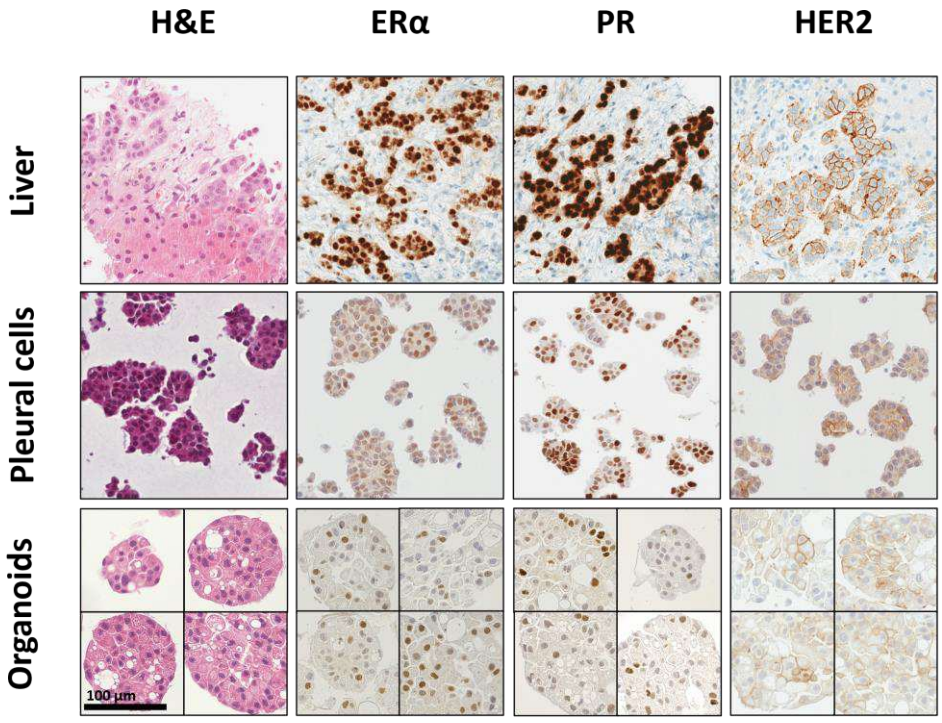

Figure 15: Histological characterization of pleural BC cells and organoids derived from MPE. *Histology (H&E staining) and receptor status of metastasized liver tissue, pleural cells, and organoids (P3) of MBC-PDO #03 are shown. Organoids consist exclusively of epithelial cells, while tissues often show tumor epithelium ringed by mesenchymal cells. The receptor status is maintained in the organoids. Scale bar: 100 µm. This figure has been previously published (9.1).*

All pleural cells and corresponding MBC-PDO lines were characterized *via* H&E and IHC staining in the same manner as MBC-PDO #03 (**Supplementary Figure 4**). Like MPE cells, initial cells from MA (MBC-PDO #02 and #05) are also referred to as pleural cells, in this study. As observed in the BC statistics, hormone receptor-positive/HER2-negative BC samples was the dominating receptor status in our collection (**Table 24**). Only MBC-PDO #02 and #03 revealed some weak expressions of HER2. In most cases, MBC-PDOs preserved the expression profile of the original cells; with MBC-PDO #04 being the exception: while pleural cells revealed low levels of ERα expression, there was no ERα signal detected in the organoids.

Additionally, the expressions of epithelial cell adhesion molecule (EpCAM), GATA3, tumor suppressor protein p53, and cadherin-1 (CDH1) were analyzed (**Supplementary Figure 5**). The expression patterns were summarized in **Table 24**. All lines, both pleural cells and organoids, demonstrated positive signals of EpCAM, GATA3, and p53 (the latter one indicates a mutation in the *TP53* gene), demonstrating, that MBC-PDO lines could preserve the expression pattern of their respective origins. The only exception was observed in MBC-PDO #05, which showed almost no signal of EpCAM. As stated, the most common subtypes are IDC (NST) and ILC [124]. Both types are represented in our MBC-PDO models (**Table 23**); while NST samples MBC-PDO #03, #04, #06, #07 were CDH1-positive, ILC samples MBC-PDO #02 and #05 did not express CDH1 **(Table 24**). Overall, the receptor status of MBC-PDOs correlated with the expression profile of their metastatic counterpart, indicating that MBC-PDOs could serve as a suitable *in vitro* model for metastatic BC.

Table 24: Results of IHC staining signals of pleural cells and/or organoid lines. *Abbreviations neg.: negative signal, pos.: positive signal. Parts of this table have been previously published (9.1).*

MBC-PDO		ERα	PR	HER2	EpCAM	GATA3	p53	CDH1
#02	**Organoids**	neg.	neg.	neg.*	pos.	pos.	pos.	neg.
#03	**Pleural cells**	pos.	pos.	neg.*	pos.	pos.	pos.	pos.
	Organoids	pos.	pos.	neg.*	pos.	pos.	pos.	pos.
#04	**Pleural cells**	pos.*	neg.	neg.	pos.	pos.*	pos.	pos.
	Organoids	neg.	neg.	neg.	pos.	pos.*	pos.	pos.
#05	**Pleural cells**	pos.	pos.	neg.	neg.*	pos.*	pos.	neg.
#06	**Pleural cells**	pos.*	neg.	neg.	pos.	pos.*	pos.	pos.
	Organoids	pos.*	neg.	neg.	pos.	pos.	pos.	pos.
#07	**Pleural cells**	pos.*	neg.	neg.	pos.	pos.*	pos.	pos.
	Organoids	pos.*	neg.	neg.	pos.	pos.*	pos.	pos.

* Samples showed a weak positivity

Finally, Ki67 (marker of proliferation) staining was performed to compare the proliferation of organoids. In MBC-PDO #02, #03, and #04, under 20% of cells were Ki67-positive, while MBC-

PDO #06 and #07 revealed a high number (more than 80%) of Ki67-positive cells (**Figure 16A, B**). These results are in accordance with the proliferation rate observed in the MBC-PDO lines.

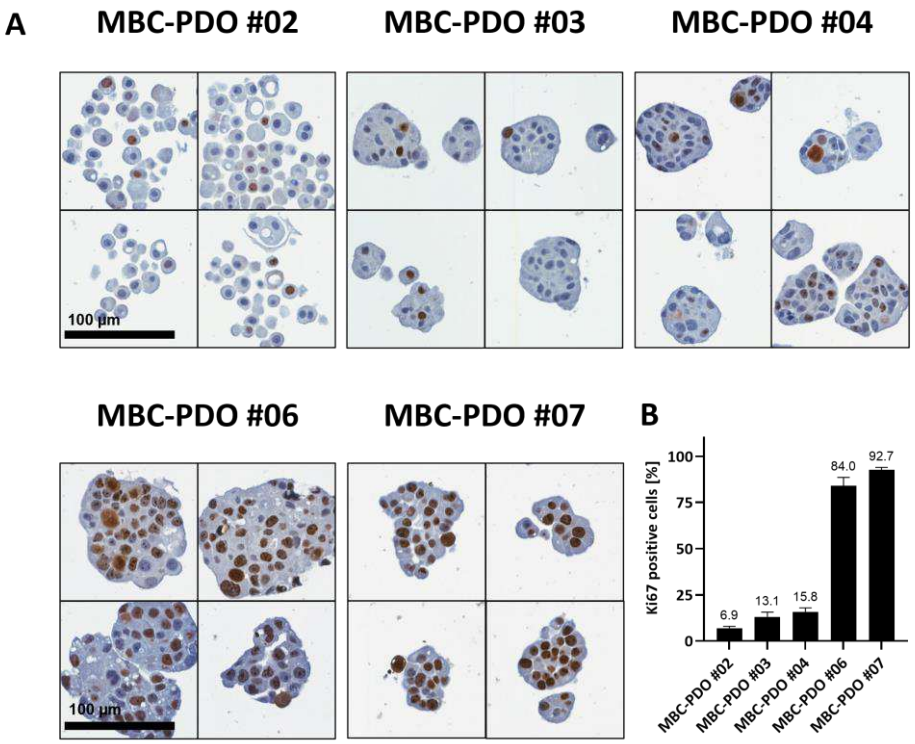

Figure 16: IHC staining of proliferation marker Ki67 in MBC-PDO lines. (A) *IHC stainings of FFPE samples from organoids. Brown nuclei indicate positivity. Scale bar: 100 µm.* ***(B)*** *Quantification of Ki67-positive cells. Ki67 stainings were quantified by counting 150 cells of each organoid line and determining the ratio of Ki67-positive cells. Quantification was done in triplicates. This figure has been previously published (9.1).*

3.2.3 Hotspot mutation analysis of MBC-PDOs

In BC, tumorigenesis can be driven by PI3K and MAPK signaling cascade [21]. Sometimes, the activation of these pathways can be traced back to mutations of key genes. Just like in any other cancer, there are genetic mutations that frequently occur in BC. For instance, mutations in the genes *PIK3CA* and *AKT1* can cause abnormal protein production and have been associated with the hyperactivation of downstream processes leading to cell proliferation and survival. This in turn can cause an increased risk of BC [22, 23]. *PIK3CA* mutations are one of the most frequent mutations in BC and have been encountered in more than 30% of BC cases [22, 25]. The most common hotspot mutations in *PIK3CA* are in E542 (11%), E545 (17%), and H1047 (35%) [24]. In approx. 6% of all BC cases, a missense mutation of *AKT1* leading to the exchange of glutamic acid (E) to lysine (K) in amino acid position 17 has been detected [26].

In this study, DNA of pleural cells and MBC-PDOs were extracted and amplified as described above using different forward and reverse primers for each hotspot position (2.4.1 and 2.4.2) (**Figure 17**). Subsequently, amplified DNA samples were checked *via* Agarose gel-electrophoresis and purified, before they were sent in for Sanger sequencing by Eurofins Genomics Germany GmbH (2.4.3). Results were analyzed via SnapGene Viewer and presented in **Table 25**.

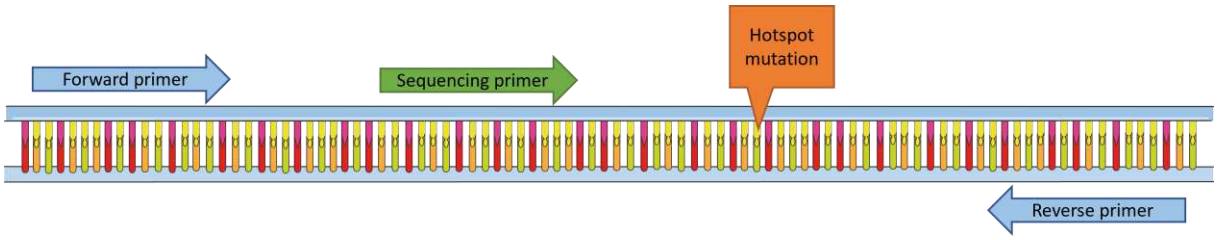

Figure 17: Schematic presentation of primers used for PCR and Sanger sequencing for the detection of hotspot mutations. *Forward and reverse primers covered the area for the sequencing primer and the hotspot mutation. The figure was created using Microsoft® PowerPoint®.*

According to clinical diagnostic reports, the hepatic metastasis of MBC-PDO #03 was analyzed and revealed a heterozygous *PIK3CA* H1047R mutation. In this study, the same mutation was detected in the MPE (pleural cells) and the corresponding organoid model MBC-PDO #03 (**Table 25**, **Figure 18**), indicating a possible hepatic origin of MBC-PDO #03. None of the samples revealed a mutation of *PIK3CA* E542, while a heterozygous E545K hotspot mutation was detected in pleural cells and/or organoids of MBC-PDO #05 and #06. The patient of MBC-PDO #05 also had the same mutation in the primary tumor biopsy (**Table 23**). The homozygous hotspot mutation of *AKT1* (E17K) was found in the pleural cells of MBC-PDO #04 and #07, as well as in the organoids (**Table 25**, **Figure 18**). The corresponding patient of MBC-PDO #07 carried the same mutation in her primary NST (**Table 23**). Due to insufficient sample material, the MAs of MBC-PDO #02 and #05 were not tested. Of note, MBC-PDO #02 was the only line with no hotspot mutation observed. Overall, five out of six MBC-PDOs carried a hotspot mutation in *PIK3CA* or *AKT1*. The hotspot mutation analysis revealed that organoids were able to retain mutations from initial MPE cells and in some cases also from the primary tumor. Also, derived organoids represent metastasized tumors, which makes them useful for downstream applications such as drug screenings.

Table 25: Mutation analysis of hotspots in AKT1 and PIK3CA. *Abbreviations WT: wild type, E: glutamic acid, K: lysine, H: histidine, R: arginine. The content of this table has been previously published (9.1).*

MBC-PDO		*AKT1*	*PIK3CA*
#02	**Organoids**	WT	WT
#03	**Pleural cells**	WT	H1047R†
	Organoids	WT	H1047R†
#04	**Pleural cells**	E17K◊	WT
	Organoids	E17K◊	WT
#05	**Organoids**	WT	E545K†
#06	**Pleural cells**	WT	E545K†
	Organoids	WT	E545K†
#07	**Pleural cells**	E17K◊	WT
	Organoids	E17K◊	WT

◊ Homozygous mutation
† Heterozygous mutation

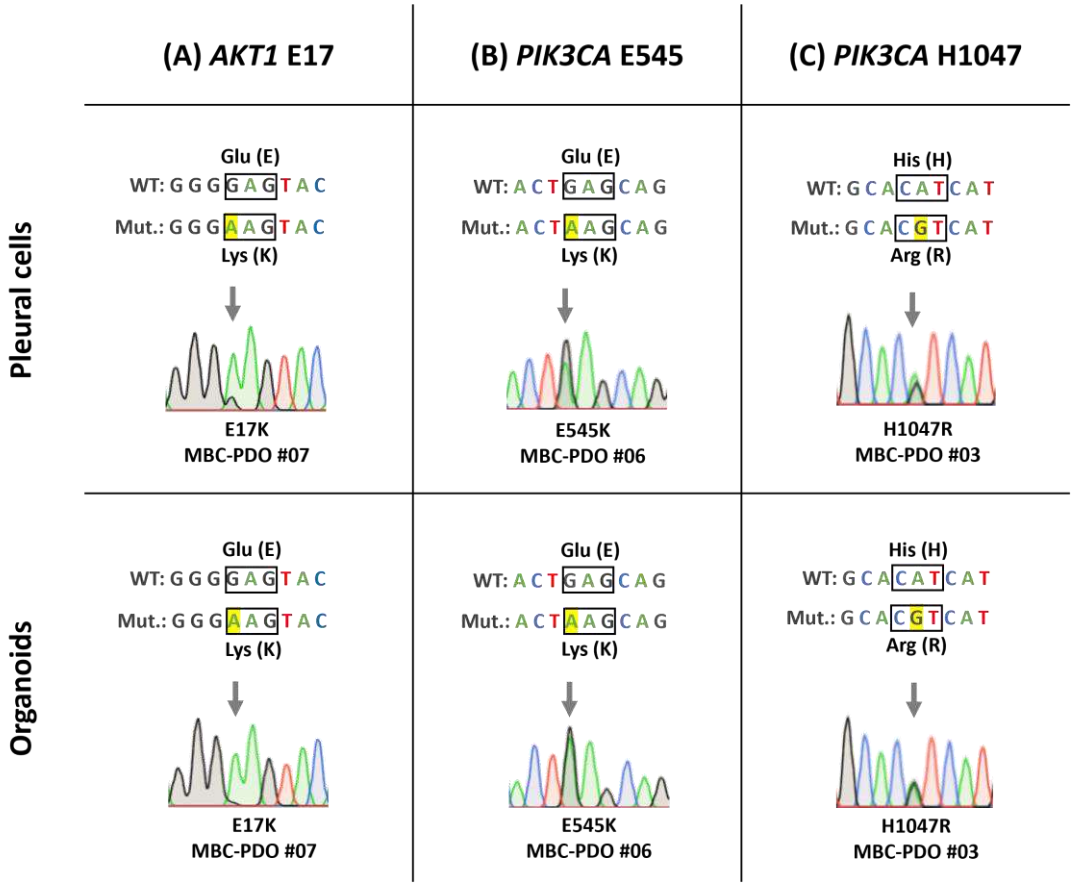

Figure 18: Examples of mutations in AKT1 and PIK3CA. *Mutation analysis of three common hotspots in AKT1 and PIK3CA genes. PCR-amplified DNA samples were sequenced by Sanger sequencing and depicted in chromatograms. Shown are wild type (WT) sequences and the sequence of mutated (Mut) samples. DNA bases are represented by the following colors: guanine (G) in black, cytosine (C) in blue, adenine (A) in green, thymine (T) in red.* ***(A)*** *Homozygous mutation of AKT1 E17K in MBC-PDO #07 pleural cells and organoids.* ***(B)*** *Heterozygous mutation of PIK3CA E545K in MBC-*

PDO #06 pleural cells and organoids. ***(C)*** *Heterozygous mutation of PIK3CA H1047R in MBC-PDO #03 pleural cells and organoids. This figure has been previously published (9.1).*

3.2.4 Drug response assays of MBC-PDOs

In the early stages of research*, in vitro* drug assays are frequently carried out in cell lines and primary cells, before continuing with *in vivo* studies [67]. Cultured cells are treated with compounds to assess their impact on cell proliferation, viability, and function [77, 78]. Systemic treatment of BC is applied to prevent the spread of metastatic cells. Once metastasized, the need of making the best treatment plan for BC is extremely high. Future therapies of BC aim for precision medicine based on tumor characteristics [76]. Consequently, the subsequent requirement would be the integration of *in vitro* drug screenings in clinical therapy. However, therapy decisions depend on clinical studies only, and do not consider interpatient heterogeneity in drug sensitivity. Here, the aim was to assess the potential of MBC-PDOs as *in vitro* models in drug-response assays and to create a reliable application for 3D drug screenings to determine the sensitivity of MBC-PDOs towards the drugs in an individualized manner.

Systemic therapy plans for BC patients depend on the tumor characteristics. For instance, hormone receptor-positive and HER2-negative BC can be treated with CDK4/6 inhibitors. HER2-positive BC is commonly treated with targeted therapy, while chemotherapy is used in TNBC. Also, BC patients with a *BRCA1/2* mutation are often treated with PARP inhibitors [28]. Of note, the HER2 inhibitors Afatinib and Neratinib also target HER4 and EGFR, while Lapatinib targets EGFR but not HER4, and Tucatinib inhibits HER2, only [84].

In the following assays, drugs that target the HER signaling pathway, CDK4/6, PARPs, DNA synthesis, and β-tubulin were selected (**Figure 19A**). Organoid lines were treated with various drugs at specific concentrations to generate a heat map (**Figure 19B**). Serial dilution assays of Lapatinib, Alpelisib, Capivasertib, Abemaciclib, and Paclitaxel were conducted to generate dose–response curves and calculate the IC50 values (**Figure 19C**).

MBC-PDO #02 has low levels of HER2 (**Table 24**) and responded well to HER2 inhibitors Afatinib, Lapatinib, and Tucatinib (**Figure 19**). As showed previously, no hotspot mutation was detected in MBC-PDO #02, which could have activated the PI3K-AKT pathway. As a result, drugs inhibiting the PI3K-AKT pathway, namely Alpelisib, Pictilisib, Ipatasertib, Capivasertib, and Everolimus, had no severe effect on cell viability. The patient of MBC-PDO #02 had previously been treated with CDK4/6 inhibitor Palbociclib prior to ascites collection. The drug screenings revealed that neither Abemaciclib nor Palbociclib affected cell viability much. Hence, resistant populations of metastasized cells likely survived the treatment. Instead, the patient of MBC-PDO #02 could have profited from a HER2 targeting therapy.

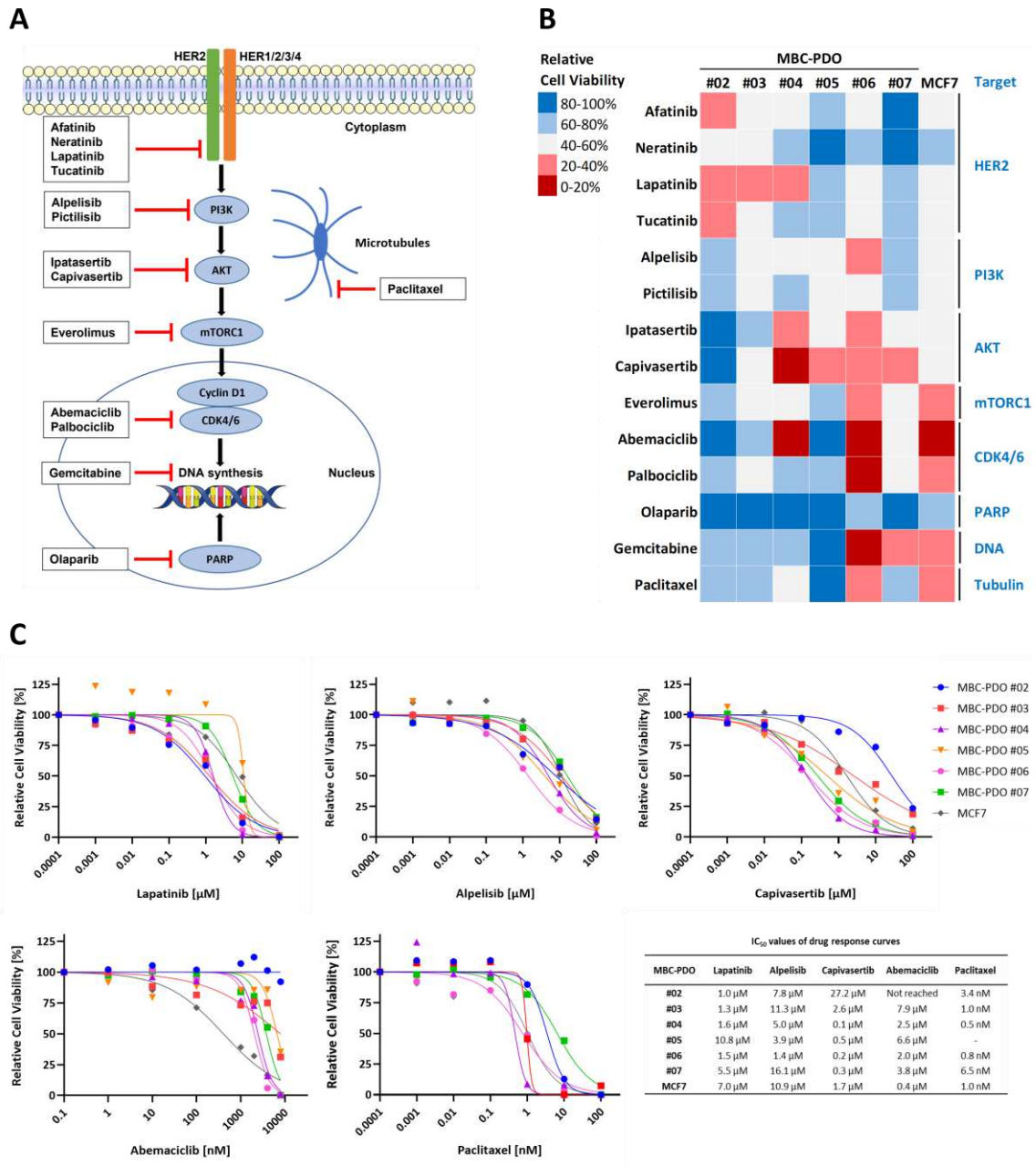

Figure 19: In vitro drug response assays of organoid lines. (A) *Overview of drugs used in the assays and their targets. Inhibitors Afatinib, Lapatinib, Neratinib, and Tucatinib target the HER2 receptor intracellularly. Alpelisib and Pictilisib target PI3K, while Ipatasertib and Capivasertib aim for AKT. Everolimus inhibits mTORC1, whereas Abemaciclib and Palbociclib target CDK4/6 in the nucleus. Olaparib, which is administered to BC patients with a BRCA1/2 mutation/deletion, inhibits PARP. Gemcitabine enters the cell through nucleoside transporters and is phosphorylated in three steps into Gemcitabine triphosphate, which is incorporated into the DNA and leads to the termination of DNA synthesis. Paclitaxel binds and stabilizes β-tubulin, upon which depolymerization is blocked. This affects the mitotic spindle assembly, chromosome segregation, and mitosis. The figure was created using Microsoft® PowerPoint®.* ***(B)*** *Heat map of relative cell viability of organoids treated with various drugs at specific concentrations for 4 days (10 µM Afatinib, 1 µM Neratinib, 4 µM Lapatinib, 10 µM Tucatinib, 10 µM Alpelisib, 1 µM Pictilisib, 1 µM Ipatasertib, 1 µM Capivasertib, 100 nM Everolimus, 4 µM Abemaciclib,*

10 µM Palbociclib, 10 µM Olaparib, 100 nM Gemcitabine, 10 nM Paclitaxel). Values were normalized to control treatment with 0.1% DMSO (set to 100%). Red fields indicate sensitive responses, while blue fields present less-responding lines. Experiments were performed in technical triplicates. ***(C)*** *Drug response curves depict organoid viabilities after 4 days of treatment with Lapatinib, Alpelisib, Capivasertib, Abemaciclib, and Paclitaxel. Error bars representing SD of three independent experiments were removed for better presentation. IC50 values of drug response curves are shown in the adjacent table. This figure has been previously published (9.1).*

MBC-PDO #03 has some HER2 expression (**Table 24**) and revealed a strong response to HER2 (and EGFR) inhibitor Lapatinib (**Figure 19B, C**). Although MBC-PDO #03 carries the hotspot mutation in *PIK3CA* H1047R (**Table 25**), which could potentially activate the PI3K-AKT pathway, the organoid line did not respond sensitively to drugs targeting that pathway. Since tumorigenesis can be promoted by PI3K and MAPK signaling pathways, the activation of these pathways was investigated in the MBC-PDOs by IHC staining of phosphorylated (p)-AKT (phosphorylation site Ser473) and p-ERK1/2 (phosphorylation sites Thr202/Tyr204 of extracellular-signal regulated kinases 1/2 (ERK)) (**Figure 20**, **Table 26).** The IHC staining of the activating phosphorylation sites of AKT and ERK showed that p-AKT was absent while p-ERK was present in MBC-PDO #03. This indicates that in the cells of MBC-PDO #03 the MAPK signaling cascade and not the PI3K-AKT pathway was activated. These results emphasize the importance of using functional *in vitro* drug assays in combination with IHC stainings of p-AKT in patient-derived organoids.

Even though MBC-PDO #04 did not reveal a positive HER2 signal (**Table 24**), it responded sensitively to Lapatinib (**Figure 19B, C**). As Lapatinib not only targets HER2 but also EGFR, these results reveal that some inhibitors can be beneficial in one way or another. MBC-PDO #04 cells carry an *AKT1* E17K hotspot mutation (**Table 25**), indicating a possible activation of the PI3K-AKT pathway. Indeed, the cell viability of these organoids was reduced upon treatment with AKT inhibitors Ipatasertib and Capivasertib. These results are in accordance with the positive IHC staining of p-AKT (**Figure 20**, **Table 26**). Furthermore, MBC-PDO #04 was sensitive towards Abemaciclib. After the collection of the effusion, the patient was treated with Everolimus, which would not have been the first choice according to **Figure 19**.

MBC-PDO #05, which carries the hotspot mutation *PIK3CA* E545K (**Table 25**), responded most sensitively to Capivasertib, followed by some response towards the other PI3K and AKT targeting drugs (**Figure 19**). There were not sufficient organoids from MBC-PDO #05 to fix and perform IHC staining with. However, the patient would have likely profited from PI3K and AKT inhibitors, instead of the actual therapy with Paclitaxel and HER2-targeting antibodies Trastuzumab and Pertuzumab, followed by Abemaciclib combined with Trastuzumab.

MBC-PDO #06 carries the *PIK3CA* E545K hotspot mutation (**Table 25**), revealed positive signals of p-AKT (**Figure 20**, **Table 26**), and reacted sensitively to PI3K and AKT inhibitors, as well as mTORC1 inhibitor Everolimus (**Figure 19B, C**). Additionally, the cell viability of these organoids was affected by the CDK4/6 inhibitors Abemaciclib and Palbociclib, as well as by the chemotherapy drugs Gemcitabine and Paclitaxel.

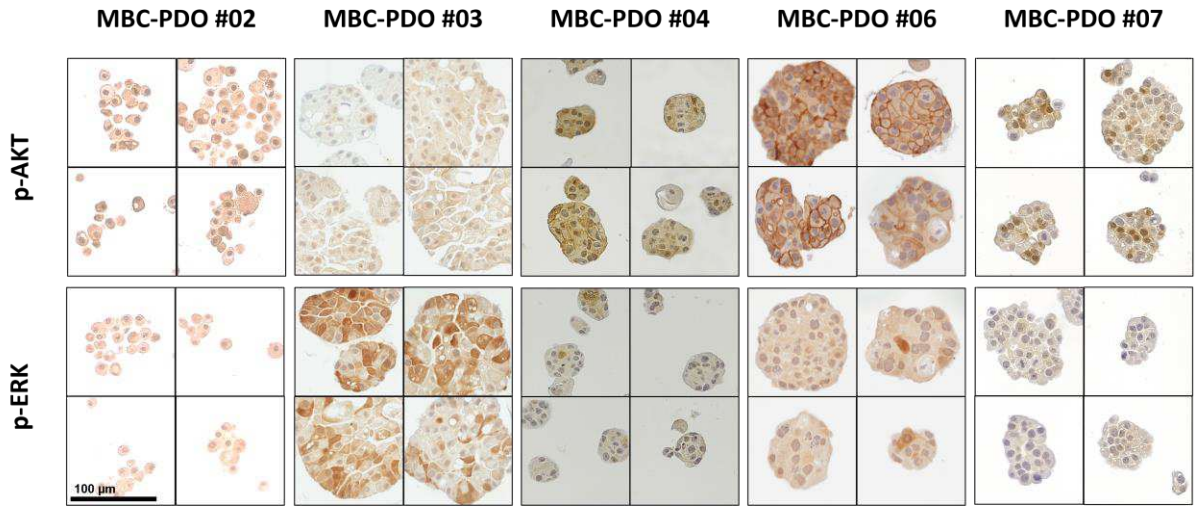

***Figure 20: IHC staining* of p-AKT and p-ERK in MBC-PDOs.** *The activation of PI3K and MAPK signaling pathways was validated by IHC staining of the activating phosphorylation sites of AKT (Ser473) and ERK1/2 (Thr202/Tyr204). Localization of p-AKT and p-ERK can be nuclear, subcellular, and cytoplasmic. Parts of this figure have been previously published (9.1).*

Table 26: Results of IHC staining of p-AKT and p-ERK in MBC-PDOs. *Abbreviations neg.: negative signal, pos.: positive signal. Some content of this table has been previously published (9.1).*

MBC-PDO		p-AKT	p-ERK
#02	**Organoids**	neg.	neg.
#03	**Organoids**	neg.	pos.
#04	**Organoids**	pos.	neg.
#06	**Organoids**	pos.	neg.
#07	**Organoids**	pos.	neg.

Lastly, MBC-PDO #07, which has an *AKT1* E17K hotspot mutation (**Table 25**) and is p-AKT-positive (**Figure 20, Table 26**), reacted most sensitively to AKT1 inhibitor Capivasertib and the chemotherapy drug Gemcitabine (**Figure 19B, C**). The patient of MBC-PDO #07 had previously received treatment with Paclitaxel and Abemaciclib. Yet, both drugs did not have a

noticeable impact on the cell viability of MBC-PDO #07, indicating a resistance to these drugs. Besides, the corresponding patient was diagnosed with a *BRCA1/2* deletion in the breast tumor sample and consequently she had been treated with the PARP inhibitor Olaparib. However, MBC-PDO #07 cells were resistant to Olaparib. Therefore, the patient could have benefited from therapy with AKT inhibitors or Gemcitabine.

Here, a reliable drug screening method is demonstrated, which helps to determine the optimal drug treatment in an individualized manner. In summary, the results highlight the significance of combining IHC stainings and mutation analysis with *in vitro* drug screenings to move a step closer to personalized BC therapy. For example, even in cancers where there is no or little HER2 signal, it could be beneficial for some patients to receive HER2-targeting therapy such as Lapatinib.

3.3 Treatment of MBC-PDOs with AdCAR-T cells

Some of the following contents and data have been previously published (see chapter 8 and 9.2). Published figures are labeled accordingly.

Onder, C.E., M. Moustafa-Oglou, S.M. Schroder, A.D. Hartkopf, A. Koch, and C.M. Seitz, Precision Immunotherapy Utilizing Adapter CAR-T Cells (AdCAR-T) in Metastatic Breast Cancer Leads to Target Specific Lysis. Cancers (Basel), 2023. 16(1).

3.3.1 Cultivation and characterization of MBC-PDOs expressing luciferase and GFP

Hematologic malignancies have been shown to be successfully treated with CAR-T cell therapy. Yet, CAR-T efficiency in attacking solid tumors, such as BC, still requires improvement. The approach of AdCAR technology allows the universal targeting of numerous cancer types, enables adjustable modulation of AdCAR function, and addresses antigen-loss-caused immune evasion. Here, the potential of utilizing MBC-PDOs for AdCAR-T cell-mediated cytotoxicity assays was tested.

The efficacy of AdCAR-T cell lysis on established MBC-PDO lines #03, #04, #06, and #07 was assessed. For visualization and analysis of cell lysis, MBC-PDO lines were virally transduced to express luciferase and green fluorescent protein (GFP). **Figure 21A** demonstrates a schematic overview of the isolation of metastatic BC cells from MPE and the establishment of MBC-PDO cultures expressing luciferase and GFP. After transduction, MBC-PDO and MCF-7 cells were cultivated, before GFP-expressing cells were sorted via FACS and expanded to be used in the following assays. The transduction efficiency of established MBC-PDO lines and MCF-7 was visualized via brightfield (BF) and fluorescence (FL) microscopy (**Figure 21B**).

To analyze the antigen profiles of MBC-PDOs and MCF-7, transduced and sorted cells were immune-profiled. Immunophenotyping (FC) was conducted using biotinylated monoclonal antibodies (mAbs), that were subsequently used in the cytotoxicity assays (**Figure 21B**). The target antigen panel was selected based on expression patterns of BC as well as their suitability for AdCAR-T treatment. The following BC-associated antigens were chosen: HER2, TROP2, EGFR, ROR1, CD276, and EpCAM. **Figure 21B** displays the expression profile of the surface antigens in normalized histograms, in which MCF-7 served as a comparative control. HER2 is one of the three receptors, which determine the receptor status of BC and the therapy the patients receive. All MBC-PDO lines showed low to medium levels of HER2, with MBC-PDO #03 showing the highest level of HER2. The EpCAM signal intensity was the highest in all five samples (lower panel, red curves), whereas the other antigens were detected in different quantities. The signal intensity for TROP2 was the highest in MBC-PDO #03 and the lowest in MBC-PDO #04, while levels of EGFR were the highest in MBC-PDO #07 and the lowest in MCF-7. ROR1 expression was elevated in MBC-PDO #07 and absent in MCF-7 as well as MBC-PDO #03. CD276 was represented in MBC-PDO #04, #06, #07, and MCF-7 in comparable high quantities, whereas MBC-PDO #03 revealed a lower quantity of CD276. In conclusion, the MBC-PDO lines can serve as *in vitro* models for the application of precision AdCAR-T cell treatment of metastatic BC cells.

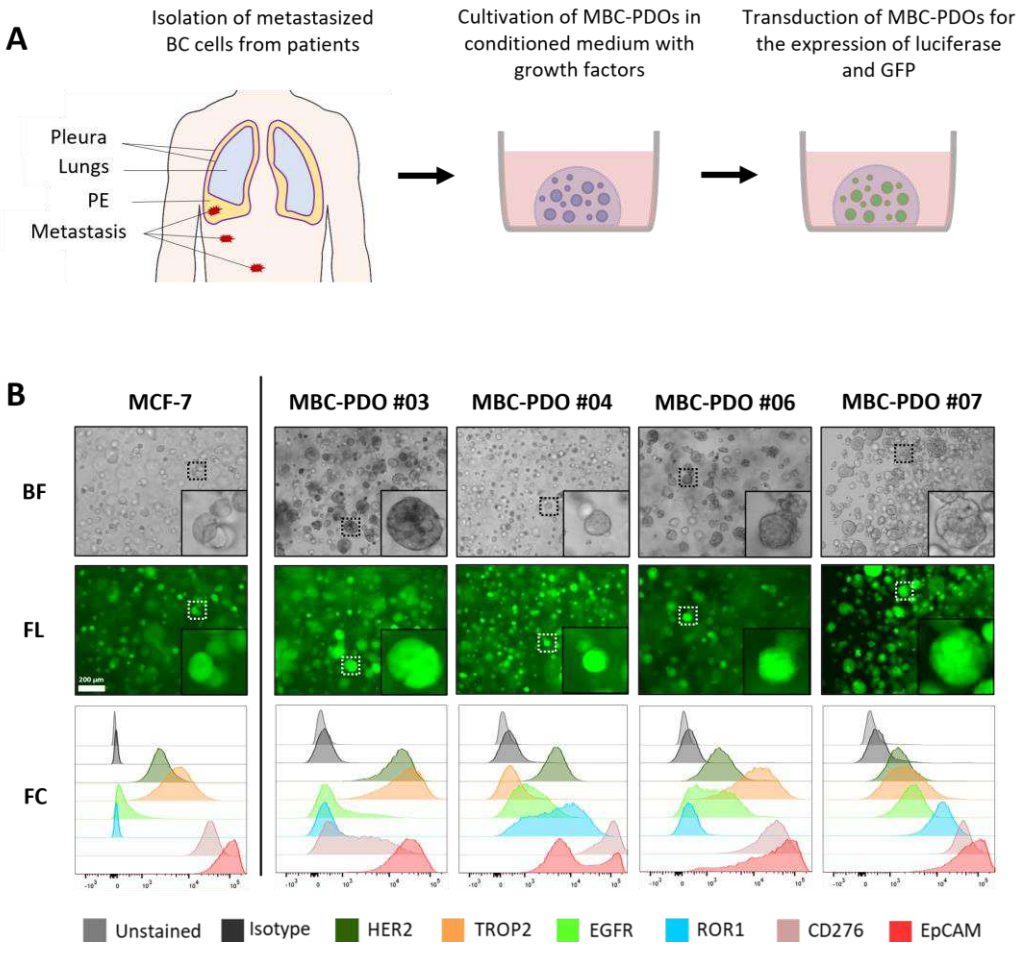

Figure 21: Cultivation and characterization of luciferase- and GFP-expressing MBC-PDOs. (A) *Schematic overview of isolation of metastatic BC cells from MPEs, cultivation in BME droplets and viral transduction of MBC-PDOs. The figure was created using Microsoft® PowerPoint®.* ***(B)*** *Brightfield (BF) and fluorescence (FL) images as well as flow cytometry (FC) analysis of luciferase- and GFP-expressing MCF-7 and MBC-PDOs. Scale bar: 200 µm. The majority of this figure has been previously published (9.2).*

3.3.2 Implementation of AdCAR treatment of organoids

In the following step, the potential of MBC-PDOs as *in vitro* models for metastatic BC and their suitability in AdCAR-T cell treatments was assessed. To show the universal antigen-specific effector function of AdCAR-T cells *in vitro*, we applied adapter molecules in the linker-label-epitope (LLE)-mAb design that target various TAAs expressed by the tumor cells. The goal was to utilize MBC-PDOs as a screening platform to evaluate AdCAR-T cell-based precision immunotherapy for flexible targeting of TAAs.

In the first approach, the application of AdCAR treatment was implemented by testing various E:T ratios on GFP and luciferase expressing MCF-7 organoids. As demonstrated above, MCF-7 cells also express the target antigen CD276 (**Figure 21B**). Consequently, MCF-7 organoids were grown, harvested, and seeded on BME beds, so they could be treated with AdCAR-T cells and LLE-CD276 mAb (**Figure 22A**). Unspecific cell lysis by AdCAR-T cells was determined by the elimination of mAbs from the application. AdCAR-T cells were added at different E:T ratios (ranging from 5:1 to 0.156:1), and the LLE-mAb concentration was used at 10 ng/mL in all experiments.

In **Figure 22B**, BF and FL images of MCF-7 organoids treated with AdCAR-T cells with and without (w/o) LLE-CD276 mAb are demonstrated. Luciferase activity and GFP signal of viable cells were captured 24 h, 48 h, and 72 h post-treatment (**Figure 22B, C**). In the absence of LLE-CD276 mAb, MCF-7 organoids remained intact even at the highest E:T ratio of 5:1 (**Figure 22B**), thus, there was no unspecific lysis identified. Yet, the GFP signal declined slightly, as the organoids were covered by proliferated AdCAR-T cells. In the presence of LLE-CD276 mAb on the other hand, MCF-7 organoids were specifically targeted and lysed by AdCAR-T cells (**Figure 22B**). The GFP signal started to disperse before it disappeared completely.

Also, the efficacy of target cell lysis was further determined by a luciferase-based cytotoxicity assay. Luciferase activity of viable cells was read, and values were normalized to untreated control MCF-7 organoids (lacking AdCAR-T cells and mAbs; **Figure 22C**). Antigen-specific cell lysis correlated positively with the E:T ratio, as AdCAR-mediated cytolysis of MCF-7 organoids reached from 7% to 62% with increasing E:T ratios (0.156:1 to 5:1), only after 24 h of treatment. Unspecific cytolysis by AdCAR-T cells (without mAbs) was relatively low (3-8%) and positively

correlated with the E:T ratio, too. After 48 h of treatment, the specific and unspecific cell lysis increased, and after 72 h of treatment, the highest target cell lysis of 94% was detected in an E:T ratio of 1.25:1 (**Figure 22C**).

In order to investigate the compatibility of MBC-PDOs in AdCAR treatments, MBC-PDO #07, which expresses CD276 (**Figure 21B**), was also treated with AdCAR-T cells combined with LLE-CD276 mAb (**Figure 23A, B**) at various E:T ratios. FL images of GFP-expressing MBC-PDO #07 demonstrate that GFP signal weakened and dispersed with increasing E:T ratios and over time (**Figure 23A**). Quantification of target cell lysis of MBC-PDO #07 supported the visual results and was conducted by measuring the luciferase activity of remaining viable cells (**Figure 23B**). The addition of LLE-CD276 mAb to AdCAR-T cells resulted in very high target-specific lysis (up to 99%) (normalized to untreated organoids), while unspecific cell lysis by AdCAR-T cells (without LLE-CD276 mAb) was reasonably low (0-17%).

In conclusion, MCF-7 and MBC-PDO #07 demonstrated high levels of CD276 expression and displayed strong reactions to the specific targeting by AdCAR-T cells combined with LLE-CD276 mAb. These outcomes indicate that our MBC-PDO lines are suitable for AdCAR treatments with various mAbs. Additionally, the E:T ratio of 1.25:1 resulted in a target cell lysis of 99% after 72 h of treatment. Therefore, all subsequent experiments were conducted with an E:T ratio of 1:1.

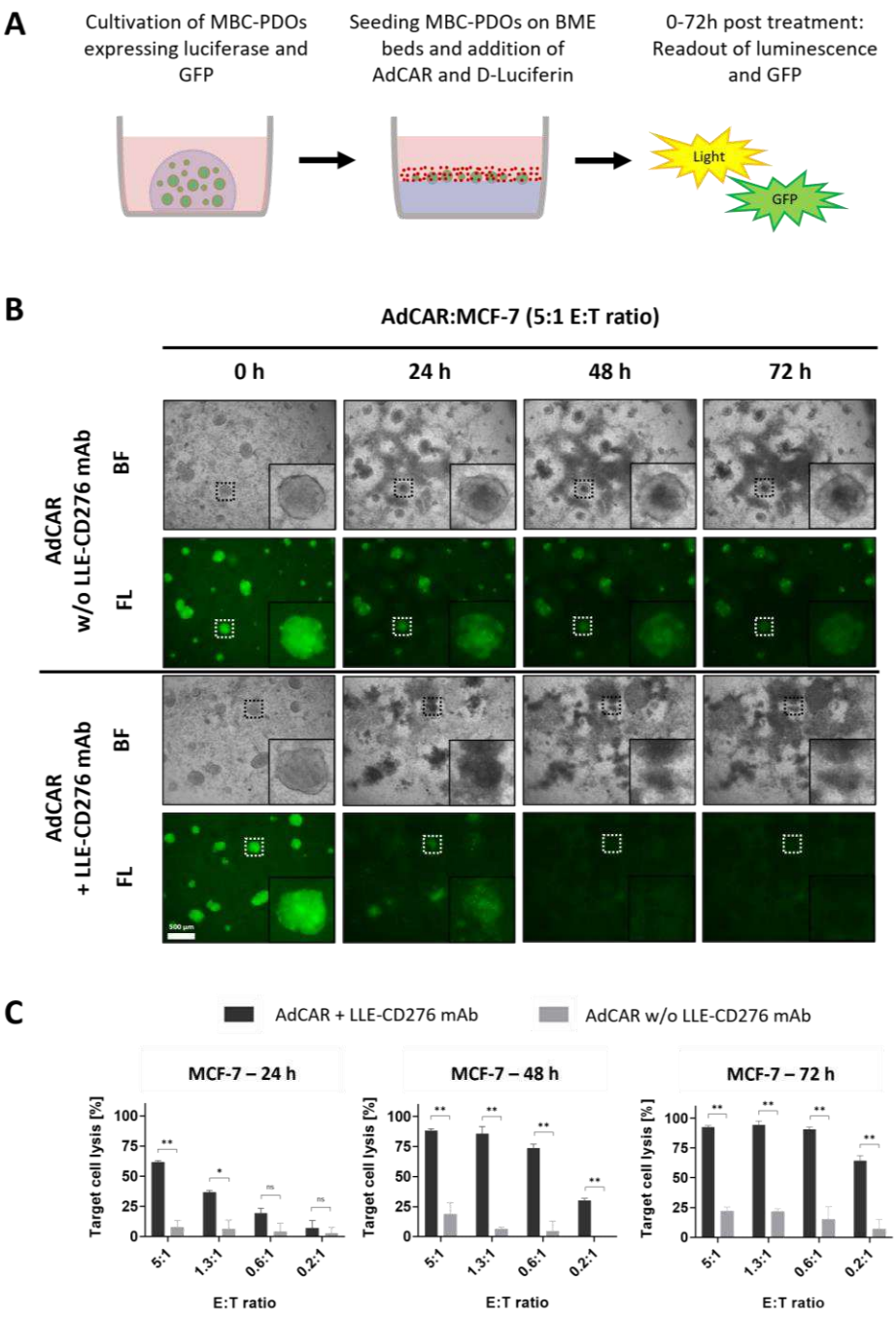

Figure 22: AdCAR treatment of MCF-7 organoids expressing luciferase and GFP. ***(A)*** *Schematic overview of the experimental setup. MCF-7 and MBC-PDOs (green) expressing luciferase and GFP were seeded on BME beds and treated with AdCAR-T cells (red) and corresponding LLE-CD276 mAb. Readouts were performed on luminescence and GFP, after 24 h, 48 h, and 72 h, using a plate reader and a fluorescence microscope. The figure was created using Microsoft® PowerPoint®.* ***(B)*** *BF and FL images of GFP-expressing MCF-7 organoids treated with AdCAR-T cells without (w/o) and with LLE-CD276 mAb. Scale bar: 500 µm.* ***(C)*** *Target cell lysis of MCF-7 organoids treated with AdCAR-T cells with (black bars) and without (grey bars) LLE-CD276 mAb, over 72 h. Target cell lysis efficiency was determined by luciferase activity of remaining cells. Data shown represents the mean ± SD of triplicates (n = 3). Negative values were set to 0. Statistical analysis was performed using paired t-test. ns, not significant. * = p ≤ 0.05; ** = p ≤ 0.01. This figure has been previously published (9.2).*

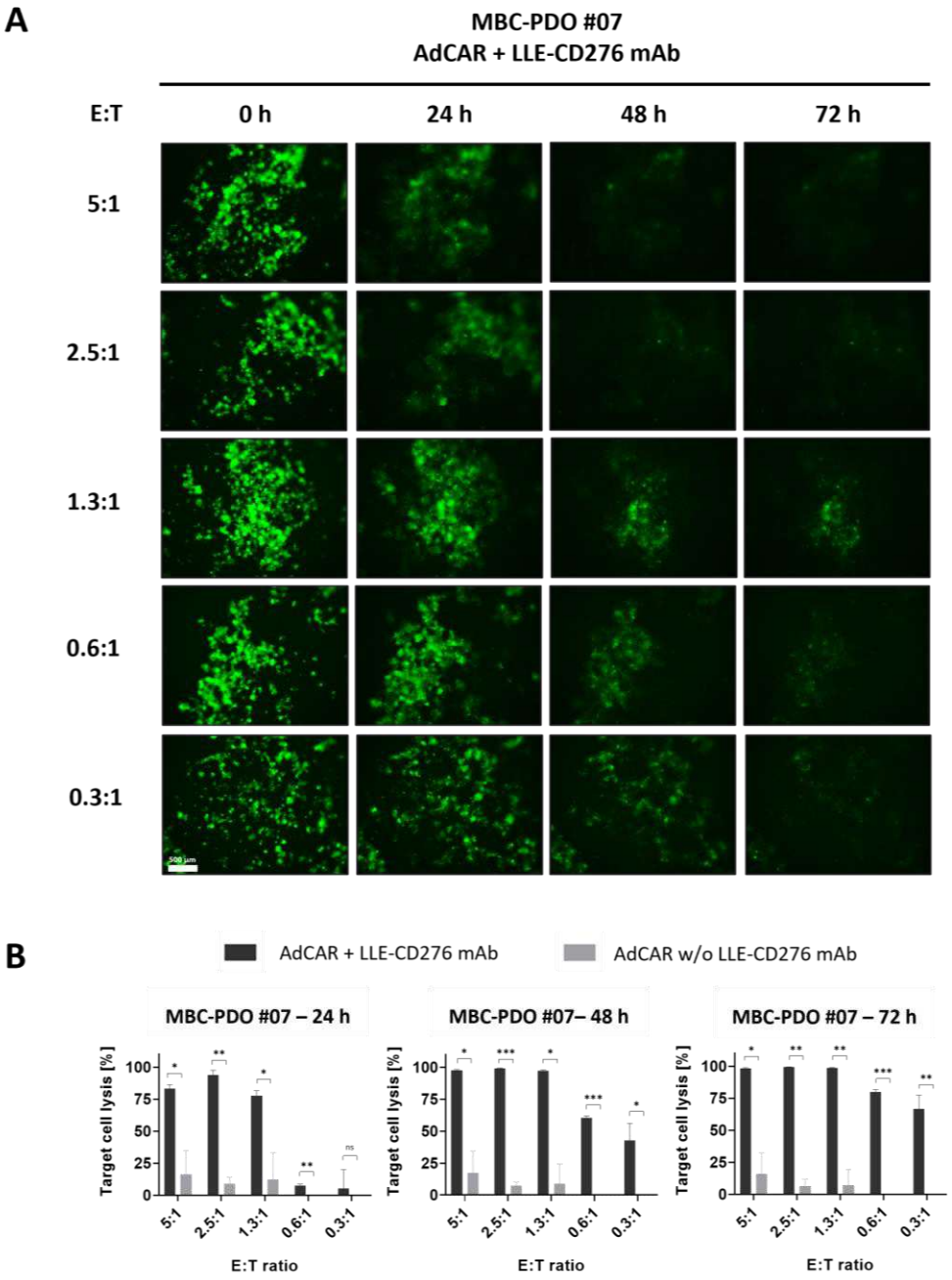

Figure 23: AdCAR treatment of luciferase- and GFP-expressing MBC-PDO #07 at various E:T ratios. ***(A)*** *Fluorescence images of GFP-expressing MBC-PDO #07 treated with AdCAR-T cells of different E:T ratios with the addition of LLE-CD276 mAb, over 72 h. Scale bar: 500 µm.* ***(B)*** *Target cell lysis of MBC-PDO #07 treated with AdCAR-T cells with (black bars) and without (w/o; grey bars) LLE-CD276 mAb, over 72 h. Target cell lysis efficiency was determined by luciferase activity of viable organoids. Data shown represents the mean ± SD of triplicates (n = 3). Negative values were set to 0. Statistical analysis was performed using paired t-test. ns, not significant. * = p ≤ 0.05; ** = p ≤ 0.01; *** = p ≤ 0.001. This figure has been previously published (9.2).*

3.3.3 AdCAR treatment of MBC-PDOs applying various LLE-mAbs

In order to examine the capability of targeting alternative antigens beyond CD276, we investigated if other LLE-mAbs have comparable effects on MBC-PDO #07. Therefore, MBC-PDO #07 was treated with AdCAR-T cells combined not only with LLE-CD276, but also with LLE-HER2, LLE-EGFR, and LLE-TROP2, at an E:T ratio of 1:1 (**Figure 24A**). In comparison to the control conditions (without LLE-mAbs and +/-AdCAR), in which the organoids were completely intact, targeted organoids (+AdCAR and +LLE-mAb) lost GFP intensity which dissolved over time. These observations correlate with the antigen profile of MBC-PDO #07 analyzed by FC, and the quantification of target cell lysis determined by luciferase activity (**Figure 24B**). After 24 h of treatment, the mAbs LLE-CD276 and LLE-EGFR initiated the highest lysis rates (84% and 87%, respectively), which are in accord with the antigen profile according to the FC data. Antigen-specific AdCAR-mediated cytolysis of MBC-PDO #07 reached from 90% to 99% after 48 h and rose to 100% (LLE-HER2) after 72 h of treatment.

Subsequently, we assessed the impact of AdCAR treatment and several LLE-mAbs on additional MBC-PDO lines. MBC-PDO #03, for instance, was treated with the mAbs LLE-CD276, LLE-HER2, LLE-EGFR, LLE-TROP2, and LLE-EpCAM for 72 h (**Figure 25A**). According to the FC data of MBC-PDO #03, levels of EGFR were lower compared to the antigens HER2, TROP2, CD276, and EpCAM. As a result, the LLE-EGFR-mediated target cell lysis was lower (38% after 24 h, and 58% after 72 h of treatment) compared to the rest of the mAbs which achieved a lysis of up to 83% (HER2) at 24 h, and up to 95% (CD276, and HER2) after 72 h of treatment. Additionally, LLE-TROP2- and LLE-EpCAM-mediated target cell lysis also reached high percentages: 81% and 61% respectively after 24 h, and 94% and 89% respectively after 72 h of treatment. At all three timepoints, unspecific cell lysis (without LLE-mAb, grey bars) was relatively low with a maximum of 12% after 24 h of treatment.

Based on the FC data, MBC-PDO #06 expressed medium to high amounts of CD276, EGFR, and TROP2, hence the AdCAR treatment of these organoids was combined with LLE-CD276, LLE-EGFR, and LLE-TROP2, respectively (**Figure 25B**). As expected, all three conditions led to complete cytolysis of up to 98% after 24 h and 100% after 72 h of treatment. However, unspecific cell lysis was relatively high in MBC-PDO #06 with 21-36%. CD276- and EGFR-expressing MBC-PDO #04 was treated with AdCAR-T cells together with LLE-CD276, and LLE-EGFR, respectively (**Figure 25C**). After 72 h of treatment, the antigen-specific cytolysis achieved 92% (CD276) and 94% (EGFR). Unspecific cell lysis was relatively low with a maximum of 11% after 24 h of treatment.

In conclusion, these results demonstrate that MBC-PDOs are suitable models for the *in vitro* screening of metastatic BC treatment by the AdCAR system. Furthermore, the antigen expression of MBC-PDOs correlates with their specific cytolysis mediated by AdCAR-T cells

and corresponding LLE-mAbs. Moreover, the potential of targeting several antigens varied, depending on antigen expression levels and the characteristics of the target antigens that had an impact on their efficiency in recruiting AdCAR-T cells to tumor cells. Although there is potential for universal targeting using a single CAR construct for all antigens, not all antigens were able to recruit AdCAR-T cells to cancer cells equally.

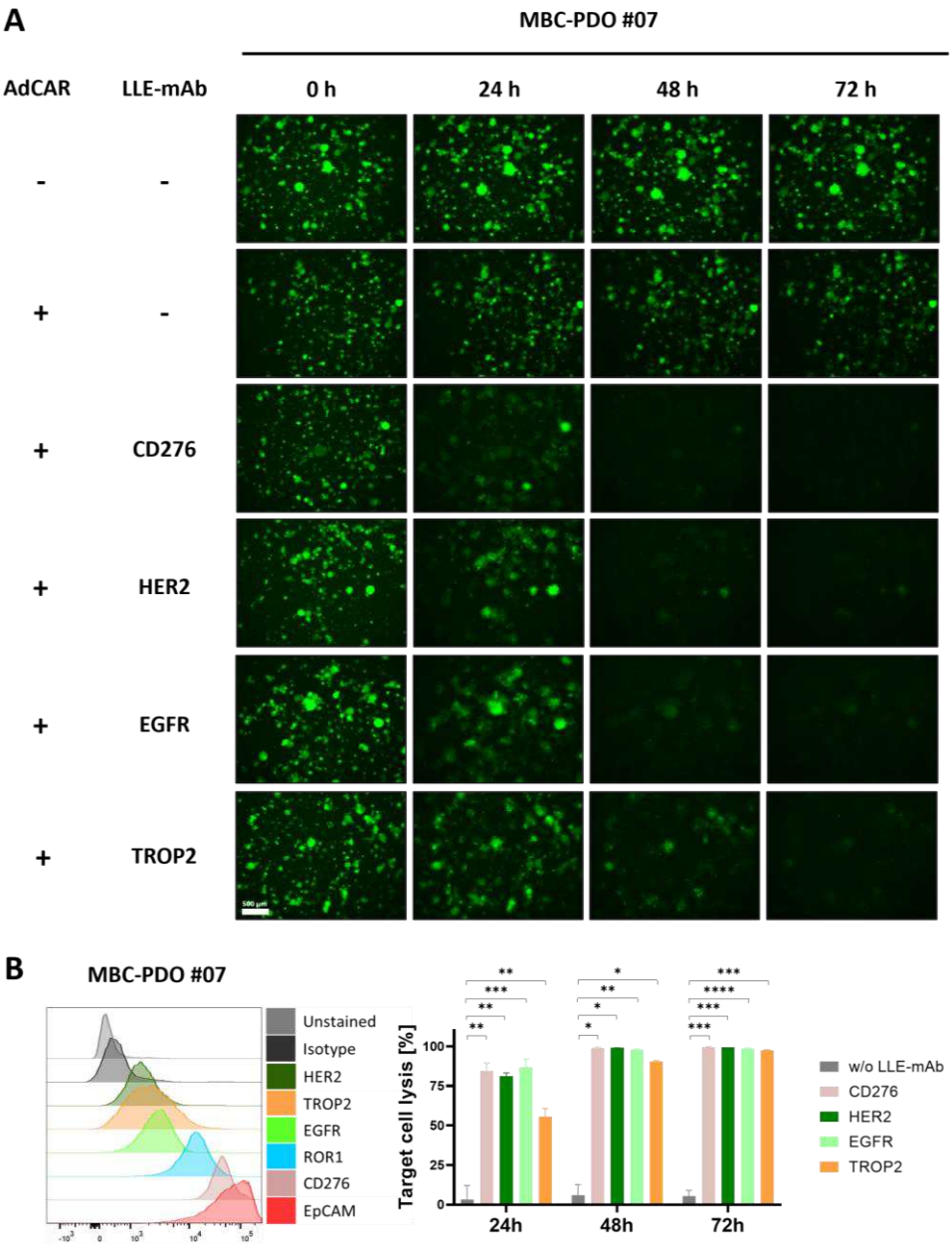

Figure 24: AdCAR treatment of MBC-PDO #07 with various LLE-mAbs. (A) *Fluorescence images of GFP-expressing MBC-PDO #07 treated with AdCAR-T cells (E:T ratio was set to 1:1) with the addition of LLE- mAbs against CD276, HER2, EGFR, and TROP2. Images were taken after 0 h, 24 h, 48 h, and 72 h of treatment. Scale bar: 500 µm.* ***(B)*** *FC analysis and target cell lysis of MBC-PDO #07 treated with AdCAR-T cells (E:T ratio was set to 1:1) with (colored bars) and without (w/o; grey bars) LLE-mAbs, over 72 h. Target cell lysis efficiency was determined by luciferase activity of viable organoids. Data shown represents the mean ± SD of triplicates (n = 3). Statistical analysis was performed using paired t-test. ns, not significant. * = p ≤ 0.05; ** = p ≤ 0.01; *** = p ≤ 0.001; **** = p ≤ 0.0001. The majority of this figure has been previously published (9.2).*

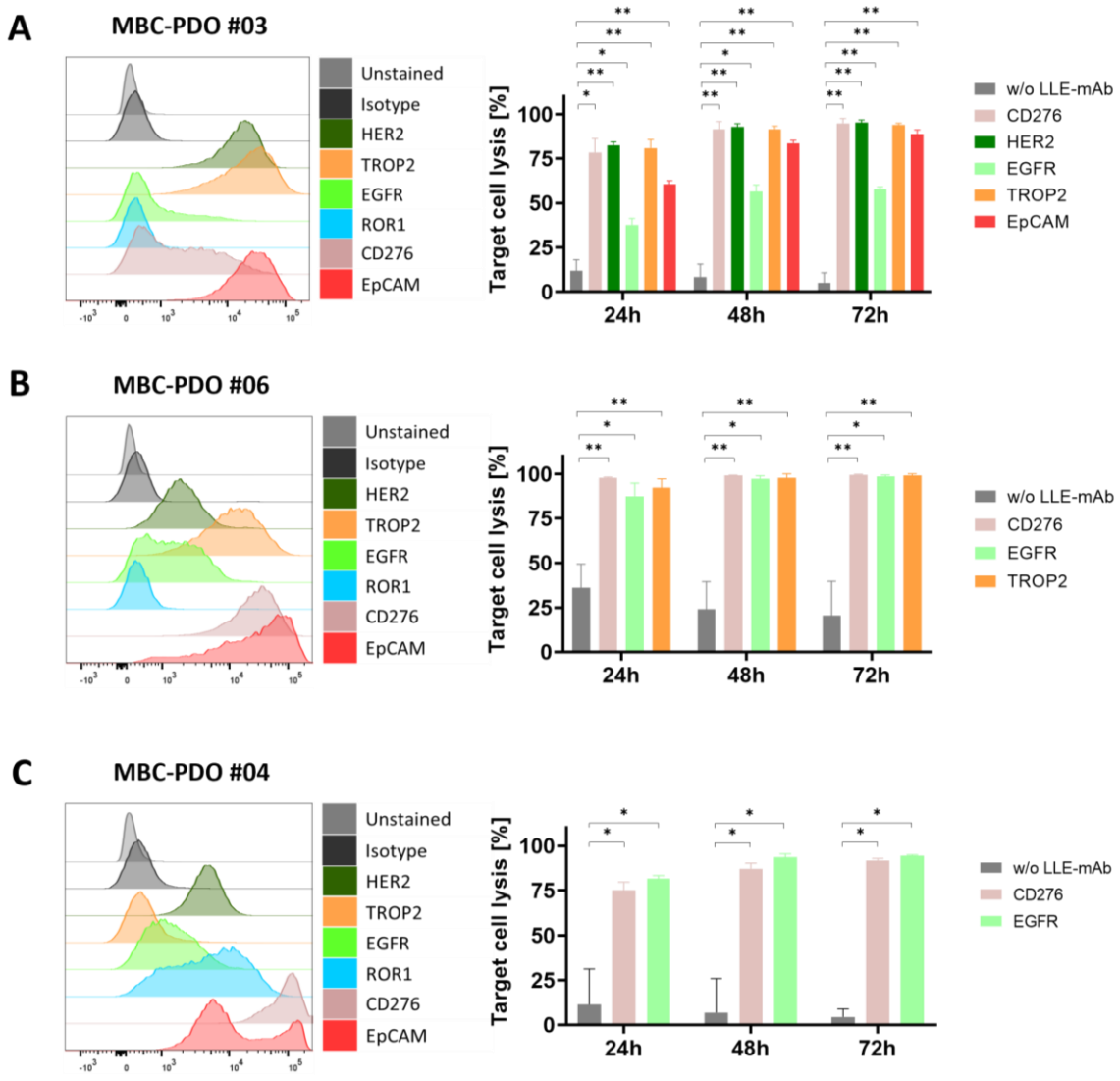

Figure 25: FC analysis and AdCAR treatment of MBC-PDOs with various LLE-mAbs. *Treatments were performed on* ***(A)*** *MBC-PDO #03,* ***(B)*** *MBC-PDO #06, and* ***(C)*** *MBC-PDO #04. AdCAR treatment of MBC-PDOs with (colored bars) and without (w/o; grey bars) LLE-mAbs was carried out in an E:T ratio of 1:1, for 72 h. Target cell lysis efficiency was determined by luciferase activity of viable organoids. Data shown represents the mean ± SD of multiple replicates (n ≥ 3). Statistical analysis was performed using paired t-test. ns, not significant. * = p ≤ 0.05; ** = p ≤ 0.01. The majority of this figure has been previously published (9.2).*

4 Discussion

Some of the following contents have been previously published (see chapter 8 and 9).

Onder, C.E., T.J. Ziegler, R. Becker, S.Y. Brucker, A.D. Hartkopf, T. Engler, and A. Koch, Advancing Cancer Therapy Predictions with Patient-Derived Organoid Models of Metastatic Breast Cancer. Cancers (Basel), 2023. 15(14).

Onder, C.E., M. Moustafa-Oglou, S.M. Schroder, A.D. Hartkopf, A. Koch, and C.M. Seitz, Precision Immunotherapy Utilizing Adapter CAR-T Cells (AdCAR-T) in Metastatic Breast Cancer Leads to Target Specific Lysis. Cancers (Basel), 2023. 16(1).

4.1 Drug response of BC cell lines

Owing to their convenience and reproducible application, 2D BC cell lines are widely used in research. Applicable to high-throughput drug screenings, 2D BC cell lines allow the analysis of multiple compounds and conditions, including the assessment of drug efficacy in preclinical and clinical studies.

Here, the sensitivity of various BC cell lines, that carry different receptor status and mutations, towards specific drugs was identified by conducting dose-dependent drug assays. Relative cell viability of BC cell lines was calculated applying one Crystal Violet staining and two CellTiter-Glo® assays per drug. Both approaches, the staining of attached cells and the metabolic readout, resulted in nearly identical dose-response curves as shown in the example of MEK inhibitor Selumetinib (**Figure 9**). Consequently, the values of each BC line and each drug could be unified as means of technical triplicates (**Figure 10-12**).

BC cell lines SKBR3 and MDA-MB-453 are HER2-positive and are a frequently used model to study HER2-targeted therapies [62, 63, 116]. As expected, treatment with HER2 inhibitors Afatinib, Neratinib, Lapatinib, and Tucatinib led to sensitive responses of SKBR3 and MDA-MB-453 (**Figure 10**, **Figure 13**). The rather sensitive response of HER2-negative MDA-MB-468 towards Afatinib, Neratinib, and Lapatinib can be justified by the fact that these drugs do not only inhibit HER2, but also EGFR. Hence, the proliferation of this BC cell line likely depends on EGFR. Another possibility is, that MDA-MB-468 is officially HER2-negative, but still expresses sufficient HER2 that results in some sensitivity towards HER2 inhibitors. Either way, these results emphasize that inhibitors such as Afatinib, that have numerous targets, can be profitable in targeting BC cells regardless of their pathological HER2 status.

Not only the receptor status influences the therapy recommendation for BC, but also genetic mutations. In BC, tumorigenesis can be driven by PI3K-AKT and the MAPK signaling pathway [21]. PI3K inhibitors Alpelisib and Pictilisib as well as AKT inhibitor Ipatasertib can be beneficial

in the treatment of BCs that have an activated PI3K-AKT signaling pathway. Sometimes, mutations of key genes, such as hotspot mutations in *PIK3CA* and *AKT1*, can lead to the hyperactivation of this signaling pathway and can result in a sensitivity of BC cells to these drugs [27]. MCF-7, which harbors a mutation in the *PIK3CA* gene, reacted most sensitively to all three inhibitors, proving its hyperactivation of the PI3K-AKT pathway (**Figure 11**, **Figure 13**). T47D on the other hand, also carries a *PIK3CA* mutation. Yet it did not respond sensitively towards the PI3K and AKT inhibitors, indicating that this line, just like MDA-MB-468 and MDA-MB-231, does not entirely depend on PI3K or AKT activation for cell proliferation. This demonstrates that mutation status alone is not sufficient for the recommendation of a certain therapy and that drug response assays ought to be conducted to determine the sensitivity of a line.

Even though MEK inhibitors are not typically applied in BC therapies, they could propose an alternative strategy to target BC cells that have an oncogenic activation of the MAPK signaling cascade. The BC cell line MDA-MB-231 for one, is known to harbor a *BRAF* mutation, which is associated with the hyperactivation of the corresponding pathway. According to our expectations, MDA-MB-231 was sensitive towards MEK inhibitors Selumetinib and Trametinib (**Figure 12**, **Figure 13**). Moreover, the moderately sensitive responses of MDA-MB-453 and MDA-MB-468 towards these MEK inhibitors was not expected and indicate that their cell proliferation depended on activated MEK to some extent. Once again, these results suggest that drug assays are inevitable since receptor and mutation status alone are not sufficient for therapy proposal.

As expected, the endocrine therapy drugs Tamoxifen and Fulvestrant successfully led to lower relative cell viabilities of all three ERα-positive BC cell lines MCF-7, T47D, and HCC1500. The ERα-negative lines on the other hand, were relatively resistant towards both drugs (**Figure 12**). However, Fulvestrant treatment did not reduce the relative cell viabilities of ERα-positive lines to below 50% even at high drug concentrations. This may be due to the presence of the pH indicator phenol red in the culture medium, which is structurally similar to estrogens and has been shown to have estrogenic activity [125]. In MCF-7, phenol red binds to ERα and stimulates the proliferation of these cells. Whereas in ERα-negative cells MDA-MB-231, phenol red showed no effect on cell proliferation [125]. Moreover, Tamoxifen has shown to inhibit cell proliferation in MCF-7 cells only when phenol red or estradiol were present [125]. Since Fulvestrant targets ERα in a slightly different manner than Tamoxifen, the medium should be adjusted by either using phenol red-free culture medium or adding estradiol to the treatments. Either way, the estrogenic stimulation of phenol red needs to be considered in assays that use ERα-positive cells.

Put together, 2D BC cell lines present a platform for testing the efficacy of different drugs and allow the identification of treatment-sensitive and -resistant lines. However, they also face limitations in assays that involve endocrine therapy drugs such as Tamoxifen and Fulvestrant. Furthermore, 2D cell lines do not capture the complex heterogeneity of BC tumors. Consequently, these observations require further validations in more complex models, such as patient-derived organoids.

4.2 Establishment and characterization of MBC-PDOs

While primary BC has a relatively good prognosis, drug-resistant metastasized BC has a very poor outcome. This emphasizes the need for reliable precision oncology and the relevance of models capturing the features of MBC [34]. Cell lines for one, are convenient to use but are not able to predict drug responses for individual patients [66]. PDX models on the other hand, have shown to be suitable for therapy predictions but their establishment is expensive and needs a long time [66]. In recent years, patient-derived organoid models have been established for personalized oncology with a great promise for clinical applications [71, 76]. Organoids are often derived from primary tumor samples, since metastatic biopsies are often small, rare, and mainly used for pathological purposes. Consequently, drug screenings are primarily conducted on organoids established from treatment-naïve primary tumors and rarely on pre-treated metastatic specimens. However, primary tumors do not necessarily represent the metastatic disease which is the main cause of cancer-death.

In some cases, metastasized BC can lead to MA and MPE. Patients with MA or MPE often suffer from discomfort, a shortness of breath, and chest or abdominal pain, which all cause a reduced quality of life. As MA and MPE often contain an abundance of metastasized cells, are easily accessible and simply removed by thoracentesis and paracentesis, collected fluids offer a great opportunity for the establishment of *in vitro* models representing metastatic BC. Therefore, our main objective is not only to improve patients' quality of life, but also to prolong their survival time by reducing MA and MPE.

In this study, we generated organoid models (MBC-PDOs) that represent metastatic BC by utilizing MA and MPE from patients with advanced BC. MBC-PDOs could be cultured for extended passages and were able to maintain their morphological features (**Figure 14**). Histochemical and mutational analyses were performed on MBC-PDOs to determine their expression profiles and detect hotspot mutations, that are common in BC. MBC-PDOs presented and preserved the histochemical and mutational characteristics of their respective sources (**Figure 15**, **Figure 18**, **Table 24, Table 25**) and sometimes even of their primary tumor (**Table 23**). Of note, the dominating receptor status in our collection was hormone receptor-positive and HER2-negative, which is mirrored in the BC statistics [10].

In some cases, mutations of key genes are responsible for the hyperactivation of the PI3K and MAPK signaling pathway, which drive the tumorigenesis in cancer cells [21]. *PIK3CA* and *AKT1* mutations are one of the most common mutations in BC and have been detected in approx. 30% and 8% of BC cases, respectively [22, 23, 25]. Here, five out of six MBC-PDO lines carried a hotspot mutation in either *AKT1* (two lines) or in *PIK3CA* (three lines). MBC-PDO #03 organoids for one, retained the receptor status and the hotspot mutation of the liver metastasis, indicating that the organoids have a hepatic origin.

All in all, the MBC-PDOs correspond to the different classifications of BC in terms of subtype, histological characteristics, receptor status and hotspot mutations, which collectively influence therapy decisions. Nonetheless, the actual objective here was to use MBC-PDOs as a platform for drug screenings and assessing therapy predictions.

4.3 Drug response of MBC-PDOs

Primary cells can serve as a useful platform for assessing the efficacy of drugs in a preclinical setting, before continuing with *in vivo* studies [67, 77]. Systemic therapy of BC aims for preventing the spread of metastatic cells. Once metastasized, making the best treatment plan for the BC becomes top priority. Future therapies of BC will sight precision medicine based on characteristics and drug sensitivities of the tumors [76]. Accordingly, there's a need for integration of *in vitro* drug screenings in clinical therapy. To date, therapy proposals depend on clinical studies, and do not take interpatient heterogeneity in drug sensitivity into account.

In this study, the objective was to assess the capability of MBC-PDOs as *in vitro* models in drug screenings and to establish a reliable application for 3D drug response assays to determine the sensitivity of MBC-PDOs towards the compounds in an individualized manner. The drug screenings were performed with compounds that target the HER signaling pathway, CDK4/6, PARPs, DNA synthesis, and β-tubulin (**Figure 19A**). While drug-response curves delivered detailed response curves of each MBC-PDO in a dose-dependent manner as well as IC50 values (**Figure 19C**), the heat map approach was more efficient in terms of saving time and organoid material.

Here, the drug assays (**Figure 19**) demonstrated that drug responses are not always in accord with expression patterns (**Table 24**), pathway activation (**Figure 20, Table 26**), and hotspot mutations (**Table 25**). This highlights the importance of personalized drug assays, in combination with the characterization of expression patterns and mutation status. For example, HER2-targeting inhibitors affected the proliferation of some of the MBC-PDO lines with zero to low levels of HER2. Importantly, some of these compounds inhibit multiple receptors including EGFR. This emphasizes the potential benefits of these inhibitors in clinical applications,

despite a pathologically negative HER2 status. Of note, clinical studies with Afatinib in HER2-negative BC have demonstrated some impact on tumor progression [126, 127].

Overall, AKT inhibitor Capivasertib demonstrated the highest effect among all drugs – four of six MBC-PDO lines responded sensitively. In terms of PI3K and AKT inhibitors, these drugs affected most hotspot mutated MBC-PDO lines, with MBC-PDO #03 being the only exception. This line harbored a *PI3KCA* H1047R mutation, which is associated with a hyperactivation of the PI3K-AKT signaling pathway. According to a recent study, modifications in the PI3K-AKT signaling pathway have been linked to higher levels of p-AKT, and responsiveness to AKT inhibitor Ipatasertib [128]. Yet, drugs targeting this pathway had little to no effect on MBC-PDO #03. In this case, the IHC staining of the activating phosphorylation sites of AKT and ERK1/2 delivered more insight. While p-AKT was absent, there was an abundance of p-ERK1/2 – a sign for activated MAPK signaling pathway. Here, alternative compounds that target the MAPK signaling pathway should be taken into consideration. MEK inhibitors such as Trametinib for instance, are already used in *BRAF*-mutated melanoma and non-small cell lung cancer [129]. Further MEK inhibitors are in clinical trials for the treatment of BC [129]. Therefore, we propose that in addition to receptor determination and mutational analysis, staining of p-AKT and p-ERK1/2 can help with the understanding of whether the corresponding pathway is activated and if targeting PI3K or AKT could be reasonable. For instance, TNBC with high p-AKT levels was associated with enriched clinical benefit of AKT inhibitor Ipatasertib regardless of the PI3K-AKT mutations [128].

Here, it has been shown that IHC staining of HER2 and mutation analysis of *PIK3CA* or *AKT1* are important but not sufficient for an accurate therapy recommendation. HER2-targeting drugs, such as Lapatinib, can also be useful for patients with HER2-negative BC. In contrast, BC patients with mutated *PIK3CA* or *AKT1* may, but do not necessarily, benefit from a treatment targeting the PI3K-AKT pathway, as we have shown for MBC-PDO #03. In general, there's a need for standardizing new biomarkers such as p-AKT in clinical diagnostics to guide therapy recommendations.

mTORC1 inhibitor Everolimus and CDK4/6 inhibitors are widely used in the clinic for hormone receptor-positive and HER2-negative BC patients [130-132]. Especially endocrine-resistant tumors could be treated with these drugs. However, our drug assays revealed that the response towards Everolimus and CDK4/6 inhibitors did not correlate with the receptor status of MBC-PDOs. One possible explanation is that some MBC-PDOs acquired resistance towards these drugs following clinical treatment. Similar effects have already been observed in previous studies [133]. This repeatedly suggests that personalized drug screenings may be valuable for individual cases, and novel biomarkers could help identify patients that would benefit from Everolimus and CDK4/6 inhibitors.

As demonstrated in MBC-PDO #07, the assays revealed accurate predictions of drug responses in a personalized fashion. The patient of MBC-PDO #07 had been treated with several drugs, including Olaparib due to a *BRCA1/2* mutation in the primary tumor, which did not have a significant impact on the relative cell viability of the organoids. In accordance with that, the patient passed away rather fast and would have likely profited from drugs that led to sensitive responses in our assays.

In summary, the discrepancy between characterization and functional assessment emphasizes the significance of linking IHC stainings and mutational analysis of metastasized BC with in vitro drug assays, to improve precision BC therapy. In a clinical setting, a fast turnaround time for organoid culture establishment and drug efficacy assessment is a crucial requirement. With our approach, culturing and screening of MBC-PDOs can take place within two weeks.

To further validate the accuracy of MBC-PDOs in predicting drug responses, initiating a study in which MBC-PDOs are treated with drugs used in the clinic for the respective patients would be favorable in order to align the results with the patients' responses to the therapy.

Here, we established six MBC-PDO lines for characterization and functional testing as proof of principle. We propose that with more models, hypotheses and biomarkers can be thoroughly examined in our setup. Generating a larger biobank of MBC-PDOs can broaden the understanding of connections between a patient's genetic as well as proteomic patterns and drug responses to identify sensitivity and resistance across BC subtypes. With an extended drug screening data, the way to making therapy decisions based on the characteristics of the organoid subtypes may be paved [134].

4.4 CAR-T treatment of MBC-PDOs

Metastatic BC faces numerous challenges such as cancer heterogeneity and treatment-resistance [34]. For instance, triple negative BC is defined by the absence of hormone receptors and HER2 and has a worse outcome, since endocrine therapy as well as HER2-targeted therapy are off the table [10]. Therefore, alternative target antigens, expressed on the surface of tumor cells, need to be investigated and clinically evaluated. CD276 for one, has shown to be expressed in various solid tumors including BC [135, 136].

In patients with hematological malignancies, the application of genetically modified T-cell treatments, which incorporate a chimeric antigen receptor (CAR), has shown successful clinical responses [96]. However, multiple obstacles have diminished successful translation of CAR-T cell therapies in solid tumors. Directing CAR-T cells to infiltrate the tumor proposes a great challenge, in addition to the immunosuppressive conditions found in the tumor

microenvironment [96]. Moreover, tumor cells are capable of reducing antigen expression under the selective pressure applied by CAR-T cells. Unrestrained antigen expression among tumor and healthy tissues can lead to on-target off-tumor effects and is associated with life-threatening toxicities [96]. This was observed in a case study, where the application of HER2-targeting CAR-T cells initiated a cascading systemic inflammation, ultimately leading to multi-organ failure [137]. This tragedy was attributed to CAR-T activation by low HER2 expression on lung epithelial cells [137]. This highlights the need for progress in the field of CAR-T cell-based therapy of BC. The progress of this approach highly depends on discovering suitable TAAs, which is especially important in TNBC.

To date, various novel CAR-based target antigens have been investigated against BC. Most of these studies have been conducted in preclinical trials [138]. Current clinical trials with BC patients embrace the targeting of HER2, GD2, ROR1, and EpCAM, amongst others [97]. Apart from targeting tumor cells, efforts have been directed towards the elimination of cells located within the extracellular matrix [139]. Combinatory plans with CAR-T cells and conventional BC therapy may result in better efficacy, especially in terms of defeating the suppressive tumor microenvironment. These strategies have yet to be assessed in clinical trials.

The AdCAR-T system offers a new approach to tackle these restrictions. This technology presents an improved safety profile by separating antigen recognition and CAR-T activation, which allows the control over CAR-T activity [108]. In terms of targeting promiscuously expressed antigens, CAR-T targeting can be controlled to react to on-target off-tumor activity. Additionally, AdCAR-T cells allow flexible targeting of multiple TAAs to avoid antigen escape and facilitate personalized targeting plans.

In this study, it has been demonstrated that MBC-PDOs preserve both receptor statuses and hotspot mutations across numerous passages. Hence, MBC-PDOs provide a reliable platform for pre-clinical assessment of therapeutic effectiveness of the AdCAR-T system. For visualization and analysis of target cell lysis, MBC-PDO lines were virally transduced to express luciferase and GFP, sorted via FACS and expanded to be used in the assays. This approach requires multiple weeks to be carried out and can lead to the selection of some of the heterogeneous tumor cells. However, in our case, the risk of selection is negligible, as we assessed the targeting efficacy of various LLE-mAbs on immunophenotyped MBC-PDOs using the AdCAR system as a proof of concept.

We conducted a comprehensive flow cytometry analysis of target antigen expression patterns in MBC-PDOs, revealing interpatient heterogeneity (**Figure 21B**). These results clearly display the necessity for patient-individualized treatment approaches. We tested AdCAR-T cells with a variety of LLE-mAbs that target different antigens on MCF-7 and MBC-PDOs. Most of the targets used in this study harbor clinical relevance [97]. In accordance with individual antigen

expression profiles, AdCAR-T combined with LLE-mAbs resulted in specific lysis of MBC-PDOs, which correlated with antigen expression levels. For instance, MBC-PDO #03 revealed minor levels of EGFR and high levels of CD276, HER2, TROP2, and EpCAM expression (**Figure 25A**). Consequently, AdCAR-mediated cytolysis using LLE-EGFR mAbs was low (38-58%), while the treatments with LLE-CD276, LLE-HER2, LLE-TROP2, and LLE-EpCAM resulted in complete target cell lysis (**Figure 25A**).

Here, we demonstrate the possibility of analyzing individual target antigen expression profiles and validating the efficacy of specific targeting on MBC-PDOs. Additionally, we highlight the potential of AdCAR-T as a tool for precision immunotherapy which allows personalized selection of target antigens. By reshaping clinically tested and approved mAbs into LLE-mAbs, this approach can allow clinical translation and availability of targeted cellular therapies to heterogeneous patient cohorts. Our MBC-PDO-based *in vitro* platform in combination with AdCAR-T cells pave the way for precision immunotherapy in female malignancies and can further be applied in the assessment of existing and novel therapeutic approaches.

4.5 Conclusions

In recent decades, cell lines and animal models were the gold standard in BC research. While both approaches present profitable advantages, they also have their limits, which can be overcome by patient-derived organoid models. Therefore, PDOs were established with promising benefits for clinical applications [71, 76]. However, PDOs are often derived from primary tumor samples, which do not necessarily represent the advanced stages of cancer diseases.

Here, we established MBC-PDOs that represent metastatic BC by utilizing MA and MPE from patients with advanced BC. Our goal was to use these models for characterization and functional testing as proof of principle. We have demonstrated that MBC-PDOs represent the characteristics of their original sample derived from MA and MPE and serve as a valuable model that can be applied in a preclinical setting for guiding therapy decisions. Also, correlating genomic and proteomic analysis with drug screenings can be useful in finding novel biomarkers for drug response in the future. A fast turnaround time for organoid culture establishment and drug efficacy assessment is required when treating patients with MBC. With our approach, culturing and drug screening of MBC-PDOs can occur within two weeks.

So far, therapy proposals depend on clinical studies, and rarely take interpatient heterogeneity in drug response into account. However, with additional models, biomarkers and hypotheses can be thoroughly investigated in our setup. Furthermore, the numerous challenges metastatic BC faces such as heterogeneity and treatment-resistance can be addressed.

As metastatic samples are very rare, MA and MPE can serve as a convenient source of metastatic cells for the establishment of PDOs. Yet only a minority of cancer patients develop MA or MPE. Therefore, gained knowledge and experience from our models can be applied to further sources of metastatic biopsies. These should be introduced as a novel standard in pathological and experimental applications. Consequently, the biobank of MBC-PDO models can be extended to operate as a pre-clinical evaluation platform.

For instance, efforts could be directed towards the extraction of metastatic cells from blood samples, also known as liquid biopsies. Liquid biopsies are non-invasive, offer the monitoring of patients' tumor dynamics, and can help guiding personalized treatment decisions [140]. Challenges of this approach include uncertainty in terms of sampling the complete genomic clones within a tumor as well as detection of rare variants and components [140].

Nevertheless, with sufficient source material, further research fields, such as cell-based immunotherapy including CAR-T cell technology, can be explored utilizing MBC-PDOs.

The progress of treating BC with CAR-T cell-based therapy highly depends on discovering suitable TAAs, which is especially important in TNBC. The AdCAR-T system proposes a new method to tackle these limitations. Furthermore, AdCAR-T cells permit flexible targeting of multiple TAAs to avoid antigen escape and facilitate personalized targeting decisions.

This work demonstrates that MBC-PDO lines serve as a reliable *in vitro* platform that can be employed for the evaluation of therapeutic outcomes in metastatic BC applying molecular as well as cellular therapies in a high throughput manner. Our setup paves the way for the establishment of novel therapeutic approaches leading to precision therapy in female malignancies.

5 Supplementary material

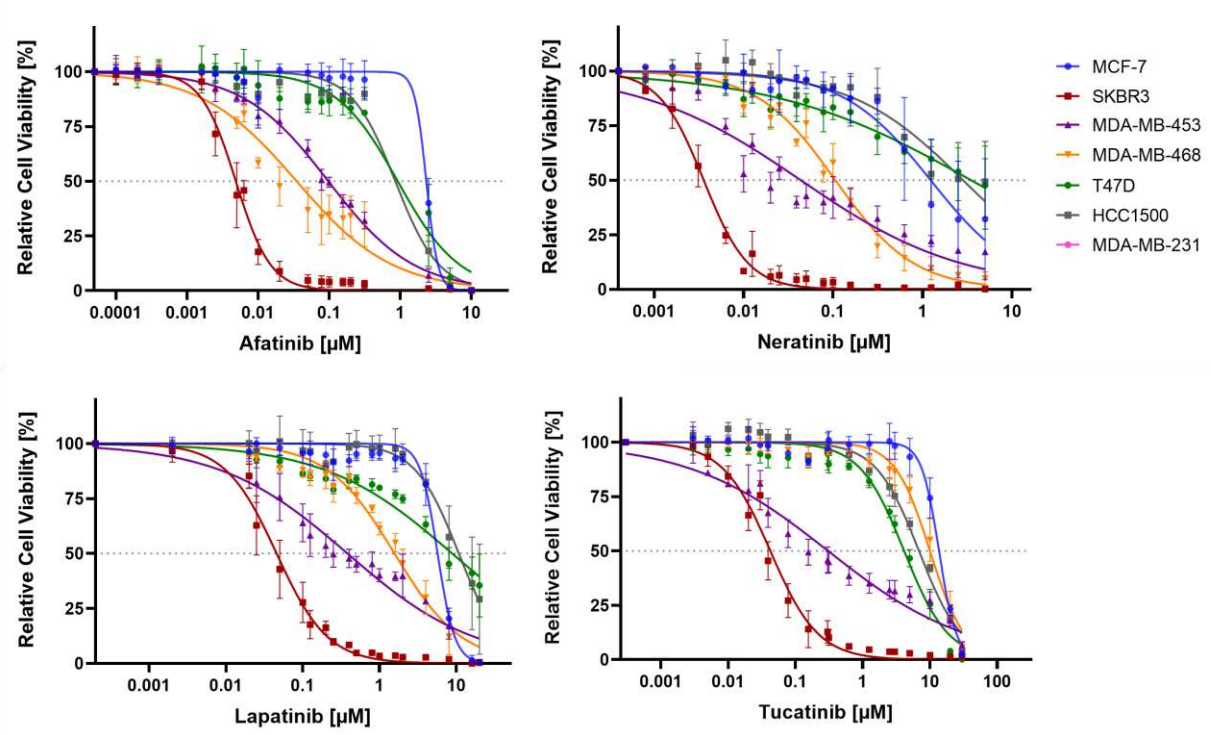

Supplementary Figure 1: 2D drug response curves with error bars of HER2 inhibitors Afatinib Neratinib, Lapatinib, and Tucatinib. *2D BC cell lines were treated with dilution series of HER2 inhibitors. For each drug, one replicate was done in clear plates and stained with Crystal Violet, and two replicates were carried out in white plates and cell viability was assessed with CellTiter Glo® 3D. Error bars representing SD of three independent experiments are illustrated here.*

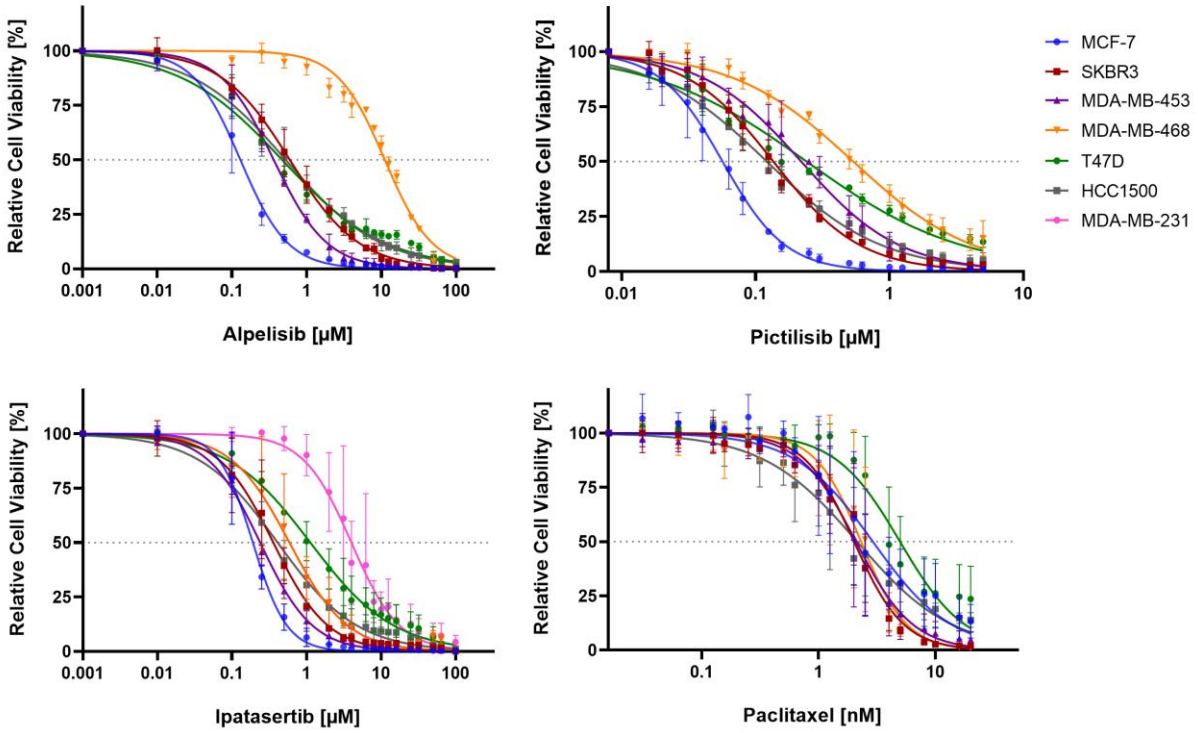

Supplementary Figure 2: 2D drug response curves with error bars of PI3K inhibitors Alpelisib and Pictilisib, as well as AKT inhibitor Ipatasertib and chemotherapeutic drug Paclitaxel. *2D BC cell lines were treated with dilution series of drugs. For each drug, one replicate was done in clear plates and stained with Crystal Violet, and two replicates were carried out in white plates and cell viability was assessed with CellTiter Glo® 3D. Error bars representing SD of three independent experiments are illustrated here.*

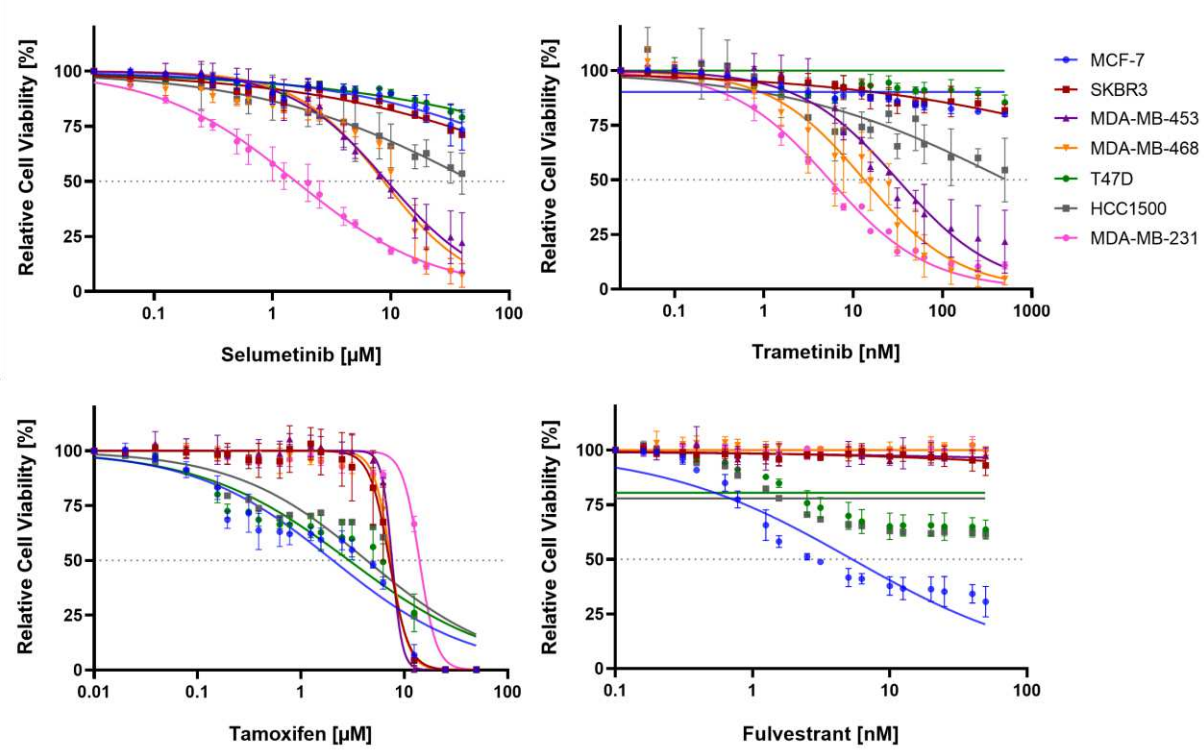

***Supplementary Figure 3*: 2D drug response curves with error bars of MEK inhibitors Selumetinib and Trametinib, as well as ER inhibitors Tamoxifen and Fulvestrant.** *2D BC cell lines were treated with dilution series of HER2 inhibitors. For each drug, one replicate was done in clear plates and stained with Crystal Violet, and two replicates were carried out in white plates and cell viability was assessed with CellTiter Glo® 3D. Error bars representing SD of three independent experiments are illustrated here.*

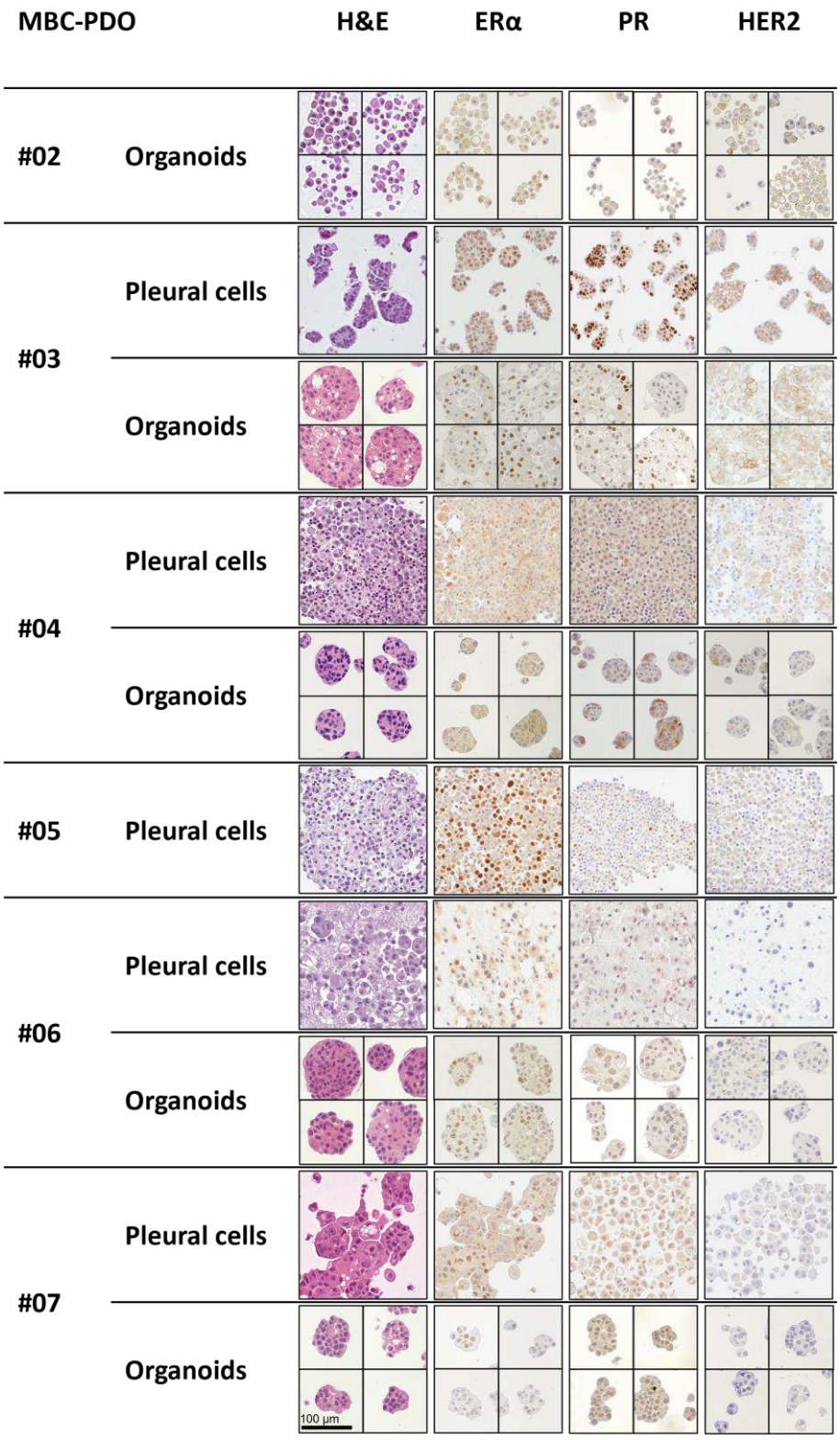

Supplementary Figure 4: Histological characterization of pleural BC cells and organoids derived from MA and MPE. *Histology (H&E staining) and receptor status of pleural cells (including cells from MA) and organoids of MBC-PDO lines are shown. Organoids consist exclusively of epithelial cells, while tissues often show tumor epithelium ringed by mesenchymal cells. The receptor status is maintained in the organoids. Scale bar: 100 µm.*

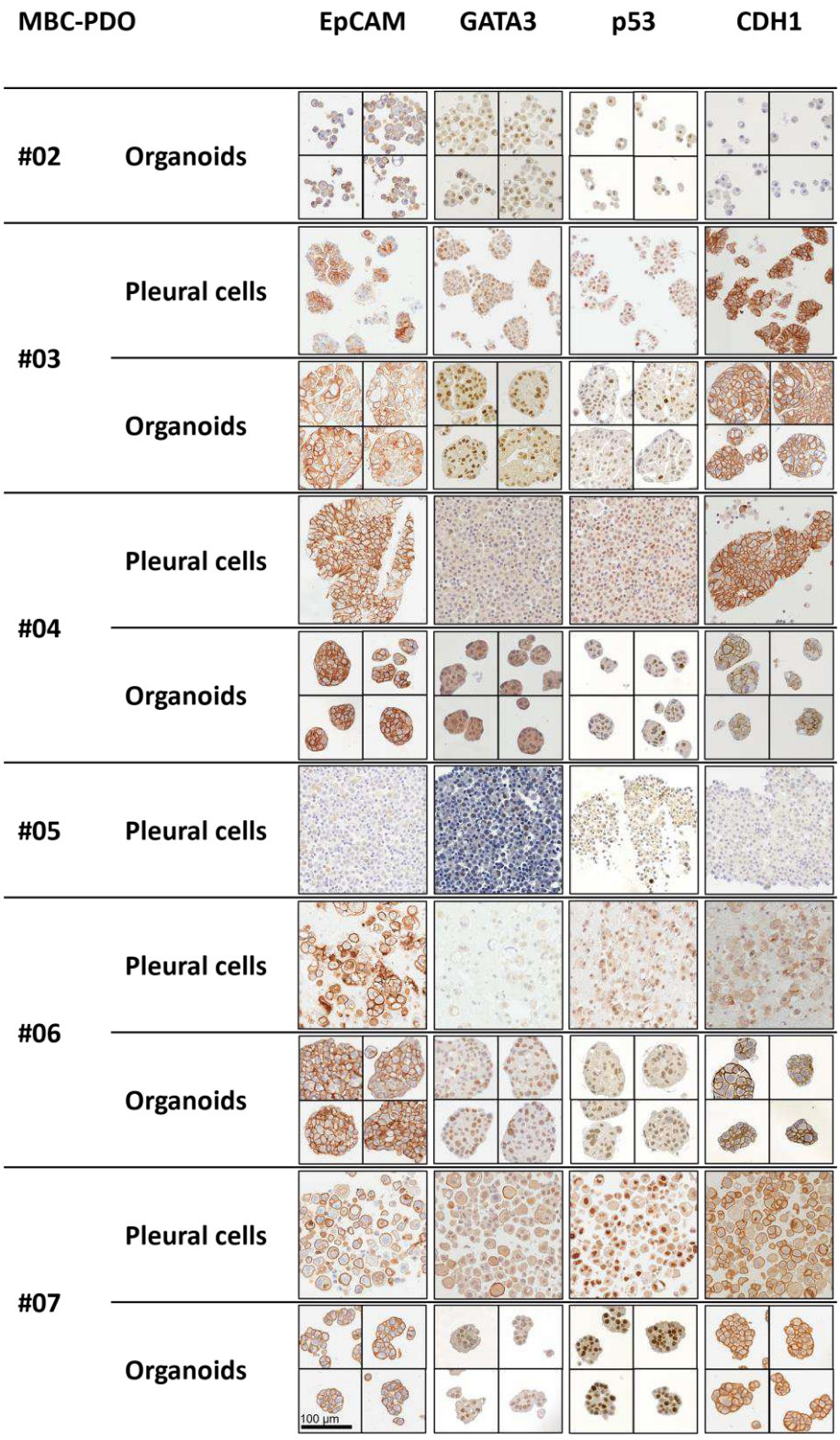

Supplementary Figure 5: EpCAM, GATA3, p53, and CDH1 expression in pleural BC cells and organoids derived from MA and MPE. *Expression profile of pleural cells (including cells from MA) and MBC-PDO lines is shown. The expression patterns of pleural cells are maintained in the corresponding MBC-PDO lines. Scale bar: 100 µm.*

6 List of references

1. Sung, H., J. Ferlay, R.L. Siegel, M. Laversanne, I. Soerjomataram, A. Jemal, and F. Bray, *Global Cancer Statistics 2020: GLOBOCAN Estimates of Incidence and Mortality Worldwide for 36 Cancers in 185 Countries.* CA Cancer J Clin, 2021. **71**(3): p. 209-249.
2. Turnbull, C. and N. Rahman, *Genetic predisposition to breast cancer: past, present, and future.* Annu Rev Genomics Hum Genet, 2008. **9**: p. 321-45.
3. American Cancer Society. *Key Statistics for Breast Cancer*. January 17, 2024 [Access Date: April 7, 2024]; Available from: https://www.cancer.org/cancer/breast-cancer/about/how-common-is-breast-cancer.html.
4. Bray, F., P. McCarron, and D.M. Parkin, *The changing global patterns of female breast cancer incidence and mortality.* Breast Cancer Res, 2004. **6**(6): p. 229-39.
5. Ma, H., L. Bernstein, R.K. Ross, and G. Ursin, *Hormone-related risk factors for breast cancer in women under age 50 years by estrogen and progesterone receptor status: results from a case-control and a case-case comparison.* Breast Cancer Res, 2006. **8**(4): p. R39.
6. Stordal, B., *Breastfeeding reduces the risk of breast cancer: A call for action in high-income countries with low rates of breastfeeding.* Cancer Med, 2023. **12**(4): p. 4616-4625.
7. Parkin, D.M., F. Bray, J. Ferlay, and P. Pisani, *Global cancer statistics, 2002.* CA Cancer J Clin, 2005. **55**(2): p. 74-108.
8. Jemal, A., R. Siegel, E. Ward, Y. Hao, J. Xu, and M.J. Thun, *Cancer statistics, 2009.* CA Cancer J Clin, 2009. **59**(4): p. 225-49.
9. Weigelt, B., F.C. Geyer, and J.S. Reis-Filho, *Histological types of breast cancer: how special are they?* Mol Oncol, 2010. **4**(3): p. 192-208.
10. Harbeck, N., F. Penault-Llorca, J. Cortes, M. Gnant, N. Houssami, P. Poortmans, K. Ruddy, J. Tsang, and F. Cardoso, *Breast cancer.* Nat Rev Dis Primers, 2019. **5**(1): p. 66.
11. Weigelt, B., H.M. Horlings, B. Kreike, M.M. Hayes, M. Hauptmann, L.F. Wessels, D. de Jong, M.J. Van de Vijver, L.J. Van't Veer, and J.L. Peterse, *Refinement of breast cancer classification by molecular characterization of histological special types.* J Pathol, 2008. **216**(2): p. 141-50.
12. Perou, C.M., T. Sorlie, M.B. Eisen, M. van de Rijn, S.S. Jeffrey, C.A. Rees, J.R. Pollack, D.T. Ross, H. Johnsen, L.A. Akslen, et al., *Molecular portraits of human breast tumours.* Nature, 2000. **406**(6797): p. 747-52.
13. Sorlie, T., C.M. Perou, R. Tibshirani, T. Aas, S. Geisler, H. Johnsen, T. Hastie, M.B. Eisen, M. van de Rijn, S.S. Jeffrey, et al., *Gene expression patterns of breast carcinomas distinguish tumor subclasses with clinical implications.* Proc Natl Acad Sci U S A, 2001. **98**(19): p. 10869-74.

14. Goldhirsch, A., J.N. Ingle, R.D. Gelber, A.S. Coates, B. Thurlimann, H.J. Senn, and m. Panel, *Thresholds for therapies: highlights of the St Gallen International Expert Consensus on the primary therapy of early breast cancer 2009.* Ann Oncol, 2009. **20**(8): p. 1319-29.
15. Baretta, Z., S. Mocellin, E. Goldin, O.I. Olopade, and D. Huo, *Effect of BRCA germline mutations on breast cancer prognosis: A systematic review and meta-analysis.* Medicine (Baltimore), 2016. **95**(40): p. e4975.
16. Shahbandi, A., H.D. Nguyen, and J.G. Jackson, *TP53 Mutations and Outcomes in Breast Cancer: Reading beyond the Headlines.* Trends Cancer, 2020. **6**(2): p. 98-110.
17. Cancer Genome Atlas, N., *Comprehensive molecular portraits of human breast tumours.* Nature, 2012. **490**(7418): p. 61-70.
18. Mahdavi, M., M. Nassiri, M.M. Kooshyar, M. Vakili-Azghandi, A. Avan, R. Sandry, S. Pillai, A.K. Lam, and V. Gopalan, *Hereditary breast cancer; Genetic penetrance and current status with BRCA.* J Cell Physiol, 2019. **234**(5): p. 5741-5750.
19. Girardi, A., F. Magnoni, E. Vicini, A. Kouloura, C. La Vecchia, P. Veronesi, and G. Corso, *CDH1 germline mutations in families with hereditary lobular breast cancer.* Eur J Cancer Prev, 2022. **31**(3): p. 274-278.
20. Takaku, M., S.A. Grimm, and P.A. Wade, *GATA3 in Breast Cancer: Tumor Suppressor or Oncogene?* Gene Expr, 2015. **16**(4): p. 163-8.
21. Kruger, D.T., M. Opdam, J. Sanders, V. van der Noort, E. Boven, and S.C. Linn, *Hierarchical clustering of PI3K and MAPK pathway proteins in breast cancer intrinsic subtypes.* APMIS, 2020. **128**(4): p. 298-307.
22. Campbell, I.G., S.E. Russell, D.Y. Choong, K.G. Montgomery, M.L. Ciavarella, C.S. Hooi, B.E. Cristiano, R.B. Pearson, and W.A. Phillips, *Mutation of the PIK3CA gene in ovarian and breast cancer.* Cancer Res, 2004. **64**(21): p. 7678-81.
23. Carpten, J.D., A.L. Faber, C. Horn, G.P. Donoho, S.L. Briggs, C.M. Robbins, G. Hostetter, S. Boguslawski, T.Y. Moses, S. Savage, et al., *A transforming mutation in the pleckstrin homology domain of AKT1 in cancer.* Nature, 2007. **448**(7152): p. 439-44.
24. Martinez-Saez, O., N. Chic, T. Pascual, B. Adamo, M. Vidal, B. Gonzalez-Farre, E. Sanfeliu, F. Schettini, B. Conte, F. Braso-Maristany, et al., *Frequency and spectrum of PIK3CA somatic mutations in breast cancer.* Breast Cancer Res, 2020. **22**(1): p. 45.
25. Shimoi, T., A. Hamada, M. Yamagishi, M. Hirai, M. Yoshida, T. Nishikawa, K. Sudo, A. Shimomura, E. Noguchi, M. Yunokawa, et al., *PIK3CA mutation profiling in patients with breast cancer, using a highly sensitive detection system.* Cancer Sci, 2018. **109**(8): p. 2558-2566.

26. Rudolph, M., T. Anzeneder, A. Schulz, G. Beckmann, A.T. Byrne, M. Jeffers, C. Pena, O. Politz, K. Kochert, R. Vonk, et al., *AKT1 (E17K) mutation profiling in breast cancer: prevalence, concurrent oncogenic alterations, and blood-based detection.* BMC Cancer, 2016. **16**: p. 622.

27. Beaver, J.A., J.P. Gustin, K.H. Yi, A. Rajpurohit, M. Thomas, S.F. Gilbert, D.M. Rosen, B. Ho Park, and J. Lauring, *PIK3CA and AKT1 mutations have distinct effects on sensitivity to targeted pathway inhibitors in an isogenic luminal breast cancer model system.* Clin Cancer Res, 2013. **19**(19): p. 5413-22.

28. American Cancer Society. *Treating Breast Cancer*. [Access Date: April 7, 2024]; Available from: https://www.cancer.org/cancer/breast-cancer/treatment.html.

29. *Breast cancer pathogenesis and histologic vs. molecular subtypes.* http://www.pathophys.org/wp-content/uploads/2012/12/breastcancer-copy.png.

30. Banys, M., I. Gruber, N. Krawczyk, S. Becker, R. Kurth, D. Wallwiener, J. Jakubowska, J. Hoffmann, R. Rothmund, A. Staebler, et al., *Hematogenous and lymphatic tumor cell dissemination may be detected in patients diagnosed with ductal carcinoma in situ of the breast.* Breast Cancer Res Treat, 2012. **131**(3): p. 801-8.

31. Hartkopf, A.D., M. Banys, N. Krawczyk, A. Staebler, S. Becker, J. Hoffmann, M. Hahn, M. Wallwiener, and T. Fehm, *Bone marrow versus sentinel lymph node involvement in breast cancer: a comparison of early hematogenous and early lymphatic tumor spread.* Breast Cancer Res Treat, 2012. **131**(2): p. 501-8.

32. Pedersen, R.N., B.O. Esen, L. Mellemkjaer, P. Christiansen, B. Ejlertsen, T.L. Lash, M. Norgaard, and D. Cronin-Fenton, *The Incidence of Breast Cancer Recurrence 10-32 Years After Primary Diagnosis.* J Natl Cancer Inst, 2022. **114**(3): p. 391-399.

33. Friberg, S. and A. Nystrom, *Cancer Metastases: Early Dissemination and Late Recurrences.* Cancer Growth Metastasis, 2015. **8**: p. 43-9.

34. Pasha, N. and N.C. Turner, *Understanding and overcoming tumor heterogeneity in metastatic breast cancer treatment.* Nat Cancer, 2021. **2**(7): p. 680-692.

35. Aurilio, G., D. Disalvatore, G. Pruneri, V. Bagnardi, G. Viale, G. Curigliano, L. Adamoli, E. Munzone, A. Sciandivasci, F. De Vita, et al., *A meta-analysis of oestrogen receptor, progesterone receptor and human epidermal growth factor receptor 2 discordance between primary breast cancer and metastases.* Eur J Cancer, 2014. **50**(2): p. 277-89.

36. Angus, L., M. Smid, S.M. Wilting, J. van Riet, A. Van Hoeck, L. Nguyen, S. Nik-Zainal, T.G. Steenbruggen, V.C.G. Tjan-Heijnen, M. Labots, et al., *The genomic landscape of metastatic breast cancer highlights changes in mutation and signature frequencies.* Nat Genet, 2019. **51**(10): p. 1450-1458.

37. Curigliano, G., V. Bagnardi, G. Viale, L. Fumagalli, N. Rotmensz, G. Aurilio, M. Locatelli, G. Pruneri, S. Giudici, M. Bellomi, et al., *Should liver metastases of breast cancer be biopsied to improve treatment choice?* Ann Oncol, 2011. **22**(10): p. 2227-33.
38. Botteri, E., D. Disalvatore, G. Curigliano, J. Brollo, V. Bagnardi, G. Viale, F. Orsi, A. Goldhirsch, and N. Rotmensz, *Biopsy of liver metastasis for women with breast cancer: impact on survival.* Breast, 2012. **21**(3): p. 284-8.
39. Walter, V., C. Fischer, T.M. Deutsch, C. Ersing, J. Nees, F. Schutz, C. Fremd, E.M. Grischke, P. Sinn, S.Y. Brucker, et al., *Estrogen, progesterone, and human epidermal growth factor receptor 2 discordance between primary and metastatic breast cancer.* Breast Cancer Res Treat, 2020. **183**(1): p. 137-144.
40. Becker, G., D. Galandi, and H.E. Blum, *Malignant ascites: systematic review and guideline for treatment.* Eur J Cancer, 2006. **42**(5): p. 589-97.
41. Dipper, A., H.E. Jones, R. Bhatnagar, N.J. Preston, N. Maskell, and A.O. Clive, *Interventions for the management of malignant pleural effusions: a network meta-analysis.* Cochrane Database Syst Rev, 2020. **4**(4): p. CD010529.
42. Weichselbaum, R., A. Marck, and S. Hellman, *Pathogenesis of pleural effusion in carcinoma of the breast.* Int J Radiat Oncol Biol Phys, 1977. **2**(9-10): p. 963-5.
43. Ayantunde, A.A. and S.L. Parsons, *Pattern and prognostic factors in patients with malignant ascites: a retrospective study.* Ann Oncol, 2007. **18**(5): p. 945-9.
44. Roberts, M.E., E. Neville, R.G. Berrisford, G. Antunes, N.J. Ali, and B.T.S.P.D.G. Group, *Management of a malignant pleural effusion: British Thoracic Society Pleural Disease Guideline 2010.* Thorax, 2010. **65 Suppl 2**: p. ii32-40.
45. Bielsa, S., A. Salud, M. Martinez, A. Esquerda, A. Martin, F. Rodriguez-Panadero, and J.M. Porcel, *Prognostic significance of pleural fluid data in patients with malignant effusion.* Eur J Intern Med, 2008. **19**(5): p. 334-9.
46. Zamboni, M.M., C.T. da Silva, Jr., R. Baretta, E.T. Cunha, and G.P. Cardoso, *Important prognostic factors for survival in patients with malignant pleural effusion.* BMC Pulm Med, 2015. **15**: p. 29.
47. Wu, H., H. Ji, W. Yang, M. Zhang, Y. Guo, B. Li, J. Wang, R. Chen, Y. Chen, and X. Wang, *Liquid biopsy using ascitic fluid and pleural effusion supernatants for genomic profiling in gastrointestinal and lung cancers.* BMC Cancer, 2022. **22**(1): p. 1020.
48. Sorolla, M.A., A. Sorolla, E. Parisi, A. Salud, and J.M. Porcel, *Diving into the Pleural Fluid: Liquid Biopsy for Metastatic Malignant Pleural Effusions.* Cancers (Basel), 2021. **13**(11).
49. Jeffries, J., M. Gayed, T.G.V. Ha, and R. Navuluri, *Management of Malignant Pleural Effusions and Malignancy-Related Ascites.* Semin Intervent Radiol, 2020. **37**(4): p. 434-440.

50. Jiang, L., P. Li, Z. Gong, B. Hu, J. Ma, J. Wang, H. Chu, L. Zhang, P. Sun, and J. Chen, *Effective Treatment for Malignant Pleural Effusion and Ascites with Combined Therapy of Bevacizumab and Cisplatin.* Anticancer Res, 2016. **36**(3): p. 1313-8.
51. Yang, L. and Y. Wang, *Malignant pleural effusion diagnosis and therapy.* Open Life Sci, 2023. **18**(1): p. 20220575.
52. Cailleau, R., M. Olive, and Q.V. Cruciger, *Long-term human breast carcinoma cell lines of metastatic origin: preliminary characterization.* In Vitro, 1978. **14**(11): p. 911-5.
53. Soule, H.D., J. Vazguez, A. Long, S. Albert, and M. Brennan, *A human cell line from a pleural effusion derived from a breast carcinoma.* J Natl Cancer Inst, 1973. **51**(5): p. 1409-16.
54. Holliday, D.L. and V. Speirs, *Choosing the right cell line for breast cancer research.* Breast Cancer Res, 2011. **13**(4): p. 215.
55. Yen, T.Y., N. Haste, L.C. Timpe, C. Litsakos-Cheung, R. Yen, and B.A. Macher, *Using a cell line breast cancer progression system to identify biomarker candidates.* J Proteomics, 2014. **96**: p. 173-83.
56. Jia, Y., Y. Chen, Q. Wang, U. Jayasinghe, X. Luo, Q. Wei, J. Wang, H. Xiong, C. Chen, B. Xu, et al., *Exosome: emerging biomarker in breast cancer.* Oncotarget, 2017. **8**(25): p. 41717-41733.
57. Wang, H.Y., D. Greenawalt, X. Cui, I.V. Tereshchenko, M. Luo, Q. Yang, M.A. Azaro, G. Hu, Y. Chu, J.Y. Li, et al., *Identification of possible genetic alterations in the breast cancer cell line MCF-7 using high-density SNP genotyping microarray.* J Carcinog, 2009. **8**: p. 6.
58. Kitaeva, K.V., C.S. Rutland, A.A. Rizvanov, and V.V. Solovyeva, *Cell Culture Based in vitro Test Systems for Anticancer Drug Screening.* Front Bioeng Biotechnol, 2020. **8**: p. 322.
59. Cao, X., B. Li, J. Chen, J. Dang, S. Chen, E.G. Gunes, B. Xu, L. Tian, S. Muend, M. Raoof, et al., *Effect of cabazitaxel on macrophages improves CD47-targeted immunotherapy for triple-negative breast cancer.* J Immunother Cancer, 2021. **9**(3).
60. Hah, N. and W.L. Kraus, *Hormone-regulated transcriptomes: lessons learned from estrogen signaling pathways in breast cancer cells.* Mol Cell Endocrinol, 2014. **382**(1): p. 652-664.
61. Brodie, A., D. Jelovac, G. Sabnis, B. Long, L. Macedo, and O. Goloubeva, *Model systems: mechanisms involved in the loss of sensitivity to letrozole.* J Steroid Biochem Mol Biol, 2005. **95**(1-5): p. 41-8.
62. Watanabe, S., K. Yonesaka, J. Tanizaki, Y. Nonagase, N. Takegawa, K. Haratani, H. Kawakami, H. Hayashi, M. Takeda, J. Tsurutani, et al., *Targeting of the HER2/HER3 signaling axis overcomes ligand-mediated resistance to trastuzumab in HER2-positive breast cancer.* Cancer Med, 2019. **8**(3): p. 1258-1268.
63. Collins, D.M., S.F. Madden, N. Gaynor, D. AlSultan, M. Le Gal, A.J. Eustace, K.A. Gately, C. Hughes, A.M. Davies, T. Mahgoub, et al., *Effects of HER Family-targeting Tyrosine Kinase*

Inhibitors on Antibody-dependent Cell-mediated Cytotoxicity in HER2-expressing Breast Cancer. Clin Cancer Res, 2021. **27**(3): p. 807-818.

64. Sahu, P., I.G. Camarillo, and R. Sundararajan, *Enhanced Antiproliferation Potency of Electrical Pulse-Mediated Metformin and Cisplatin Combination Therapy on MDA-MB-231 Cells.* Appl Biochem Biotechnol, 2022. **194**(1): p. 18-36.
65. Burdall, S.E., A.M. Hanby, M.R. Lansdown, and V. Speirs, *Breast cancer cell lines: friend or foe?* Breast Cancer Res, 2003. **5**(2): p. 89-95.
66. Vargo-Gogola, T. and J.M. Rosen, *Modelling breast cancer: one size does not fit all.* Nat Rev Cancer, 2007. **7**(9): p. 659-72.
67. Bahcecioglu, G., G. Basara, B.W. Ellis, X. Ren, and P. Zorlutuna, *Breast cancer models: Engineering the tumor microenvironment.* Acta Biomater, 2020. **106**: p. 1-21.
68. Hofer, M. and M.P. Lutolf, *Engineering organoids.* Nat Rev Mater, 2021. **6**(5): p. 402-420.
69. Zhao, Z., X. Chen, A.M. Dowbaj, A. Sljukic, K. Bratlie, L. Lin, E.L.S. Fong, G.M. Balachander, Z. Chen, A. Soragni, et al., *Organoids.* Nat Rev Methods Primers, 2022. **2**.
70. Wensink, G.E., S.G. Elias, J. Mullenders, M. Koopman, S.F. Boj, O.W. Kranenburg, and J.M.L. Roodhart, *Patient-derived organoids as a predictive biomarker for treatment response in cancer patients.* NPJ Precis Oncol, 2021. **5**(1): p. 30.
71. Sachs, N., J. de Ligt, O. Kopper, E. Gogola, G. Bounova, F. Weeber, A.V. Balgobind, K. Wind, A. Gracanin, H. Begthel, et al., *A Living Biobank of Breast Cancer Organoids Captures Disease Heterogeneity.* Cell, 2018. **172**(1-2): p. 373-386 e10.
72. Calar, K., S. Plesselova, S. Bhattacharya, M. Jorgensen, and P. de la Puente, *Human Plasma-Derived 3D Cultures Model Breast Cancer Treatment Responses and Predict Clinically Effective Drug Treatment Concentrations.* Cancers (Basel), 2020. **12**(7).
73. Katt, M.E., A.L. Placone, A.D. Wong, Z.S. Xu, and P.C. Searson, *In Vitro Tumor Models: Advantages, Disadvantages, Variables, and Selecting the Right Platform.* Front Bioeng Biotechnol, 2016. **4**: p. 12.
74. Friedrich, J., C. Seidel, R. Ebner, and L.A. Kunz-Schughart, *Spheroid-based drug screen: considerations and practical approach.* Nat Protoc, 2009. **4**(3): p. 309-24.
75. Ebrahimi, N., A. Nasr Esfahani, S. Samizade, A. Mansouri, M. Ghanaatian, S. Adelian, V. Shadman Manesh, and M.R. Hamblin, *The potential application of organoids in breast cancer research and treatment.* Hum Genet, 2022. **141**(2): p. 193-208.
76. Drost, J. and H. Clevers, *Organoids in cancer research.* Nat Rev Cancer, 2018. **18**(7): p. 407-418.
77. Larsson, P., H. Engqvist, J. Biermann, E. Werner Ronnerman, E. Forssell-Aronsson, A. Kovacs, P. Karlsson, K. Helou, and T.Z. Parris, *Optimization of cell viability assays to improve replicability and reproducibility of cancer drug sensitivity screens.* Sci Rep, 2020. **10**(1): p. 5798.

78. Trilla-Fuertes, L., A. Gamez-Pozo, J.M. Arevalillo, M. Diaz-Almiron, G. Prado-Vazquez, A. Zapater-Moros, H. Navarro, R. Aras-Lopez, I. Dapia, R. Lopez-Vacas, et al., *Molecular characterization of breast cancer cell response to metabolic drugs.* Oncotarget, 2018. **9**(11): p. 9645-9660.

79. Lv, Q., Z. Meng, Y. Yu, F. Jiang, D. Guan, C. Liang, J. Zhou, A. Lu, and G. Zhang, *Molecular Mechanisms and Translational Therapies for Human Epidermal Receptor 2 Positive Breast Cancer.* Int J Mol Sci, 2016. **17**(12).

80. Martinez-Pacheco, S. and L. O'Driscoll, *Pre-Clinical In Vitro Models Used in Cancer Research: Results of a Worldwide Survey.* Cancers (Basel), 2021. **13**(23).

81. Lin, A., C.J. Giuliano, A. Palladino, K.M. John, C. Abramowicz, M.L. Yuan, E.L. Sausville, D.A. Lukow, L. Liu, A.R. Chait, et al., *Off-target toxicity is a common mechanism of action of cancer drugs undergoing clinical trials.* Sci Transl Med, 2019. **11**(509).

82. Hsu, J.L. and M.C. Hung, *The role of HER2, EGFR, and other receptor tyrosine kinases in breast cancer.* Cancer Metastasis Rev, 2016. **35**(4): p. 575-588.

83. Oh, D.Y. and Y.J. Bang, *HER2-targeted therapies - a role beyond breast cancer.* Nat Rev Clin Oncol, 2020. **17**(1): p. 33-48.

84. Schlam, I. and S.M. Swain, *HER2-positive breast cancer and tyrosine kinase inhibitors: the time is now.* NPJ Breast Cancer, 2021. **7**(1): p. 56.

85. Zhu, K., Y. Wu, P. He, Y. Fan, X. Zhong, H. Zheng, and T. Luo, *PI3K/AKT/mTOR-Targeted Therapy for Breast Cancer.* Cells, 2022. **11**(16).

86. Piezzo, M., S. Cocco, R. Caputo, D. Cianniello, G.D. Gioia, V.D. Lauro, G. Fusco, C. Martinelli, F. Nuzzo, M. Pensabene, et al., *Targeting Cell Cycle in Breast Cancer: CDK4/6 Inhibitors.* Int J Mol Sci, 2020. **21**(18).

87. Wang, J., S. Jain, C.R. Coombes, and C. Palmieri, *Fulvestrant in advanced breast cancer following tamoxifen and aromatase inhibition: a single center experience.* Breast J, 2009. **15**(3): p. 247-53.

88. Tutt, A.N.J., J.E. Garber, B. Kaufman, G. Viale, D. Fumagalli, P. Rastogi, R.D. Gelber, E. de Azambuja, A. Fielding, J. Balmana, et al., *Adjuvant Olaparib for Patients with BRCA1- or BRCA2-Mutated Breast Cancer.* N Engl J Med, 2021. **384**(25): p. 2394-2405.

89. Hu, X.C., J. Zhang, B.H. Xu, L. Cai, J. Ragaz, Z.H. Wang, B.Y. Wang, Y.E. Teng, Z.S. Tong, Y.Y. Pan, et al., *Cisplatin plus gemcitabine versus paclitaxel plus gemcitabine as first-line therapy for metastatic triple-negative breast cancer (CBCSG006): a randomised, open-label, multicentre, phase 3 trial.* Lancet Oncol, 2015. **16**(4): p. 436-46.

90. Pandit, B. and M. Royzen, *Recent Development of Prodrugs of Gemcitabine.* Genes (Basel), 2022. **13**(3).

91. Abu Samaan, T.M., M. Samec, A. Liskova, P. Kubatka, and D. Busselberg, *Paclitaxel's Mechanistic and Clinical Effects on Breast Cancer.* Biomolecules, 2019. **9**(12).

92. Han, J., Y. Liu, S. Yang, X. Wu, H. Li, and Q. Wang, *MEK inhibitors for the treatment of non-small cell lung cancer.* J Hematol Oncol, 2021. **14**(1): p. 1.

93. Wester, L., S. Venneker, M. Hazenoot, C. Pont, E. Koedoot, A.M. Timmermans, J.W.M. Martens, M. Jansen, C.E.M. Kockx, I.W.F.J. van, et al., *A kinase inhibitor screen reveals MEK1/2 as a novel therapeutic target to antagonize IGF1R-mediated antiestrogen resistance in ERalpha-positive luminal breast cancer.* Biochem Pharmacol, 2022. **204**: p. 115233.

94. Ghanaatgar-Kasbi, S., M. Khazaei, A. Rastgar-Moghadam, G.A. Ferns, S.M. Hassanian, and A. Avan, *The Therapeutic Potential of MEK1/2 Inhibitors in the Treatment of Gynecological Cancers: Rational Strategies and Recent Progress.* Curr Cancer Drug Targets, 2020. **20**(6): p. 417-428.

95. Wang, J. and P. Zhou, *New Approaches in CAR-T Cell Immunotherapy for Breast Cancer.* Adv Exp Med Biol, 2017. **1026**: p. 371-381.

96. Sterner, R.C. and R.M. Sterner, *CAR-T cell therapy: current limitations and potential strategies.* Blood Cancer J, 2021. **11**(4): p. 69.

97. Yang, Y.H., J.W. Liu, C. Lu, and J.F. Wei, *CAR-T Cell Therapy for Breast Cancer: From Basic Research to Clinical Application.* Int J Biol Sci, 2022. **18**(6): p. 2609-2626.

98. Lu, J. and G. Jiang, *The journey of CAR-T therapy in hematological malignancies.* Mol Cancer, 2022. **21**(1): p. 194.

99. Han, D., Z. Xu, Y. Zhuang, Z. Ye, and Q. Qian, *Current Progress in CAR-T Cell Therapy for Hematological Malignancies.* J Cancer, 2021. **12**(2): p. 326-334.

100. Kim, D.W. and J.Y. Cho, *Recent Advances in Allogeneic CAR-T Cells.* Biomolecules, 2020. **10**(2).

101. Firor, A.E., A. Jares, and Y. Ma, *From humble beginnings to success in the clinic: Chimeric antigen receptor-modified T-cells and implications for immunotherapy.* Exp Biol Med (Maywood), 2015. **240**(8): p. 1087-98.

102. Sadelain, M., R. Brentjens, and I. Riviere, *The basic principles of chimeric antigen receptor design.* Cancer Discov, 2013. **3**(4): p. 388-98.

103. Chmielewski, M. and H. Abken, *TRUCKs: the fourth generation of CARs.* Expert Opin Biol Ther, 2015. **15**(8): p. 1145-54.

104. Kagoya, Y., S. Tanaka, T. Guo, M. Anczurowski, C.H. Wang, K. Saso, M.O. Butler, M.D. Minden, and N. Hirano, *A novel chimeric antigen receptor containing a JAK-STAT signaling domain mediates superior antitumor effects.* Nat Med, 2018. **24**(3): p. 352-359.

105. Mackall, C.L. and D.B. Miklos, *CNS Endothelial Cell Activation Emerges as a Driver of CAR T Cell-Associated Neurotoxicity.* Cancer Discov, 2017. **7**(12): p. 1371-1373.

106. Gardner, R., D. Wu, S. Cherian, M. Fang, L.A. Hanafi, O. Finney, H. Smithers, M.C. Jensen, S.R. Riddell, D.G. Maloney, et al., *Acquisition of a CD19-negative myeloid phenotype allows immune escape of MLL-rearranged B-ALL from CD19 CAR-T-cell therapy.* Blood, 2016. **127**(20): p. 2406-10.

107. Shalabi, H., I.L. Kraft, H.W. Wang, C.M. Yuan, B. Yates, C. Delbrook, J.D. Zimbelman, R. Giller, M. Stetler-Stevenson, E.S. Jaffe, et al., *Sequential loss of tumor surface antigens following chimeric antigen receptor T-cell therapies in diffuse large B-cell lymphoma.* Haematologica, 2018. **103**(5): p. e215-e218.

108. Seitz, C.M., J. Mittelstaet, D. Atar, J. Hau, S. Reiter, C. Illi, V. Kieble, F. Engert, B. Drees, G. Bender, et al., *Novel adapter CAR-T cell technology for precisely controllable multiplex cancer targeting.* Oncoimmunology, 2021. **10**(1): p. 2003532.

109. Atar, D., A.S. Mast, S. Scheuermann, L. Ruoff, C.M. Seitz, and P. Schlegel, *Adapter CAR T Cell Therapy for the Treatment of B-Lineage Lymphomas.* Biomedicines, 2022. **10**(10).

110. Grote, S., J. Mittelstaet, C. Baden, K.C. Chan, C. Seitz, P. Schlegel, A. Kaiser, R. Handgretinger, and S. Schleicher, *Adapter chimeric antigen receptor (AdCAR)-engineered NK-92 cells: an off-the-shelf cellular therapeutic for universal tumor targeting.* Oncoimmunology, 2020. **9**(1): p. 1825177.

111. Carter, M.E., A.D. Hartkopf, A. Wagner, L.L. Volmer, S.Y. Brucker, S. Berchtold, U.M. Lauer, and A. Koch, *A Three-Dimensional Organoid Model of Primary Breast Cancer to Investigate the Effects of Oncolytic Virotherapy.* Front Mol Biosci, 2022. **9**: p. 826302.

112. Goldhammer, N., J. Kim, V. Timmermans-Wielenga, and O.W. Petersen, *Characterization of organoid cultured human breast cancer.* Breast Cancer Res, 2019. **21**(1): p. 141.

113. Baker, C.L., C.P. Vaughn, and W.S. Samowitz, *A PIK3CA pyrosequencing-based assay that excludes pseudogene interference.* J Mol Diagn, 2012. **14**(1): p. 56-60.

114. Guzman, C., M. Bagga, A. Kaur, J. Westermarck, and D. Abankwa, *ColonyArea: an ImageJ plugin to automatically quantify colony formation in clonogenic assays.* PLoS One, 2014. **9**(3): p. e92444.

115. Seeger, H., X. Ruan, H. Neubauer, and A.O. Mueck, *Effect of drospirenone on proliferation of human benign and cancerous epithelial breast cells.* Horm Mol Biol Clin Investig, 2011. **6**(2): p. 211-4.

116. Yan, Y.Y., H. Bi, W. Zhang, Q. Wen, H. Liu, J.X. Li, H.Z. Zhang, Y.X. Zhang, and J.S. Li, *Downregulation and subcellular distribution of HER2 involved in MDA-MB-453 breast cancer cell apoptosis induced by lapatinib/celastrol combination.* J BUON, 2017. **22**(3): p. 644-651.

117. Spear, J.M., Z. Lu, and W.A. Russu, *Pharmacological Inhibition of CDK8 in Triple-Negative Breast Cancer Cell Line MDA-MB-468 Increases E2F1 Protein, Induces Phosphorylation of STAT3 and Apoptosis.* Molecules, 2020. **25**(23).

118. Wang, L., Q. Lu, K. Jiang, R. Hong, S. Wang, and F. Xu, *BRAF V600E Mutation in Triple-Negative Breast Cancer: A Case Report and Literature Review.* Oncol Res Treat, 2022. **45**(1-2): p. 54-61.

119. ATCC. *American Type Culture Collection*. [Access Date: April 7, 2024]; Available from: https://www.atcc.org/.

120. Dai, X., H. Cheng, Z. Bai, and J. Li, *Breast Cancer Cell Line Classification and Its Relevance with Breast Tumor Subtyping.* J Cancer, 2017. **8**(16): p. 3131-3141.

121. Smith, S.E., P. Mellor, A.K. Ward, S. Kendall, M. McDonald, F.S. Vizeacoumar, F.J. Vizeacoumar, S. Napper, and D.H. Anderson, *Molecular characterization of breast cancer cell lines through multiple omic approaches.* Breast Cancer Res, 2017. **19**(1): p. 65.

122. Cellosaurus. *Cellosaurus - a knowledge resource on cell lines*. [Access Date: April 7, 2024]; Available from: https://www.cellosaurus.org/.

123. COSMIC. *Cancer Sanger - Cell Lines*. [Access Date: April 7, 2024]; Available from: https://cancer.sanger.ac.uk/cell_lines.

124. Vuong, D., P.T. Simpson, B. Green, M.C. Cummings, and S.R. Lakhani, *Molecular classification of breast cancer.* Virchows Arch, 2014. **465**(1): p. 1-14.

125. Berthois, Y., J.A. Katzenellenbogen, and B.S. Katzenellenbogen, *Phenol red in tissue culture media is a weak estrogen: implications concerning the study of estrogen-responsive cells in culture.* Proc Natl Acad Sci U S A, 1986. **83**(8): p. 2496-500.

126. Lin, P.H., L.M. Tseng, Y.H. Lee, S.T. Chen, D.C. Yeh, M.S. Dai, L.C. Liu, M.Y. Wang, C. Lo, S. Chang, et al., *Neoadjuvant afatinib with paclitaxel for triple-negative breast cancer and the molecular characteristics in responders and non-responders.* J Formos Med Assoc, 2022. **121**(12): p. 2538-2547.

127. Schuler, M., A. Awada, P. Harter, J.L. Canon, K. Possinger, M. Schmidt, J. De Greve, P. Neven, L. Dirix, W. Jonat, et al., *A phase II trial to assess efficacy and safety of afatinib in extensively pretreated patients with HER2-negative metastatic breast cancer.* Breast Cancer Res Treat, 2012. **134**(3): p. 1149-59.

128. Shi, Z., J. Wulfkuhle, M. Nowicka, R.I. Gallagher, C. Saura, P.G. Nuciforo, I. Calvo, J. Andersen, J.L. Passos-Coelho, M.J. Gil-Gil, et al., *Functional Mapping of AKT Signaling and Biomarkers of Response from the FAIRLANE Trial of Neoadjuvant Ipatasertib plus Paclitaxel for Triple-Negative Breast Cancer.* Clin Cancer Res, 2022. **28**(5): p. 993-1003.

129. Cheng, Y. and H. Tian, *Current Development Status of MEK Inhibitors.* Molecules, 2017. **22**(10).

130. Corona, S.P. and D. Generali, *Abemaciclib: a CDK4/6 inhibitor for the treatment of HR+/HER2- advanced breast cancer.* Drug Des Devel Ther, 2018. **12**: p. 321-330.

131. Finn, R.S., J.P. Crown, J. Ettl, M. Schmidt, I.M. Bondarenko, I. Lang, T. Pinter, K. Boer, R. Patel, S. Randolph, et al., *Efficacy and safety of palbociclib in combination with letrozole as first-line treatment of ER-positive, HER2-negative, advanced breast cancer: expanded analyses of subgroups from the randomized pivotal trial PALOMA-1/TRIO-18.* Breast Cancer Res, 2016. **18**(1): p. 67.

132. Shtivelband, M.I., *Everolimus in hormone receptor-positive advanced breast cancer: targeting receptor-based mechanisms of resistance.* Breast, 2013. **22**(4): p. 405-10.

133. Braal, C.L., E.M. Jongbloed, S.M. Wilting, R.H.J. Mathijssen, S.L.W. Koolen, and A. Jager, *Inhibiting CDK4/6 in Breast Cancer with Palbociclib, Ribociclib, and Abemaciclib: Similarities and Differences.* Drugs, 2021. **81**(3): p. 317-331.

134. Onder, C.E., T.J. Ziegler, R. Becker, S.Y. Brucker, A.D. Hartkopf, T. Engler, and A. Koch, *Advancing Cancer Therapy Predictions with Patient-Derived Organoid Models of Metastatic Breast Cancer.* Cancers (Basel), 2023. **15**(14).

135. Arigami, T., N. Narita, R. Mizuno, L. Nguyen, X. Ye, A. Chung, A.E. Giuliano, and D.S. Hoon, *B7-h3 ligand expression by primary breast cancer and associated with regional nodal metastasis.* Ann Surg, 2010. **252**(6): p. 1044-51.

136. Liu, S., J. Liang, Z. Liu, C. Zhang, Y. Wang, A.H. Watson, C. Zhou, F. Zhang, K. Wu, F. Zhang, et al., *The Role of CD276 in Cancers.* Front Oncol, 2021. **11**: p. 654684.

137. Morgan, R.A., J.C. Yang, M. Kitano, M.E. Dudley, C.M. Laurencot, and S.A. Rosenberg, *Case report of a serious adverse event following the administration of T cells transduced with a chimeric antigen receptor recognizing ERBB2.* Mol Ther, 2010. **18**(4): p. 843-51.

138. Seitz, C.M., S. Schroeder, P. Knopf, A.C. Krahl, J. Hau, S. Schleicher, M. Martella, L. Quintanilla-Martinez, M. Kneilling, B. Pichler, et al., *GD2-targeted chimeric antigen receptor T cells prevent metastasis formation by elimination of breast cancer stem-like cells.* Oncoimmunology, 2020. **9**(1): p. 1683345.

139. Schepisi, G., C. Gianni, M. Palleschi, S. Bleve, C. Casadei, C. Lolli, L. Ridolfi, G. Martinelli, and U. De Giorgi, *The New Frontier of Immunotherapy: Chimeric Antigen Receptor T (CAR-T) Cell and Macrophage (CAR-M) Therapy against Breast Cancer.* Cancers (Basel), 2023. **15**(5).

140. Noor, J., A. Chaudhry, R. Noor, and S. Batool, *Advancements and Applications of Liquid Biopsies in Oncology: A Narrative Review.* Cureus, 2023. **15**(7): p. e42731.

7 Publications

Relevant for this thesis

1. Onder, C.E., T.J. Ziegler, R. Becker, S.Y. Brucker, A.D. Hartkopf, T. Engler, and A. Koch, Advancing Cancer Therapy Predictions with Patient-Derived Organoid Models of Metastatic Breast Cancer. Cancers (Basel), 2023. 15(14).

2. Onder, C.E., M. Moustafa-Oglou, S.M. Schroder, A.D. Hartkopf, A. Koch, and C.M. Seitz, Precision Immunotherapy Utilizing Adapter CAR-T Cells (AdCAR-T) in Metastatic Breast Cancer Leads to Target Specific Lysis. Cancers (Basel), 2023. 16(1).

Not relevant for this thesis

1. Orlich, M.M., R. Dieguez-Hurtado, R. Muehlfriedel, V. Sothilingam, H. Wolburg, C.E. Oender, P. Woelffing, C. Betsholtz, K. Gaengel, M. Seeliger, et al., Mural Cell SRF Controls Pericyte Migration, Vessel Patterning and Blood Flow. Circ Res, 2022. 131(4): p. 308-327.

2. Volmer, L.L., C.E. Önder, B. Volz, A.R. Singh, S.Y. Brucker, T. Engler, A.D. Hartkopf, and A. Koch, Microfluidic Isolation of Disseminated Tumor Cells from the Bone Marrow of Breast Cancer Patients. International Journal of Molecular Sciences, 2023. 24: p. 13930.

3. Anderle, N., F. Schafer-Ruoff, A. Staebler, N. Kersten, A. Koch, C. Onder, A.L. Keller, S. Liebscher, A. Hartkopf, M. Hahn, et al., Breast cancer patient-derived microtumors resemble tumor heterogeneity and enable protein-based stratification and functional validation of individualized drug treatment. J Exp Clin Cancer Res, 2023. 42(1): p. 210.

8 Declaration of contributions

This thesis was written by the author Cansu Ebru Önder with the exception that some contents were extracted from the author's publications as indicated in the beginning of each chapter. The author contributions of the two publications relevant for this thesis are listed on the following two pages.

The use of artificial intelligence (ChatGPT) was restricted to research information alongside Google and publications for some paragraphs of the introduction. Language aids including DeepL and Thesaurus were utilized sporadically.

Contribution to the publication that is included in this thesis

Titel of the paper: Advancing Cancer Therapy Predictions with Patient-Derived Organoid Models of Metastatic Breast Cancer

Authors contributed to the paper: Cansu E. Önder, Teresa J. Ziegler, Ronja Becker, Sara Y. Brucker, Andreas D. Hartkopf, Tobias Engler, André Koch

Author position: 1

Status in publication process: Published in Cancers (13th July 2023)

Detailed contribution to the publication

- **Scientific ideas (40% contributed by Cansu E. Önder)**
  - The initial idea was conceptualized by Dr. André Koch
  - Methodology originated from Dr. André Koch, Cansu E. Önder, Teresa J. Ziegler, and Ronja Becker
    - MBC-PDO culture establishment was carried out by the four authors
    - IHC staining protocol was established by Dr. Andre Koch
    - Experimental design for mutation analysis and drug assays was done by Cansu E. Önder
- **Data generation (75% contributed by Cansu E. Önder)**
  - MBC-PDO lines were cultured by Cansu E. Önder and Teresa J. Ziegler
  - IHC stainings were conducted by Teresa J. Ziegler and Ingrid Teufel
  - Mutation analysis was performed by Cansu E. Önder and Teresa J. Ziegler
  - Drug assays were performed by Cansu E. Önder
- **Analysis & interpretation (80% contributed by Cansu E. Önder)**
  - Data was mainly analyzed by Cansu E. Önder, with the aid from Teresa J. Ziegler
  - Interpretation was carried out by Cansu E. Önder, Teresa J. Ziegler, Ronja Becker, and Dr. André Koch
- **Paper writing (80% contributed by Cansu E. Önder)**
  - The first draft of the manuscript was completely written by Cansu E. Önder
  - This was further improved and revised first by Dr. André Koch, followed by the co-authors Dr. Tobias Engler, Prof. Dr. Andreas D. Hartkopf, and Prof. Dr. Sara Y. Brucker

Contribution to the publication that is included in this thesis

Titel of the manuscript: Precision Immunotherapy Utilizing Adapter CAR-T Cells (AdCAR-T) in Metastatic Breast Cancer Leads to Target Specific Lysis

Authors contributed to the paper: Cansu E. Önder, Moustafa Moustafa-Oglou, Sarah M. Schröder, Andreas D. Hartkopf, André Koch, Christian M. Seitz

Author position: 1 (shared first authorship with Moustafa Moustafa-Oglou)

Status in publication process: Published in Cancers (29th December 2023)

Detailed contribution to the manuscript

- **Scientific ideas (20% contributed by Cansu E. Önder)**
    - The initial idea was conceptualized by Dr. André Koch and Dr. Christian M. Seitz
    - Methodology originated from Dr. André Koch, Cansu E. Önder, Christian M. Seitz, and Moustafa-Moustafa-Oglou
        - Experimental design for cytotoxicity assays was done by Cansu E. Önder and Moustafa Moustafa-Oglou with input by Dr. André Koch and Dr. Christian M. Seitz
- **Data generation (50% contributed by Cansu E. Önder)**
    - Data of 2D assays was generated by Sarah M. Schröder
    - MBC-PDO culture establishment was carried out by Cansu E. Önder
    - Transduction, FACS, and flow cytometry was conducted by Moustafa Moustafa-Oglou
    - Cytotoxicity assays of MBC-PDOs were performed by Cansu E. Önder and Moustafa Moustafa-Oglou
- **Analysis & interpretation (60% contributed by Cansu E. Önder)**
    - Data was analyzed by Cansu E. Önder and Moustafa Moustafa-Oglou
    - Interpretation was carried out by Cansu E. Önder, Moustafa Moustafa-Oglou, Dr. André Koch, and Dr. Christian M. Seitz
- **Paper writing (60% contributed by Cansu E. Önder)**
    - The first draft of the manuscript was written by Cansu E. Önder and Moustafa Moustafa-Oglou
    - This was further improved and revised first by Dr. André Koch and Dr. Christian M. Seitz

9 Appendix (publications involved in this thesis)

9.1 Advancing Cancer Therapy Predictions with Patient-Derived Organoid Models of Metastatic Breast Cancer

Published paper in Cancers

9.2 Precision Immunotherapy Utilizing Adapter CAR-T Cells (AdCAR-T) in Metastatic Breast Cancer Leads to Target Specific Lysis

Published paper in Cancers

cancers

MDPI

Article

Advancing Cancer Therapy Predictions with Patient-Derived Organoid Models of Metastatic Breast Cancer

Cansu E. Önder [1], Teresa J. Ziegler [1], Ronja Becker [1], Sara Y. Brucker [1,2], Andreas D. Hartkopf [2], Tobias Engler [2] and André Koch [1,2,*]

[1] Research Institute for Women's Health, University of Tübingen, 72076 Tübingen, Germany
[2] Department of Women's Health, University of Tübingen, 72076 Tübingen, Germany
* Correspondence: andre.koch@med.uni-tuebingen.de; Tel.: +49-7071-29-85380

Simple Summary: A frequent disabling symptom during metastasized breast cancer is the development of ascites and pleural effusion, which is associated with poor outcomes. Malignant cells in ascites and pleural effusions derived from the primary tumor site indicate the spreading of cancer and can serve as a model for metastatic breast cancer. Therefore, we cultured metastatic cells from six patients with ascites or pleural effusion in a three-dimensional fashion to obtain organoids. The organoids recapitulated the characteristics of metastatic samples, as shown by immunohistochemistry and mutation analysis. Drug assays of organoids were performed to assess individual responses in a personalized manner. Overall, metastatic organoid cultures derived from malignant pleural effusion and malignant ascites demonstrated in vivo-like phenotypes and drug responses. Hence, these metastatic organoids can serve as an accurate model for the investigation of breast cancer progression and therapy predictions.

Abstract: The poor outcome of metastasized breast cancer (BC) stresses the need for reliable personalized oncology and the significance of models recapitulating the heterogeneous nature of BC. Here, we cultured metastatic tumor cells derived from advanced BC patients with malignant ascites (MA) or malignant pleural effusion (MPE) using organoid technology. We identified the characteristics of tumor organoids by applying immunohistochemistry and mutation analysis. Tumor organoids preserved their expression patterns and hotspot mutations when compared to their original metastatic counterpart and are consequently a well-suited in vitro model for metastasized BC. We treated the tumor organoids to implement a reliable application for drug screenings of metastasized cells. Drug assays revealed that responses are not always in accord with expression patterns, pathway activation, and hotspot mutations. The discrepancy between characterization and functional testing underlines the relevance of linking IHC stainings and mutational analysis of metastasized BC with in vitro drug assays. Our metastatic BC organoids recapitulate the characteristics of their original sample derived from MA and MPE and serve as an invaluable tool that can be utilized in a preclinical setting for guiding therapy decisions.

Keywords: metastasis; breast cancer; organoid culture; pleural effusion; ascites; drug response; cancer biology; personalized medicine; patient-derived organoids

Citation: Önder, C.E.; Ziegler, T.J.; Becker, R.; Brucker, S.Y.; Hartkopf, A.D.; Engler, T.; Koch, A. Advancing Cancer Therapy Predictions with Patient-Derived Organoid Models of Metastatic Breast Cancer. *Cancers* **2023**, *15*, 3602. https://doi.org/10.3390/cancers15143602

Academic Editors: Loretta L. del Mercat and Enza Lonardo

Received: 20 June 2023
Revised: 3 July 2023
Accepted: 11 July 2023
Published: 13 July 2023

1. Introduction

Breast cancer (BC) is the most prevalent type of cancer and one of the leading causes of cancer-associated deaths among women worldwide [1]. The most common kind is invasive BC of no special type (NST), also known as invasive ductal carcinoma (IDC), followed by the special type invasive lobular carcinoma (ILC) [2]. The status of estrogen receptor α (ERα), progesterone receptor (PR), and human epidermal growth factor receptor 2 (HER2) defines the subtype, determines the treatment, and predicts the prognosis [3–5]. Breast tumors that express ER and/or PR are categorized as "hormone receptor-positive", accounting for approximately 65% of cases. The second most common subtype, comprising about 15–20% of cases, involves tumors that overexpress HER2, either alone or in combination with

ER/PR. Tumors that do not express ER, PR, or HER2 are referred to as "triple-negative" and constitute around 10–15% of breast cancer cases [6].

Invasive tumor cells can spread through the bloodstream or the lymphatic system to different locations and organs of the body and form metastasis [7]. While primary BC is well understood and has favorable outcomes, metastatic BC remains a challenge. Heterogeneity is one of the causes of metastatic BC and a common reason why therapies are often not successful [8]. Additionally, metastatic BC has a poor prognosis due to persistent and treatment-resistant malignant cells and their impact on vital organs [8].

Due to the rarity of metastatic biopsies, therapy recommendation usually depends on the characteristics of primary tumors. However, it is important to note that primary tumors may not fully reflect the attributes of metastatic lesions, which often exhibit discordance in phenotypic markers such as ER, PR, and HER2 expression [9]. Moreover, there can be alterations in mutational signatures and mutational burden during the progression to metastasis [10]. Therefore, therapy decisions that are based on the characteristics of the primary tumor alone can result in a poor prognosis [11,12].

Malignant ascites (MA) and malignant pleural effusion (MPE) are a widespread concern for cancer patients and describe the presence of malignant cells in the peritoneal and pleural cavity [13,14]. BC is a frequent driver of MA and MPE, with 7% of BC patients developing MPE and 3% developing MA [15,16]. Patients suffering from MPE or MA endure a poor quality of life defined by chest and abdominal pain and difficulty breathing [16,17]. The median survival rate of these patients is relatively low and varies from 5 to 13 months [16,18,19]. MPE and MA, containing metastasized tumor cells, offer opportunities for metastatic biopsies since the fluid can be obtained through a simple puncture to relieve pressure and pain for the patients [20,21]. Consequently, MPE and MA present a beneficial source for the characterization of metastasized BC and the creation of in vitro models to improve therapy outcomes.

The poor prognosis of metastasized BC demonstrates the demand for reliable personalized oncology and the relevance of models representing the characteristics of BC. Cell lines, although widely used in BC research, only represent a small subset of the diversity of BC and are not capable of predicting specific drug responses for patients [19]. Patient-derived xenograft (PDX) models are utilized in translational research and considered crucial for drug development and response studies. Despite their value, high costs and limited efficiency interfere with the use of PDX models [22].

Patient-derived BC organoids, cultured in an extracellular matrix, have proven to be an important three-dimensional model for research as they accurately recapitulate the characteristics of their respective origin and can be used for long-term culturing [20]. Organoids of different sources have already been utilized in various methods including drug development and the determination of drug response [23]. Therefore, organoids have been shown to be inexpensive and valuable in vitro models for individualized oncology and high-throughput drug assays [24–26].

Since studies addressing BC organoids usually use primary tumor tissue for establishing patient-derived models [24,27,28], we focused exclusively on advanced-stage BC and derived models from MA and MPE, as there is an unmet clinical need in this condition. We further identified the characteristics of these metastatic BC patient-derived organoids (MBC-PDOs) using immunohistochemistry and mutation analysis. Our aim was to utilize these MBC-PDOs to establish a reliable application for drug screenings. Once established, representative organoids can further serve as models to study the most lethal BCs—drug-resistant, metastatic tumors. In the future, research on such patient-derived models could help prolong patients' survival time and improve their quality of life.

2. Materials and Methods

2.1. Patient Cohort

All MPE and MA samples were obtained from advanced BC patients treated at the Department of Women's Health in Tübingen after informed written consent. The study

was approved by the Ethics Committee of the Eberhard Karl University of Tübingen (Ethical approval 150/2018BO2 and 288/2022BO2) and is compliant with all relevant ethical regulations regarding research involving human participants. PE (by thoracentesis) and ascites (by paracentesis) from six patients with metastatic BC were collected in sterile containers. For full patient characteristics, see Table S1.

2.2. Culturing 2D Cell Lines

BC cell line MCF-7 was purchased from American Type Culture Collection (Manassas, VA, USA, HTB-22) and served as a control cell line for 3D drug response assays. Cells were cultured in DMEM-FBS (Dulbecco's Modified Eagle Medium (41965-062), containing 10% FBS (10270-106), 1% Pen/Strep (15140-122); all from Thermo Fisher, Waltham, MA, USA) and incubated at 37 °C and 5% CO_2. Cells were regularly checked for mycoplasma using a PCR Detection Kit (abm, Richmond, BC, Canada, G238).

2.3. Processing of Pleural Effusions and Ascites

MPE and MA samples were centrifuged at 500× *g* for 10 min. Cell pellets were pooled, and when necessary, red blood cells were lysed with 10 mL of RBC lysis buffer (155 mM NH_4Cl, 10 mM $KHCO_3$, 100 µM Na_2EDTA in H_2O, pH 7.4) on ice for 5–10 min. Cells were diluted in DPBS (Dulbecco's Phosphate Buffered Saline, Pan Biotech GmbH, Aidenbach, Germany, P04-36500) and centrifuged at 500× *g* for 10 min. The final cell pellet was resuspended in AdvDMEM+++ (Advanced DMEM/F-12 (12634-028), 1% Pen/Strep (15140-122), 1x GlutaMAXTM-I (35050-038), 10 mM HEPES (15630-056); all from Thermo Fisher). When applicable, the resulting pellet was subjected to 40 µm and 100 µm cell strainers (Greiner Bio-One GmbH, Frickenhausen, Germany, 42040 and 42000) to obtain various fractions and single-cell solutions. Fractions were used for cryopreservation, culturing organoids, and/or FFPE embedding.

2.4. Organoid Culture Setup

For organoid culture setup, the desired amount of cell suspension was mixed with Basement Membrane Extract (BME; Cultrex Reduced Growth Factor Basement Membrane Extract, Type 2 Select, Bio-techne, Minneapolis, MN, USA, 3533-005-02) at a ratio of 30% cell suspension to 70% BME. Twenty µL droplets were plated out on 48-well plates and placed upside down in an incubator (37 °C, 5% CO_2) to solidify for 30 min. BC culture medium (BCM; Table S2, composition previously described [24,27]) was added to each well and renewed every 3–4 days. Cells were incubated at 37 °C and 5% CO_2, and pictures were taken regularly with an EVOS M7000 microscope (Thermo Fisher).

2.5. Passaging of Organoid Cultures

MBC-PDOs were passaged every 7 to 21 days, depending on organoid size and density. Organoids were recovered from the wells by resuspending the BME droplets in ice-cold DPBS containing 5 µM Y-27632 (DPBS/Y-27632). The organoid suspension was centrifuged at 500× *g* for 10 min, and the supernatant was removed. The BME-organoid pellet was enzymatically dispersed with 1 mL of TrypLE Express Enzyme (1X; Thermo Fisher, 12604013) at 37 °C in a water bath for 5 min. The suspension was then centrifuged at 500× *g* for 10 min, and the supernatant was removed. For further culture, the desired amount of cell pellet was resuspended in AdvDMEM+++ and mixed with BME at a ratio of 30% cell suspension to 70% BME and cultured as described above. To stock organoids, passaged cells were cryopreserved in Recovery Cell Culture Freezing Medium (Thermo Fisher, Waltham, MA, USA, 12648010) and stored in cryovials in liquid nitrogen.

2.6. Three-Dimensional Drug Screening

For the heat-map assays, specific concentrations of the drugs were used. For the dose-dependent assays, dilution series of various drugs were prepared in BC medium. Drugs applied in the assays are listed in Table S3.

MBC-PDOs were passaged as follows: Two BME droplets containing organoids were resuspended in 500 µL of TrypLE, incubated at 37 °C for 10 min, and afterward thoroughly pipetted up and down to disrupt organoids into single cells. Cells were shortly spun down and resuspended in AdvDMEM+++. Cells were counted using the Bio-Rad TC20 Automated Cell Counter according to the manufacturer's protocol. To seed 1000 cells/well, the required cell number of each line was resuspended in BME in a ratio of 30% cell suspension and 70% BME. Three µL of this suspension, containing 1000 cells, was seeded in each well of white flat-bottom 96-well plates (Thermo Fisher, 136102). Plates were turned upside down and incubated at 37 °C and 5% CO_2 for 30 min. Finally, drug dilutions in BCM were added to the wells.

After four days of treatment, relative cell viability was determined using CellTiter-Glo 3D Cell Viability Assay reagent (Promega, Madison, WI, USA, G9682). The reagent was mixed 1:1 with the same volume of AdvDMEM+++. The content of the wells was removed, and 100 µL of reagent mixture (1:1 mix with AdvDMEM+++) was added to the wells. Then, plates were incubated at room temperature on an orbital plate shaker for 15 min (900 rpm). After a 10 min resting phase, luminescence values were read using a Varioskan LUX (Thermo Fisher). Assays were performed in technical triplicates. For the drug response curves, results were normalized to the lowest drug concentration. For the heat-map assay, results were normalized to viability in 0.1% DMSO (set as 100% cell viability).

2.7. Paraffin Sections and Immunohistochemistry of Tissue and MBC-PDOs

Samples were fixed in 4% formaldehyde, followed by dehydration, paraffin embedding, sectioning (2.5 µm), and standard hematoxylin and eosin (H&E) staining. Immunohistochemistry (IHC) was performed using the ZytoChem Plus HRP Polymer Kit (Zytomed Systems GmbH, Bargteheide, Germany, POLHRP-100) and DAB Substrate Kit (Zytomed Systems GmbH, DAB057) according to the manufacturer's protocol. IHC was performed using antibodies listed in Table S4. Images were captured with ScanScope (Leica, Wetzlar, Germany) or EVOS M7000 microscope (Thermo Fisher) and processed with Aperio ImageScope (version 12.4.6.5003), Image J (version 1.53e), and Photoshop (version 13.0.1).

2.8. Mutation Analysis

Four different hotspot regions were investigated for mutation analysis. Primers were designed using NCBI (see Table S5). The reverse primer for *PIK3CA* E542 and E545 mutation was designed based on a previous publication, to eliminate the amplification of a pseudogene [29]. Nucleic acids were extracted using the Quick-DNA/RNA miniprep kit (Zymo Research, Irvine, CA, USA, D7001) according to the manufacturer's protocol. DNA concentration was determined using a Varioskan LUX (Thermo Fisher).

Polymerase chain reaction (PCR) was performed by preparing 20 µL reactions with 1x Phusion HF buffer, 200 µM dNTPs, 0.5 µM of forward and reverse primer (Table S5), 40 ng of template DNA, 0.4 units Phusion DNA polymerase, and nuclease-free water up to 20 µL. After an initial denaturation at 98 °C for 60 s, PCR was run for 34 cycles: denaturation at 98 °C for 10 s, annealing at 62 °C for 30 s, elongation at 72 °C for 60 s. Final elongation was performed at 72 °C for 10 min. PCR products were analyzed via agarose gel electrophoresis and purified using the QIAquick PCR Purification Kit (QIAGEN GmbH, Hilden, Germany, 28106) according to the manufacturer's instructions. Amplified DNAs were sequenced by Eurofins Genomics Germany GmbH, applying Sanger sequencing. Results were analyzed and aligned using SnapGene Viewer (version 6.0.2).

3. Results

3.1. Establishing a Biobank of Metastasized BC Organoids Derived from Pleural Effusion and Ascites

To generate suitable models for metastasized BC, pleural effusion and ascites were obtained from patients with metastasized BC. Isolated tumor cells were seeded in BME droplets and cultured in BC medium as previously described [24]. Figure 1A shows an example of an established organoid line (MBC-PDO #07) that has been cultured for at least 10 passages. The morphology of the organoids was maintained in high passage (P) numbers. We successfully

established organoid lines with various morphologies, including grape-like structures, dense and massive organoids, and lines with smooth or rough structures (Figure 1B).

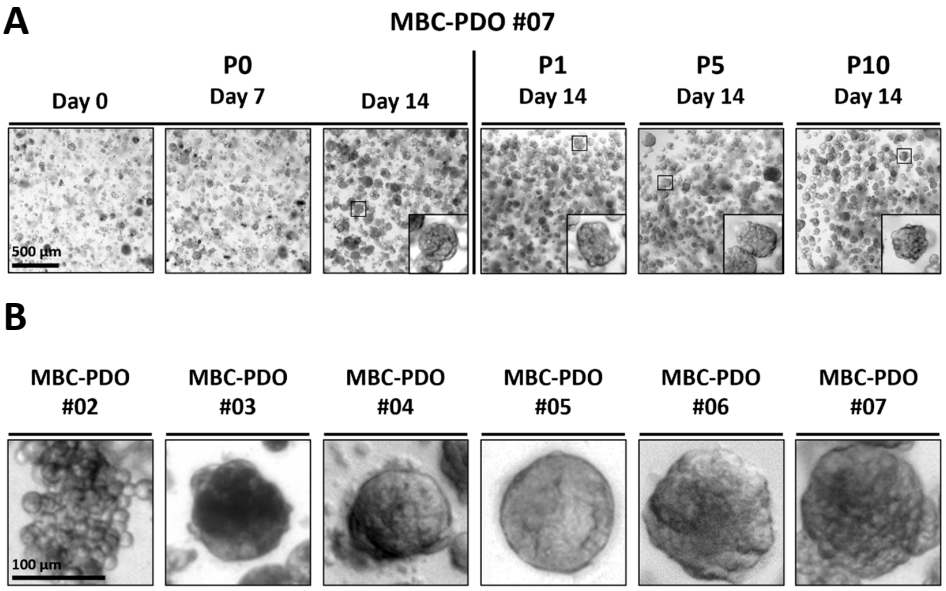

Figure 1. Establishing a biobank of breast cancer (BC) organoids derived from pleural effusion and ascites. (**A**) Brightfield images of metastatic BC patient-derived organoid (MBC-PDO) #07 in passage (P)0, P1, P5, and P10. Morphology was preserved throughout the whole culturing period. Scale bar: 500 µm. (**B**) Brightfield images of organoid lines displaying different phenotypes. The first image with grape-like morphology illustrates the ILC sample MBC-PDO #02, and images with dense, smooth, and rough structures illustrate NST samples of MBC-PDO #03–#07. Scale bar: 100 µm.

BC is known to be classified into specific subtypes based on histological characteristics and receptor status (ERα, PR, and HER2) [30]. The most common BC subtypes are invasive ductal carcinoma (IDC) of no special type (NST) and invasive lobular carcinoma (ILC) [31]. Both types are represented in our organoid models (Table S1). The dominating receptor status is hormone receptor-positive/HER2-negative BC, which is also represented by the MBC-PDO lines (Table 1).

Table 1. Results of immunohistochemistry (IHC) staining signals of pleural cells and/or organoid lines, and mutation analysis of hotspots in *AKT1* and *PIK3CA*. Abbreviations neg.: negative signal, pos.: positive signal, WT: wild type, E: glutamic acid, K: lysine, H: histidine, R: arginine.

MBC-PDO		ERα	PR	HER2	*AKT1*	*PIK3CA*	p-AKT
#02	Organoids	neg.	neg.	neg. *	WT	WT	neg.
#03	PE	pos.	pos.	neg. *	WT	H1047R †	-
	Organoids	pos.	pos.	neg. *	WT	H1047R †	neg.
#04	PE	pos. *	neg.	neg.	E17K ◊	WT	-
	Organoids	neg.	neg.	neg.	E17K ◊	WT	pos.
#05	PE	pos.	pos.	neg.	-	-	-
	Organoids	-	-	-	WT	E545K †	-
#06	PE	pos. *	neg.	neg.	WT	E545K †	-
	Organoids	pos.*	neg.	neg.	WT	E545K †	pos.
#07	PE	pos. *	neg.	neg.	E17K ◊	WT	-
	Organoids	pos. *	neg.	neg.	E17K ◊	WT	pos.

* Samples showed a weak positivity, ◊ homozygous mutation, † heterozygous mutation.

3.2. Immunohistochemical Characterization of Patient-Derived Organoids

The receptor status of BC influences the type of therapy the patients receive and is an indicator for prognosis. For example, triple-negative BC is associated with a poor prognosis as it lacks hormone receptors and has limited therapy options, while hormone receptor (ERα and PR)-positive tumors can be treated with endocrine therapy. HER2-positive BC can be targeted with antibodies and inhibitors.

We studied the suitability of organoid lines as a model for metastasized BC and their conservation of histological characteristics through H&E and IHC staining of pleural samples and the corresponding organoid lines. The phenotype and expression pattern of the liver metastasis, MPE, and the corresponding MPE organoids of MBC-PDO #03 were compared. The corresponding patient was diagnosed with primary NST in 2008 and developed PE 13 years later. To confirm that expression patterns are retained in organoids, organoid samples of MBC-PDO #03 were taken at P3 for FFPE embedding and IHC staining (Figure 2). H&E staining revealed comparable histology of liver metastasis, pleural cells, and organoids. IHC staining of nuclear hormone receptors ER and PR demonstrated positive signals in all three samples (Figure 2). Membranous receptor HER2 could be observed in some of the cells. According to pathology, HER2 expression had an IHC score of 2+ (out of 3+), which was represented in the patient-derived organoids. Thus, organoids of MBC-PDO #03 not only preserved the expression patterns of pleural cells, but also had the same receptor status as the respective liver metastasis.

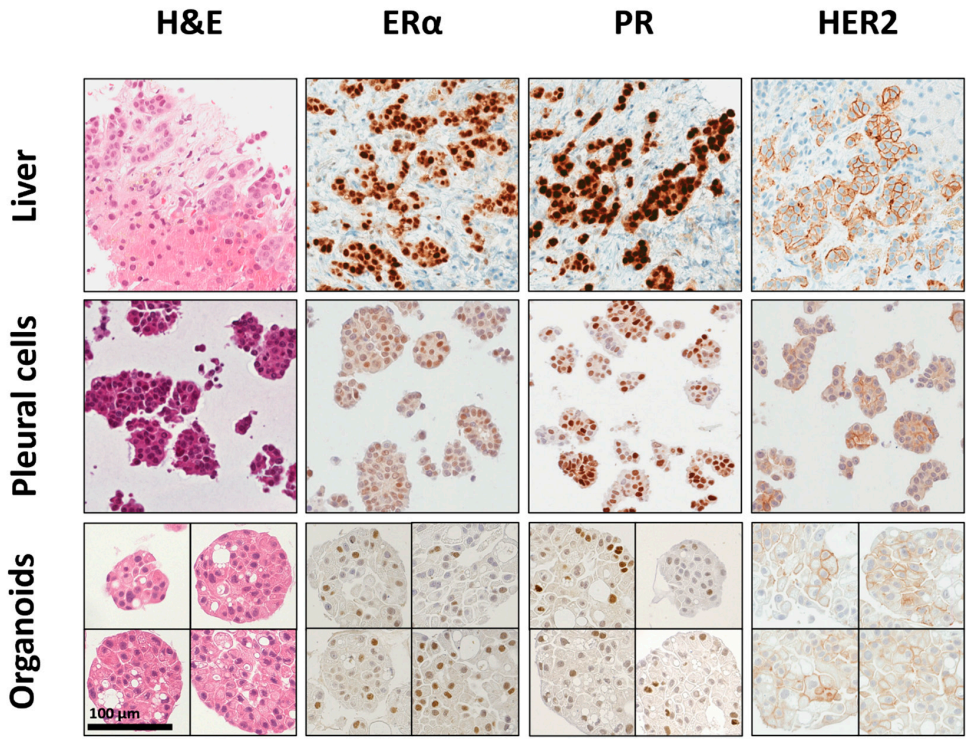

Figure 2. Histological characterization of pleural BC cells and organoids derived from pleural effusion. Histology (H&E staining) and receptor status of metastasized liver tissue, pleural cells, and organoids (P3) of MBC-PDO #03 are shown. Organoids consist exclusively of epithelial cells, while tissues often show tumor epithelium ringed by mesenchymal cells. The receptor status is maintained in the organoids. Scale bar: 100 µm.

IHC staining of additional markers (epithelial marker EpCAM, GATA3, tumor suppressor protein p53, and cadherin-1) in the pleural effusion sample revealed positive signals, which were equally preserved in the derived organoid culture (Figure S1). Ki-67 staining was applied to compare the proliferation of organoids. Only a small number of Ki67-positive cells were observed for MBC-PDO #02, #03, and #04, whereas MBC-PDO #06 and

#07 presented a higher number of Ki67-positive cells (Figure S2A,B). This is in accordance with the proliferation rate we observed in the organoid lines. An overview of the IHC staining results of all lines is provided in Table 1. In most cases, organoids preserved the expression patterns of the original cells. One exception was observed in MBC-PDO #04: no ERα expression was detected in the organoids, while pleural cells displayed low levels of ERα expression. In conclusion, the receptor status of tumor organoids correlates with the expression patterns of their metastatic counterpart, suggesting that these organoids could serve as a well-suited in vitro model for metastasized BC.

3.3. Hotspot Mutation Analysis of Patient-Derived Organoid Lines

Tumorigenesis in BC cells can be driven by both the phosphoinositide 3-kinase (PI3K) and mitogen-activated protein kinase (MAPK) signaling pathway [32]. Activation of these pathways can sometimes be traced back to mutations of key proteins. Mutations in *AKT1* and *PIK3CA* can lead to abnormal protein production and have been associated with the activation of downstream processes (proliferation, survival, etc.) and increased risk of BC [33–35].

A missense mutation of *AKT1* leading to the exchange of glutamic acid (E) to lysine (K) in amino acid position 17 has been observed in approx. 6% of all BC cases [36]. Mutations in *PIK3CA* are one of the most common mutations in BC and have been observed in more than 30% of BC cases [35,37]. The three most common mutation hotspots in this gene are E542 (11%), E545 (17%), and H1047 (35%) [38].

Sanger sequencing of the hepatic metastasis of MBC-PDO #03 revealed a *PIK3CA* H1047R mutation that was also detected in the MPE as well as the corresponding organoid model (Table 1 and Figure S3). Whereas none of the samples presented with a *PIK3CA* E542 mutation, MBC-PDO #05 and MBC-PDO #06 had an E545 hotspot mutation that was also present in the primary tumor of the corresponding patients. A mutation in *AKT1* (E17K) was found in the MPE of MBC-PDO #04 and #07 as well as the primary tumor samples. The MPEs of MBC-PDO #02 and MBC-PDO #05 could not be tested due to insufficient sample material from the initial MPE. MBC-PDO #02 was also the only organoid line with no hotspot mutation detected. Thus, five out of six organoid lines carried a mutation in either *AKT1* or *PIK3CA*.

Mutation analysis of hotspot gene mutations showed that the organoids retained mutations from initial MPE (and often the primary tumor) and that derived organoids represent the metastasized tumors. These findings indicate that the organoid lines could be useful for downstream applications like drug response assays.

3.4. Drug Response Assays

To examine the potential of organoids derived from MPE and MA as in vitro models of BC metastasis, we assessed their suitability for use in drug response assays. We selected drugs that target the HER signaling pathway, cyclin-dependent kinases 4 and 6 (CDK4/6), poly ADP ribose polymerases (PARPs), DNA synthesis, and β-tubulin (Figure 3A). Organoid lines were treated with various drugs at specific concentrations, and the results are presented in a heat map (Figure 3B). Serial dilution drug assays of Lapatinib, Alpelisib, Capivasertib, Abemaciclib, and Paclitaxel were performed to generate dose–response curves and calculate the half-maximal inhibitory concentrations (IC50) (Figure 3C).

MBC-PDO #03, which has medium levels of HER2 expression (Figure 2), showed a strong response to the HER2 pathway inhibitor Lapatinib. Despite having the H1047R hotspot mutation in the *PIK3CA* gene (Table 1), which could potentially activate the corresponding signaling pathway, MBC-PDO #03 did not respond positively to drugs targeting the PI3K pathway (Figure 3). As tumorigenesis in BC cells can be driven by the PI3K and MAPK signaling pathways, we examined if the PI3K signaling cascade was activated. IHC staining for the activating phosphorylation site Ser473 of AKT showed that p-AKT was absent in MBC-PDO #03 compared to the positive staining in MBC-PDO #06, suggesting that the PI3K pathway was not activated in MBC-PDO #03 (Figure S4). This demonstrates the value of using functional in vitro drug assays in combination with p-AKT IHC stainings in patient-derived organoids.

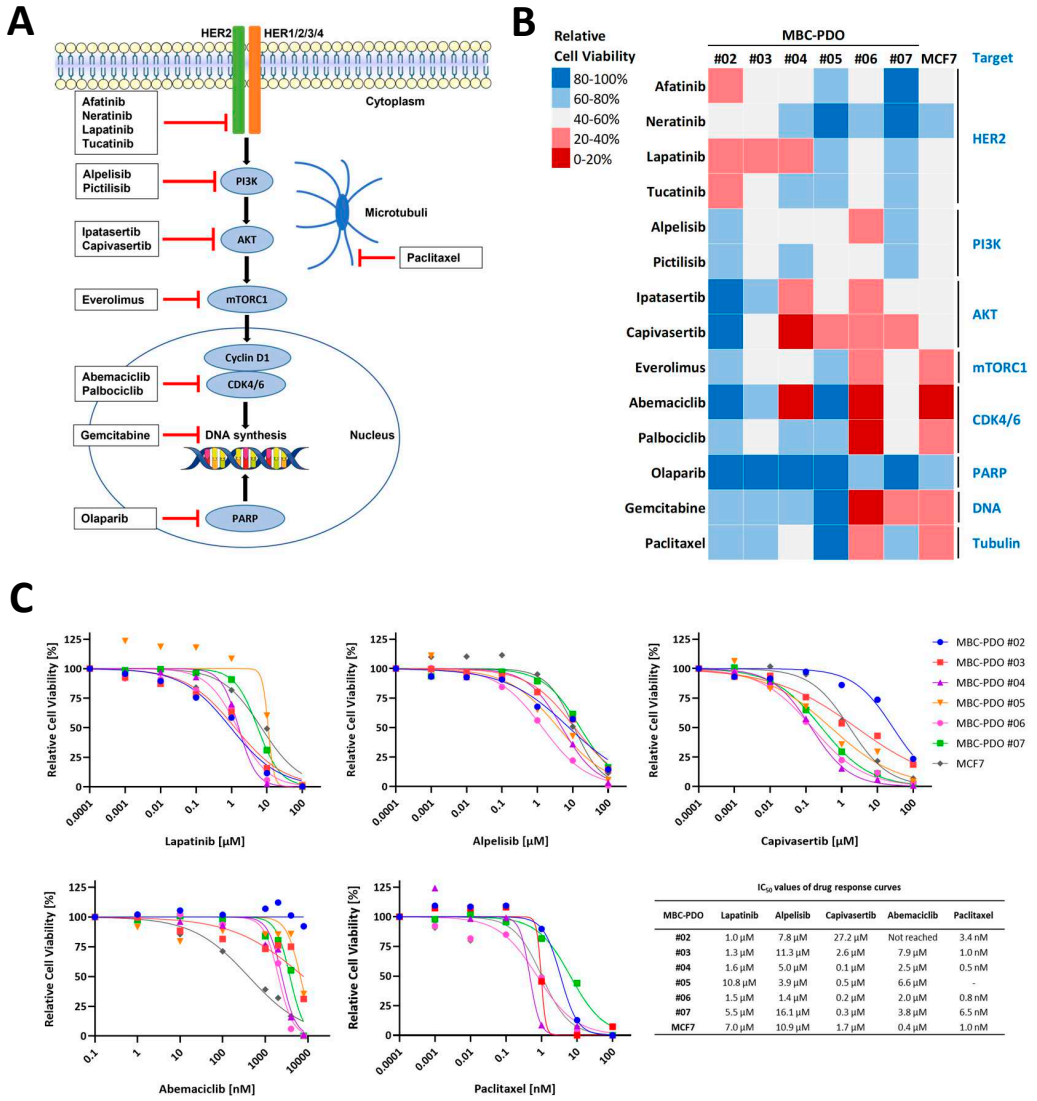

Figure 3. In vitro drug response assays of organoid lines. (**A**) Overview of drugs used in the assays and their targets. Inhibitors Afatinib, Lapatinib, Neratinib, and Tucatinib target the HER2 receptor intracellularly. Alpelisib and Pictilisib target PI3K, while Ipatasertib and Capivasertib aim for AKT. Everolimus inhibits mTORC1, whereas Abemaciclib and Palbociclib target CDK4/6 in the nucleus. Olaparib, which is administered to BC patients with a *BRCA1/2* mutation/deletion, inhibits PARP. Gemcitabine enters the cell through nucleoside transporters and is phosphorylated in three steps into Gemcitabine triphosphate, which is incorporated into the DNA and leads to the termination of DNA synthesis. Paclitaxel binds and stabilizes β-tubulin, upon which depolymerization is blocked. This affects the mitotic spindle assembly, chromosome segregation, and mitosis. (**B**) Heat map of relative cell viability of organoids treated with various drugs at specific concentrations for 4 days (10 µM Afatinib, 1 µM Neratinib, 4 µM Lapatinib, 10 µM Tucatinib, 10 µM Alpelisib, 1 µM Pictilisib, 1 µM Ipatasertib, 1 µM Capivasertib, 100 nM Everolimus, 4 µM Abemaciclib, 10 µM Palbociclib, 10 µM Olaparib, 100 nM Gemcitabine, 10 nM Paclitaxel). Values were normalized to control treatment with 0.1% DMSO (set to 100%). Red fields indicate sensitive responses, while blue fields present less-responding lines. Experiments were performed in technical triplicates. (**C**) Drug response curves depict organoid viabilities after 4 days of treatment with Lapatinib, Alpelisib, Capivasertib, Abemaciclib, and Paclitaxel. Error bars representing standard deviation (SD) of three independent experiments were removed for better presentation. IC50 values of drug response curves are shown in the adjacent table.

MBC-PDO #05 carries the *PIK3CA* E545K hotspot mutation and reacted most sensitively to AKT inhibitor Capivasertib, followed by the other PI3K and AKT drugs. We did not have sufficient organoids from MBC-PDO #05 to fix and perform IHC staining. However, the patient would likely have profited from treatment with PI3K or AKT inhibitors like Alpelisib, instead of the actual therapy with Paclitaxel combined with HER2-targeting Trastuzumab and Pertuzumab, followed by CDK4/6 inhibitor Abemaciclib combined with Trastuzumab.

MBC-PDO #07, which is positive for p-AKT (Table 1) and carries an *AKT1* E17K mutation, responded most sensitively to the AKT inhibitor Capivasertib. This line was also sensitive to Gemcitabine. Interestingly, the patient of MBC-PDO #07 had previously been treated with Paclitaxel and Abemaciclib, and both drugs did not affect the cell viability of MBC-PDO #07, suggesting a resistance to these drugs. Furthermore, the corresponding patient was diagnosed with a *BRCA1/2* deletion in the breast tumor sample and therefore had previously received treatment with the PARP inhibitor Olaparib. Nonetheless, the organoid line was resistant to Olaparib. Consequently, the patient may have benefited from treatment with AKT inhibitors or Gemcitabine.

In summary, our results emphasize the relevance of combining IHC staining and mutation analysis with in vitro drug assays in order to move a step closer to personalized BC therapy. For instance, even in cases where the HER2 signal is negative or low, it may be beneficial for some patients to receive HER2-targeting therapy like Lapatinib.

4. Discussion

The poor outcome of metastasized BC underscores the need for reliable personalized oncology and the importance of models recapitulating the characteristics of MBC [8]. Two of the most used approaches involve cell lines as well as PDX models. While cell lines are readily available but often do not recapitulate drug responses in patients [22], PDX models are good in therapy predictions but are expensive and need a long time for their establishment [22]. Recent years have seen the rise of organoid technology for personalized oncology with an enormous potential for clinical applications [24,25]. However, while organoids are often established from primary tumor specimens obtained during resection of the tumor, metastases are often underrepresented due to insufficient bioavailability of specimen material. Biopsies are often small and are still widely used for pathological characterization only. Drug efficacy screenings are therefore mainly performed on organoids derived from treatment-naïve primary tumors rather than on already heavily pre-treated metastatic samples. These pose the disadvantage of not being representative of metastatic disease and often do not help the patients in need. Here, we were trying to close this gap by utilizing MPE and MA from breast cancer patients as a source for the generation of such metastatic models. One great advantage of this approach is the facile accessibility to metastasized tumor cells, which can easily be obtained by clinical routine procedures, such as thoracentesis and paracentesis. BC patients with MA or MPE can suffer from a shortness of breath, discomfort, and chest or abdominal pain, which collectively lead to a reduced quality of life. Hence, one of the main objectives is to improve patients' quality of life and prolong their survival time by reducing MPE and MA.

This study shows the feasibility of culturing metastatic tumor cells derived from advanced BC patients with MA or MPE utilizing organoid technology. The derived tumor organoid lines could be cultured for extended passages (Figure 1) and presented characteristics of their respective source materials (see IHC and mutation analysis; Figure 2, Table 1). The collection of tumor organoid lines represents the different classifications of BC regarding subtype, histological features, and receptor status, which to date are key factors in therapy recommendation. However, the main objective here was to utilize these models for drug screenings and therapy predictions.

In our study, drug assays revealed that responses are not always in accord with expression patterns, pathway activation, and hotspot mutations. This emphasizes the value of personalized drug assays, in combination with the characterization of expression

patterns and mutation status. For instance, HER2-targeting drugs affected some of the MBC-PDO lines with zero to low levels of HER2 (Figure 3, Table 1). It is noteworthy that some of these drugs target multiple receptors, including EGFR, highlighting potential benefits in clinical applications, despite a negative HER2 status. In fact, clinical trials with Afatinib in HER2-negative BC have shown some effect on tumor progression [39,40].

PI3K- and AKT-targeting drugs affected most hotspot mutated tumor organoid lines, as anticipated. Overall, AKT inhibitor Capivasertib showed the highest effect among all drugs—four of six MBC-PDO lines responded sensitively. According to a study, alterations in the PI3K-AKT signaling pathway have been linked to higher levels of p-AKT, and responsiveness to AKT inhibitor Ipatasertib [41].

Here, however, one *PIK3CA*-mutated line showed less sensitivity, as the IHC staining of p-AKT indicated an inactive PI3K cascade in those organoids (Figure S4, MBC-PDO #03). This stresses the necessity of including a biomarker such as p-AKT in clinical diagnostics to guide therapy decisions. According to the mentioned study, triple-negative BC tumors with phosphorylated AKT levels were associated with enriched clinical benefit of AKT inhibitor Ipatasertib regardless of the absence of PI3K-AKT alterations [41].

According to the SOLAR-1 study, the combination of Alpelisib and Fulvestrant resulted in a higher median overall survival for patients with *PIK3CA*-mutated, HR+, HER2- advanced BC [42]. Here, we have demonstrated that IHC staining of HER2 and mutation analysis of *PIK3CA* or *AKT1* genes are relevant but not sufficient for a proper therapy recommendation. Drugs targeting HER2, such as Lapatinib, can also be beneficial for patients with HER2-, advanced BC. In contrast, patients with an altered *PIK3CA* or *AKT1* can, but do not necessarily, profit from a treatment targeting the PI3K-AKT pathway, as we have shown for MBC-PDO #03 (Figure 3 and Table 1). We propose that in addition to receptor determination and mutational diagnosis, staining of p-AKT can help with the understanding of whether the corresponding pathway is activated and if targeting PI3K or AKT could be reasonable.

CDK4/6 inhibitors and mTORC1 inhibitor Everolimus are widely used in the clinic for hormone receptor-positive and HER2-negative BC patients [43–45]. In particular, patients with endocrine-resistant BC may profit from these drugs. In our drug assays, however, the response to CDK4/6 inhibitors and Everolimus did not correlate with the receptor status of the tumor organoids. One possible explanation would be that some MBC-PDOs acquired resistance towards these drugs upon clinical treatment. Similar effects have already been observed in previous studies [46]. These results repeatedly suggest that personalized drug response assays can be beneficial for individual cases, and new biomarkers could help identify patients that would profit from CDK4/6 inhibitors and Everolimus.

In summary, the discrepancy between characterization and functional testing underlines the relevance of linking IHC stainings and mutational analysis of metastasized BC with in vitro drug assays, to improve personalized BC therapy. To make organoid-based drug screening practical in a clinical setting, it is crucial to have a fast turnaround time for organoid culture establishment and drug response assessment, preferably within the same time interval as the treatment. Here, we were able to culture and screen tumor organoid lines within two weeks. To further confirm the accuracy of metastatic organoids in predicting drug response, it would be beneficial to conduct a study in which metastatic organoids derived from patients with MA or MPE are screened with drugs used in the clinic. Consequently, the results can then be aligned with the patients' response to the treatment.

We established six MBC-PDO lines and discovered that with more models, hypotheses and biomarkers can be thoroughly investigated in our setup. Generating a larger biobank of metastatic BC organoids will help with the understanding of correlations between a patient's genetic as well as proteomic makeup and drug responses to identify sensitivity and resistance across BC subtypes. With a larger collection of drug screening data, it could be possible to create therapy plans based on the characteristics of the organoid subtypes.

5. Conclusions

In conclusion, our metastatic BC organoids recapitulate the characteristics of their original sample derived from MA and MPE and serve as an invaluable model that can be utilized in a preclinical setting for guiding therapy decisions. Further research is necessary to prove the validity of these models for clinical relevance. Since the minority of BC patients develop MA or MPE, alternative sources for liquid biopsies, e.g., blood samples, should be standardized in pathological and experimental applications to maximize the patient numbers that are included in these studies. Additionally, correlating drug screenings with genomic and proteomic analysis can be beneficial in finding new biomarkers for drug response in the future.

Supplementary Materials: The following supporting information can be downloaded at: https://www.mdpi.com/article/10.3390/cancers15143602/s1, Table: S1: List of data of BC patients from whom the organoid lines were established. Table S2: Composition of BC culture medium (BCM). Table S3: List of inhibitors applied in 3D drug screenings. Table S4: List of antibodies used for IHC stainings. Table S5: Primers used for the amplification of hotspot mutations and for sequencing. Figure S1: Histological characterization of pleural BC cells and organoids derived from pleural effusion. Figure S2: IHC staining of the proliferation marker Ki67 in organoids. Figure S3: Examples of mutations in *AKT* and *PIK3CA*. Figure S4: IHC staining of p-AKT.

Author Contributions: Conceptualization, A.K.; methodology, A.K., C.E.Ö., T.J.Z. and R.B.; formal analysis, C.E.Ö. and T.J.Z.; resources, T.E., S.Y.B. and A.D.H.; data curation, C.E.Ö., T.J.Z., R.B. and T.E.; writing—original draft preparation, C.E.Ö. and A.K.; writing—review and editing, C.E.Ö., A.K., T.E., A.D.H. and S.Y.B.; supervision, A.K. All authors have read and agreed to the published version of the manuscript.

Funding: Part of this research was supported by the German Cancer Aid (Priority program 'Translational Oncology'; Project: DETECT-CTC-HIGH—70114705). We acknowledge support from the Open Access Publication Fund of the University of Tübingen.

Institutional Review Board Statement: The study was approved by the Ethics Committee of the Eberhard Karl University of Tübingen (Ethical approval 150/2018BO2 and 288/2022) and is compliant with all relevant ethical regulations regarding research studies involving humans.

Informed Consent Statement: Written informed consent was obtained from all subjects involved in the study.

Data Availability Statement: The data demonstrated in this study are available on request from the corresponding author.

Acknowledgments: We thank Ingrid Teufel for her excellent technical assistance. Furthermore, we thank Alica Fehrenbach and Anjali Ralhan Singh for their contribution to this project.

Conflicts of Interest: The authors declare no conflict of interest. The funders had no role in the design of the study; in the collection, analyses, or interpretation of data; in the writing of the manuscript; or in the decision to publish the results.

References

1. Sung, H.; Ferlay, J.; Siegel, R.L.; Laversanne, M.; Soerjomataram, I.; Jemal, A.; Bray, F. Global cancer statistics 2020: GLOBOCAN estimates of incidence and mortality worldwide for 36 cancers in 185 countries. *CA Cancer J. Clin.* **2021**, *71*, 209–249. [CrossRef] [PubMed]
2. Weigelt, B.; Horlings, H.; Kreike, B.; Hayes, M.; Hauptmann, M.; Wessels, L.; de Jong, D.; Van de Vijver, M.; Veer, L.V.; Peterse, J. Refinement of breast cancer classification by molecular characterization of histological special types. *J. Pathol.* **2008**, *216*, 141–150. [CrossRef]
3. Perou, C.M.; Sørlie, T.; Eisen, M.B.; Van De Rijn, M.; Jeffrey, S.S.; Rees, C.A.; Pollack, J.R.; Ross, D.T.; Johnsen, H.; Akslen, L.A.; et al. Molecular portraits of human breast tumours. *Nature* **2000**, *406*, 747–752. [CrossRef]
4. Sørlie, T.; Perou, C.M.; Tibshirani, R.; Aas, T.; Geisler, S.; Johnsen, H.; Hastie, T.; Eisen, M.B.; van de Rijn, M.; Jeffrey, S.S.; et al. Gene expression patterns of breast carcinomas distinguish tumor subclasses with clinical implications. *Proc. Natl. Acad. Sci. USA* **2001**, *98*, 10869–10874. [CrossRef]

5. Goldhirsch, A.; Ingle, J.N.; Gelber, R.D.; Coates, A.S.; Thürlimann, B.; Senn, H.-J. Thresholds for therapies: Highlights of the St Gallen International Expert Consensus on the Primary Therapy of Early Breast Cancer 2009. *Ann. Oncol.* **2009**, *20*, 1319–1329. [CrossRef] [PubMed]
6. Harbeck, N.; Penault-Llorca, F.; Cortes, J.; Gnant, M.; Houssami, N.; Poortmans, P.; Ruddy, K.; Tsang, J.; Cardoso, F. Breast Cancer. *Nat. Rev. Dis. Prim.* **2019**, *5*, 66. [CrossRef] [PubMed]
7. Hartkopf, A.D.; Banys, M.; Krawczyk, N.; Staebler, A.; Becker, S.; Hoffmann, J.; Hahn, M.; Wallwiener, M.; Fehm, T. Bone marrow versus sentinel lymph node involvement in breast cancer: A comparison of early hematogenous and early lymphatic tumor spread. *Breast Cancer Res. Treat.* **2011**, *131*, 501–508. [CrossRef]
8. Pasha, N.; Turner, N.C. Understanding and overcoming tumor heterogeneity in metastatic breast cancer treatment. *Nat. Cancer* **2021**, *2*, 680–692. [CrossRef]
9. Aurilio, G.; Disalvatore, D.; Pruneri, G.; Bagnardi, V.; Viale, G.; Curigliano, G.; Adamoli, L.; Munzone, E.; Sciandivasci, A.; De Vita, F.; et al. A meta-analysis of oestrogen receptor, progesterone receptor and human epidermal growth factor receptor 2 discordance between primary breast cancer and metastases. *Eur. J. Cancer* **2013**, *50*, 277–289. [CrossRef]
10. Angus, L.; Smid, M.; Wilting, S.M.; van Riet, J.; Van Hoeck, A.; Nguyen, L.; Nik-Zainal, S.; Steenbruggen, T.G.; Tjan-Heijnen, V.C.G.; Labots, M.; et al. The genomic landscape of metastatic breast cancer highlights changes in mutation and signature frequencies. *Nat. Genet.* **2019**, *51*, 1450–1458. [CrossRef]
11. Curigliano, G.; Bagnardi, V.; Viale, G.; Fumagalli, L.; Rotmensz, N.; Aurilio, G.; Locatelli, M.; Pruneri, G.; Giudici, S.; Bellomi, M.; et al. Should liver metastases of breast cancer be biopsied to improve treatment choice? *Ann. Oncol.* **2011**, *22*, 2227–2233. [CrossRef]
12. Walter, V.; Fischer, C.; Deutsch, T.M.; Ersing, C.; Nees, J.; Schütz, F.; Fremd, C.; Grischke, E.-M.; Sinn, P.; Brucker, S.Y.; et al. Estrogen, progesterone, and human epidermal growth factor receptor 2 discordance between primary and metastatic breast cancer. *Breast Cancer Res. Treat.* **2020**, *183*, 137–144. [CrossRef]
13. Dipper, A.; Jones, H.E.; Bhatnagar, R.; Preston, N.J.; Maskell, N.; Clive, A.O. Interventions for the management of malignant pleural effusions: A network meta-analysis. *Cochrane Database Syst. Rev.* **2020**, *4*, CD010529. [CrossRef]
14. Runyon, B.A. Care of Patients with Ascites. *N. Engl. J. Med.* **1994**, *330*, 337–342. [CrossRef]
15. Weichselbaum, R.; Marck, A.; Hellman, S. Pathogenesis of pleural effusion in carcinoma of the breast. *Int. J. Radiat. Oncol.* **1977**, *2*, 963–965. [CrossRef]
16. Ayantunde, A.; Parsons, S. Pattern and prognostic factors in patients with malignant ascites: A retrospective study. *Ann. Oncol.* **2007**, *18*, 945–949. [CrossRef]
17. Roberts, M.E.; Neville, E.; Berrisford, R.G.; Antunes, G.; Ali, N.J.; on behalf of the BTS Pleural Disease Guideline Group. Management of a malignant pleural effusion: British Thoracic Society pleural disease guideline 2010. *Thorax* **2010**, *65* (Suppl. S2), ii32–ii40. [CrossRef]
18. Bielsa, S.; Salud, A.; Martínez, M.; Esquerda, A.; Martín, A.; Rodríguez-Panadero, F.; Porcel, J.M. Prognostic significance of pleural fluid data in patients with malignant effusion. *Eur. J. Intern. Med.* **2008**, *19*, 334–339. [CrossRef] [PubMed]
19. Zamboni, M.M.; da Silva, C.T., Jr.; Baretta, R.; Cunha, E.T.; Cardoso, G.P. Important prognostic factors for survival in patients with malignant pleural effusion. *BMC Pulm. Med.* **2015**, *15*, 29. [CrossRef] [PubMed]
20. Wu, H.; Ji, H.; Yang, W.; Zhang, M.; Guo, Y.; Li, B.; Wang, J.; Chen, R.; Chen, Y.; Wang, X. Liquid biopsy using ascitic fluid and pleural effusion supernatants for genomic profiling in gastrointestinal and lung cancers. *BMC Cancer* **2022**, *22*, 1020. [CrossRef] [PubMed]
21. Sorolla, M.A.; Sorolla, A.; Parisi, E.; Salud, A.; Porcel, J.M. Diving into the Pleural Fluid: Liquid Biopsy for Metastatic Malignant Pleural Effusions. *Cancers* **2021**, *13*, 2798. [CrossRef] [PubMed]
22. Vargo-Gogola, T.; Rosen, J.M. Modelling breast cancer: One size does not fit all. *Nat. Rev. Cancer* **2007**, *7*, 659–672. [CrossRef] [PubMed]
23. Vlachogiannis, G.; Hedayat, S.; Vatsiou, A.; Jamin, Y.; Fernández-Mateos, J.; Khan, K.; Lampis, A.; Eason, K.; Huntingford, I.; Burke, R.; et al. Patient-derived organoids model treatment response of metastatic gastrointestinal cancers. *Science* **2018**, *359*, 920–926. [CrossRef] [PubMed]
24. Sachs, N.; de Ligt, J.; Kopper, O.; Gogola, E.; Bounova, G.; Weeber, F.; Balgobind, A.V.; Wind, K.; Gracanin, A.; Begthel, H.; et al. A Living Biobank of Breast Cancer Organoids Captures Disease Heterogeneity. *Cell* **2018**, *172*, 373–386.e10. [CrossRef]
25. Drost, J.; Clevers, H. Organoids in cancer research. *Nat. Rev. Cancer* **2018**, *18*, 407–418. [CrossRef]
26. Zhao, Z.; Chen, X.; Dowbaj, A.M.; Sljukic, A.; Bratlie, K.; Lin, L.; Fong, E.L.S.; Balachander, G.M.; Chen, Z.; Soragni, A.; et al. Organoids. *Nat. Rev. Methods Prim.* **2022**, *2*, 94. [CrossRef]
27. Carter, M.E.; Hartkopf, A.D.; Wagner, A.; Volmer, L.L.; Brucker, S.Y.; Berchtold, S.; Lauer, U.M.; Koch, A. A Three-Dimensional Organoid Model of Primary Breast Cancer to Investigate the Effects of Oncolytic Virotherapy. *Front. Mol. Biosci.* **2022**, *9*, 826302. [CrossRef]
28. Goldhammer, N.; Kim, J.; Timmermans-Wielenga, V.; Petersen, O.W. Characterization of organoid cultured human breast cancer. *Breast Cancer Res.* **2019**, *21*, 141. [CrossRef]
29. Baker, C.L.; Vaughn, C.P.; Samowitz, W.S. A PIK3CA Pyrosequencing-Based Assay that Excludes Pseudogene Interference. *J. Mol. Diagn.* **2012**, *14*, 56–60. [CrossRef]

30. Shaath, H.; Elango, R.; Alajez, N.M. Molecular Classification of Breast Cancer Utilizing Long Non-Coding RNA (lncRNA) Transcriptomes Identifies Novel Diagnostic lncRNA Panel for Triple-Negative Breast Cancer. *Cancers* **2021**, *13*, 5350. [CrossRef]
31. Vuong, D.; Simpson, P.; Green, B.; Cummings, M.; Lakhani, S.R. Molecular classification of breast cancer. *Virchows Arch.* **2014**, *465*, 1–14. [CrossRef] [PubMed]
32. Kruger, D.T.; Opdam, M.; Sanders, J.; Van Der Noort, V.; Boven, E.; Linn, S.C. Hierarchical clustering of PI3K and MAPK pathway proteins in breast cancer intrinsic subtypes. *Apmis* **2020**, *128*, 298–307. [CrossRef] [PubMed]
33. Zhang, Q.X.; Borg, A.; Wolf, D.M.; Oesterreich, S.; Fuqua, S.A. An estrogen receptor mutant with strong hormone-independent activity from a metastatic breast cancer. *Cancer Res.* **1997**, *57*, 1244–1249. [PubMed]
34. Carpten, J.D.; Faber, A.L.; Horn, C.; Donoho, G.P.; Briggs, S.L.; Robbins, C.M.; Hostetter, G.; Boguslawski, S.; Moses, T.Y.; Savage, S.; et al. A transforming mutation in the pleckstrin homology domain of AKT1 in cancer. *Nature* **2007**, *448*, 439–444. [CrossRef] [PubMed]
35. Campbell, I.G.; Russell, S.E.; Choong, D.Y.H.; Montgomery, K.G.; Ciavarella, M.L.; Hooi, C.S.F.; Cristiano, B.E.; Pearson, R.B.; Phillips, W.A. Mutation of the *PIK3CA* Gene in Ovarian and Breast Cancer. *Cancer Res.* **2004**, *64*, 7678–7681. [CrossRef]
36. Rudolph, M.; Anzeneder, T.; Schulz, A.; Beckmann, G.; Byrne, A.T.; Jeffers, M.; Pena, C.; Politz, O.; Köchert, K.; Vonk, R.; et al. AKT1 E17K mutation profiling in breast cancer: Prevalence, concurrent oncogenic alterations, and blood-based detection. *BMC Cancer* **2016**, *16*, 622. [CrossRef]
37. Shimoi, T.; Hamada, A.; Yamagishi, M.; Hirai, M.; Yoshida, M.; Nishikawa, T.; Sudo, K.; Shimomura, A.; Noguchi, E.; Yunokawa, M.; et al. PIK 3 CA mutation profiling in patients with breast cancer, using a highly sensitive detection system. *Cancer Sci.* **2018**, *109*, 2558–2566. [CrossRef]
38. Martínez-Sáez, O.; Chic, N.; Pascual, T.; Adamo, B.; Vidal, M.; González-Farré, B.; Sanfeliu, E.; Schettini, F.; Conte, B.; Brasó-Maristany, F.; et al. Frequency and spectrum of PIK3CA somatic mutations in breast cancer. *Breast Cancer Res.* **2020**, *22*, 45. [CrossRef]
39. Lin, P.-H.; Tseng, L.-M.; Lee, Y.-H.; Chen, S.-T.; Yeh, D.-C.; Dai, M.-S.; Liu, L.-C.; Wang, M.-Y.; Lo, C.; Chang, S.; et al. Neoadjuvant afatinib with paclitaxel for triple-negative breast cancer and the molecular characteristics in responders and non-responders. *J. Formos. Med. Assoc.* **2022**, *121*, 2538–2547. [CrossRef] [PubMed]
40. Schuler, M.; Awada, A.; Harter, P.; Canon, J.L.; Possinger, K.; Schmidt, M.; De Grève, J.; Neven, P.; Dirix, L.; Jonat, W.; et al. A phase II trial to assess efficacy and safety of afatinib in extensively pretreated patients with HER2-negative metastatic breast cancer. *Breast Cancer Res. Treat.* **2012**, *134*, 1149–1159. [CrossRef] [PubMed]
41. Shi, Z.; Wulfkuhle, J.; Nowicka, M.; Gallagher, R.I.; Saura, C.; Nuciforo, P.G.; Calvo, I.; Andersen, J.; Passos-Coelho, J.L.; Gil-Gil, M.J.; et al. Functional Mapping of AKT Signaling and Biomarkers of Response from the FAIRLANE Trial of Neoadjuvant Ipatasertib plus Paclitaxel for Triple-Negative Breast Cancer. *Clin. Cancer Res.* **2021**, *28*, 993–1003. [CrossRef] [PubMed]
42. André, F.; Ciruelos, E.M.; Juric, D.; Loibl, S.; Campone, M.; Mayer, I.A.; Rubovszky, G.; Yamashita, T.; Kaufman, B.; Lu, Y.S.; et al. Alpelisib plus fulvestrant for PIK3CA-mutated, hormone receptor-positive, human epidermal growth factor receptor-2–negative advanced breast cancer: Final overall survival results from SOLAR-1. *Ann. Oncol.* **2021**, *32*, 208–217. [CrossRef] [PubMed]
43. Corona, S.P.; Generali, D. Abemaciclib: A CDK4/6 inhibitor for the treatment of HR+/HER2− advanced breast cancer. *Drug Des. Dev. Ther.* **2018**, *12*, 321–330. [CrossRef] [PubMed]
44. Finn, R.S.; Martin, M.; Rugo, H.S.; Jones, S.; Im, S.-A.; Gelmon, K.; Harbeck, N.; Lipatov, O.N.; Walshe, J.M.; Moulder, S.; et al. Palbociclib and Letrozole in Advanced Breast Cancer. *N. Engl. J. Med.* **2016**, *375*, 1925–1936. [CrossRef] [PubMed]
45. Shtivelband, M.I. Everolimus in hormone receptor–positive advanced breast cancer: Targeting receptor-based mechanisms of resistance. *Breast* **2013**, *22*, 405–410. [CrossRef] [PubMed]
46. Braal, C.L.; Jongbloed, E.M.; Wilting, S.M.; Mathijssen, R.H.; Koolen, S.L.; Jager, A. Inhibiting CDK4/6 in breast cancer with palbociclib, ribociclib, and abemaciclib: Similarities and differences. *Drugs* **2021**, *81*, 317–331. [CrossRef]

cancers

MDPI

Article

Precision Immunotherapy Utilizing Adapter CAR-T Cells (AdCAR-T) in Metastatic Breast Cancer Leads to Target Specific Lysis

Cansu E. Önder [1,†], Moustafa Moustafa-Oglou [2,†], Sarah M. Schröder [3,4], Andreas D. Hartkopf [5], André Koch [1,5,*,‡] and Christian M. Seitz [2,6,7,*,‡]

1 Research Institute for Women's Health, University of Tübingen, 72076 Tübingen, Germany; cansu.onder@live.de
2 Department of Pediatric Oncology and Hematology, University Hospital Tübingen, 72076 Tübingen, Germany; moustafa.moustafa-oglou@med.uni-tuebingen.de
3 Department of Otorhinolaryngology, Head and Neck Surgery, University of Ulm, 89081 Ulm, Germany
4 Department of Peptide-Based Immunotherapy, University and University Hospital Tübingen, 72076 Tübingen, Germany
5 Department of Women's Health, University of Tübingen, 72076 Tübingen, Germany
6 Cluster of Excellence iFIT (EXC 2180) "Image-Guided and Functionally Instructed Tumor Therapies", University of Tübingen, 72076 Tübingen, Germany
7 German Cancer Consortium (DKTK), Partner Site Tübingen, a Partnership between German Cancer Research Center (DKFZ) and University Hospital Tübingen, 81675 Munich, Germany
* Correspondence: andre.koch@med.uni-tuebingen.de (A.K.); christian.seitz@med.uni-tuebingen.de (C.M.S.); Tel.: +49-70701-29-85380 (A.K.); +49-7071-29-61803 (C.M.S.)
† These authors contributed equally to this work.
‡ These authors contributed equally to this work.

Simple Summary: The development of pleural effusion is a common debilitating occurrence during metastasized breast cancer. Malignant cells in pleural effusions originating from the primary tumor suggest the spread of the disease and can serve as a model for metastatic breast cancer. Hence, we established three-dimensional organoid lines from four patients with malignant pleural effusion. Patient-derived organoids were characterized by flow cytometry for individual target antigen expression profiles. Adapter CAR-T cells (AdCAR-T) and biotinylated monoclonal antibodies were evaluated to specifically target patient-derived organoids and assess responses in a personalized fashion. This study demonstrates the feasibility of precision immunotherapy utilizing AdCAR-T to target patient-individualized antigen patterns.

Abstract: A frequent symptom of metastasized breast cancer (BC) includes the development of malignant pleural effusion (MPE), which contains malignant cells derived from the primary tumor site. The poor prognosis of MPE in metastasized BC indicates the necessity for dependable precision oncology and the importance of models representing the heterogenous nature of metastatic BC. In this study, we cultured MPE-derived metastatic tumor cells from four advanced BC patients using organoid technology. We assessed the expression of tumor-associated antigens on MPE-derived organoid lines by flow cytometry (FC). Based on an individual antigen expression pattern, patient-derived organoids were treated with adapter CAR-T cells (AdCAR-T) and biotinylated monoclonal antibodies targeting CD276, HER2, EGFR, TROP2, or EpCAM. Co-culture assays revealed specific organoid lysis by AdCAR-T depending on individual antigen expression patterns. Our results demonstrate that MPE-derived organoids can serve as a reliable tool for assessing the efficacy of AdCAR-T on metastatic BC in a patient-individualized manner. This approach could potentially be applied in a preclinical setting to instruct therapy decisions. Further, our study demonstrates the feasibility of precision immunotherapy utilizing AdCAR-T to target patient-individualized antigen patterns.

Keywords: precision immunotherapy; adapter CAR-T cells; metastasis; breast cancer; organoid culture; pleural effusion; cancer biology; patient-derived organoids

Citation: Önder, C.E.; Moustafa-Oglou, M.; Schröder, S.M.; Hartkopf, A.D.; Koch, A.; Seitz, C.M. Precision Immunotherapy Utilizing Adapter CAR-T Cells (AdCAR-T) in Metastatic Breast Cancer Leads to Target Specific Lysis. *Cancers* **2024**, *16*, 168. https://doi.org/10.3390/cancers16010168

Academic Editor: Simone Krebs

Received: 31 October 2023
Revised: 22 December 2023
Accepted: 27 December 2023
Published: 29 December 2023

1. Introduction

Globally, breast cancer (BC) stands out as the most diagnosed cancer and a leading contributor to cancer-related fatalities in women [1]. BC presents itself with four molecular subtypes (luminal A, luminal B, HER2-enriched, and basal-like) based on a 50-gene expression signature (PAM50) [2]. Besides this molecular classification, a more traditional classification based on the immunohistochemistry expression of key proteins such as estrogen receptor (ER), progesterone receptor (PR), human epidermal growth factor receptor 2 (HER2), and the proliferation marker Ki67, are commonly employed (reviewed in [3]). BC cells can acquire invasiveness, leading to the formation of metastases, as they spread through the bloodstream or lymphatic system to various organs and sites in the body. Primary BC has been extensively studied and generally has a positive prognosis. In contrast, metastatic BC presents numerous challenges, including the presence of diverse cell types and resistance to treatment. These factors often contribute to the failure of therapeutic interventions [4].

Therapy decisions usually depend on the features of primary tumors, as metastatic biopsies are relatively rare. Yet, primary tumors may not fully represent the heterogeneous characteristics of metastatic tumors. Frequently, these attributes demonstrate inconsistency in phenotypic markers [5]. Consequently, therapy recommendations based on the characteristics of primary tumors alone might lead to poorer outcomes [6,7].

Malignant pleural effusion (MPE), which describes the presence of malignant cells in the pleural cavity, develops in 7% of BC patients [8,9]. The quality of life and prognosis of patients suffering from MPE are relatively poor and defined by chest pain and breathing difficulties [10]. However, as MPE contains metastatic BC cells and can be obtained through a simple puncture, it offers more options for metastatic biopsies [11]. Moreover, malignant cells in MPEs can serve as a source for the establishment of in vitro models that represent the characteristics of metastasized BC to improve therapy outcomes and approach precision oncology. The most common approaches include cell lines and patient-derived xenograft (PDX) models. While cell lines are widely used in BC research but are not capable of predicting drug response in patients, PDX models are invaluable for translational research but are expensive and limited in efficiency [12].

Recently, patient-derived BC organoids have been shown to be valuable three-dimensional models for research and personalized oncology, as they represent the characteristics of their respective origin and can be used for long-term culturing [13,14]. Cultured in an extracellular matrix, organoids of different sources have already been used in various methods, such as high-throughput drug assays [13,15].

In the area of BC treatment, standard therapeutic approaches involve surgery, chemotherapy, radiotherapy, endocrine therapy, and targeted therapy [16]. The latter approach includes immunotherapy, which has risen as a crucial element, presenting promising effectiveness and minimal safety concerns [17]. The emergence of genetically modified T cell therapies, incorporating a chimeric antigen receptor (CAR) has achieved remarkable success in long-lasting clinical responses among individuals with hematologic malignancies [18]. This sparked immense enthusiasm in the potential to address various types of cancer including BC. CAR-T cell therapy, a type of immunotherapy derived from adoptive T cell transfer, has been established to harness the patient's own immune cells to fight cancer by triggering antigen-specific cytotoxic response [19].

Conventional CAR constructs are limited in their ability to provide adjustable cytotoxicity and flexible selectivity against heterogenous tumors. These limitations result in potential risks such as uncontrolled CAR-T expansion, depletion of normal tissues expressing the target antigen, CAR-T exhaustion, and lack of activation toward antigen-negative tumor cells [20–22].

One sophisticated approach to circumvent these limitations is to separate target antigen recognition from CAR-T activation through the introduction of adapter molecules (AMs) and adapter CARs (AdCARs) [23]. These AMs combine the functional components of an antigen-binding moiety and a CAR-binding moiety. Being able to conjugate clinically

approved therapeutical antibodies, effectively turning them into AMs, enables flexible redirection of CAR-T cells toward different tumor-associated antigens (TAAs) and furthermore introduces a controllable on/off-switch.

In previous studies, we have demonstrated the remarkable effectiveness of AdCAR-T cells in vitro and in vivo by specifically targeting tumors associated with a broad spectrum of tumor-associated antigens (TAAs) across different cancer types [23,24]. This CAR technology provides the advantage of universal targeting of various cancer types and furthermore allows for the finely adjustable modulation of effector function and ultimately addresses the challenge of immune evasion due to antigen loss.

While CAR-T cell therapy has proven great achievements in hematologic malignancies, its effectiveness in battling solid tumors, including BC, still has room for improvement. In a previous study, we cultured tumor cells derived from MPE of advanced BC patients employing organoid technology and generated metastatic BC patient-derived organoids (MBC-PDOs). MBC-PDOs were then used as a platform to perform drug screenings applying various inhibitors [14].

In this study, we cultured MBC-PDOs and analyzed their antigen expression patterns utilizing flow cytometry (FC). Our goal was to utilize MBC-PDOs as a screening platform to demonstrate feasibility of an AdCAR-T-based precision immunotherapy approach for flexible targeting of various tumor-associated target antigens. In the future, research on patient-derived models could have enormous potential for clinical applications, such as extending patients' survival time and improving their quality of life.

2. Materials and Methods

2.1. Patient Cohort

All MBC-PDOs were previously established and characterized [14]. The study was approved by the Ethics Committee of the Eberhard Karl University of Tübingen (ethical approval 288/2022BO2) and is compliant with all relevant ethical regulations regarding research involving human participants. For full patient characteristics see Table S1.

2.2. Culturing 2D Cell Lines

BC cell lines MDA-MB-468 and MCF-7 were acquired from American Type Culture Collection (Manassas, VA, USA, HTB-22 and HTB-132). Cells were handled in DMEM-FBS (Dulbecco's Modified Eagle Medium (41965-062), containing 10% FBS (10270-106), 1% Pen/Strep (15140-122) from Thermo Fisher Scientific, Waltham, MA, USA). Cells were recurrently checked for mycoplasma using a PCR Detection Kit (abm, Richmond, BC, Canada, G238).

2.3. Freezing and Thawing of CAR-T Cells

Cultured cells were centrifuged at 350× *g* for 5 min and resuspended in human serum albumin (HSA, CSL Behring GmbH, Marburg, Germany, 4356500002) containing 10% dimethyl sulfoxide (DMSO, PanReac Applichem, Darmstadt, Germany, A3672) at a cell density of 1–10 × 10^7 cells/mL; 1 mL aliquots were frozen overnight at −80 °C and subsequently transferred to liquid nitrogen storage. To thaw cells, frozen aliquots were rapidly thawed in a 37 °C water bath, diluted in pre-warmed TexMACS™ medium (Miltenyi Biotec, Bergisch Gladbach, Germany, 31870) without interleukins or antibiotics and centrifuged at 350× *g* for 5 min. Then, T cells were resuspended in TexMACS™ medium without supplementation at a density of 4 × 10^6 cells/mL and incubated for 4 h before adding IL-7/IL-15-supplemented (Miltenyi Biotec, Bergisch Gladbach, Germany, 130-095-367 and 130-093-955) TexMACS™ media to achieve a cell density of 1 × 10^6 cells/mL.

2.4. Isolation and Transduction of T Cells

Peripheral blood mononuclear cells (PBMCs) were isolated from freshly collected peripheral blood samples via Ficoll centrifugation (Biocoll®, BIO&SELL GmbH, Nürnberg, Germany, L 6115) from healthy voluntary donors at the University Children's Hospital

Tübingen. T cell isolation was performed using anti-CD4 and anti-CD8 microbeads (Miltenyi Biotec, Bergisch Gladbach, Germany, 130-045-101 and 130-045-201), subsequently activated with TransAct™ (Miltenyi Biotec, Bergisch Gladbach, Germany, 130-128-758) and cultivated in TexMACS™ media supplemented with 10 ng/mL IL-7 and 5 ng/mL IL-15. After 36 h, activated T cells were transduced with AdCAR (LLE-CAR) lentivirus (provided by Miltenyi Biotec, Bergisch Gladbach, Germany) at a multiplicity of infection (MOI) of 3. Transduced T cells were maintained at 0.5–2 × 10^6 cells/mL in IL-7/IL-15-supplemented TexMACS™ media and furthermore monitored for lactate. CAR transduction efficiency was determined by flow cytometry at day 7 using AdCAR detection reagent (provided by Miltenyi Biotec, Bergisch Gladbach, Germany).

2.5. Adapter Molecule Conjugation

Biotin adapter conjugation was achieved at 30 °C for 1 h in DPBS buffer (Thermo Fisher Scientific, Waltham, MA, USA, 14190-094) using 5-fold molar excess of biotin-LC-LC-NHS (Thermo Fisher Scientific, Waltham, MA, USA, CAS-No. 89889-52-1). This was followed by separation of the antibody/label mix on a Sephadex G25 column (Cytiva Europe GmbH, Freiburg, Germany, 17085101). Protein holding fractions were collected, analyzed by absorption at 280 nm, and subsequently united. Successful conjugation was confirmed via flow cytometry on cell lines expressing the target.

2.6. Organoid Culture Setup

Cryopreserved MBC-PDOs from our previous study were used for the study [14]. For the setup of organoid cultures, the required amount of cell suspension was mixed with basement membrane extract (BME; Cultrex Reduced Growth Factor Basement Membrane Extract, Type 2 Select, Bio-techne, Minneapolis, MN, USA, 3533-005-02) at a ratio of 30% cell suspension to 70% BME; 20 µL droplets were seeded on 48-well plates and placed upside down in an incubator (37 °C, 5% CO_2) to solidify for 30 min. BC culture medium (BCM; Table S2, composition previously described [13,25]) was added to each well and renewed every 3–4 days. Cells were incubated at 37 °C and 5% CO_2 and pictures were taken frequently with EVOS M7000 microscope (Thermo Fisher Scientific, Waltham, MA, USA).

2.7. Passaging of MBC-PDOs

MBC-PDOs were passaged every 7 to 21 days, depend on organoid size and density. Organoids were recovered from the wells by resuspending the BME droplets in ice-cold DPBS containing 5 µM Y-27632 (DPBS/Y-27632). The organoid suspension was centrifuged at 500× *g* for 10 min and the supernatant was discarded. The BME-organoid pellet was dispersed with 1 mL of TrypLE™ Express Enzyme (1X; Thermo Fisher Scientific, Waltham, MA, USA, 12604013) at 37 °C in a water bath for 5 min. The suspension was then centrifuged (500× *g* for 10 min) and the supernatant was discarded. For further culture, the desired amount of cell pellet was resuspended in AdvDMEM+++ and mixed with BME at a ratio of 30% cell suspension to 70% BME and cultured as described above. To stock organoids, passaged cells were cryopreserved in Recovery™ Cell Culture Freezing Medium (Thermo Fisher Scientific, Waltham, MA, USA, 12648010) and stored in cryovials in liquid nitrogen.

2.8. Generation of Lentiviral Vector

Luciferase and GFP containing lentivirus were produced as previously described [23]. After lipofection (Lipofectamine 3000, Thermo Fisher) of Lenti-XTM 293 T (Clontech/TaKaRa Bio Company, San Jose, CA, USA, 631231) with second-generation packaging plasmid, VSV-G envelope plasmid and transfer plasmid, lentivirus containing supernatants were concentrated (Lenti-X concentrator, TaKaRa Bio Company, San Jose, CA, USA, 631231) and cryopreserved at −80 °C.

2.9. Viral Transduction and Sorting of MBC-PDOs

Third-generation-based lentiviral vector transfer plasmids containing luciferase and GFP were kindly provided by Irmela Jeremias, Helmholtz Center Munich, Munich, Germany (Irmela Jeremias, Helmholtz Center Munich, Germany, 12260). Lentiviral particles were produced as described above. All MBC-PDO lines were transduced at an MOI of 3. Subsequent transgene expression was analyzed by flow cytometry using the co-expressed fluorescent protein. Transduced cells were enriched by bulk fluorescence-activated cell sorting (FACS).

2.10. Flow Cytometry

Flow cytometry analysis was performed by staining 0.2×10^6 cells in fluorescence-activated cell sorting (FACS) tubes. The following antibodies by Miltenyi Biotec (Bergisch Gladbach, Germany) were used to determine antigen expression. Anti-CD47 (anti-human, Biotin, 130-101-342), anti-CD66 (anti-human, Biotin, 130-093-156), anti-CD112 (anti-human, Biotin, 130-109-000), anti-CD133 (anti-human, Biotin, 130-112-193), anti-CD146 (anti-human, Biotin, 130-092-850), anti-CD171 (anti-human, Biotin, 130-100-702), anti-CD276 (anti-human, Biotin, 130-118-579), anti-ROR1 (anti-human, Biotin, 130-118-018), anti-TROP2 (anti-human, Biotin, 130-115-096), anti-CD326 (EpCAM) (anti-human, Biotin, 130-111-114), HER2 (biotin-conjugated Trastuzumab, Kanjinti, 1144554A), and EGFR (biotin conjugated Cetuximab, Erbitux, G0157D) (Table S3). CliniMACS® buffer (Miltenyi Biotec, Bergisch Gladbach, Germany, 700-25) containing antibodies at an equimolar concentration of 20 µg/mL was added to each sample. The cells were furthermore stained with anti-Biotin (APC; Miltenyi Biotec, Bergisch Gladbach, Germany, 130-111-069) and analyzed via BD FACSCanto II (BD Biosciences, Franklin Lakes, NJ, USA).

2.11. Two-Dimensional Luciferase-Based Cytotoxicity Assay (LCA)

Tumor cells were plated in complete RPMI media (Thermo Fisher Scientific, Waltham, MA, USA, 31870) in white 96-well flat-bottomed plates (Greiner Holding, Kremsmünster, Austria, 655083) with 15,000 cells per well and were co-cultured with AdCAR-T cells at a 2:1 ratio. At timepoint 0 h, adapter molecules and synthetic D-luciferin (Sigma Aldrich, St. Louis, MO, USA, L9504) were added to each well at a final concentration of 10 ng/mL and 4 µg/mL, respectively. Bioluminescence was assessed after 24 h, 48 h, and 72 h using the Tecan SPARK microplate reader (Perkin Elmer, Waltham, MA, USA, 30086376) at 37 °C. Lysis was evaluated by the relative luminescence to tumor control wells without AdCAR-T cells.

2.12. Real-Time Impedance-Based Cytotoxicity Assay (ICA)

The impedance-based Real-Time Cytotoxicity Analyzer (RTCA) xCELLigence device (ACEA Biosciences Inc., Santa Clara, CA, USA, 106-0534) was used to assess label-free real-time cytotoxicity [23]. MCF-7 and MD-MBA-468 cell lines were plated at 30,000 cells per well in RPMI 1640-based complete media in 96-well electronic microtiter plates E-Plate® 96 (ACEA Biosciences Inc., Santa Clara, CA, USA, 2801035). After 24 h, effector cells were added according to indicated effector to target ratio. Therapeutic antibodies (AMs) were used at 10 ng/mL. Plates were incubated under 37 °C, 95% humidity, and 5% CO_2, and impedance was assessed every 15 min for 24 h.

2.13. Three-Dimensional Luciferase-Based Cytotoxicity Assay (LCA)

For the AdCAR-T cell treatment of MBC-PDOs and MCF-7, cells were cultured 7 to 21 days as described in Section 2.7. The day before treatment, MBC-PDOs were recovered from the BME droplets by incubating the droplets in 1 mg/mL Dispase (Sigma-Aldrich, St. Louis, MO, USA, D4693) at 37 °C for 20 min. Droplet suspensions were diluted in 1% BSA and centrifuged at 250× *g* for 10 min. The supernatant was removed, and organoid pellets were resuspended in the required amount of assay medium (BCM without Nicotinamide and Y-27632). Per well, 125 µL of organoid suspensions was seeded in 96-well plates (clear

plates, 353072; white plates, 136102; both from Thermo Fisher Scientific, Waltham, MA, USA) coated with 40 µL BME-advDMEM (in a ratio of 50% BME and 50% AdvDMEM+++).

CAR-T cells were thawed the day before treatment and cultured in TexMacs™ medium lacking cytokines and including 10% FBS at 37 °C for 4 h. Cells were then diluted to a concentration of 1×10^6 cells/mL with TexMacs™ supplemented with IL-7 (10 ng/mL), IL-15 (5 ng/mL), penicillin (100 units/mL)/streptomycin (100 µg/mL), and cultured at 37 °C until the following day.

The following day, MBC-PDO cells were counted by the addition of TrypLE to one well per line. Organoids dispersed into single cells at 37 °C for 10 min and were pelleted and resuspended in 100 µL of AdvDMEM+++. MBC-PDO and CAR-T cells were counted using the Bio-Rad TC20™ Automated Cell Counter (Bio-Rad Laboratories, Inc., Hercules, CA, USA) according to manufacturer's protocol.

Diluted in assay medium, 25 µL of CAR-T cells (various E:T ratios), 25 µL of biotinylated antibodies (80 ng/mL), and 25 µL D-Luciferin (2 ng/µL) were added to the wells, reaching a total volume of 200 µL. Wells of clear plates received assay medium instead of D-Luciferin; also, control wells received assay medium as a replacement for CAR-T cells and/or biotinylated antibodies. Readouts were performed after 24 h, 48 h, and 72 h by measuring the luminescence (white plates) with a Varioskan LUX (Thermo Fisher Scientific, Waltham, MA, USA) and capturing brightfield and fluorescence images (clear plates) of MCF-7 organoids and MBC-PDOs. Assays were carried out in multiple technical replicates, and results were normalized to untreated controls.

3. Results

3.1. Design of AdCAR-T Cell System and Functional Targeting of BC Cell Lines

The AdCAR-T system was designed by conjugating the murine clone mBio3-derived scFvs on a third-generation CAR backbone consisting of extracellular spacer domains, CD28 and 4-1BB co-stimulatory, as well as the CD3-ζ signaling domain (Figure 1A) [23]. Unlike conventional CAR-T cells, the AdCAR-T cell system is designed to separate target antigen recognition from T cell activation. This can be achieved by a two-component approach, where AdCAR-T cells identify the linker–labeled–epitope (LLE) of biotin-conjugated adapter molecules (AMs), effectively utilizing their specific antigen-binding capacity (Figure 1B). This two-component system enables targeting a multitude of antigens expressed on target cells, utilizing biotin-conjugated monoclonal antibodies (mAbs) that are in clinical use (Table S3).

To validate the effectiveness of AdCAR-T cells against a range of target antigens, we conducted a cytotoxicity assay using luciferase-expressing MCF-7 (Figure 1C) and MD-MBA-468 (Figure 1D) cell lines. Expression levels of potential BC target antigens such as HER2, EGFR, and TROP2, among others, were assessed via flow cytometry (FC). Immunophenotyping (FC) was performed using the very same biotinylated mAbs, that were subsequently used in cytotoxicity assays. Target cell lysis (of MCF-7 and MDA-MB-468) was compared to the target antigen expression, which reveals a clear correlation between high antigen expression and target cell lysis (Figure 1E,F). When plotting target cell lysis against antigen expression using linear and exponential regression models, the Spearman correlation coefficient value indicates 0.66 and 0.77, respectively. To further validate our observation, we replicated these findings in an impedance-based cytotoxicity assay (ICA), as Supplementary Figure S1 shows.

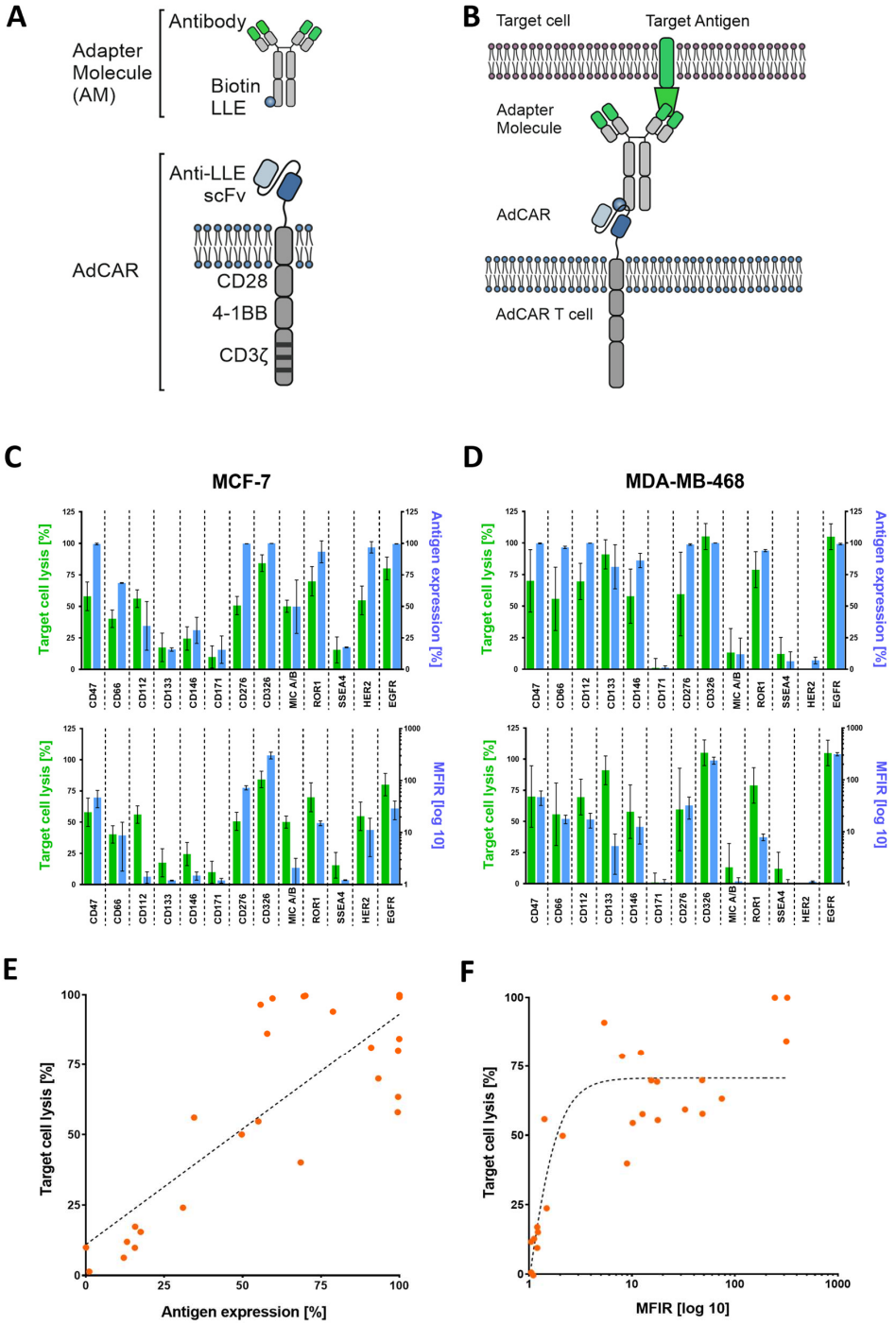

Figure 1. AdCAR-T cell design and functional targeting of BC cell lines using adapter molecules (AMs). (**A**) Schematic illustration of an adapter molecule and AdCAR-T cell receptor. (**B**) AdCAR-T cells are directed towards the target antigen via LLE-conjugated biotinylated antibodies referred to as AMs. (**C**,**D**) Comparison of target cell lysis of MCF-7 and MB-MDA-468 (green bars) to either overtone positive antigen expression (upper blue bars) or mean fluorescence intensity ratio (MFIR) log 10 of antigen expression (lower blue bars). Target cell lysis was determined via luciferin-based cytotoxicity assay after 48 h with an E:T ratio of 2:1. Antigen screening with respective antibodies was performed via flow cytometry (FC) and is represented by mean values (n = 6) ± SD. (**E**) Correlation between target cell lysis and antigen expression of both cell lines analyzed via linear regression resulted in a Spearman correlation coefficient of 0.66. (**F**) Analyzing exponential regression for the correlation of target cell lysis and MFIR log 10 of both cell lines showed a Spearman coefficient of 0.77. All data used in (**E**,**F**) are depicted by mean values (n = 6).

3.2. Cultivation and Characterization of MBC-PDOs Expressing Luciferase and GFP

In order to test the efficacy of AdCAR-T cell lysis on BC patient-derived cells, we used our previously established in vitro models for metastasized BC derived from pleural effusions [14]. Figure 2A shows a schematic overview of the isolation of MBC cells from pleural effusions and the establishment of MBC-PDO cultures. For better visualization and analysis of cell lysis, MBC-PDO lines were virally transduced to express luciferase and GFP (Figure 2A,B). The transduction efficiency of each generated MBC-PDO line was visualized via brightfield and fluorescence microscopy (Figure 2B).

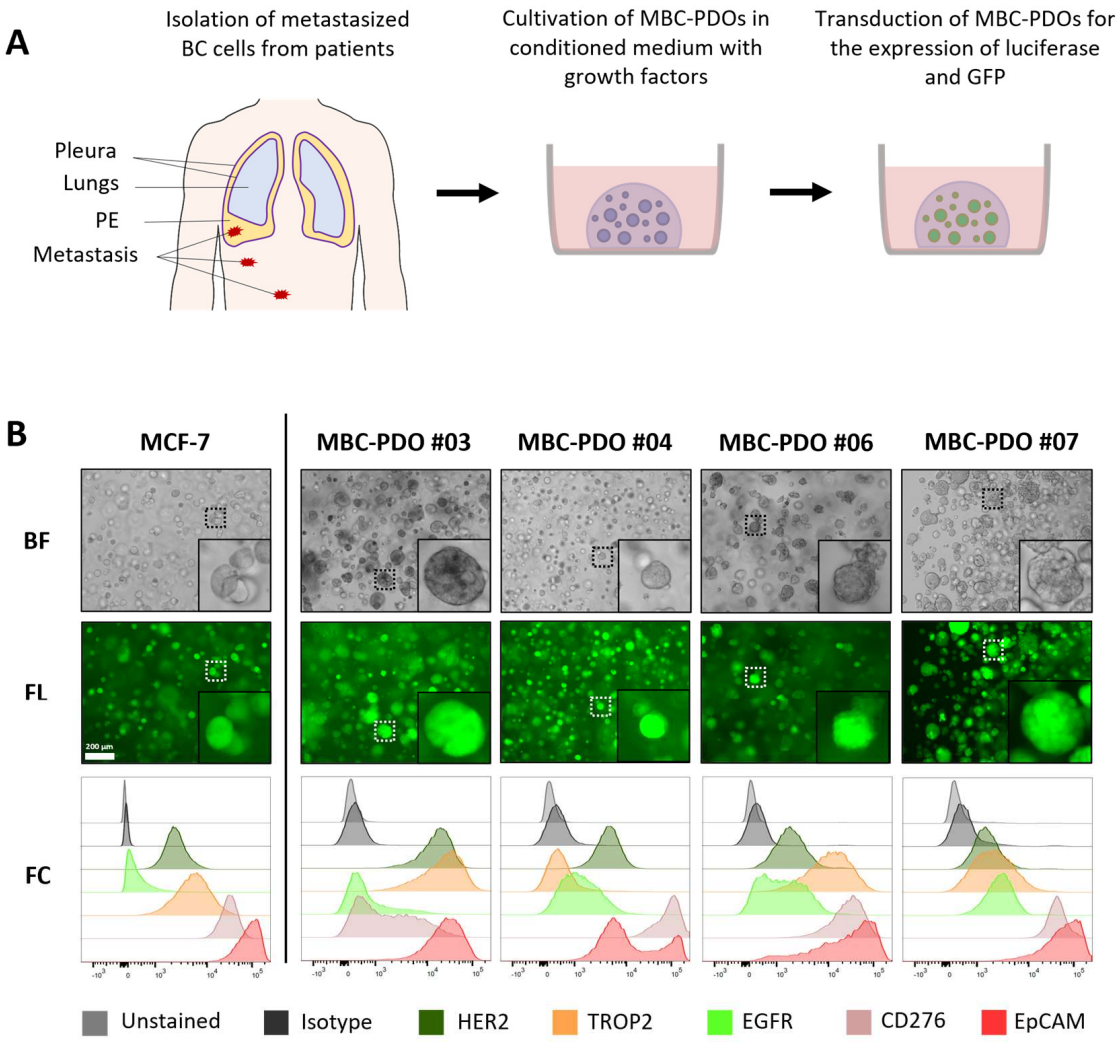

Figure 2. Cultivation and characterization of metastatic breast cancer (BC) patient-derived organoids (MBC-PDO), originated from malignant pleural effusion (MPE). (**A**) Schematic overview of isolation of metastatic BC cells from MPEs, as well as cultivation in BME droplets and viral transduction of MBC-PDOs. (**B**) Brightfield (BF) and fluorescence (FL) images as well as FC analysis of luciferase- and GFP-expressing MCF-7 and MBC-PDO #03, #04, #06, and #07. Scale bar: 200 µm.

To assess the antigen patterns of MBC-PDOs, we immune-profiled all transduced and sorted MBC-PDOs. Immunophenotyping (FC) was performed using biotinylated mAbs that were subsequently used in cytotoxicity assays (Figure 2B). The target antigen panel was chosen based on the expression levels found in BC and their suitability for CAR-T cell therapy. We focused on the following tumor-related antigens found in BC: HER2, TROP2, EGFR, CD276, and EpCAM. Figure 2B shows the expression of the surface antigens in normalized histograms, in which MCF-7 organoids served as a control.

Based on histological characteristics and receptor status (ERα, PR, and HER2), BC is categorized into different subtypes [3]. The receptor status of BC determines the therapy the patients receive and indicates the prognosis. While receptor-positive tumors can be treated with endocrine therapy, or targeted with antibodies and inhibitors, receptor-negative (triple-negative) BC has a poorer prognosis as it is treated with chemotherapy only.

Here, all MBC-PDO lines presented low to medium levels of HER2, with MBC-PDO #03 having the highest level of HER2. The signal for EpCAM was the highest in all five samples (lower panel, red curves), while the other antigens were represented in different quantities. Consequently, the MBC-PDO lines may serve as well-suited in vitro models for the application of personalized AdCAR treatment of metastatic BC cells.

3.3. Implementation of AdCAR Treatment of Organoids

We explored the potential of MBC-PDOs as in vitro models of BC metastasis and their suitability to evaluate AdCAR-T-mediated cytotoxicity. To demonstrate the universal antigen-specific effector function of AdCAR-T cells in vitro, we used adapter molecules in the LLE-mAb format targeted to various tumor-associated antigens expressed by the malignant cells. To implement the application of AdCAR treatment, we first tested various E:T ratios on GFP- and luciferase-expressing MCF-7 organoids. As previously shown, MCF-7 cells strongly express the target antigen CD276 (Figure 2B). Hence, organoids were grown, harvested, and seeded on BME beds to be treated with AdCAR-T cells and LLE-CD276 mAb (Figure 3A). AdCAR-T cells were incubated at different E:T ratios (ranging from 5:1 to 0.2:1). The LLE-mAb concentration was used at 10 ng/mL in all experiments.

Figure 3B presents brightfield and fluorescence images of MCF-7 organoids treated with AdCAR with and without LLE-CD276 mAb. GFP signal and luciferase activity of viable cells were captured after 24 h, 48 h, and 72 h (Figure 3B,C). In the absence of LLE-CD276 mAb, organoids stayed intact even at the highest E:T ratio of 5:1 (Figure 3B), hence, there was no unspecific lysis detected. Yet, the GFP signal decreased slightly, as the organoids were covered by proliferated AdCAR-T cells. In the presence of LLE-CD276 mAb however, MCF-7 organoids were specifically targeted and lysed by AdCAR-T cells, as Figure 3B illustrates. The GFP signal started to diffuse before it disappeared completely.

Furthermore, the efficiency of target cell lysis was determined by luciferase-based cytotoxicity assay. Luciferase activity of remaining viable cells was measured, and values were normalized to untreated control organoids (lacking AdCAR-T cells and mAbs; Figure 3C). With increasing E:T ratios (0.2:1 to 5:1), the antigen-specific AdCAR-mediated cytolysis of MCF-7 organoids reached from 7% to 62% after 24 h of treatment. Thus, antigen-specific cell lysis correlated positively with the E:T ratio. The unspecific cytolysis by AdCAR-T cells (without mAbs) was relatively low (3–8%) and correlated with the E:T ratio as well. After 72 h of treatment, organoids were completely lysed, even at a low E:T of 0.6:1. No significant difference in target cell lysis was observed when comparing direct CD276 CAR T-cells on MCF-7 organoids (Figure S2).

To further assess the suitability of MBC-PDOs for evaluating the efficacy of AdCAR-T, CD276-positive MBC-PDO #07 was treated with AdCAR-T cells in combination with LLE-CD276 mAb (Figure 4A,B) at different E:T ratios. Fluorescence images of GFP-expressing organoids illustrate that the GFP signal decreased and diffused with higher E:T ratios and over time (Figure 4A). Quantification of target cell lysis of MBC-PDO #07 confirmed the visual results (Figure 4B). While the addition of LLE-CD276 mAb to AdCAR-T cells led to very high target-specific lysis (up to 99%) (normalized to untreated organoids), unspecific cell lysis by AdCAR-T cells (without LLE-CD276 mAb) was relatively low (0–17%).

In summary, both MCF-7 and MBC-PDO #07 displayed high levels of CD276 antigen expression and revealed strong responses to the specific targeting by AdCAR-T cells combined with LLE-CD276 mAb. These findings suggest that our organoid lines are suitable for AdCAR treatments with various mAbs. Furthermore, the E:T ratio of 1.3:1 led to a target cell lysis of 99% after 72 h of treatment. Subsequent experiments were performed with an E:T ratio of 1:1.

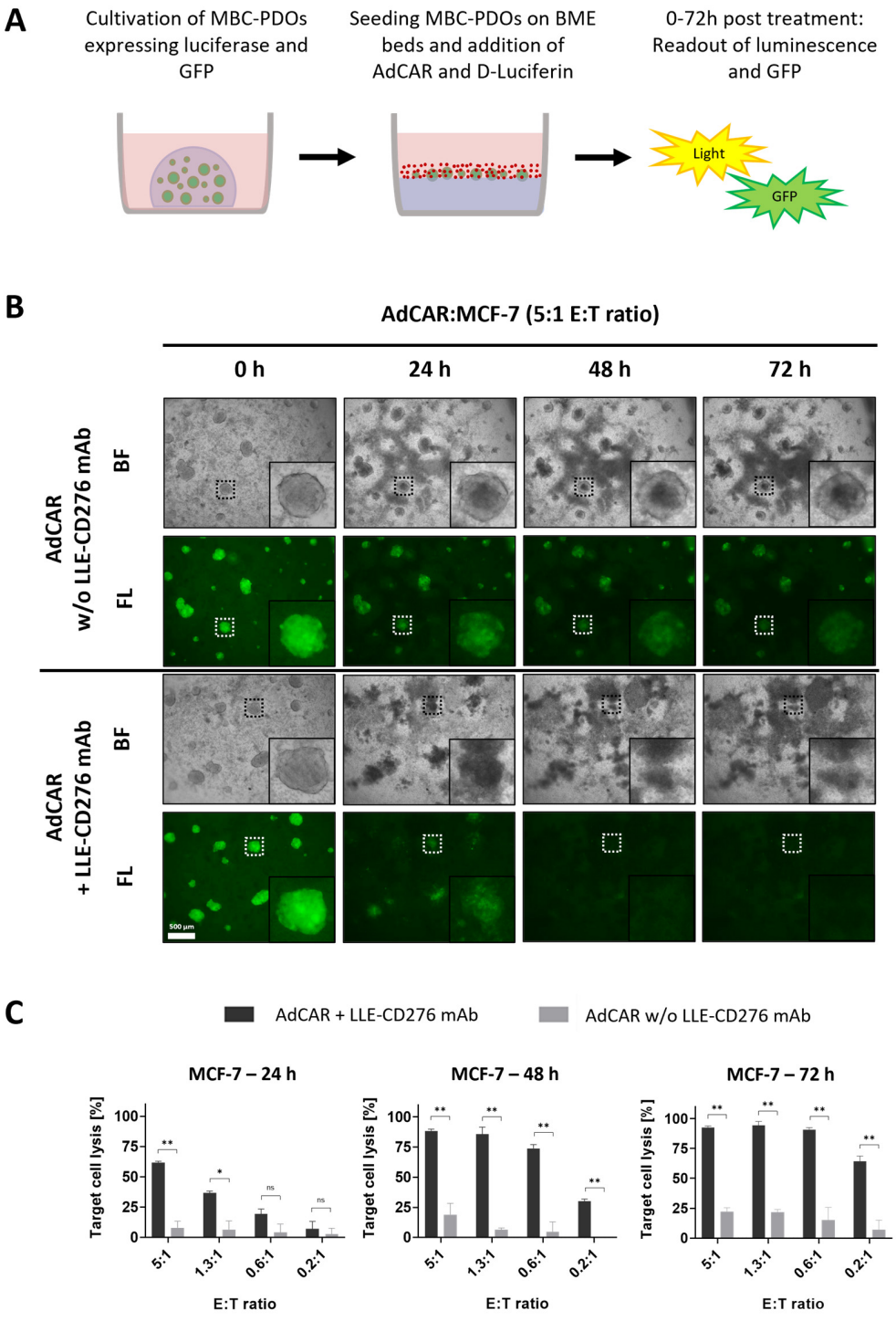

Figure 3. AdCAR treatment of MCF-7 organoids expressing luciferase and GFP. (**A**) Schematic overview of the experimental setup. MCF-7 and MBC-PDOs (green) expressing luciferase and GFP were seeded on BME beds and treated with AdCAR-T cells (red) and corresponding LLE-CD276 mAb. Readouts were performed on luminescence and GFP after 24 h, 48 h, and 72 h using a plate reader and a fluorescence microscope. (**B**) Brightfield (BF) and fluorescence (FL) images of GFP-expressing MCF-7 organoids treated with AdCAR-T cells without (−) and with (+) LLE-CD276 mAb. Scale bar: 500 µm. (**C**) Target cell lysis of MCF-7 organoids treated with AdCAR-T cells with (black bars) and without (gray bars) LLE-CD276 mAb over 72 h. Target cell lysis efficiency was determined by luciferase activity of remaining cells. Data shown represent the mean ± SD of biological triplicates ($n = 3$). Negative values were set to 0. Statistical analysis was performed using paired *t*-test. ns, not significant. * = $p \leq 0.05$; ** = $p \leq 0.01$.

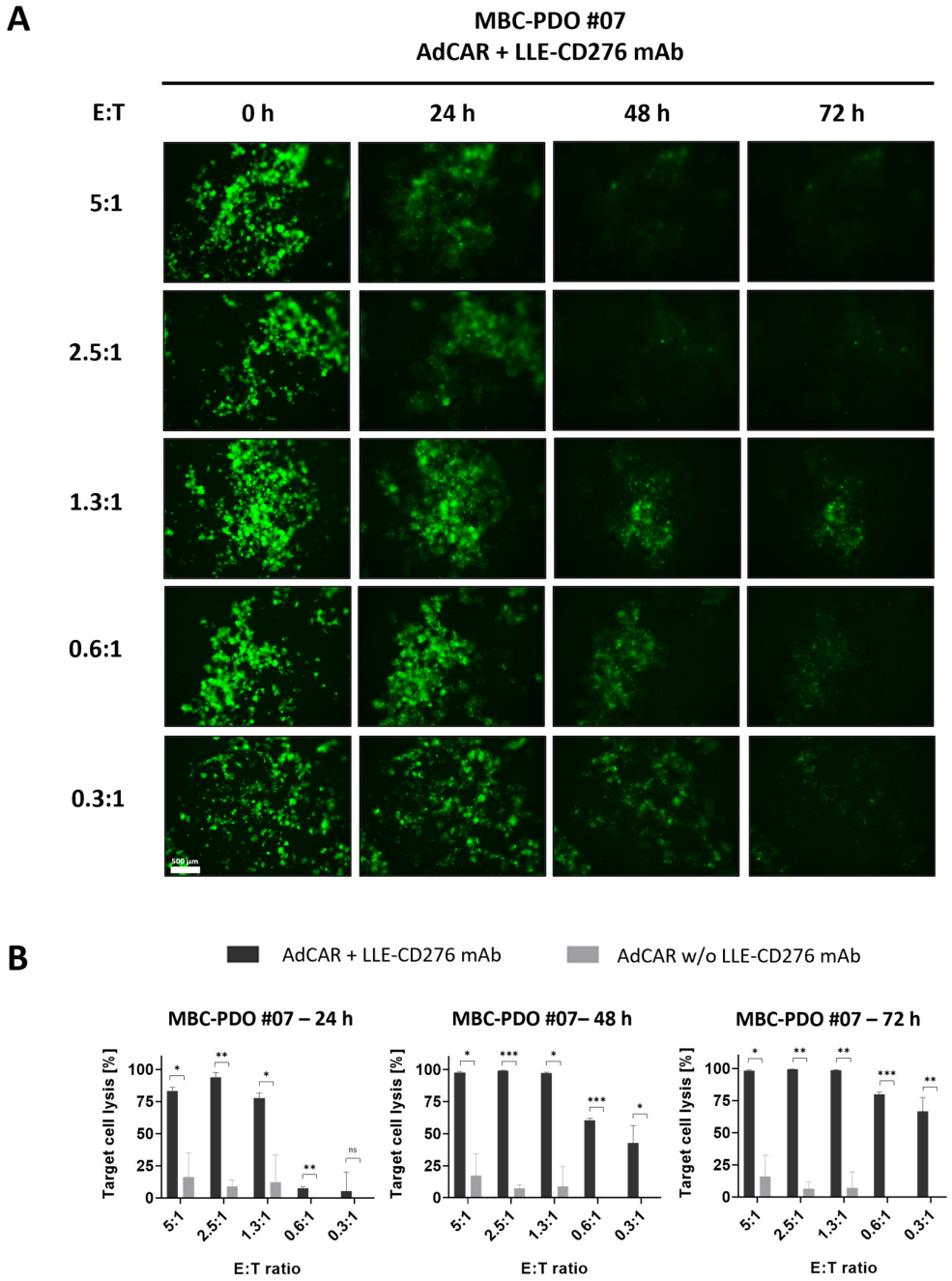

Figure 4. AdCAR treatment of luciferase- and GFP-expressing MBC-PDO #07 at various E:T ratios. (**A**) Fluorescence images of GFP-expressing MBC-PDO #07 treated with AdCAR-T cells of different E:T ratios with the addition of LLE-CD276 mAb over 72 h. Scale bar: 500 µm. (**B**) Target cell lysis of MBC-PDO #07 treated with AdCAR-T cells with (black bars) and without (gray bars) LLE-CD276 mAb over 72 h. Target cell lysis efficiency was determined by luciferase activity of viable organoids. Data shown represent the mean ± SD of biological triplicates (n = 3). Negative values were set to 0. Statistical analysis was performed using paired t-test. ns, not significant. * = $p \leq 0.05$; ** = $p \leq 0.01$; *** = $p \leq 0.001$.

3.4. AdCAR Treatment of MBC-PDOs Using Multiple LLE-mAbs

To investigate the potential of targeting alternative antigens beyond CD276, we tested if further LLE-mAbs have similar effects on MBC-PDO #07. Hence, this line was treated with AdCAR-T cells in combination with LLE-CD276, LLE-HER2, LLE-EGFR, and LLE-TROP2 at an E:T ratio of 1:1 (Figure 5A). Compared to the control conditions (without

LLE-mAbs, +/− AdCAR), in which organoids were fully intact, treated organoids lost GFP intensity and dissolved over time. These results are in accord with the antigen expression pattern analyzed by FC, and the quantification of target cell lysis determined by luciferase activity (Figure 5B). After 24 h of treatment, LLE-CD276 and LLE-EGFR resulted in the highest lysis rates, which correlated with the antigen expression according to the FC data. At 48 h, the antigen-specific AdCAR-mediated cytolysis of MBC-PDO #07 reached from 90% to 99%, and further increased up to 100% (LLE-HER2) after 72 h of treatment.

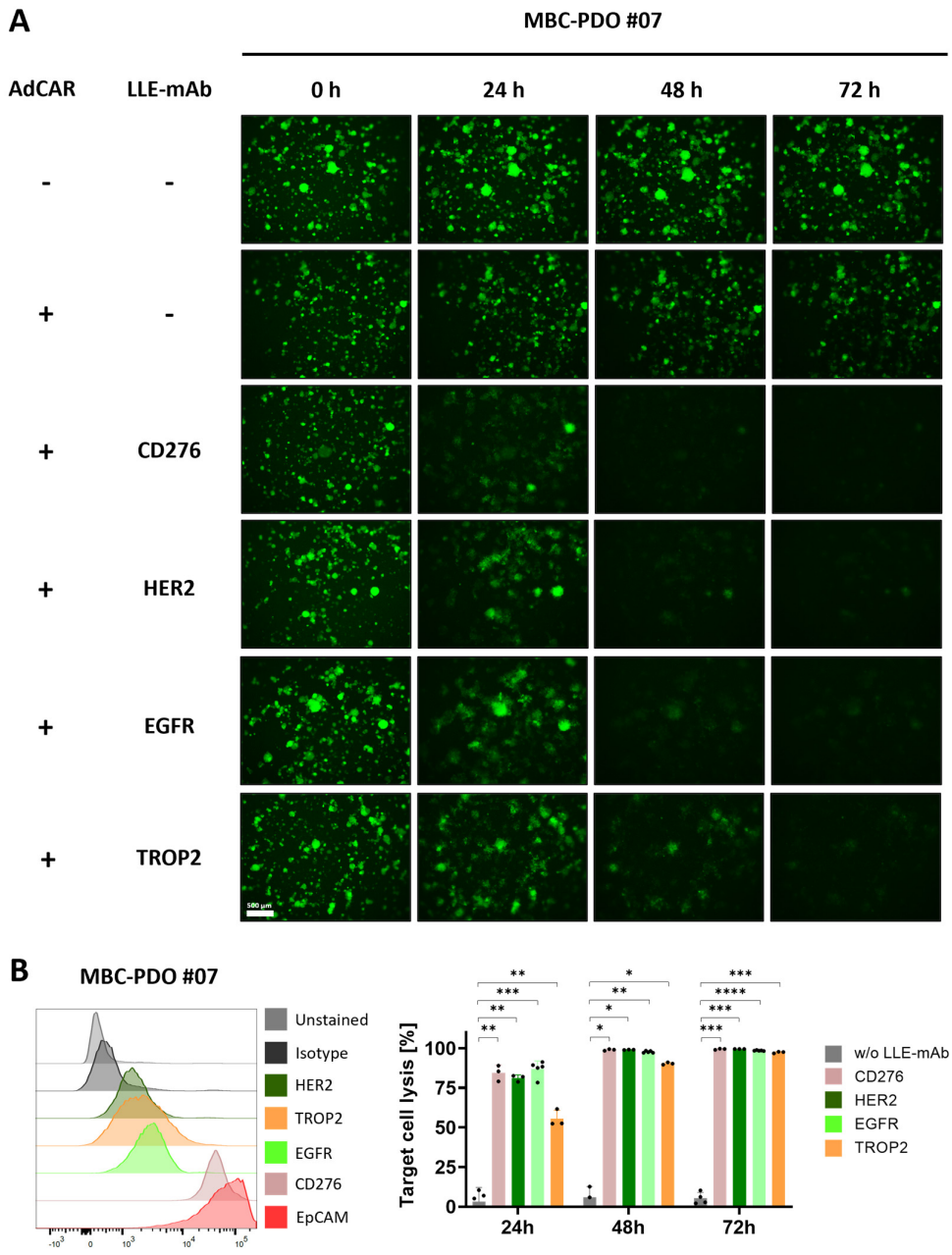

Figure 5. AdCAR treatment of MBC-PDO #07 with various LLE-mAbs. (**A**) Fluorescence images of GFP-expressing MBC-PDO #07 treated with AdCAR-T cells (E:T ratio was set to 1:1) with the addition of LLE-mAbs against CD276, HER2, EGFR, and TROP2. Images were taken after 0 h, 24 h, 48 h, and 72 h of treatment. Scale bar: 500 µm. (**B**) FC analysis and target cell lysis of MBC-PDO #07 treated with AdCAR-T cells (E:T ratio was set to 1:1) with (colored bars) and without (gray bars) LLE-mAbs over 72 h. Target cell lysis efficiency was determined by luciferase activity of viable organoids. Data shown represent the mean ± SD of biological triplicates (n = 3). Statistical analysis was performed using paired t-test. ns, not significant. * = $p \leq 0.05$; ** = $p \leq 0.01$; *** = $p \leq 0.001$; **** = $p \leq 0.0001$.

Next, we tested the influence of AdCAR treatment and various LLE-mAbs on additional MBC-PDO lines. MBC-PDO #03 was treated with the mAbs LLE-CD276, LLE-HER2, LLE-EGFR, LLE-TROP2, and LLE-EpCAM for 72 h (Figure 6A). According to the FC data, levels of EGFR in MBC-PDO #03 were lower compared to the other antigens. Consequently, the LLE-EGFR-mediated target cell lysis was lower compared to the rest of the mAbs which achieved a lysis of up to 95%. The AdCAR treatment of MBC-PDO #06, which expressed CD276, EGFR, and TROP2, was combined with LLE-CD276, LLE-EGFR, and LLE-TROP2, respectively (Figure 6B). As expected, all three conditions led to complete cytolysis. Finally, CD276- and EGFR-expressing MBC-PDO #04 were treated with AdCAR-T cells together with LLE-CD276 and LLE-EGFR, respectively (Figure 6C). After 48 h and 72 h of treatment, the antigen-specific cytolysis achieved approx. 90%.

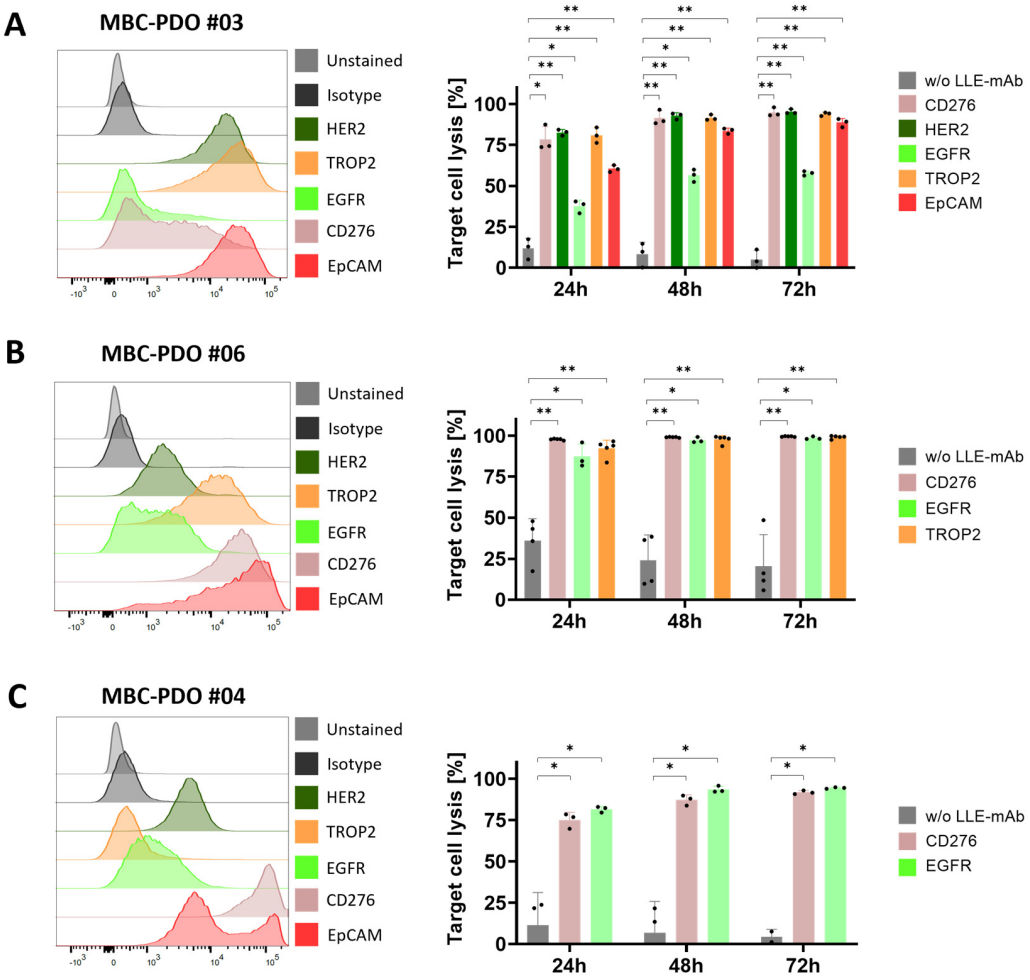

Figure 6. FC analysis and AdCAR treatment of MBC-PDOs with various LLE-mAbs. Treatments were performed on (**A**) MBC-PDO #03, (**B**) MBC-PDO #06, and (**C**) MBC-PDO #04. AdCAR treatment of MBC-PDOs with (colored bars) and without (gray bars) LLE-mAbs was carried out in an E:T ratio of 1:1 for 72 h. Target cell lysis efficiency was determined by luciferase activity of viable organoids. Data shown represent the mean ± SD of multiple biological replicates ($n \geq 3$). Statistical analysis was performed using paired *t*-test. ns, not significant. * = $p \leq 0.05$; ** = $p \leq 0.01$.

In conclusion, our findings illustrate that MBC-PDOs are suitable models for the in vitro screening of metastatic BC treatment by the AdCAR system and that antigen expression of MBC-PDOs correlates with their specific cytolysis mediated by AdCAR-T cells and compatible LLE-mAbs. Furthermore, the capability of targeting various antigens varied, depending on antigen expression levels and the characteristics of the target antigens that had an influence on their effectiveness in recruiting AdCAR-T cells

to malignant cells. Hence, even though there is potential for universal targeting using a single CAR construct for all antigens, not all antigens were capable of recruiting AdCAR-T cells to cancer cells equally. Nevertheless, our data clearly demonstrate the potential of AdCAR-T for personalized therapies based on individual target antigen expression patterns.

4. Discussion

Metastatic BC is associated with various challenges including cancer heterogeneity and treatment-resistant cells [4]. As metastatic biopsies are relatively rare, most therapy decisions depend on the characteristics of primary tumors. However, primary tumors may not represent the heterogeneous features of metastatic tumors. Therefore, therapy decisions based solely on the characteristics of primary tumors can lead to a poor outcome [6,7].

BC exhibits significant heterogeneity and can be clinically categorized into various subtypes based on the presence or absence of hormone receptors (HRs) and the status of HER2 [3]. Triple-negative BC, for one, which is defined by the absence of both HRs and HER2, is associated with a poorer prognosis, as endocrine therapy and HER2-targeted therapy are off the table [3]. In this case, alternative target antigens, expressed on the tumor cell surface, need to be explored and clinically evaluated. For instance, CD276 has shown to be expressed in numerous solid tumors including BC [26,27]. In the present study, we provide a comprehensive analysis of target antigen expression patterns in BC cell lines and MBC-PDOs, demonstrating inter-individual heterogeneity. These results clearly demonstrate the need for patient-individualized treatment approaches.

The application of genetically engineered T cell treatments, which integrate a chimeric antigen receptor (CAR), has demonstrated impressive clinical responses in patients with hematological malignancies [18]. Thus far, multiple obstacles have restricted successful translation of CAR-T therapies in solid tumors. Guiding CAR-T cells to reach and infiltrate the tumor poses a significant challenge, which is furthermore magnified by the immunosuppressive conditions found in the tumor microenvironment [18]. Additionally, tumor cells have the capability to reduce antigen expression under the selective pressure exerted by CAR-T cells. Promiscuous antigen expression between tumor and physiological tissues can result in on-target off-tumor effects and associated life-threatening toxicities [18]. This is particularly highlighted in the case study conducted by Morgan et al., where the application of HER2-targeted CAR-T cells triggered a cascading systemic inflammation, ultimately resulting in multi-organ failure that was attributed to CAR-T activation by a low-level expression of HER2 on lung epithelial cells [28]. This emphasizes the necessity for advancements in the emerging field of CAR-T cell-based therapy in BC, where progress depends on discovering suitable TAAs and mechanisms for stringent control of CAR-T activity. This is especially pronounced in the context of triple-negative BC.

To date, numerous novel CAR-based target antigens have been evaluated against BC. The majority of these studies have been conducted in preclinical trials. Ongoing clinical trials with BC patients include the targeting of HER2, GD2, and EpCAM amongst others [19]. In addition to targeting tumor cells, efforts have been directed toward the elimination of cells residing within the extracellular matrix [29]. Combinatorial strategies with CAR-T cells and conventional BC therapy may lead to better efficacy, especially in terms of overcoming the suppressive tumor microenvironment. These approaches have yet to be assessed in clinical trials.

One elegant way to improve safety and flexibility of CAR-T cells in comparison to conventional CAR-T cell designs is to split antigen recognition from CAR-T cell activation. By introducing "adapter" molecules that bridge between TAA and CAR, this approach allows maximal control of CAR-T cell activity. Pioneered by the expression of an Fcγ receptor (CD16) [30] or CD16-derived CAR construct [31] in T cells to enable antibody-dependent cellular cytotoxicity (ADCC), multiple groups have re-invented the concept of "adapter"-mediated CAR-T activation [32–35]. We have recently reported on the development of the

AdCAR platform [23]. The AdCAR is directed against biotin in the context of a specific linker structure, referred to as linker–label–epitope (LLE). We did not see any interference with serum or protein-bound biotin. The LLE-tag can be chemically conjugated on any kind of binding molecule (e.g., mAbs, mAb fragments, natural or synthetic ligands), allowing highly flexible and convenient AM generation. This flexibility in AM generation provides an advantage over AMs that incorporate recombinant tags [32,33,35], facilitating to build on clinically available mAbs. Moreover, we use the physiologically available vitamin biotin as a label. In contrast to other approaches using, for example, FITC, we expect less immunogenicity. Inherent to the design of all "adapter"-CAR systems is the beneficial safety profile, rendering these approaches a perfect fit for promiscuously expressed TAA. Moreover, AdCAR-T allows highly flexible and multiple targeting to prevent antigen escape and enable individualized targeting the regiment's platform [23]. First "adapter"-CAR systems have already entered the clinic (NCT04230265), targeting CD123 in adult AML, demonstrating complete remission in 2 out of 3 patients and underscoring the feasibility of "adapter"-CAR approaches [36]. To explore this concept, we tested AdCAR-T cells with a variety of adapter molecules that target different antigens on MCF-7 and triple-negative MDA-MB-468 in 2D cultures (Figure 1C–F). Most of the targets used in this study harbor clinical relevance [19]. We observed a positive correlation between antigen expression and target cell lysis.

To demonstrate the feasibility of patient-individualized targeting and co-clinical functional validation, we utilized our MBC-PDOs' platform [14]. As shown before, MBC-PDOs preserve both receptor statuses and hotspot mutations across numerous passages. Therefore, MBC-PDOs provide a reliable in vitro platform for pre-clinical assessment of therapeutic effectiveness [14]. For the first time, we applied this platform for systematic testing in the context of immunotherapy, particularly CAR-T cells. In accordance with individual antigen expression profiles assessed by flow cytometry (Figure 2B), AdCAR-T in combination with specific adapter molecules delivered potent lysis of MBC-PDOs. Specific lyses strongly correlated with antigen expression. For instance, MBC-PDO #03 demonstrated minor levels of EGFR and high levels of CD276, HER2, TROP2, and EpCAM expression (Figure 6A). As a result, AdCAR-mediated cytolysis applying LLE-EGFR mAbs was low (38–58%), while the treatments with LLE-CD276, LLE-HER2, LLE-TROP2, and LLE-EpCAM led to complete target cell lysis. Future studies can include combinatorial approaches with multiple targets, as this was demonstrated to be superior compared to monotargeting [24]. Whether targeting specific TAAs results in enhanced target cell lysis can be investigated in further studies While our approach is clearly functional and shows a correlation between antigen expression and target cell lysis in 2D culture (Figure 1E,F), further investigation is needed within the 3D setting. Here, antigen staining alone does not seem to provide a clear prediction of AdCAR activity.

We, however, clearly demonstrate the feasibility of individually analyzing target antigen expression profiles and functionally validating patient-derived organoids' efficacy of specific targeting. We further underscore the potential of AdCAR-T as an ideal tool for precision immunotherapy allowing individual selection target antigens, streamlining complex manufacturing and safety assessment of engineered cellular therapeutics. By building clinically tested and approved antibodies, this approach will facilitate clinical translation and accessibility of targeted cellular therapies to a very heterogeneous patient cohort.

Our MBC-PDO-based in vitro platform in combination with AdCAR-T cells pave the way for precision immunotherapy in solid tumor malignancies and can further be utilized in the assessment of existing and novel therapeutic approaches.

5. Conclusions

In conclusion, MBC-PDO lines serve as a reliable in vitro platform that can be utilized in the assessment of AdCAR-T cell effectiveness in treating metastatic BC. Further research is required to demonstrate the soundness of these promising models for clinical relevance.

As a minuscule number of BC patients develop MA or MPE, further sources for metastatic biopsies should be introduced as a novel standard in pathological and experimental applications. Consequently, the biobank of patient-derived BC organoid models can be extended to increase access to this pre-clinical evaluation platform. This study clearly demonstrates the feasibility of precision immunotherapy utilizing AdCAR-T to target patient-individualized antigen patterns.

Supplementary Materials: The following supporting information can be downloaded at: https://www.mdpi.com/article/10.3390/cancers16010168/s1, Table S1: List of BC patient data from whom the organoid lines were established. Table S2: Composition of breast cancer medium (BCM). Table S3: Antibody information chart. Figure S1: Correlation between LCA and real-time ICA. Figure S2: Direct CD276 CAR-T cell treatment of MCF-7 organoids expressing GFP.

Author Contributions: Conceptualization, A.K. and C.M.S.; methodology, A.K., C.M.S., C.E.Ö., M.M.-O. and S.M.S.; formal analysis, C.E.Ö. and M.M.-O.; resources, A.K., C.M.S. and A.D.H.; data curation, C.E.Ö. and M.M.-O.; writing—original draft preparation, C.E.Ö., M.M.-O., A.K. and C.M.S.; writing—review and editing, C.E.Ö., M.M.-O., A.K. and C.M.S.; supervision, A.K. and C.M.S. All authors have read and agreed to the published version of the manuscript.

Funding: Part of this research was supported by the German Cancer Aid (Priority program 'Translational Oncology'; Project: DETECT-CTC-HIGH—70114705). We acknowledge support from the Open Access Publication Fund of the University of Tübingen.

Institutional Review Board Statement: The study was approved by the Ethics Committee of the Eberhard Karl University of Tübingen (Ethical approval 150/2018BO2, 288/2022 and 761/2015BO2) and is compliant with all relevant ethical regulations regarding research studies involving humans.

Informed Consent Statement: Written informed consent was obtained from all subjects involved in the study.

Data Availability Statement: The data demonstrated in this study are available upon request from the corresponding author.

Acknowledgments: We thank Alica Fehrenbach for her contribution to this project.

Conflicts of Interest: The authors declare no conflict of interest. The funders had no role in the design of the study; in the collection, analyses, or interpretation of data; in the writing of the manuscript; or in the decision to publish the results.

References

1. Sung, H.; Ferlay, J.; Siegel, R.L.; Laversanne, M.; Soerjomataram, I.; Jemal, A.; Bray, F. Global Cancer Statistics 2020: GLOBOCAN Estimates of Incidence and Mortality Worldwide for 36 Cancers in 185 Countries. *CA Cancer J. Clin.* **2021**, *71*, 209–249. [CrossRef] [PubMed]
2. Sorlie, T.; Perou, C.M.; Tibshirani, R.; Aas, T.; Geisler, S.; Johnsen, H.; Hastie, T.; Eisen, M.B.; van de Rijn, M.; Jeffrey, S.S.; et al. Gene expression patterns of breast carcinomas distinguish tumor subclasses with clinical implications. *Proc. Natl. Acad. Sci. USA* **2001**, *98*, 10869–10874. [CrossRef] [PubMed]
3. Harbeck, N.; Penault-Llorca, F.; Cortes, J.; Gnant, M.; Houssami, N.; Poortmans, P.; Ruddy, K.; Tsang, J.; Cardoso, F. Breast cancer. *Nat. Rev. Dis. Primers* **2019**, *5*, 66. [CrossRef]
4. Pasha, N.; Turner, N.C. Understanding and overcoming tumor heterogeneity in metastatic breast cancer treatment. *Nat. Cancer* **2021**, *2*, 680–692. [CrossRef] [PubMed]
5. Aurilio, G.; Disalvatore, D.; Pruneri, G.; Bagnardi, V.; Viale, G.; Curigliano, G.; Adamoli, L.; Munzone, E.; Sciandivasci, A.; De Vita, F.; et al. A meta-analysis of oestrogen receptor, progesterone receptor and human epidermal growth factor receptor 2 discordance between primary breast cancer and metastases. *Eur. J. Cancer* **2014**, *50*, 277–289. [CrossRef] [PubMed]
6. Curigliano, G.; Bagnardi, V.; Viale, G.; Fumagalli, L.; Rotmensz, N.; Aurilio, G.; Locatelli, M.; Pruneri, G.; Giudici, S.; Bellomi, M.; et al. Should liver metastases of breast cancer be biopsied to improve treatment choice? *Ann. Oncol.* **2011**, *22*, 2227–2233. [CrossRef]
7. Walter, V.; Fischer, C.; Deutsch, T.M.; Ersing, C.; Nees, J.; Schutz, F.; Fremd, C.; Grischke, E.M.; Sinn, P.; Brucker, S.Y.; et al. Estrogen, progesterone, and human epidermal growth factor receptor 2 discordance between primary and metastatic breast cancer. *Breast Cancer Res. Treat.* **2020**, *183*, 137–144. [CrossRef]
8. Dipper, A.; Jones, H.E.; Bhatnagar, R.; Preston, N.J.; Maskell, N.; Clive, A.O. Interventions for the management of malignant pleural effusions: A network meta-analysis. *Cochrane Database Syst. Rev.* **2020**, *4*, CD010529. [CrossRef]

9. Weichselbaum, R.; Marck, A.; Hellman, S. Pathogenesis of pleural effusion in carcinoma of the breast. *Int. J. Radiat. Oncol. Biol. Phys.* **1977**, *2*, 963–965. [CrossRef]
10. Roberts, M.E.; Neville, E.; Berrisford, R.G.; Antunes, G.; Ali, N.J.; on behalf of the BTS Pleural Disease Guideline Group. Management of a malignant pleural effusion: British Thoracic Society Pleural Disease Guideline 2010. *Thorax* **2010**, *65* (Suppl. 2), ii32–ii40. [CrossRef]
11. Sorolla, M.A.; Sorolla, A.; Parisi, E.; Salud, A.; Porcel, J.M. Diving into the Pleural Fluid: Liquid Biopsy for Metastatic Malignant Pleural Effusions. *Cancers* **2021**, *13*, 2798. [CrossRef] [PubMed]
12. Vargo-Gogola, T.; Rosen, J.M. Modelling breast cancer: One size does not fit all. *Nat. Rev. Cancer* **2007**, *7*, 659–672. [CrossRef] [PubMed]
13. Sachs, N.; de Ligt, J.; Kopper, O.; Gogola, E.; Bounova, G.; Weeber, F.; Balgobind, A.V.; Wind, K.; Gracanin, A.; Begthel, H.; et al. A Living Biobank of Breast Cancer Organoids Captures Disease Heterogeneity. *Cell* **2018**, *172*, 373–386. [CrossRef] [PubMed]
14. Onder, C.E.; Ziegler, T.J.; Becker, R.; Brucker, S.Y.; Hartkopf, A.D.; Engler, T.; Koch, A. Advancing Cancer Therapy Predictions with Patient-Derived Organoid Models of Metastatic Breast Cancer. *Cancers* **2023**, *15*, 3602. [CrossRef]
15. Drost, J.; Clevers, H. Organoids in cancer research. *Nat. Rev. Cancer* **2018**, *18*, 407–418. [CrossRef]
16. Trayes, K.P.; Cokenakes, S.E.H. Breast Cancer Treatment. *Am. Fam. Physician* **2021**, *104*, 171–178.
17. Wang, J.; Zhou, P. New Approaches in CAR-T Cell Immunotherapy for Breast Cancer. *Adv. Exp. Med. Biol.* **2017**, *1026*, 371–381. [CrossRef]
18. Sterner, R.C.; Sterner, R.M. CAR-T cell therapy: Current limitations and potential strategies. *Blood Cancer J.* **2021**, *11*, 69. [CrossRef]
19. Yang, Y.H.; Liu, J.W.; Lu, C.; Wei, J.F. CAR-T Cell Therapy for Breast Cancer: From Basic Research to Clinical Application. *Int. J. Biol. Sci.* **2022**, *18*, 2609–2626. [CrossRef]
20. Mackall, C.L.; Miklos, D.B. CNS Endothelial Cell Activation Emerges as a Driver of CAR T Cell-Associated Neurotoxicity. *Cancer Discov.* **2017**, *7*, 1371–1373. [CrossRef]
21. Gardner, R.; Wu, D.; Cherian, S.; Fang, M.; Hanafi, L.A.; Finney, O.; Smithers, H.; Jensen, M.C.; Riddell, S.R.; Maloney, D.G.; et al. Acquisition of a CD19-negative myeloid phenotype allows immune escape of MLL-rearranged B-ALL from CD19 CAR-T-cell therapy. *Blood* **2016**, *127*, 2406–2410. [CrossRef] [PubMed]
22. Shalabi, H.; Kraft, I.L.; Wang, H.W.; Yuan, C.M.; Yates, B.; Delbrook, C.; Zimbelman, J.D.; Giller, R.; Stetler-Stevenson, M.; Jaffe, E.S.; et al. Sequential loss of tumor surface antigens following chimeric antigen receptor T-cell therapies in diffuse large B-cell lymphoma. *Haematologica* **2018**, *103*, e215–e218. [CrossRef] [PubMed]
23. Seitz, C.M.; Mittelstaet, J.; Atar, D.; Hau, J.; Reiter, S.; Illi, C.; Kieble, V.; Engert, F.; Drees, B.; Bender, G.; et al. Novel adapter CAR-T cell technology for precisely controllable multiplex cancer targeting. *Oncoimmunology* **2021**, *10*, 2003532. [CrossRef] [PubMed]
24. Atar, D.; Mast, A.S.; Scheuermann, S.; Ruoff, L.; Seitz, C.M.; Schlegel, P. Adapter CAR T Cell Therapy for the Treatment of B-Lineage Lymphomas. *Biomedicines* **2022**, *10*, 2420. [CrossRef]
25. Carter, M.E.; Hartkopf, A.D.; Wagner, A.; Volmer, L.L.; Brucker, S.Y.; Berchtold, S.; Lauer, U.M.; Koch, A. A Three-Dimensional Organoid Model of Primary Breast Cancer to Investigate the Effects of Oncolytic Virotherapy. *Front. Mol. Biosci.* **2022**, *9*, 826302. [CrossRef]
26. Arigami, T.; Narita, N.; Mizuno, R.; Nguyen, L.; Ye, X.; Chung, A.; Giuliano, A.E.; Hoon, D.S. B7-h3 ligand expression by primary breast cancer and associated with regional nodal metastasis. *Ann. Surg.* **2010**, *252*, 1044–1051. [CrossRef]
27. Liu, S.; Liang, J.; Liu, Z.; Zhang, C.; Wang, Y.; Watson, A.H.; Zhou, C.; Zhang, F.; Wu, K.; Zhang, F.; et al. The Role of CD276 in Cancers. *Front. Oncol.* **2021**, *11*, 654684. [CrossRef]
28. Morgan, R.A.; Yang, J.C.; Kitano, M.; Dudley, M.E.; Laurencot, C.M.; Rosenberg, S.A. Case report of a serious adverse event following the administration of T cells transduced with a chimeric antigen receptor recognizing ERBB2. *Mol. Ther.* **2010**, *18*, 843–851. [CrossRef]
29. Schepisi, G.; Gianni, C.; Palleschi, M.; Bleve, S.; Casadei, C.; Lolli, C.; Ridolfi, L.; Martinelli, G.; De Giorgi, U. The New Frontier of Immunotherapy: Chimeric Antigen Receptor T (CAR-T) Cell and Macrophage (CAR-M) Therapy against Breast Cancer. *Cancers* **2023**, *15*, 1597. [CrossRef]
30. Clemenceau, B.; Congy-Jolivet, N.; Gallot, G.; Vivien, R.; Gaschet, J.; Thibault, G.; Vie, H. Antibody-dependent cellular cytotoxicity (ADCC) is mediated by genetically modified antigen-specific human T lymphocytes. *Blood* **2006**, *107*, 4669–4677. [CrossRef]
31. Kudo, K.; Imai, C.; Lorenzini, P.; Kamiya, T.; Kono, K.; Davidoff, A.M.; Chng, W.J.; Campana, D. T lymphocytes expressing a CD16 signaling receptor exert antibody-dependent cancer cell killing. *Cancer Res.* **2014**, *74*, 93–103. [CrossRef] [PubMed]
32. Tamada, K.; Geng, D.; Sakoda, Y.; Bansal, N.; Srivastava, R.; Li, Z.; Davila, E. Redirecting gene-modified T cells toward various cancer types using tagged antibodies. *Clin. Cancer Res.* **2012**, *18*, 6436–6445. [CrossRef] [PubMed]
33. Rodgers, D.T.; Mazagova, M.; Hampton, E.N.; Cao, Y.; Ramadoss, N.S.; Hardy, I.R.; Schulman, A.; Du, J.; Wang, F.; Singer, O.; et al. Switch-mediated activation and retargeting of CAR-T cells for B-cell malignancies. *Proc. Natl. Acad. Sci. USA* **2016**, *113*, E459–E468. [CrossRef] [PubMed]
34. Cartellieri, M.; Feldmann, A.; Koristka, S.; Arndt, C.; Loff, S.; Ehninger, A.; von Bonin, M.; Bejestani, E.P.; Ehninger, G.; Bachmann, M.P. Switching CAR T cells on and off: A novel modular platform for retargeting of T cells to AML blasts. *Blood Cancer J.* **2016**, *6*, e458. [CrossRef]

35. Cho, J.H.; Collins, J.J.; Wong, W.W. Universal Chimeric Antigen Receptors for Multiplexed and Logical Control of T Cell Responses. *Cell* **2018**, *173*, 1426–1438. [CrossRef]
36. Wermke, M.; Kraus, S.; Ehninger, A.; Bargou, R.C.; Goebeler, M.E.; Middeke, J.M.; Kreissig, C.; von Bonin, M.; Koedam, J.; Pehl, M.; et al. Proof of concept for a rapidly switchable universal CAR-T platform with UniCAR-T-CD123 in relapsed/refractory AML. *Blood* **2021**, *137*, 3145–3148. [CrossRef]